Diverse roles of Phosphatidylinositol transfer protein PITPβ in eukaryotic cells

Kristina Elizabeth Ile

A dissertation submitted to the faculty of the University of North Carolina at Chapel Hill in partial fulfillment of the requirements for the degree of Doctor of Philosophy in the School of Medicine (Cell and Developmental Biology)

Chapel Hill
2009

Approved by:

Vytas Bankaitis

Patrick Brennwald

Mohanish Deshmukh

Kendall Harden

Sally A. Kornbluth

Abstract

Kristina Ile: Diverse roles of phosphatidylinositol transfer protein PITPβ in eukaryotic cells
(Under the direction of Vytas A. Bankaitis)

Phosphatidylinositol transfer proteins (PITPs) provide a dynamic interface between membrane dynamics and lipid signaling. PITPα and PITPβ encode for two soluble class I, metazoan specific PITPs. However, despite the fact that PITPα and PITPβ share 77 and 95% primary sequence identity and similarity (respectively), PITPα and PITPβ are functionally distinct and play nonredundant functions in cells. Whereas PITPα knockout mice have been created, and these mice display neuronal, intestinal, and liver pathologies, PITPβ functionality remains largely unknown.

In this work, I addressed the distinguishing properties of PITPβ and its role in mammalian and zebrafish cells. We identified regions of PITPβ that contributed to its unique properties: Golgi localization and sphingomyelin (SM) binding. Two single point mutations are sufficient to ablate the SM binding properties of PITPβ, and the Golgi localization was attributed to the combination of two regions of the protein. Next, siRNA and morpholino analyses, in mammalian cells and zebrafish respectively, were developed to understand the physiological role of PITPβ in cells. In mammalian cells, PITPβ was essential for cell survival. Particularly, PITPβ-depleted cells displayed disorganized Golgi networks and anterograde trafficking defects. Surprisingly, PITPβ was not required for cell survival or early development in zebrafish. Instead, PITPβ maintains the

outer segment of the double cone cells of the eye – a cell type required for detection of red and green light. The lack of a housekeeping role for PITPβ led us to examine the roles of other PITPs in zebrafish. A novel third soluble PITP in zebrafish, PITPγ, was identified, though its function is not yet determined because we have no means of detecting the protein levels to ascertain knockdown. PITPα, however, had an unexpected role in early development: reduction of PITPα led to an arrest at an early stage of development (about 12 hpf), ultimately leading to embryonic lethality. Together, this dissertation presents novel roles for class I PITPs in zebrafish, and represents the first functional characterization of PITPβ.

Acknowledgments

I would like to thank my advisor, Vytas Bankaitis, for his excellent mentoring. He has provided me both freedom to learn and explore on my own, and helpful advice when I needed it. I will always be grateful for all that I have learned from him.

I would also like to thank the members of the Bankaitis lab, from whom I've learned a lot, and who have made the lab a fun place to work. Thanks especially to my bench neighbors Carl, Jim, Malika, Sweety and Shriya, and to fellow graduate students Emily and Lydia, all of whom have been great colleagues and friends.

Thank you to my parents, sister, and brother-in-law, who have always supported me in graduate school and in everything else.

Finally, thanks to my colleague, friend, and husband Gabriel Schaaf. I am forever grateful for his help, understanding, and support throughout this experience.

Table of Contents

List of Tables

List of Figures

List of abbreviations

BFA: Brefeldin A

BSA: bovine serum albumin

DAG: diacylglycerol

FBS: fetal bovine serum

GFP: green fluorescent protein

MEF: mouse embryo fibroblasts

PITP: phosphatidylinositol transfer protein

PKD: protein kinase D

PtdCho: phosphatidylcholine

PtdIns: phosphatidylinositol

SM: sphingomyelin

Chapter 1 - Introduction

Chapter 1a

Reference: Ile KE, Schaaf G, Bankaitis VA. Phosphatidylinositol transfer proteins and cellular nanoreactors for lipid signaling. Nat Chem Biol. 2006 Nov;2(11):576-83.

Abstract

Membrane lipids function as structural molecules, reservoirs for second messengers, membrane platforms that scaffold protein assembly and regulators of enzymes and ion channels. Such diverse lipid functions contribute substantially to cellular mechanisms for fine-tuning membrane-signaling events. Meaningful coordination of these events requires exquisite spatial and temporal control of lipid metabolism and organization, and reliable mechanisms for specifically coupling these parameters to dedicated physiological processes. Recent studies suggest such integration is linked to the action of phosphatidylinositol transfer proteins that operate at the interface of the metabolism, trafficking and organization of specific lipids.

Intro

An important feature of eukaryotic membranes is their lipid heterogeneity (van Meer, 2005). There are over 100 distinct lipid species in a mammalian cell based on the

criteria of lipid headgroup and backbone composition alone. When one also considers acyl-chain heterogeneity (that is, heterogeneity in the chemical nature of the fatty-acyl groups that are incorporated into lipid molecules), the number of lipid molecular species rises to over 1,000. Why such diversity if the role of membranes is simply to act as barriers that define the boundary of the cell and physically segregate biochemically distinct internal compartments from one another? We now know that membrane surfaces are sites of robust interfacial chemical reactions that are necessary for proper maintenance of organellar and cellular homeostasis. Thus, membranes serve as platforms for intricate orchestration of the complex biochemistry of signal transduction. Because signaling systems are intrinsic properties of eukaryotic cells, the microanatomy of the membrane surface must also be sufficiently complex to satisfy the intricacies in the organization of such systems.

Recent progress in many laboratories is leading to an increasing appreciation for the complexity of the interface between lipids and proteins, even when one considers only the cytoplasmic leaflet of cellular membranes. As one simple example, phosphatidylinositol-4,5-bisphosphate (PtdIns(4,5)P2) constitutes only ~1 mole percent of total lipid in mammalian plasma membranes (van Meer, 2005). Yet PtdIns(4,5)P2 has many roles in production of second messengers(Berridge and Irvine, 1989; Majerus, 1992; Nishizuka, 1995; Rhee, 2001). PtdIns(4,5)P2 also regulates membrane-protein interactions (Shaw, 1996; Hurley and Meyer, 2001; Lemmon, 2003), enzyme and ion-channel activity (Suh and Hille, 2005), membrane trafficking to and from the plasma membrane (Martin, 2001; Simonsen *et al.*, 2001; Wenk and De Camilli, 2004), activity of actin-binding proteins (York *et al.*, 1999; Defacque *et al.*, 2002; Janmey and Lindberg,

2004) and, indirectly, transcription and mRNA transport (Kronke, 1999; Odom *et al.*, 2000). The picture becomes even more complicated when other phosphorylated forms of phosphatidylinositol (PtdIns) are considered. There are seven distinct species of phosphoinositides (PIPs) in higher eukaryotic cell membranes, of which PtdIns(4,5)P2 is one. There is growing evidence that each of these individual PIP isomers also has unique biological activity. This chemical diversity offers impressive prospects for intricate and combinatorial fine-tuning of PIP-dependent regulation of complex cell functions. In this regard, PIPs are uniquely eukaryotic phospholipids.

Other lipids, previously relegated to 'housekeeping' status, are also more functionally versatile than first believed. Enzyme activation by ceramide-based lipids is a highly active area of investigation (Pettus *et al.*, 2002; Spiegel and Milstien, 2003; Pettus *et al.*, 2004). Phosphatidylserine (PtdSer) activates specific protein kinase C isozymes (Stahelin *et al.*, 2003), phosphatidylethanolamine (PtdEtN) organization imparts spatial organization to the actin cytoskeleton (Iwamoto *et al.*, 2004) and phosphatidylcholine (PtdCho) is a substrate for various phospholipases that release hydrolytic products (for example, phosphatidic acid, lysophosphatidic acid and arachidonic acid) having diverse signaling capabilities (Exton, 1990; Moolenaar, 1995; Singer *et al.*, 1997). The cellular lipid signaling circuitry that connects these regulatory pathways is very complex. For example, PtdCho metabolism intersects at several points with PIP metabolism, which indicates a cross-talk between these two signaling systems that permits their integration (Liscovitch and Cantley, 1995; Sciorra *et al.*, 2002). It is now clear that lipids are not homogeneously distributed along the surface of any membrane system. Rather, they are dynamically organized into sets of domains that, in turn, impose spatial and temporal

regulation on interfacial protein binding and/or enzymatic reactions. Moreover, it is becoming increasingly apparent that populations of lipid molecules are functionally segregated from others of the same species with respect to their involvements in specific intracellular activities. Such functionally distinct populations of specific lipids are operationally referred to as 'pools' (Cleves *et al.*, 1991a; Hinchliffe *et al.*, 1998). A precise definition of what 'pools' means in a physical sense is often unclear because there are many physical explanations for how a functional lipid pool can be created and maintained. Some of these concepts are developed further below.

How are lipid pools segregated in the face of powerful subversive forces, such as lateral lipid diffusion and membrane trafficking, that one might expect to erase higher order blueprints for lipid organization? Unrestrained lipids are mobile in the plane of a membrane bilayer (with diffusion coefficients in the range of 0.1–1.0 $\mu m^2\ s^{-1}$) after all (Schwille *et al.*, 1999). Given that yeast cells have a diameter of 5 μm, whereas mammalian cells are roughly 10–20 μm in each dimension, this is a considerable rate of movement. Vesicle trafficking is also a highly active process that would be expected to confound mechanisms for maintaining nonrandom distribution of lipids. The entire picture becomes even more confused when the robust contributions of 'household' lipid metabolism (both biosynthesis and turnover) are superimposed, particularly when one considers that lipids with signaling power are continuously generated and consumed by such constitutive metabolic pathways (Schwille *et al.*, 1999). Obviously, the coupling of lipid pools to privileged biological functions demands the timely metabolism and/or organization of specific lipids. One mechanism for doing so is to interface lipid metabolism and signaling with spatial and temporal regulators that can control the

metabolic steps themselves, or the organization of the products of such metabolism. This concept implies the existence of very small machines, or nanoreactors, in which metabolic and signaling reactions take place and their products are subsequently organized.

Herein, we explore the notion that the biological functions of an understudied class of eukaryotic proteins, the phosphatidylinositol transfer proteins (PITPs), adhere to some of the key principles implicit in a nanoreactor concept. We also discuss the emerging evidence that PITPs have key roles in defining the functional identities of individual lipid pools. These individual pools are, in turn, dedicated to the regulation of specific biological functions. For the purpose of this review, we define nanoreactor to mean a functional network connecting a phospholipid-bound PITP, at least one phospholipid metabolic enzyme, and a specific lipid-binding component in addition to the PITP (or PITP domain in the case of multidomain proteins; Fig. 1). This basic notion is inspired by work done some 15 years ago by Konrad Sandhoff and colleagues, who demonstrated the existence of activator proteins required for efficient turnover of sphingolipids in lysosomes. Although these sphingolipid activator proteins resemble PITPs in their behavior as lipid transfer proteins in vitro (see below), they actually function as substrate-presentation subunits that mark a bound phospholipid for degradation (Furst and Sandhoff, 1992). The metabolic channeling, by a subunit with lipid-transfer activity, of a privileged lipid molecule to a specific enzyme is an example of what we define as a lipid metabolic nanoreactor.

PITPs: convergent evolution or something else?

To place this discussion in historical context, it has long been appreciated that cells express lipid transfer proteins; that is, provisionally cytosolic proteins that catalyze the desorption of lipid monomers from bilayers in vitro. In some (but not all) cases, these transfer proteins have lipid-binding specificity and are stable as lipid–protein complexes in solution. The sphingolipid activator proteins introduced above belong to this general class of lipid transfer proteins and have binding specificity for sphingolipids (Furst and Sandhoff, 1992). PITPs are uniquely eukaryotic proteins that also have both the property of lipid-binding specificity and the ability to form stable protein–phospholipid complexes in solution. PITPs catalyze exchange of either PtdIns or PtdCho between membranes in vitro (Wirtz, 1997; Hsuan and Cockcroft, 2001; Phillips *et al.*, 2006b). A cycle for such a transfer reaction is illustrated in Figure 2. PITPs contain one phospholipid binding site per monomer, with a decided preference for PtdIns over PtdCho. PITPs exchange a bound phospholipid for a PtdIns or PtdCho monomer that resides in a bona fide membrane bilayer. This is done very efficiently and without ATP or other cofactors. PITPs abstract a phospholipid molecule from a monolayer, which indicates that bilayer organization is not an obligatory requirement for action. As a result, it has been taken somewhat as an article of faith that PITPs do not access, or otherwise disturb, the luminal leaflet of intracellular membranes. Whether this is actually true remains to be rigorously shown. How PITPs couple conformational changes to phospholipid recognition, and eject a bound phospholipid in favor of binding and desorbtion of another phospholipid molecule, remains unknown.

PITPs fall into two families on the basis of primary sequence relationships and structural fold. We refer to these as the Sec14 family and the metazoan PITP family.

Sec14-like and metazoan PITPs have nearly identical in vitro activities but share no primary sequence similarity and, as shown in Figure 3, have unrelated three-dimensional folds. The Sec14 fold defined a novel fold when a crystal structure for the yeast Sec14p PITP was solved (Sha *et al.*, 1998; Phillips *et al.*, 1999). By contrast, the metazoan PITP fold belongs to the steroidogenic acute response protein–related START-domain family (Yoder *et al.*, 2001; Schouten *et al.*, 2002; Tilley *et al.*, 2004). In that respect, it groups with other lipid transfer proteins (for example, ceramide transfer protein (Hanada *et al.*, 2003), PtdCho transfer protein (Roderick *et al.*, 2002) and the putative Kes1p (also called Osh4p) sterol transfer protein (Li *et al.*, 2002; Im *et al.*, 2005)) that either share primary sequence similarity with START domains or are otherwise known to adopt similar structural shapes.

If the extent of gene expansion is a fair measure of functional importance, then the Sec14 family is an important one indeed. Sec14-like proteins make up a protein superfamily for which >500 member proteins can be discerned in available databases, and the expansion of this superfamily is clear in even the simplest unicellular eukaryotes. The yeast Saccharomyces cerevisiae expresses six Sec14-like proteins, whereas higher eukaryotes (humans, mice, Drosophila melanogaster, Caenorhabditis elegans, Arabidopsis thaliana) each harbor in excess of 20. The founding member of this superfamily is the yeast Sec14p, and it is arguably the best studied of the group (see below). It is almost certain that not all Sec14p-like proteins are PITPs. Some Sec14-like proteins (or proteins with Sec14 domains) have specific PIP-binding activities, and these comprise an interesting class in their own right. Some examples include the GTPase-activating RhoGAP proteins (Kostenko *et al.*, 2005; Sirokmany *et al.*, 2006), the Meg2

protein tyrosine phosphatase (Gu *et al.*, 1992; Huynh *et al.*, 2003), Rho nucleotide exchange factors such as Dbl and Ost/Dbs (Whitehead *et al.*, 1997; Cheng *et al.*, 2002; Rossman *et al.*, 2002), the rasGAP neurofibromin (D'Angelo *et al.*, 2006) and plant PIP-binding proteins implicated in osmoregulation (Kearns *et al.*, 1998; Monks *et al.*, 2001). The sheer number of Sec14-like proteins in eukaryotic cells argues for extensive diversification of function, but it remains uncertain whether PtdIns and PIP binding is a common feature of all Sec14p-like proteins. Some bind other hydrophobic ligands (such as vitamin E and retinaldehyde) (Stocker *et al.*, 2002; Min *et al.*, 2003; Panagabko *et al.*, 2003). However, functional studies already suggest that this evolutionary expansion cannot be explained by diversification of substrate binding specificity alone. We anticipate that many mammalian Sec14-like proteins retain PITP activity, and that the PITP complement in metazoans is underestimated.

By contrast, the metazoan PITP family is not highly expanded, and no members of this family have yet been recognized in the genomes of even the higher plants. An enigmatic case is presented by the slime mold Dictyostelium discoideum, which expresses four Sec14-like and four metazoan PITP–like proteins. It is notable that the two classes of PITPs are so similar with respect to in vitro activity yet so different in structural construction and evolutionary expansion. Is this a case for convergent evolution, or does it reflect some functional distinction that is invisible in in vitro systems? In our view, the evidence suggests the latter. The difficulties in interpreting the in vitro lipid-transfer assays are known (Rogers and Bankaitis, 2000). Even in cell-free assays that are more directed, metazoan PITPs and Sec14p are functionally interchangeable (Hay and Martin, 1993; Ohashi *et al.*, 1995; Cunningham *et al.*, 1996;

Jones *et al.*, 1998; Simon *et al.*, 1998). This equivalence is not recapitulated in in vivo studies, however. Those studies consistently report a high degree of functional distinction between individual PITPs. In this review, we will primarily discuss the lipid nanoreactor concept in the context of the Sec14-like PITP family. We will close with a discussion of how this concept may also apply to the metazoan PITPs.

Yeast Sec14p and Sec14-like proteins

We now appreciate that a primary function for PITPs in cells is to coordinate lipid metabolism and signaling with membrane trafficking. The first indications to this effect came from studies of the main yeast PITP (Sec14p), which is essential for protein transport from the yeast trans-Golgi network (TGN) and for yeast cell viability (Bankaitis *et al.*, 1990; Cleves *et al.*, 1991b). Sec14p uses both its PtdIns- and PtdCho-bound forms to regulate many aspects of lipid metabolism. The net purpose of this is to generate a membrane-lipid environment conducive to optimal activity of core components of the TGN vesicle-budding machinery (Fig. 4). Both PtdCho metabolism and conversion of PtdIns to PtdIns(4)phosphate are subject to regulation by Sec14p. That is, Sec14p regulates the metabolic fate of specific pools of PtdCho and PtdIns that are specifically interfaced with the activity of a yeast Golgi subcompartment (Bankaitis *et al.*, 1990; Cleves *et al.*, 1991b; Guo *et al.*, 1999; Hama *et al.*, 1999; Rivas *et al.*, 1999). The localized interplay among Sec14p, lipid metabolism, and proteins of the Arf GTPase cycle define at least one, and perhaps two, TGN lipid nanoreactors (that is, Sec14p-PtdCho-based and Sec14p-PtdIns-based nanoreactors; see below).

Why argue the nanoreactor concept for Sec14p, when it seems equally plausible that Sec14p simply delivers lipids from the endoplasmic reticulum (ER) to the TGN (for

example, PtdIns) or vice versa (for example, PtdCho)? The reasons are several. First, unlike the case for mammalian cells, PtdCho and PtdIns are the most abundant phospholipids in yeast cell membranes. Elevating PtdIns levels to 40 mole percent of total bulk phospholipid in yeast membranes does not circumvent the Sec14p requirement for protein transport from the TGN (Jones *et al.*, 1998). Second, loss of activity of one specific pathway for PtdCho biosynthesis is one of the mechanisms that permits cell viability and TGN functionality in the absence of Sec14p (ref. (Cleves *et al.*, 1991b)). Third, a mutant Sec14p that retains PtdCho-transfer activity but is ablated for PtdIns-transfer activity retains substantial function in vivo (Phillips *et al.*, 1999). Presumably, this mutant Sec14p is incapable of driving vectorial movement of any phospholipid species—a seemingly necessary condition for meaningful lipid transfer between membranes in cells. It is difficult to conceive how these various data are consistent with lipid transfer mechanisms, but the data are readily consistent with precisely tuned metabolic control mechanisms for Sec14p function.

Though the details of this Sec14p-dependent combinatorial regulation of TGN vesicle trafficking await resolution, the ability of a peripheral membrane protein to execute function at the TGN provides a clear example of a dedicated coupling of a PITP to a specific physiological function. In the case of PtdCho metabolism, Sec14p is proposed to act as a lipid sensor that modulates the antagonistic effects of household lipid metabolism on an essential TGN process regulated by multiple lipids (for example, PtdCho, diacylglycerol and PIPs). This set of reactions is proposed to couple to activity of the Arf GTPase cycle (Fig. 4) and defines a Sec14p-PtdCho nanoreactor in the TGN (see also Fig. 1b). In the case of PtdIns(4)phosphate synthesis, Sec14p channels PtdIns to

the Pik1p PtdIns-4-OH kinase of the yeast TGN (Pik1p and Stt4p are the two demonstrated PtdIns-4-OH kinases). Which proteins couple to this particular metabolic reaction remains unknown, but one candidate is the sterol-binding protein Kes1p/Osh4p (Fig. 4). This Sec14p-PtdIns/Pik1p circuit defines a Sec14p-PtdIns nanoreactor in the TGN (see also Fig. 1a).

Other studies in yeast are also inconsistent with the notion that PITPs execute the types of 'one size fits all' activities that are reported by in vitro reconstitutions. Sec14p is only one of six yeast Sec14-like proteins, and several of the other Sec14 homologs (SFHs) are biochemically related to Sec14p on the basis of phenotypic rescue or determined phospholipid-transfer activities (Li *et al.*, 2000; Schnabl *et al.*, 2003; Routt *et al.*, 2005). Testimony to the diversification of biological function of Sec14-domain proteins is apparent from analysis of these SFH proteins. First, SFH proteins are required for optimal activation of the yeast PtdCho-hydrolyzing enzyme phospholipase D (PLD). This is in contrast to the case for Sec14p, whose deficiency activates PLD (Sreenivas *et al.*, 1998; Xie *et al.*, 1998; Xie *et al.*, 2001). Second, the Sec14-like Sfh4p is uniquely required for coordinating the localization and assembly of an enzymatic machinery dedicated to nonmitochondrial decarboxylation of PtdSer to PtdEtN (Wu *et al.*, 2000; Wu and Voelker, 2004; Routt *et al.*, 2005). This machinery is posited to involve formation of intermembrane contact sites between the ER and a TGN or endosomal compartment. Such contact sites serve as portals for nonvesicular trafficking of lipids between distinct compartments, and lipid trafficking via this mechanism is likely to represent a quantitatively significant and underappreciated pathway for intracellular lipid transport (Wu and Voelker, 2002). Present evidence suggests that assembly of this intermembrane

contact site requires an intricate organization of acidic phospholipids that help orchestrate the activity of proteins that chaperone formation of this class of intermembrane contact site. In other words, this particular intermembrane contact machine is coupled to an Sfh4p-dependent metabolic nanoreactor. Third, Sfh5p has the unique ability to promote expansion of what seems to be a plasma-membrane pool of PtdIns(4,5)P2 (ref. (Routt *et al.*, 2005). This pool optimizes the activity of specific t-SNARES (components of the plasma-membrane machinery for vesicle docking and fusion). We propose that the Sfh5p-dependent nanoreactor consists of Sfh5p, the Stt4p PtdIns-4-OH kinase, the Mss4p PtdIns(4)phosphate-5-OH kinase and specific t-SNAREs (Routt *et al.*, 2005). Finally, yeast PITPs control actin organization in yeast. But, whereas Sec14p has a constitutive role in this process, SFH isoforms are involved in evoked pathways for actin reorganization (Routt *et al.*, 2005).

The conclusions derived from study of the SFH proteins are instructive on several counts with regard to the nanoreactor concept. The budding yeast PITPs execute functions unique to individual members of this family, and one can imagine that the coupling of any single PITP to a particular PtdIns kinase may underly functional specification. Yet these proteins, including Sec14p, act at least in part through the same Stt4p PtdIns-4-OH kinase isoform (Routt *et al.*, 2005). Thus, specific PIP pools are defined not only by the lipid kinases that generate them, but also by the individual PITP that couples to a particular lipid kinase. This interface demonstrates a considerable plasticity. Coupling of both the PtdIns kinase isoform and the PITP is subject to developmental regulation in that the activation of PLD is dependent on SFH proteins and

Stt4p in vegetative cells, but it is dependent on Sec14p and Pik1p in sporulating cells (Engebrecht, 2003; Rudge *et al.*, 2004).

Multidomain Sec14-like PITPs and nanoreactors

Potentially the most notable example of a PITP-dependent nanoreactor comes from studies of two-domain Sec14-nodulin proteins of higher plants (Fig. 5a). Unlike Sec14p, these are membrane-associated proteins, at least on the basis of the one case that has been analyzed (Kapranov *et al.*, 2001; Vincent *et al.*, 2005). The Sec14 domains are PITP modules that stimulate PIP synthesis, whereas the C-terminal nodulin domains represent membrane targeting units. Root-hair PtdIns(4,5)P2 homeostasis and organization is dependent on AtSfh1p function, and there are strong similarities between the nonrandom distributions of the AtSfh1p Sec14-nodulin and PtdIns(4,5)P2 in *A. thaliana* root hairs (Vincent *et al.*, 2005). This is a prime example in which the distribution of a PITP sets the distribution of a PIP, and Sec14-nodulin proteins may do so via PIP binding. There are examples of multidomain Sec14-like proteins that bind PIPs, such as the Sec14-GOLD proteins that are conserved across the higher Eukaryota (including mammals) (Anantharaman and Aravind, 2002; McLaughlin and Murray, 2005; Phillips *et al.*, 2006b). Multidomain Sec14 proteins present interesting cases for the PITP nanoreactor concept.

The chemical properties of nodulin domains suggest the way in which PIP synthesis and organization may be coordinated by a multidomain PITP. Nodulin domains have highly basic C-terminal tails with properties reminiscent of PIP-binding motifs (Fig. 5b). Given the ability of unstructured and highly basic protein domains to sequester PtdIns(4,5)P2 on the basis of membrane surface electrostatics (McLaughlin and Murray,

2005), Sec14-nodulin proteins theoretically have the capability to regulate the spatial organization of the very PIP molecules whose synthesis they promote. Available evidence, though admittedly scant, does suggest that Sec14-nodulin proteins can functionally discriminate PIP pools in the context of polarized membrane-trafficking pathways. As PIPs are known regulators of membrane trafficking and of actin cytoskeleton dynamics, we posit that it is through the functional specification of PIP pools that Sec14-nodulin proteins evoke their specific biological effects.

The concept of PIP pools in the context of Sec14-nodulin function suggests other interesting possibilities. One attractive conjecture is that nodulin domains sequester PIPs via high-affinity, but regulated, electrostatic interactions. This sequestration could potentially be controlled so that these PIPs are rendered accessible to the proper effectors (or enzymes) on cue. One hypothetical mechanism for such regulated 'release' involves calmodulin. Basic unstructured polypeptides are excellent binding substrates for Ca2+-calmodulin (Yamniuk and Vogel, 2004; McLaughlin and Murray, 2005), which suggests the possibility that calmodulin activation could loosen the 'nodulin clamp' and release a spatially restricted PIP pool in response to a temporal program responsive to cytosolic Ca2+ flux. The fact that A. thaliana encodes 13 distinct Sec14-nodulin proteins (Vincent *et al.*, 2005) provides an indication of the potential diversity such a strategy may hold for the coupling of distinct Sec14-nodulin–dependent PIP metabolic nanoreactors to developmental pathways for membrane morphogenesis.

Metazoan PITPs: few but potent

As indicated above, the metazoan PITP family is quantitatively much more sparse than the Sec14-like PITP family. Even mammalian cells express no more than five PITP

genes, two of which encode membrane-bound isoforms (Fig. 6). Yet some of the same functional principles discussed above for Sec14p-like PITPs are likely to apply to these proteins. For example, the ability of these PITPs to stimulate PIP synthesis is a common denominator in their involvements in numerous exocytic reactions (for which they act as reconstituted stimulators) and in plasma-membrane receptor and G protein–coupled hydrolysis of PIPs by phospholipase C (Ohashi *et al.*, 1995; Cunningham *et al.*, 1996; Jones *et al.*, 1998; Simon *et al.*, 1998). This is in contrast to the results of in vivo studies that highlight the importance and functional specificities of individual metazoan PITPs. Genetic insufficiencies for the soluble PITPα lead to a perinatal morbidity in mice characterized by chylomicron retention disease (CRD), hypoglycemia and spinocerebellar neurodegeneration (Weimar *et al.*, 1982; Hamilton *et al.*, 1997; Alb *et al.*, 2003). With regard to the neurological component of this disease, recent results indicate that efficient recognition of axonal guidance cues via the netrin receptor requires PITPα (Xie *et al.*, 2005). Soluble-PITP defects in D. melanogaster lead to defective oogenesis that results from dysfunction of the actin cytoskeleton (Gatt and Glover, 2006; Giansanti *et al.*, 2006).

Membrane-associated isoforms of metazoan PITPs also exist (but why, if lipid transfer is the operative function?), and these isoforms may yet prove to be analogs of the higher plant Sec14-nodulin proteins discussed above. An inherited and light-enhanced retinal degeneration in flies results from loss of function of the membrane-associated RdgB protein. RdgB expression is highly tissue-specific, and the 280-residue PITP domain of this protein lies at the N terminus of a much larger polypeptide (Fig. 6)

(Milligan *et al.*, 1997). One mammalian RdgB ortholog is Nir2, and mice lacking this protein die before embryonic day 7.5 (ref. (Chang *et al.*, 1997)).

Why do metazoans invest in development of a small PITP family that is unrelated to Sec14 PITPs when trivial expansion of the already large Sec14 protein superfamily would presumably generate sufficient numbers of functionally unique PITPs to satisfy the same requirements? This puzzle is deepened by indications that mammals apply the same sets of functional-specificity rules to the small cohort of PITPs that they apply to the Sec14-like proteins. The PITPα and PITPβ isoforms are very similar, but they are functionally nonredundant (Alb *et al.*, 2003). In part, this is likely the result of differential distribution of these isoforms within cells. PITPβ is a TGN-associated protein (Phillips *et al.*, 2006a), whereas PITPα is localized to the cytosol and the nuclear matrix (De Vries *et al.*, 1996; Phillips *et al.*, 2006a). However, the cases of PITPβ and the membrane-associated Nir2 cannot be so easily dismissed. Both Nir2 and PITPβ localize to TGN membranes (Litvak *et al.*, 2005; Phillips *et al.*, 2006a), yet these two proteins define a functionally nonredundant pair of PITPs.

The building evidence suggests that a lipid metabolic nanoreactor concept applies to metazoan PITPs as well as the Sec14-like PITPs. What is perhaps more notable, given the structural dissimilarity between these classes of proteins, is that the lipid metabolic nanoreactors under metazoan PITP control resemble those described for Sec14-like PITPs. For example, the Nir2 PITP regulates a TGN lipid metabolic nanoreactor that coordinates diacylglycerol and PtdCho metabolism with protein trafficking in a fashion very similar to that seen in yeast for Sec14p (Litvak *et al.*, 2005). In this instance, the effectors of this lipid regulation include diacylglycerol-binding proteins of the protein

kinase D family (Liljedahl *et al.*, 2001; Baron and Malhotra, 2002; Litvak *et al.*, 2005). The function of PITPβ in the TGN is unknown, but speculations have been made about a PITP-PLD interface on mammalian Golgi membranes (Liscovitch and Cantley, 1995). Such a PITP-PLD interface offers the prospect of a lipid metabolic nanoreactor that couples with the Arf small GTPase cycle in regulating vesicle trafficking. A role for PITPβ in regulating the Arf GTPase cycle and Golgi vesicle trafficking would also be directly analogous to models for Sec14p function in yeast (Phillips *et al.*, 2006b). Returning to comparisons of the functional scenarios for Nir2 and PITPβ, the data further emphasize that the functional specification of PITPs can be achieved via differential coupling of distinct lipid metabolic nanoreactors to sets of distinct effectors.

Along those same lines, mouse PITPα nullizygosity evokes some phenotypes that resemble human CRD (Alb *et al.*, 2003), a disorder caused by ER-localized Sar1 GTPase insuffiency (Jones *et al.*, 2003). Sar1 is a distant member of the Arf GTPase family. Thus, physiological coupling of the soluble metazoan PITPs to the action of small GTPase catalytic cycles may prove a common theme. Why a specialized trafficking cargo transport pathway from the ER (the primary site of lipid synthesis in the cell) requires PITPα for efficient operation is an intriguing question—one that again suggests that lipid delivery is not the final word in terms of metazoan PITP function.

Future directions and future challenges

The idea that PITPs functionally define specific lipid metabolic pools, and do so via the action of dedicated lipid metabolic nanoreactors, is supported by a growing body of data. Much remains to be discovered, however. As a first step, we need to decipher the in vivo wiring diagram that connects individual PITPs to the regulation of lipid

metabolism and ultimately to biological readout. The physical nature of PITP-dependent nanoreactors also begs analysis. Certainly intermembrane contact sites provide one appealing (but not well-supported) notion (Holthuis and Levine, 2005). Functional analyses are obviously required for assessing the nature of PITP-dependent lipid metabolic nanoreactors, but these will likely prove tricky. For instance, the physiological fidelity of PITP activity is sensitive to protein dosage (Skinner *et al.*, 1993; Li *et al.*, 2000). New ideas for how to approach these questions are needed.

From a more general perspective, lipid metabolism cannot be viewed as an averaged activity in any single membrane system—much less in the cell. Unfortunately, we are ill equipped to analyze the mosaic nature of lipid metabolism in vivo. Development of new technologies that report, with spatial and temporal resolution, the activities of specific lipid metabolic nanoreactors in living cells would represent a tremendous advance. New and powerful vital-imaging approaches are required, and possibilities for exploration include methods based on fluorescence resonance energy transfer (FRET) that score activated conformations of protein components of specific nanoreactors. Such status-sensitive reporters are available for Cdc42 GTPases (Nalbant *et al.*, 2004). PITPs provide at least a conceptual starting point for thinking about how one would design such vital 'activity' sensors.

Finally, the concepts discussed herein will extend beyond the PITPs. There are other lipid transfer proteins (for example, ceramide transfer protein; (Hanada *et al.*, 2003), the putative sterol transporter Kes1p/Osh4p and other members of the large oxysterol-binding protein family (Li *et al.*, 2002; Im *et al.*, 2005; Raychaudhuri *et al.*, 2006)) that may define additional lipid metabolic nanoreactors whose activities are

interfaced with signaling events. Finally, a highly diverse system of metabolic nanoreactors clearly demands multiple levels of higher order integration of these machines. The physical basis for regulation of cellular lipid metabolism and signaling in such microenvironments, and how the action of lipid metabolic nanoreactors is integrated at higher levels, are two important questions for the next decade.

Acknowledgments

This work was supported by grants from the US National Institutes of Health to V.A.B. K.E.I. and G.S. were also supported by a Predoctoral Training Grant from the US National Institutes of Health and a Postdoctoral Fellowship from the Deutsche Forschungsgemeinschaft, respectively.

Figures

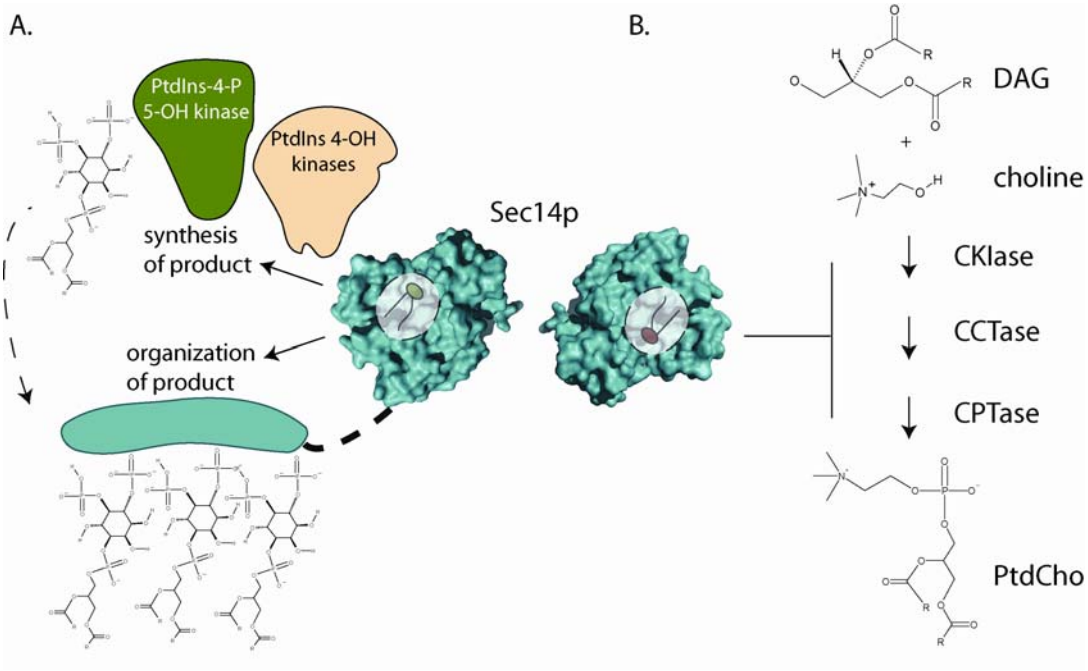

Figure 1.1 A lipid metabolic nanoreactor.

Two scenarios for Sec14p-dependent nanoreactors relevant to this discussion are shown. (**a**) Sec14p binds substrate PtdIns and channels the bound PtdIns to a metabolic enzyme (for example, PtdIns kinases), and the ultimate metabolic product (in this illustration, PtdIns(4,5)P_2) then binds another protein (or protein domain), thereby leading to a nonrandom organization of the product. (**b**) Sec14p binds PtdCho and is thereby programmed to regulate a specific phospholipid metabolic pathway (in this case the cytidine diphosphocholine pathway for PtdCho biosynthesis that involves the sequential activity of a choline kinase (CKIase), a choline-phosphate cytidylyltransferase (CCTase) and a cholinephosphotransferase (CPTase)). The lipid compositional consequences of the Sec14p-dependent regulation in that nanoreactor are transmitted to the action of lipid-responsive proteins. DAG, diacylglycerol.

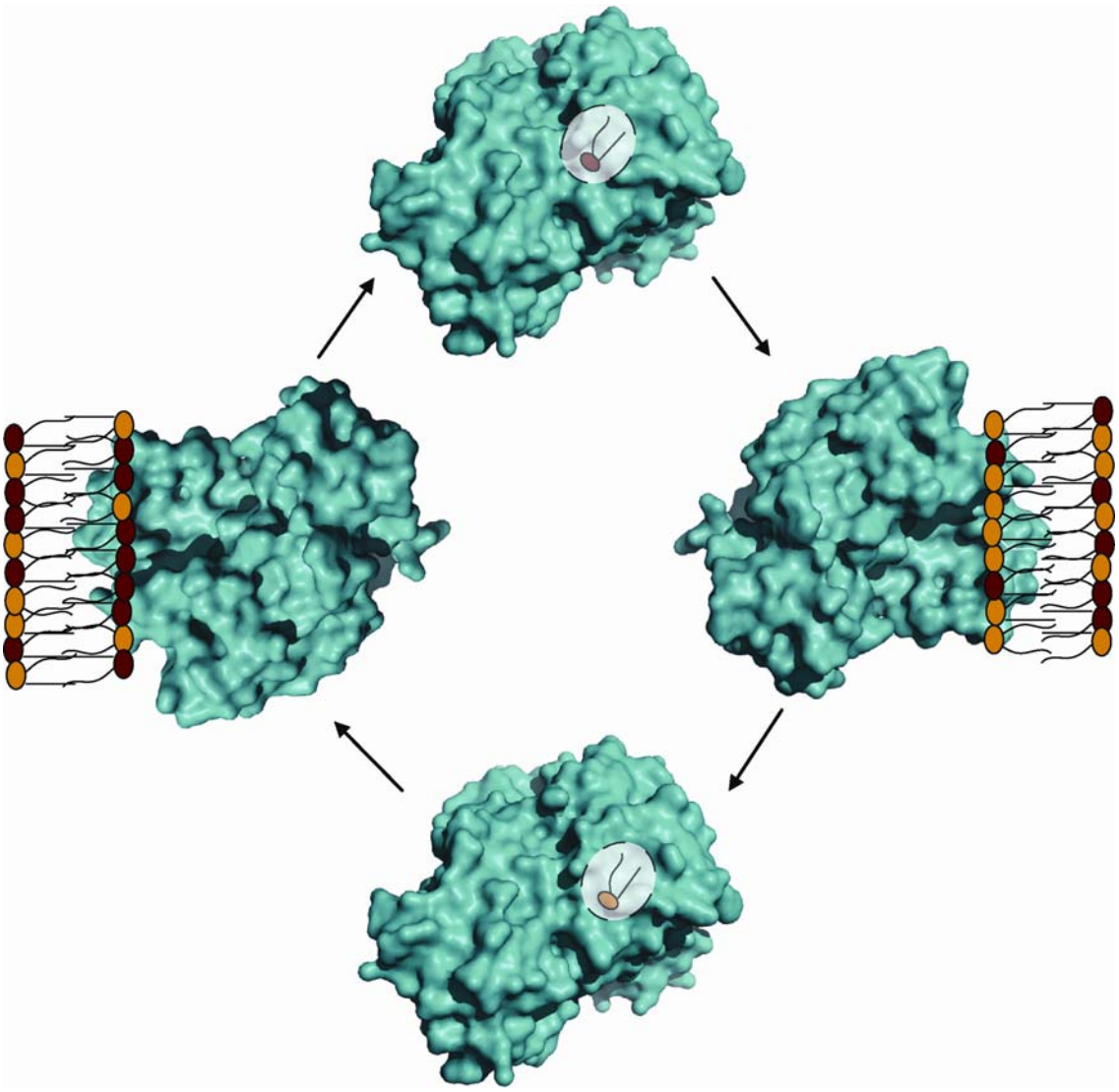

Figure 1.2: Phospholipid transfer reaction.

A cycle for PITP-mediated phospholipid exchange is shown. This reaction proceeds down a concentration gradient *in vitro*.

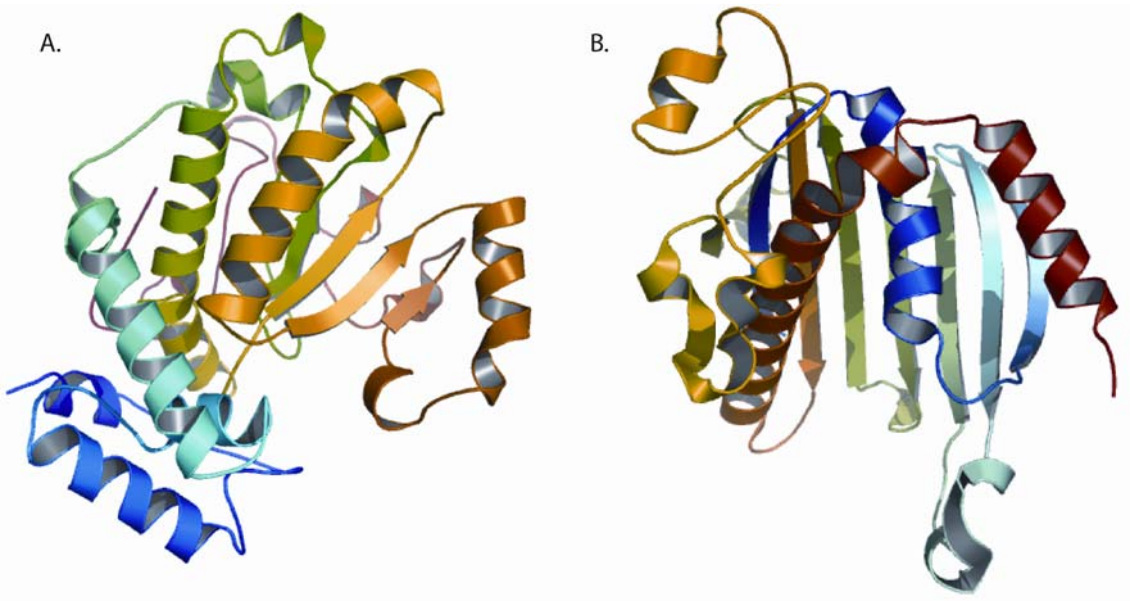

Figure 1.3: PITP crystal structures.

(**a,b**) Three-dimensional structures of apo forms of yeast Sec14p (**a**) and mammalian PITPα (**b**). The apo-Sec14p fold consists of twelve α-helices, six β-strands and eight 3_{10}-helices (bound detergent not shown). PITPα is a START-domain protein, and the fold consists of seven α-helices and eight β-sheets.

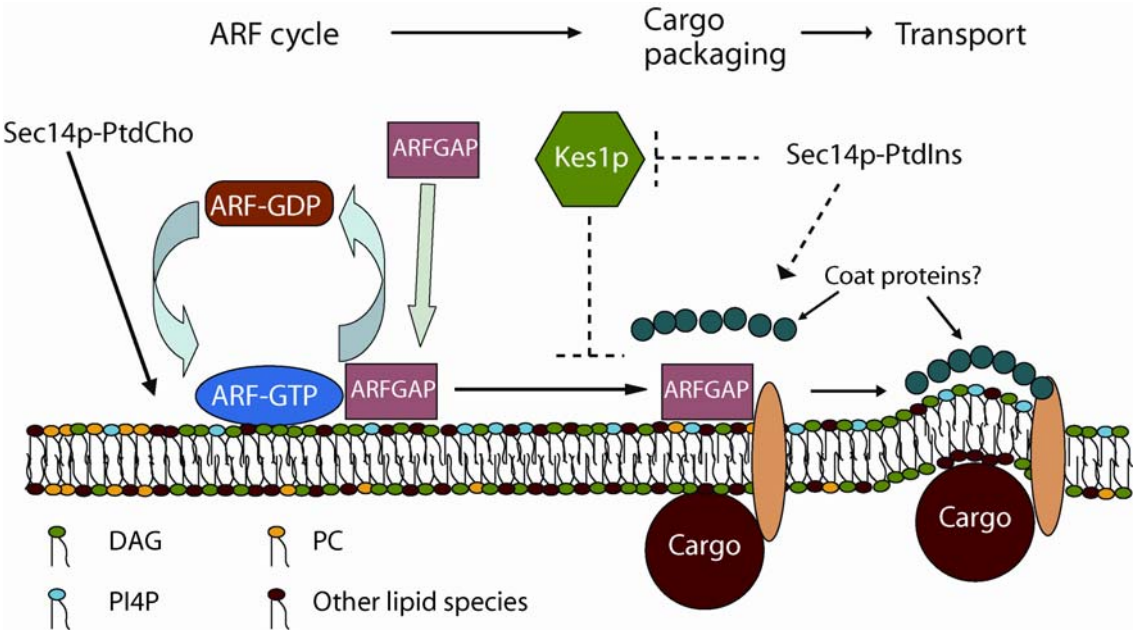

Figure 1.4: The proposed Sec14p nanoreactor.

Sec14p bound to PtdCho downregulates PtdCho biosynthesis to generate a DAG-rich, PtdCho-poor membrane domain that is conducive to the recruitment and activation of specific ArfGAPs. Genetic and biochemical data indicate that the relevant ArfGAPs are activated by DAG and inhibited by PtdCho (Yanagisawa *et al.*, 2002). These ArfGAPs potentiate later steps in secretory cargo packaging and vesicle biogenesis on TGN membranes (Lewis *et al.*, 2004; Lee *et al.*, 2005; Robinson *et al.*, 2006). The PtdIns-bound form of Sec14p independently potentiates a distinct step in the vesicle biogenesis pathway by promoting synthesis of a PtdIns(4)phosphate (PI4P) pool that regulates downstream effector proteins (perhaps the PIP and sterol-binding protein Kes1p/Osh4p, whose action is antagonistic to TGN vesicle biogenesis). PC, phosphatidylcholine.

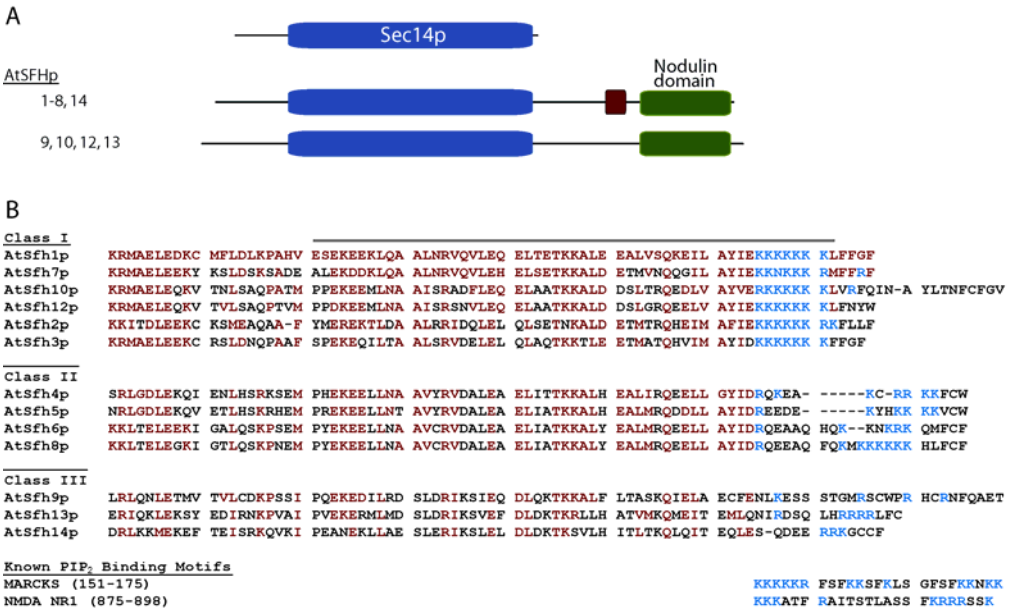

Figure 1.5: The Sec14-nodulin PITP family in *A. thaliana*.

(**a**) Schematic of the two general domain arrangements of the 13 *A. thaliana* Sec14-nodulin proteins. The Sec14p (blue), nodulin (green) and hydrophobic (red) domains are shown. Members of the family that conform to each arrangement are identified at left. (**b**) Shown is an alignment of the C-terminal half of each of 13 *A. thaliana* nodulin domains of Sec14-nodulin proteins. These nodulin domains are grouped into three classes on the basis of sequence similarity. Conserved residues are highlighted in red and basic residues in the extreme C termini of these proteins are highlighted in blue. The bar at the top highlights sequences predicted to reside in coiled coils. For purposes of comparison, known high-affinity PtdIns(4,5)P_2 binding sites for myristoylated alanine-rich C-kinase substrate (MARCKS) protein and the NMDA (*N*-methyl-D-aspartate) receptor are shown at bottom (from ref. McLaughlin and Murray, 2005).

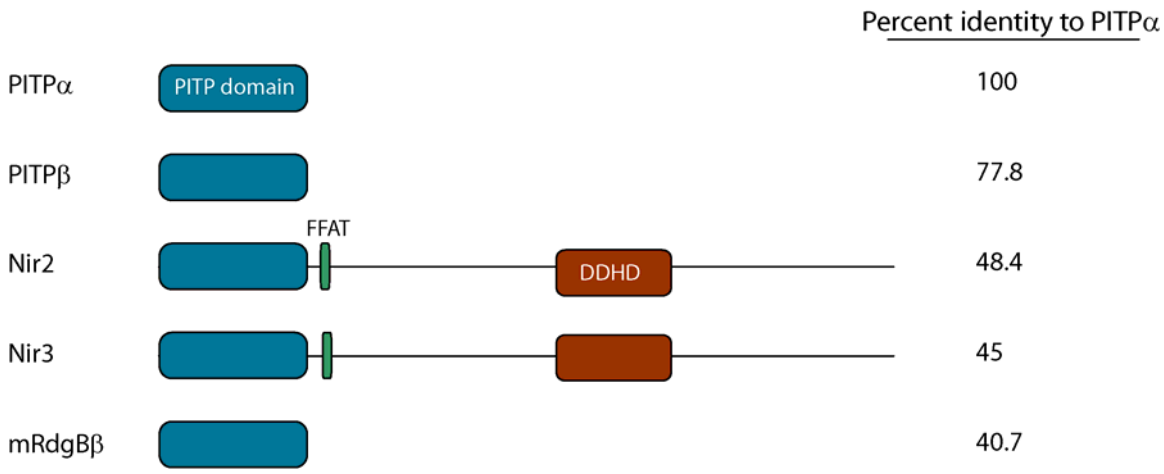

Figure 1.6: The metazoan PITP family in humans.

Schematic alignment of the five human PITPs of the metazoan PITP family. The PITP domain (blue), FFAT (green; sequence that binds an ER-localized receptor of the VAP/Scs2 family; (Loewen *et al.*, 2003) and DDHD (brown; a putative metal-binding domain) are shown. The primary sequence identities shared by each PITP domain to PITPα is given at right.

References

Alb, J.G., Jr., Cortese, J.D., Phillips, S.E., Albin, R.L., Nagy, T.R., Hamilton, B.A., and Bankaitis, V.A. (2003). Mice lacking phosphatidylinositol transfer protein-alpha exhibit spinocerebellar degeneration, intestinal and hepatic steatosis, and hypoglycemia. J Biol Chem *278*, 33501-33518.

Anantharaman, V., and Aravind, L. (2002). The GOLD domain, a novel protein module involved in Golgi function and secretion. Genome Biol *3*, research0023.

Bankaitis, V.A., Aitken, J.R., Cleves, A.E., and Dowhan, W. (1990). An essential role for a phospholipid transfer protein in yeast Golgi function. Nature *347*, 561-562.

Baron, C.L., and Malhotra, V. (2002). Role of diacylglycerol in PKD recruitment to the TGN and protein transport to the plasma membrane. Science *295*, 325-328.

Berridge, M.J., and Irvine, R.F. (1989). Inositol phosphates and cell signalling. Nature *341*, 197-205.

Chang, J.T., Milligan, S., Li, Y., Chew, C.E., Wiggs, J., Copeland, N.G., Jenkins, N.A., Campochiaro, P.A., Hyde, D.R., and Zack, D.J. (1997). Mammalian homolog of Drosophila retinal degeneration B rescues the mutant fly phenotype. J Neurosci *17*, 5881-5890.

Cheng, L., Rossman, K.L., Mahon, G.M., Worthylake, D.K., Korus, M., Sondek, J., and Whitehead, I.P. (2002). RhoGEF specificity mutants implicate RhoA as a target for Dbs transforming activity. Mol Cell Biol *22*, 6895-6905.

Cleves, A., McGee, T., and Bankaitis, V. (1991a). Phospholipid transfer proteins: a biological debut. Trends Cell Biol *1*, 30-34.

Cleves, A.E., McGee, T.P., Whitters, E.A., Champion, K.M., Aitken, J.R., Dowhan, W., Goebl, M., and Bankaitis, V.A. (1991b). Mutations in the CDP-choline pathway for phospholipid biosynthesis bypass the requirement for an essential phospholipid transfer protein. Cell *64*, 789-800.

Cunningham, E., Tan, S.K., Swigart, P., Hsuan, J., Bankaitis, V., and Cockcroft, S. (1996). The yeast and mammalian isoforms of phosphatidylinositol transfer protein can all restore phospholipase C-mediated inositol lipid signaling in cytosol-depleted RBL-2H3 and HL-60 cells. Proc Natl Acad Sci U S A *93*, 6589-6593.

D'Angelo, I., Welti, S., Bonneau, F., and Scheffzek, K. (2006). A novel bipartite phospholipid-binding module in the neurofibromatosis type 1 protein. EMBO Rep *7*, 174-179.

De Vries, K.J., Westerman, J., Bastiaens, P.I., Jovin, T.M., Wirtz, K.W., and Snoek, G.T. (1996). Fluorescently labeled phosphatidylinositol transfer protein isoforms (alpha and beta), microinjected into fetal bovine heart endothelial cells, are targeted to distinct intracellular sites. Exp Cell Res *227*, 33-39.

Defacque, H., Bos, E., Garvalov, B., Barret, C., Roy, C., Mangeat, P., Shin, H.W., Rybin, V., and Griffiths, G. (2002). Phosphoinositides regulate membrane-dependent actin assembly by latex bead phagosomes. Mol Biol Cell *13*, 1190-1202.

Engebrecht, J. (2003). Cell signaling in yeast sporulation. Biochem Biophys Res Commun *306*, 325-328.

Exton, J.H. (1990). Signaling through phosphatidylcholine breakdown. J Biol Chem *265*, 1-4.

Furst, W., and Sandhoff, K. (1992). Activator proteins and topology of lysosomal sphingolipid catabolism. Biochim Biophys Acta *1126*, 1-16.

Gatt, M.K., and Glover, D.M. (2006). The Drosophila phosphatidylinositol transfer protein encoded by vibrator is essential to maintain cleavage-furrow ingression in cytokinesis. J Cell Sci *119*, 2225-2235.

Giansanti, M.G., Bonaccorsi, S., Kurek, R., Farkas, R.M., Dimitri, P., Fuller, M.T., and Gatti, M. (2006). The class I PITP giotto is required for Drosophila cytokinesis. Curr Biol *16*, 195-201.

Gu, M., Warshawsky, I., and Majerus, P.W. (1992). Cloning and expression of a cytosolic megakaryocyte protein-tyrosine-phosphatase with sequence homology to retinaldehyde-binding protein and yeast SEC14p. Proc Natl Acad Sci U S A *89*, 2980-2984.

Guo, S., Stolz, L.E., Lemrow, S.M., and York, J.D. (1999). SAC1-like domains of yeast SAC1, INP52, and INP53 and of human synaptojanin encode polyphosphoinositide phosphatases. J Biol Chem *274*, 12990-12995.

Hama, H., Schnieders, E.A., Thorner, J., Takemoto, J.Y., and DeWald, D.B. (1999). Direct involvement of phosphatidylinositol 4-phosphate in secretion in the yeast Saccharomyces cerevisiae. J Biol Chem *274*, 34294-34300.

Hamilton, B.A., Smith, D.J., Mueller, K.L., Kerrebrock, A.W., Bronson, R.T., van Berkel, V., Daly, M.J., Kruglyak, L., Reeve, M.P., Nemhauser, J.L., Hawkins, T.L., Rubin, E.M., and Lander, E.S. (1997). The vibrator mutation causes neurodegeneration via reduced expression of PITP alpha: positional complementation cloning and extragenic suppression. Neuron *18*, 711-722.

Hanada, K., Kumagai, K., Yasuda, S., Miura, Y., Kawano, M., Fukasawa, M., and Nishijima, M. (2003). Molecular machinery for non-vesicular trafficking of ceramide. Nature *426*, 803-809.

Hay, J.C., and Martin, T.F. (1993). Phosphatidylinositol transfer protein required for ATP-dependent priming of Ca(2+)-activated secretion. Nature *366*, 572-575.

Hinchliffe, K.A., Ciruela, A., and Irvine, R.F. (1998). PIPkins1, their substrates and their products: new functions for old enzymes. Biochim Biophys Acta *1436*, 87-104.

Holthuis, J.C., and Levine, T.P. (2005). Lipid traffic: floppy drives and a superhighway. Nat Rev Mol Cell Biol *6*, 209-220.

Hsuan, J., and Cockcroft, S. (2001). The PITP family of phosphatidylinositol transfer proteins. Genome Biol *2*, REVIEWS3011.

Hurley, J.H., and Meyer, T. (2001). Subcellular targeting by membrane lipids. Curr Opin Cell Biol *13*, 146-152.

Huynh, H., Wang, X., Li, W., Bottini, N., Williams, S., Nika, K., Ishihara, H., Godzik, A., and Mustelin, T. (2003). Homotypic secretory vesicle fusion induced by the protein tyrosine phosphatase MEG2 depends on polyphosphoinositides in T cells. J Immunol *171*, 6661-6671.

Im, Y.J., Raychaudhuri, S., Prinz, W.A., and Hurley, J.H. (2005). Structural mechanism for sterol sensing and transport by OSBP-related proteins. Nature *437*, 154-158.
Iwamoto, K., Kobayashi, S., Fukuda, R., Umeda, M., Kobayashi, T., and Ohta, A. (2004). Local exposure of phosphatidylethanolamine on the yeast plasma membrane is implicated in cell polarity. Genes Cells *9*, 891-903.

Janmey, P.A., and Lindberg, U. (2004). Cytoskeletal regulation: rich in lipids. Nat Rev Mol Cell Biol *5*, 658-666.

Jones, B., Jones, E.L., Bonney, S.A., Patel, H.N., Mensenkamp, A.R., Eichenbaum-Voline, S., Rudling, M., Myrdal, U., Annesi, G., Naik, S., Meadows, N., Quattrone, A., Islam, S.A., Naoumova, R.P., Angelin, B., Infante, R., Levy, E., Roy, C.C., Freemont, P.S., Scott, J., and Shoulders, C.C. (2003). Mutations in a Sar1 GTPase of COPII vesicles are associated with lipid absorption disorders. Nat Genet *34*, 29-31.

Jones, S.M., Alb, J.G., Jr., Phillips, S.E., Bankaitis, V.A., and Howell, K.E. (1998). A phosphatidylinositol 3-kinase and phosphatidylinositol transfer protein act synergistically in formation of constitutive transport vesicles from the trans-Golgi network. J Biol Chem *273*, 10349-10354.

Kapranov, P., Routt, S.M., Bankaitis, V.A., de Bruijn, F.J., and Szczyglowski, K. (2001). Nodule-specific regulation of phosphatidylinositol transfer protein expression in Lotus japonicus. Plant Cell *13*, 1369-1382.

Kearns, M.A., Monks, D.E., Fang, M., Rivas, M.P., Courtney, P.D., Chen, J., Prestwich, G.D., Theibert, A.B., Dewey, R.E., and Bankaitis, V.A. (1998). Novel developmentally regulated phosphoinositide binding proteins from soybean whose expression bypasses the requirement for an essential phosphatidylinositol transfer protein in yeast. Embo J *17*, 4004-4017.

Kostenko, E.V., Mahon, G.M., Cheng, L., and Whitehead, I.P. (2005). The Sec14 homology domain regulates the cellular distribution and transforming activity of the Rho-specific guanine nucleotide exchange factor Dbs. J Biol Chem *280*, 2807-2817.

Kronke, M. (1999). Biophysics of ceramide signaling: interaction with proteins and phase transition of membranes. Chem Phys Lipids *101*, 109-121.

Lee, S.Y., Yang, J.S., Hong, W., Premont, R.T., and Hsu, V.W. (2005). ARFGAP1 plays a central role in coupling COPI cargo sorting with vesicle formation. J Cell Biol *168*, 281-290.

Lemmon, M.A. (2003). Phosphoinositide recognition domains. Traffic *4*, 201-213.
Lewis, S.M., Poon, P.P., Singer, R.A., Johnston, G.C., and Spang, A. (2004). The ArfGAP Glo3 is required for the generation of COPI vesicles. Mol Biol Cell *15*, 4064-4072.

Li, X., Rivas, M.P., Fang, M., Marchena, J., Mehrotra, B., Chaudhary, A., Feng, L., Prestwich, G.D., and Bankaitis, V.A. (2002). Analysis of oxysterol binding protein homologue Kes1p function in regulation of Sec14p-dependent protein transport from the yeast Golgi complex. J Cell Biol *157*, 63-77.

Li, X., Routt, S.M., Xie, Z., Cui, X., Fang, M., Kearns, M.A., Bard, M., Kirsch, D.R., and Bankaitis, V.A. (2000). Identification of a novel family of nonclassic yeast phosphatidylinositol transfer proteins whose function modulates phospholipase D activity and Sec14p-independent cell growth. Mol Biol Cell *11*, 1989-2005.

Liljedahl, M., Maeda, Y., Colanzi, A., Ayala, I., Van Lint, J., and Malhotra, V. (2001). Protein kinase D regulates the fission of cell surface destined transport carriers from the trans-Golgi network. Cell *104*, 409-420.

Liscovitch, M., and Cantley, L.C. (1995). Signal transduction and membrane traffic: the PITP/phosphoinositide connection. Cell *81*, 659-662.

Litvak, V., Dahan, N., Ramachandran, S., Sabanay, H., and Lev, S. (2005). Maintenance of the diacylglycerol level in the Golgi apparatus by the Nir2 protein is critical for Golgi secretory function. Nat Cell Biol *7*, 225-234.

Loewen, C.J., Roy, A., and Levine, T.P. (2003). A conserved ER targeting motif in three families of lipid binding proteins and in Opi1p binds VAP. Embo J *22*, 2025-2035.

Majerus, P.W. (1992). Inositol phosphate biochemistry. Annu Rev Biochem *61*, 225-250.
Martin, T.F. (2001). PI(4,5)P(2) regulation of surface membrane traffic. Curr Opin Cell Biol *13*, 493-499.

McLaughlin, S., and Murray, D. (2005). Plasma membrane phosphoinositide organization by protein electrostatics. Nature *438*, 605-611.

Milligan, S.C., Alb, J.G., Jr., Elagina, R.B., Bankaitis, V.A., and Hyde, D.R. (1997). The phosphatidylinositol transfer protein domain of Drosophila retinal degeneration B protein is essential for photoreceptor cell survival and recovery from light stimulation. J Cell Biol *139*, 351-363.

Min, K.C., Kovall, R.A., and Hendrickson, W.A. (2003). Crystal structure of human alpha-tocopherol transfer protein bound to its ligand: implications for ataxia with vitamin E deficiency. Proc Natl Acad Sci U S A *100*, 14713-14718.

Monks, D.E., Aghoram, K., Courtney, P.D., DeWald, D.B., and Dewey, R.E. (2001). Hyperosmotic stress induces the rapid phosphorylation of a soybean phosphatidylinositol transfer protein homolog through activation of the protein kinases SPK1 and SPK2. Plant Cell *13*, 1205-1219.

Moolenaar, W.H. (1995). Lysophosphatidic acid signalling. Curr Opin Cell Biol *7*, 203-210.

Nalbant, P., Hodgson, L., Kraynov, V., Toutchkine, A., and Hahn, K.M. (2004). Activation of endogenous Cdc42 visualized in living cells. Science *305*, 1615-1619.
Nishizuka, Y. (1995). Protein kinase C and lipid signaling for sustained cellular responses. Faseb J *9*, 484-496.

Odom, A.R., Stahlberg, A., Wente, S.R., and York, J.D. (2000). A role for nuclear inositol 1,4,5-trisphosphate kinase in transcriptional control. Science *287*, 2026-2029.

Ohashi, M., Jan de Vries, K., Frank, R., Snoek, G., Bankaitis, V., Wirtz, K., and Huttner, W.B. (1995). A role for phosphatidylinositol transfer protein in secretory vesicle formation. Nature *377*, 544-547.

Panagabko, C., Morley, S., Hernandez, M., Cassolato, P., Gordon, H., Parsons, R., Manor, D., and Atkinson, J. (2003). Ligand specificity in the CRAL-TRIO protein family. Biochemistry *42*, 6467-6474.

Pettus, B.J., Chalfant, C.E., and Hannun, Y.A. (2002). Ceramide in apoptosis: an overview and current perspectives. Biochim Biophys Acta *1585*, 114-125.

Pettus, B.J., Chalfant, C.E., and Hannun, Y.A. (2004). Sphingolipids in inflammation: roles and implications. Curr Mol Med *4*, 405-418.

Phillips, S.E., Ile, K.E., Boukhelifa, M., Huijbregts, R.P., and Bankaitis, V.A. (2006a). Specific and nonspecific membrane-binding determinants cooperate in targeting phosphatidylinositol transfer protein beta-isoform to the mammalian trans-Golgi network. Mol Biol Cell *17*, 2498-2512.

Phillips, S.E., Sha, B., Topalof, L., Xie, Z., Alb, J.G., Klenchin, V.A., Swigart, P., Cockcroft, S., Martin, T.F., Luo, M., and Bankaitis, V.A. (1999). Yeast Sec14p deficient in phosphatidylinositol transfer activity is functional in vivo. Mol Cell *4*, 187-197.

Phillips, S.E., Vincent, P., Rizzieri, K.E., Schaaf, G., Bankaitis, V.A., and Gaucher, E.A. (2006b). The diverse biological functions of phosphatidylinositol transfer proteins in eukaryotes. Crit Rev Biochem Mol Biol *41*, 21-49.

Raychaudhuri, S., Im, Y.J., Hurley, J.H., and Prinz, W.A. (2006). Nonvesicular sterol movement from plasma membrane to ER requires oxysterol-binding protein-related proteins and phosphoinositides. J Cell Biol *173*, 107-119.

Rhee, S.G. (2001). Regulation of phosphoinositide-specific phospholipase C. Annu Rev Biochem *70*, 281-312.

Rivas, M.P., Kearns, B.G., Xie, Z., Guo, S., Sekar, M.C., Hosaka, K., Kagiwada, S., York, J.D., and Bankaitis, V.A. (1999). Pleiotropic alterations in lipid metabolism in yeast sac1 mutants: relationship to "bypass Sec14p" and inositol auxotrophy. Mol Biol Cell *10*, 2235-2250.

Robinson, M., Poon, P.P., Schindler, C., Murray, L.E., Kama, R., Gabriely, G., Singer, R.A., Spang, A., Johnston, G.C., and Gerst, J.E. (2006). The Gcs1 Arf-GAP mediates Snc1,2 v-SNARE retrieval to the Golgi in yeast. Mol Biol Cell *17*, 1845-1858.

Roderick, S.L., Chan, W.W., Agate, D.S., Olsen, L.R., Vetting, M.W., Rajashankar, K.R., and Cohen, D.E. (2002). Structure of human phosphatidylcholine transfer protein in complex with its ligand. Nat Struct Biol *9*, 507-511.

Rogers, D.P., and Bankaitis, V.A. (2000). Phospholipid transfer proteins and physiological functions. Int Rev Cytol *197*, 35-81.

Rossman, K.L., Worthylake, D.K., Snyder, J.T., Siderovski, D.P., Campbell, S.L., and Sondek, J. (2002). A crystallographic view of interactions between Dbs and Cdc42: PH domain-assisted guanine nucleotide exchange. Embo J *21*, 1315-1326.

Routt, S.M., Ryan, M.M., Tyeryar, K., Rizzieri, K.E., Mousley, C., Roumanie, O., Brennwald, P.J., and Bankaitis, V.A. (2005). Nonclassical PITPs activate PLD via the

Stt4p PtdIns-4-kinase and modulate function of late stages of exocytosis in vegetative yeast. Traffic *6*, 1157-1172.

Rudge, S.A., Sciorra, V.A., Iwamoto, M., Zhou, C., Strahl, T., Morris, A.J., Thorner, J., and Engebrecht, J. (2004). Roles of phosphoinositides and of Spo14p (phospholipase D)-generated phosphatidic acid during yeast sporulation. Mol Biol Cell *15*, 207-218.

Schnabl, M., Oskolkova, O.V., Holic, R., Brezna, B., Pichler, H., Zagorsek, M., Kohlwein, S.D., Paltauf, F., Daum, G., and Griac, P. (2003). Subcellular localization of yeast Sec14 homologues and their involvement in regulation of phospholipid turnover. Eur J Biochem *270*, 3133-3145.

Schouten, A., Agianian, B., Westerman, J., Kroon, J., Wirtz, K.W., and Gros, P. (2002). Structure of apo-phosphatidylinositol transfer protein alpha provides insight into membrane association. Embo J *21*, 2117-2121.

Schwille, P., Haupts, U., Maiti, S., and Webb, W.W. (1999). Molecular dynamics in living cells observed by fluorescence correlation spectroscopy with one- and two-photon excitation. Biophys J *77*, 2251-2265.

Sciorra, V.A., Rudge, S.A., Wang, J., McLaughlin, S., Engebrecht, J., and Morris, A.J. (2002). Dual role for phosphoinositides in regulation of yeast and mammalian phospholipase D enzymes. J Cell Biol *159*, 1039-1049.

Sha, B., Phillips, S.E., Bankaitis, V.A., and Luo, M. (1998). Crystal structure of the Saccharomyces cerevisiae phosphatidylinositol-transfer protein. Nature *391*, 506-510.

Shaw, G. (1996). The pleckstrin homology domain: an intriguing multifunctional protein module. Bioessays *18*, 35-46.

Simon, J.P., Morimoto, T., Bankaitis, V.A., Gottlieb, T.A., Ivanov, I.E., Adesnik, M., and Sabatini, D.D. (1998). An essential role for the phosphatidylinositol transfer protein in the scission of coatomer-coated vesicles from the trans-Golgi network. Proc Natl Acad Sci U S A *95*, 11181-11186.

Simonsen, A., Wurmser, A.E., Emr, S.D., and Stenmark, H. (2001). The role of phosphoinositides in membrane transport. Curr Opin Cell Biol *13*, 485-492.

Singer, W.D., Brown, H.A., and Sternweis, P.C. (1997). Regulation of eukaryotic phosphatidylinositol-specific phospholipase C and phospholipase D. Annu Rev Biochem *66*, 475-509.

Sirokmany, G., Szidonya, L., Kaldi, K., Gaborik, Z., Ligeti, E., and Geiszt, M. (2006). Sec14 homology domain targets p50RhoGAP to endosomes and provides a link between Rab and Rho GTPases. J Biol Chem *281*, 6096-6105.

Skinner, H.B., Alb, J.G., Jr., Whitters, E.A., Helmkamp, G.M., Jr., and Bankaitis, V.A. (1993). Phospholipid transfer activity is relevant to but not sufficient for the essential function of the yeast SEC14 gene product. Embo J *12*, 4775-4784.

Spiegel, S., and Milstien, S. (2003). Sphingosine-1-phosphate: an enigmatic signalling lipid. Nat Rev Mol Cell Biol *4*, 397-407.

Sreenivas, A., Patton-Vogt, J.L., Bruno, V., Griac, P., and Henry, S.A. (1998). A role for phospholipase D (Pld1p) in growth, secretion, and regulation of membrane lipid synthesis in yeast. J Biol Chem *273*, 16635-16638.

Stahelin, R.V., Rafter, J.D., Das, S., and Cho, W. (2003). The molecular basis of differential subcellular localization of C2 domains of protein kinase C-alpha and group IVa cytosolic phospholipase A2. J Biol Chem *278*, 12452-12460.

Stocker, A., Tomizaki, T., Schulze-Briese, C., and Baumann, U. (2002). Crystal structure of the human supernatant protein factor. Structure *10*, 1533-1540.

Suh, B.C., and Hille, B. (2005). Regulation of ion channels by phosphatidylinositol 4,5-bisphosphate. Curr Opin Neurobiol *15*, 370-378.

Tilley, S.J., Skippen, A., Murray-Rust, J., Swigart, P.M., Stewart, A., Morgan, C.P., Cockcroft, S., and McDonald, N.Q. (2004). Structure-function analysis of human [corrected] phosphatidylinositol transfer protein alpha bound to phosphatidylinositol. Structure *12*, 317-326.

van Meer, G. (2005). Cellular lipidomics. Embo J *24*, 3159-3165.

Vincent, P., Chua, M., Nogue, F., Fairbrother, A., Mekeel, H., Xu, Y., Allen, N., Bibikova, T.N., Gilroy, S., and Bankaitis, V.A. (2005). A Sec14p-nodulin domain phosphatidylinositol transfer protein polarizes membrane growth of Arabidopsis thaliana root hairs. J Cell Biol *168*, 801-812.

Weimar, W.R., Lane, P.W., and Sidman, R.L. (1982). Vibrator (vb): a spinocerebellar system degeneration with autosomal recessive inheritance in mice. Brain Res *251*, 357-364.

Wenk, M.R., and De Camilli, P. (2004). Protein-lipid interactions and phosphoinositide metabolism in membrane traffic: insights from vesicle recycling in nerve terminals. Proc Natl Acad Sci U S A *101*, 8262-8269.

Whitehead, I.P., Campbell, S., Rossman, K.L., and Der, C.J. (1997). Dbl family proteins. Biochim Biophys Acta *1332*, F1-23.

Wirtz, K.W. (1997). Phospholipid transfer proteins revisited. Biochem J *324 (Pt 2)*, 353-360.

Wu, W.I., Routt, S., Bankaitis, V.A., and Voelker, D.R. (2000). A new gene involved in the transport-dependent metabolism of phosphatidylserine, PSTB2/PDR17, shares sequence similarity with the gene encoding the phosphatidylinositol/phosphatidylcholine transfer protein, SEC14. J Biol Chem *275*, 14446-14456.

Wu, W.I., and Voelker, D.R. (2002). Biochemistry and genetics of interorganelle aminoglycerophospholipid transport. Semin Cell Dev Biol *13*, 185-195.

Wu, W.I., and Voelker, D.R. (2004). Reconstitution of phosphatidylserine transport from chemically defined donor membranes to phosphatidylserine decarboxylase 2 implicates specific lipid domains in the process. J Biol Chem *279*, 6635-6642.

Xie, Y., Ding, Y.Q., Hong, Y., Feng, Z., Navarre, S., Xi, C.X., Zhu, X.J., Wang, C.L., Ackerman, S.L., Kozlowski, D., Mei, L., and Xiong, W.C. (2005). Phosphatidylinositol transfer protein-alpha in netrin-1-induced PLC signalling and neurite outgrowth. Nat Cell Biol *7*, 1124-1132.

Xie, Z., Fang, M., and Bankaitis, V.A. (2001). Evidence for an intrinsic toxicity of phosphatidylcholine to Sec14p-dependent protein transport from the yeast Golgi complex. Mol Biol Cell *12*, 1117-1129.

Xie, Z., Fang, M., Rivas, M.P., Faulkner, A.J., Sternweis, P.C., Engebrecht, J.A., and Bankaitis, V.A. (1998). Phospholipase D activity is required for suppression of yeast phosphatidylinositol transfer protein defects. Proc Natl Acad Sci U S A *95*, 12346-12351.

Yamniuk, A.P., and Vogel, H.J. (2004). Calmodulin's flexibility allows for promiscuity in its interactions with target proteins and peptides. Mol Biotechnol *27*, 33-57.

Yanagisawa, L.L., Marchena, J., Xie, Z., Li, X., Poon, P.P., Singer, R.A., Johnston, G.C., Randazzo, P.A., and Bankaitis, V.A. (2002). Activity of specific lipid-regulated ADP ribosylation factor-GTPase-activating proteins is required for Sec14p-dependent Golgi secretory function in yeast. Mol Biol Cell *13*, 2193-2206.

Yoder, M.D., Thomas, L.M., Tremblay, J.M., Oliver, R.L., Yarbrough, L.R., and Helmkamp, G.M., Jr. (2001). Structure of a multifunctional protein. Mammalian phosphatidylinositol transfer protein complexed with phosphatidylcholine. J Biol Chem *276*, 9246-9252.

York, J.D., Odom, A.R., Murphy, R., Ives, E.B., and Wente, S.R. (1999). A phospholipase C-dependent inositol polyphosphate kinase pathway required for efficient messenger RNA export. Science *285*, 96-100.

Chapter 1b

The PITP proteins

The PITP superfamily of proteins is defined by the ability of the proteins to transfer lipids between membranes *in vitro*. Within the superfamily, there are two subfamilies that share the same biochemical activity, but do not have any sequence or structural similarity. These families are called the Sec14 PITP family, named for the founding yeast PITP, and the Class I or Metazoan PITPs. In many cases, there are more Sec14 family proteins in a given organism than PITP members. The most striking case is Drosophila, where there are 15 Sec14 family members and just three metazoan PITPs (Phillips et al, 2006). The reason for the many family members in the Sec14 family may be related to the ability of these proteins to bind to different lipids (such as the α-tocopherol transfer proteins), and the fact that Sec14 domains are often found in association with other domains such as the GOLD or nodulin domains. The PITP family, which is the focus of my thesis, and thus this review, is a smaller family with members that are often essential for survival.

Sec14

While Sec14 is not related to the PITPs in structure or sequence, the functional interchangability of these molecules suggests that Sec14 is still a relevant model for PITP function.

The first clues to Sec14 function came from finding mutations in yeast genes that allowed yeast to grow despite a non-functional Sec14 molecule (known as bypass mutations). Seven molecules were found that fell into three groups. The first group of

bypass mutations inactivated the phosphatidylcholine biosynthesis pathway, suggesting a role for Sec14 in downregulating PtdCho levels, while keeping DAG levels high (Cleves *et al.*, 1991; McGee *et al.*, 1994a; McGee *et al.*, 1994b; Skinner *et al.*, 1995; Xie *et al.*, 2001). The second bypass mutation allowing growth in the absence of Sec14 is Sac1, a PtdIns (4)P phosphatase (Cleves *et al.*, 1989). The inactivation of Sac1 is believed to increase PtdIns (4)P levels, and compensate for the wild type Sec14 function of maintaining PtdIns (4)P levels. The final and least well understood bypass mutation is in Kes1 (Fang *et al.*, 1996), a member of the oxysterol binding protein (OSBP) family. Deletion of Kes1 can restore viability to a strain with a temperature sensitive mutation in the yeast kinase pik1, suggesting that the deletion of Kes1 "frees up" PtdIns-4P molecules (Li *et al.*, 2002).

Together, the bypass mutant data demonstrate a role for Sec14 in regulation of two lipid pathways: PtdIns to PtdIns-4P and PtdCho/DAG. In the PtdCho/DAG pathway, Sec14 maintains high levels of the pro-secretory lipid DAG through preventing its consumption in synthesis of PtdCho, which is itself inhibitory towards secretion. Sec14p increases the levels of PtdIns-4P in the TGN, though the mechanism is not clear from the genetic data.

Recent work provided clues to a molecular mechanism by which Sec14 could work. Crystal structures of the closely related Sfh1 protein revealed overlapping, but distinct binding sites for PtdIns and PtdCho. Subsequent mutagenesis of Sec14p revealed that the binding sites were conserved. Surprisingly, Sec14 required both PtdIns and PtdCho binding sites in the same molecule in order to function. Thus, the regulation of PtdCho/DAG and PtdIns are not distinct functions, but rather are related, leading to the

current model that as a heterotypic exchange reaction occurs, lipids are presented to modifying enzymes (Schaaf *et al.*, 2008).

The Sec14 model demonstrates a mechanism of action that could be universal for PITP molecules. However, it is also important to emphasize that there are distinctions between the Sec14 and PITP classes of proteins. PITPs bind lipid with the headgroup buried within the molecule, unlike Sec14p (discussed in more detail below). In addition, it is known that the PtdIns and PtdCho lipid headgroups bind in the same pocket of PITPs, rather than in distinct sites, as seen in Sec14/Sfh1. To better understand the unique features of PITPs, I'll discuss what is known about the structure and function of these molecules.

Structural Insights into PITP function

The solved crystal structures for PITPα in the apo-, PI- and PC-bound forms, along with a PC-bound form of PITPβ, have given a clear picture of how mammalian PITPs bind lipids (Oliver *et al.*, 1999; Yoder *et al.*, 2001; Schouten *et al.*, 2002; Tilley *et al.*, 2004; Vordtriede *et al.*, 2005). The PITP molecules are constructed of a lipid-binding core consisting of an 8-stranded β sheet, and 6 alpha-helices. In contrast to Sec14p, the lipid headgroup is buried within the pocket with the acyl chains facing the membrane binding site (Oliver *et al.*, 1999; Yoder *et al.*, 2001). Genetic studies showed a role for the T59 residue in PI transfer, and the crystal structure made clear why this residue was important (Alb *et al.*, 1995; Yoder *et al.*, 2001). The T59 residue is located within the binding pocket and forms a hydrogen bond with PtdIns. In addition to the T59 residue, residues K61 and N90 were also identified from the crystal structure and confirmed by binding and transfer assays to be essential for PtdIns binding/transfer (Tilley *et al.*, 2004).

The crystal structure of the PITPs indicated surprisingly few differences between PITP species or lipid bound forms. The closed form of the protein is the same when it is bound to PI or PC, dispelling previous predictions that PITPα would have different binding partners depending on which lipid is bound. As predicted by their high sequence similarity, PITPβ bound to PC is almost identical to lipid-bound PITPα (Tilley *et al.*, 2004).

The C-terminal tail of the PITPs is shown in this work (Chapter 2) and others to be of key importance. The C-terminal tail displays increased movement and increased trypsin sensitivity in the presences of vesicles. When the C-terminal tail is deleted, the protein displays conformational changes, increased membrane binding, and decreased transfer ability. (Tremblay *et al.*, 1996; Voziyan *et al.*, 1996; Tremblay *et al.*, 2005). Together, these data indicate that the C-terminal is both sensitive to and responsible for the membrane bound status of the protein, and the C-terminal tail is critical for function.

PITP biochemistry

Early clues to the function of PITPs came from *in vitro* experiments using permeabilized cells. These experiments showed a role for PITPs in a wide variety of signaling and secretion pathways. In particular, PITPs were shown to restore activity of PLC-β and PLC-γ isoforms in response to various stimuli(Thomas *et al.*, 1993; Cunningham *et al.*, 1995; Kauffmann-Zeh *et al.*, 1995; Cunningham *et al.*, 1996; Currie *et al.*, 1997). Additionally, PITPs supported both constitutive secretion in neuroendocrine and HL60 cells and regulated secretion in PC12 cells and mast cells (Hay and Martin, 1993; Ohashi *et al.*, 1995; Fensome *et al.*, 1996; Jones *et al.*, 1998; Simon *et al.*, 1998). The requirement for PITPs in these experiments is not specific; when tested,

the yeast PITP (Sec14p) could restore activity at levels comparable to either of the mammalian isoforms (Hay and Martin, 1993; Ohashi *et al.*, 1995; Cunningham *et al.*, 1996).

That the common role of PITP in the *in vitro* studies was PI transfer/presentation, was indicated by several lines of evidence: i) the non-specific PITP requirement in *in vitro* assays suggests that the necessary activity is a biochemical one, not a protein-protein interaction. ii) Some studies show an increase in cellular PtdIns-4P or PtdInsP2 when PITPs are present and several secretion assays require a PI-kinase as an additional factor, suggesting that PITP presents PI to the kinase (Cunningham *et al.*, 1995; Hay *et al.*, 1995; Kauffmann-Zeh *et al.*, 1995; Fensome *et al.*, 1996; Jones *et al.*, 1998). iii) Kinetics suggest that in some cases, PITP is not required for initial phases of PLC activation, but rather for extended signaling, which is consistent with a role in providing PI once PI on the membrane has been used up (Currie *et al.*, 1997) .

The notion of PITPs as PtdIns presenting molecules, suggested by permeabilized cell studies, is consistent with what is known about Sec14. For a true understanding of how these molecules work, however, they must be considered in the context of intact cells and animals. Studies of several PITP family members in animals displayed a range of functions for these molecules.

In vivo Function of Metazoan PITPs

Metazoan PITPs have been found in Dictyostelium, C. elegans, Drosophila, and mammals, however *in vivo* studies have focused mainly on Drosophila and mammalian isoforms. These PITPs can be divided into two groups based on homology: the RdgB subfamily and the soluble PITP subfamily.

Some of the soluble PITPs have well characterized roles. The *Drosophila* RdgB isoform RdgBα (or RdgB) is involved in phototransduction light response in flies; in the absence of RdgB, flies have an initial response to light, but this response cannot be terminated and the photoreceptor cells degenerate. The PITP domain of RdgB is essential in this process: the PITP domain alone can rescue the loss of RdgB (Milligan *et al.*, 1997).

Another well characterized RdgB isoform is the mammalian protein RdgB1 (Nir2). Nir2 is a multidomain protein is required for embryogenesis with roles in lipid homeostasis of the Golgi and in cytokinesis (Lu *et al.*, 2001; Litvak *et al.*, 2004). The role of Nir2 in cytokinesis is related to its Rho inhibitory domain (Rid), and there is no evidence for a role of the PITP domain in regulation of cytokinesis. A clear role for the Nir2 PITP domain, however, was demonstrated in Golgi lipid dynamics. Like Sec14p yeast mutants, knockdown of Nir2 causes Golgi dysmorphology and a decrease in diacylglycerol (DAG) due to upregulation of the CDP-choline pathway (Litvak *et al.*, 2005). These defects cannot be rescued by Nir2 with a PI binding site mutant.

Soluble PITP family

Within the soluble PITP family, a *Drosophila* and a mouse protein provide two different examples of how soluble PITPs can function. *Drosophila* have one soluble PITP family member, which shares 59% and 61% identity with mammalian PITPα and PITPβ respectively, and this protein (called *vibrator* or *giotto*) is critical for cytokinesis during spermatid meiosis and neuroblast mitosis (Gatt and Glover, 2006; Giansanti *et al.*, 2006). In *vib*-null cells, spindle and contractile ring form normally, but do not fully constrict, which is proposed to be because Golgi-like vesicles don't reach the cell poles.

Consistent with a role in cytokinesis, P-element insertions in the *vib* gene are lethal as early as larvae second instar(Gatt and Glover, 2006; Giansanti *et al.*, 2006).

There are two mammalian soluble PITPs: PITPα and PITPβ. As discussed above, *in vitro* studies indicated an interchangable role for these proteins in presenting PI for modification and in promoting signaling or vesicle budding reactions. Cell culture and *in vivo* studies, however, indicate distinct cellular roles for these proteins. PITPα-null ES cells have no defects in cell survival, nor is there a difference in lipid levels, secretion, endocytosis, or growth (Alb *et al.*, 2002).

Reduction of PITPα levels does result in profound effects on the organism. In the *vibrator* mouse, where PITPα levels are decreased 5-fold, mice are viable but exhibit whole body tremors and die 30 days after birth (Hamilton *et al.*, 1997; Alb *et al.*, 2003). The complete ablation of PITPα leads to hypoglycemia, intestine and liver steatosis, and neurodegeneration. While all of the phenotypes seen in PITPα knockout mice can be rescued by a construct expressing wild type PITPα, expression of a T59D construct (the PtdIns binding mutant) rescues none of the phenotypes (Alb *et al.*, 2007). This indicates a clear importance for PtdIns binding in PITPα activity, though the molecular mechanism of action is not yet known.

One role of PITPα in the brain seems to be in neurite outgrowth. PITPα is reported to interact via its C-terminal tail with the netrin receptors DCC and neogenin, and this netrin-1 induced interaction stimulates PITPα PtdIns transfer ability and PIP2 hydrolysis. In vibrator mouse neurons, the PIP2 hydrolysis response is completely abolished and neurite outgrowth from cortical explants is diminished (Xie *et al.*, 2005). While studies in our lab have not been able to replicate the PITPα interaction with DCC,

axonal guidance is strongly defective in PITPα knockout mice (Malika Boukhelifa, unpublished data).

In vivo studies of PITPβ are hampered by the fact that PITPβ-null cells cannot be obtained, which suggests that PITPβ is an essential housekeeping protein. Despite the clear importance of PITPβ, little is known about its function.

My dissertation focuses on the in vivo role of PITPβ in mammals and zebrafish. We demonstrate that PITPβ localizes to the TGN, and identify regions of the protein that contribute to the localization. PITPβ is not localized to the Golgi by a single region of the protein; several regions are necessary for correct localization. I then examined the effects of loss of PITPβ expression in human cell lines and zebrafish. In mammalian cells, PITPβ is required for survival, and its loss leads to abnormal Golgi formation and decreased secretion kinetics. PITPs in zebrafish demonstrate completely different roles than their mammalian counterparts. PITPβ is not an essential gene for embryonic development in zebrafish. Instead, it proves to be essential for the normal formation of the outer cone cells of the retina. A novel zebrafish PITP, termed PITPγ, is identified and its function is so far unclear. PITPα, however, is essential for early development, unlike its mammalian counterpart. Together, this thesis demonstrates the range of functions performed by PITPs in eukaryotes.

References

Alb, J.G., Jr., Cortese, J.D., Phillips, S.E., Albin, R.L., Nagy, T.R., Hamilton, B.A., and Bankaitis, V.A. (2003). Mice lacking phosphatidylinositol transfer protein-alpha exhibit spinocerebellar degeneration, intestinal and hepatic steatosis, and hypoglycemia. J Biol Chem *278*, 33501-33518.

Alb, J.G., Jr., Gedvilaite, A., Cartee, R.T., Skinner, H.B., and Bankaitis, V.A. (1995). Mutant rat phosphatidylinositol/phosphatidylcholine transfer proteins specifically defective in phosphatidylinositol transfer: implications for the regulation of phospholipid transfer activity. Proc Natl Acad Sci U S A *92*, 8826-8830.

Alb, J.G., Jr., Phillips, S.E., Rostand, K., Cui, X., Pinxteren, J., Cotlin, L., Manning, T., Guo, S., York, J.D., Sontheimer, H., Collawn, J.F., and Bankaitis, V.A. (2002). Genetic ablation of phosphatidylinositol transfer protein function in murine embryonic stem cells. Mol Biol Cell *13*, 739-754.

Alb, J.G., Jr., Phillips, S.E., Wilfley, L.R., Philpot, B.D., and Bankaitis, V.A. (2007). The pathologies associated with functional titration of phosphatidylinositol transfer protein alpha activity in mice. J Lipid Res *48*, 1857-1872.

Cleves, A.E., McGee, T.P., Whitters, E.A., Champion, K.M., Aitken, J.R., Dowhan, W., Goebl, M., and Bankaitis, V.A. (1991). Mutations in the CDP-choline pathway for phospholipid biosynthesis bypass the requirement for an essential phospholipid transfer protein. Cell *64*, 789-800.

Cleves, A.E., Novick, P.J., and Bankaitis, V.A. (1989). Mutations in the SAC1 gene suppress defects in yeast Golgi and yeast actin function. J Cell Biol *109*, 2939-2950.

Cunningham, E., Tan, S.K., Swigart, P., Hsuan, J., Bankaitis, V., and Cockcroft, S. (1996). The yeast and mammalian isoforms of phosphatidylinositol transfer protein can all restore phospholipase C-mediated inositol lipid signaling in cytosol-depleted RBL-2H3 and HL-60 cells. Proc Natl Acad Sci U S A *93*, 6589-6593.

Cunningham, E., Thomas, G.M., Ball, A., Hiles, I., and Cockcroft, S. (1995). Phosphatidylinositol transfer protein dictates the rate of inositol trisphosphate production by promoting the synthesis of PIP2. Curr Biol *5*, 775-783.

Currie, R.A., MacLeod, B.M., and Downes, C.P. (1997). The lipid transfer activity of phosphatidylinositol transfer protein is sufficient to account for enhanced phospholipase C activity in turkey erythrocyte ghosts. Curr Biol *7*, 184-190.

Fang, M., Kearns, B.G., Gedvilaite, A., Kagiwada, S., Kearns, M., Fung, M.K., and Bankaitis, V.A. (1996). Kes1p shares homology with human oxysterol binding protein and participates in a novel regulatory pathway for yeast Golgi-derived transport vesicle biogenesis. Embo J *15*, 6447-6459.

Fensome, A., Cunningham, E., Prosser, S., Tan, S.K., Swigart, P., Thomas, G., Hsuan, J., and Cockcroft, S. (1996). ARF and PITP restore GTP gamma S-stimulated protein secretion from cytosol-depleted HL60 cells by promoting PIP2 synthesis. Curr Biol *6*, 730-738.

Gatt, M.K., and Glover, D.M. (2006). The Drosophila phosphatidylinositol transfer protein encoded by vibrator is essential to maintain cleavage-furrow ingression in cytokinesis. J Cell Sci *119*, 2225-2235.

Giansanti, M.G., Bonaccorsi, S., Kurek, R., Farkas, R.M., Dimitri, P., Fuller, M.T., and Gatti, M. (2006). The class I PITP giotto is required for Drosophila cytokinesis. Curr Biol *16*, 195-201.

Hamilton, B.A., Smith, D.J., Mueller, K.L., Kerrebrock, A.W., Bronson, R.T., van Berkel, V., Daly, M.J., Kruglyak, L., Reeve, M.P., Nemhauser, J.L., Hawkins, T.L., Rubin, E.M., and Lander, E.S. (1997). The vibrator mutation causes neurodegeneration via reduced expression of PITP alpha: positional complementation cloning and extragenic suppression. Neuron *18*, 711-722.

Hay, J.C., Fisette, P.L., Jenkins, G.H., Fukami, K., Takenawa, T., Anderson, R.A., and Martin, T.F. (1995). ATP-dependent inositide phosphorylation required for Ca(2+)-activated secretion. Nature *374*, 173-177.

Hay, J.C., and Martin, T.F. (1993). Phosphatidylinositol transfer protein required for ATP-dependent priming of Ca(2+)-activated secretion. Nature *366*, 572-575.

Jones, S.M., Alb, J.G., Jr., Phillips, S.E., Bankaitis, V.A., and Howell, K.E. (1998). A phosphatidylinositol 3-kinase and phosphatidylinositol transfer protein act synergistically in formation of constitutive transport vesicles from the trans-Golgi network. J Biol Chem *273*, 10349-10354.

Kauffmann-Zeh, A., Thomas, G.M., Ball, A., Prosser, S., Cunningham, E., Cockcroft, S., and Hsuan, J.J. (1995). Requirement for phosphatidylinositol transfer protein in epidermal growth factor signaling. Science *268*, 1188-1190.

Li, X., Rivas, M.P., Fang, M., Marchena, J., Mehrotra, B., Chaudhary, A., Feng, L., Prestwich, G.D., and Bankaitis, V.A. (2002). Analysis of oxysterol binding protein homologue Kes1p function in regulation of Sec14p-dependent protein transport from the yeast Golgi complex. J Cell Biol *157*, 63-77.

Litvak, V., Argov, R., Dahan, N., Ramachandran, S., Amarilio, R., Shainskaya, A., and Lev, S. (2004). Mitotic phosphorylation of the peripheral Golgi protein Nir2 by Cdk1 provides a docking mechanism for Plk1 and affects cytokinesis completion. Mol Cell *14*, 319-330.

Litvak, V., Dahan, N., Ramachandran, S., Sabanay, H., and Lev, S. (2005). Maintenance of the diacylglycerol level in the Golgi apparatus by the Nir2 protein is critical for Golgi secretory function. Nat Cell Biol *7*, 225-234.

Lu, C., Peng, Y.W., Shang, J., Pawlyk, B.S., Yu, F., and Li, T. (2001). The mammalian retinal degeneration B2 gene is not required for photoreceptor function and survival. Neuroscience *107*, 35-41.

McGee, T.P., Skinner, H.B., and Bankaitis, V.A. (1994a). Functional redundancy of CDP-ethanolamine and CDP-choline pathway enzymes in phospholipid biosynthesis: ethanolamine-dependent effects on steady-state membrane phospholipid composition in Saccharomyces cerevisiae. J Bacteriol *176*, 6861-6868.

McGee, T.P., Skinner, H.B., Whitters, E.A., Henry, S.A., and Bankaitis, V.A. (1994b). A phosphatidylinositol transfer protein controls the phosphatidylcholine content of yeast Golgi membranes. J Cell Biol *124*, 273-287.

Milligan, S.C., Alb, J.G., Jr., Elagina, R.B., Bankaitis, V.A., and Hyde, D.R. (1997). The phosphatidylinositol transfer protein domain of Drosophila retinal degeneration B protein is essential for photoreceptor cell survival and recovery from light stimulation. J Cell Biol *139*, 351-363.

Ohashi, M., Jan de Vries, K., Frank, R., Snoek, G., Bankaitis, V., Wirtz, K., and Huttner, W.B. (1995). A role for phosphatidylinositol transfer protein in secretory vesicle formation. Nature *377*, 544-547.

Oliver, R.L., Tremblay, J.M., Helmkamp, G.M., Jr., Yarbrough, L.R., Breakfield, N.W., and Yoder, M.D. (1999). X-ray analysis of crystals of rat phosphatidylinositol-transfer protein with bound phosphatidylcholine. Acta Crystallogr D Biol Crystallogr *55*, 522-524.

Schaaf, G., Ortlund, E.A., Tyeryar, K.R., Mousley, C.J., Ile, K.E., Garrett, T.A., Ren, J., Woolls, M.J., Raetz, C.R., Redinbo, M.R., and Bankaitis, V.A. (2008). Functional anatomy of phospholipid binding and regulation of phosphoinositide homeostasis by proteins of the sec14 superfamily. Mol Cell *29*, 191-206.

Schouten, A., Agianian, B., Westerman, J., Kroon, J., Wirtz, K.W., and Gros, P. (2002). Structure of apo-phosphatidylinositol transfer protein alpha provides insight into membrane association. Embo J *21*, 2117-2121.

Simon, J.P., Morimoto, T., Bankaitis, V.A., Gottlieb, T.A., Ivanov, I.E., Adesnik, M., and Sabatini, D.D. (1998). An essential role for the phosphatidylinositol transfer protein in the scission of coatomer-coated vesicles from the trans-Golgi network. Proc Natl Acad Sci U S A *95*, 11181-11186.

Skinner, H.B., McGee, T.P., McMaster, C.R., Fry, M.R., Bell, R.M., and Bankaitis, V.A. (1995). The Saccharomyces cerevisiae phosphatidylinositol-transfer protein effects a

ligand-dependent inhibition of choline-phosphate cytidylyltransferase activity. Proc Natl Acad Sci U S A *92*, 112-116.

Thomas, G.M., Cunningham, E., Fensome, A., Ball, A., Totty, N.F., Truong, O., Hsuan, J.J., and Cockcroft, S. (1993). An essential role for phosphatidylinositol transfer protein in phospholipase C-mediated inositol lipid signaling. Cell *74*, 919-928.

Tilley, S.J., Skippen, A., Murray-Rust, J., Swigart, P.M., Stewart, A., Morgan, C.P., Cockcroft, S., and McDonald, N.Q. (2004). Structure-function analysis of human [corrected] phosphatidylinositol transfer protein alpha bound to phosphatidylinositol. Structure *12*, 317-326.

Tremblay, J.M., Helmkamp, G.M., and Yarbrough, L.R. (1996). Limited proteolysis of rat phosphatidylinositol transfer protein by trypsin cleaves the C terminus, enhances binding to lipid vesicles, and reduces phospholipid transfer activity. J Biol Chem *271*, 21075-21080.

Tremblay, J.M., Unruh, J.R., Johnson, C.K., and Yarbrough, L.R. (2005). Mechanism of interaction of PITPalpha with membranes: conformational changes in the C-terminus associated with membrane binding. Arch Biochem Biophys *444*, 112-120.

Vordtriede, P.B., Doan, C.N., Tremblay, J.M., Helmkamp, G.M., Jr., and Yoder, M.D. (2005). Structure of PITPbeta in complex with phosphatidylcholine: comparison of structure and lipid transfer to other PITP isoforms. Biochemistry *44*, 14760-14771.

Voziyan, P.A., Tremblay, J.M., Yarbrough, L.R., and Helmkamp, G.M., Jr. (1996). Truncations of the C-terminus have different effects on the conformation and activity of phosphatidylinositol transfer protein. Biochemistry *35*, 12526-12531.

Xie, Y., Ding, Y.Q., Hong, Y., Feng, Z., Navarre, S., Xi, C.X., Zhu, X.J., Wang, C.L., Ackerman, S.L., Kozlowski, D., Mei, L., and Xiong, W.C. (2005). Phosphatidylinositol transfer protein-alpha in netrin-1-induced PLC signalling and neurite outgrowth. Nat Cell Biol *7*, 1124-1132.

Xie, Z., Fang, M., and Bankaitis, V.A. (2001). Evidence for an intrinsic toxicity of phosphatidylcholine to Sec14p-dependent protein transport from the yeast Golgi complex. Mol Biol Cell *12*, 1117-1129.

Yoder, M.D., Thomas, L.M., Tremblay, J.M., Oliver, R.L., Yarbrough, L.R., and Helmkamp, G.M., Jr. (2001). Structure of a multifunctional protein. Mammalian phosphatidylinositol transfer protein complexed with phosphatidylcholine. J Biol Chem *276*, 9246-9252.

Chapter 2: Targeting of PITPβ to the trans-Golgi network

Chapter 2 is reproduced from Molecular Biology of the Cell, published by the American Society of Cell Biology (ASCB).

Citation: Phillips SE*, Ile KE*, Boukhelifa M, Huijbregts RP, Bankaitis VA (2006) Specific and nonspecific membrane-binding determinants cooperate in targeting phosphatidylinositol transfer protein beta-isoform to the mammalian trans-Golgi network, *Mol Biol Cell*. Jun;17(6):2498-512.

* These authors contributed equally to this work

Abstract

Phosphatidylinositol transfer proteins (PITPs) regulate the interface between lipid metabolism and specific steps in membrane trafficking through the secretory pathway in eukaryotes. Herein, we describe the cis-acting information that controls PITPβ localization in mammalian cells. We demonstrate PITPβ localizes predominantly to the trans-Golgi network (TGN) and that this localization is independent of the phospholipid-bound state of PITPβ. Domain mapping analyses show the targeting information within PITPβ consists of three short C-terminal specificity elements and a nonspecific membrane-binding element defined by a small motif consisting of adjacent tryptophan residues (the $W_{202}W_{203}$ motif). Combination of the specificity elements with the $W_{202}W_{203}$ motif is necessary and sufficient to generate an efficient TGN-targeting

module. Finally, we demonstrate that PITPβ association with the TGN is tolerant to a range of missense mutations at residue serine 262, we describe the TGN localization of a novel PITPβ isoform with a naturally occurring $S_{262}Q$ polymorphism, and we find no other genetic or pharmacological evidence to support the concept that PITPβ localization to the TGN is obligately regulated by conventional protein kinase C (PKC) or the Golgi-localized PKC isoforms δ or ε. These latter findings are at odds with a previous report that conventional PKC-mediated phosphorylation of residue Ser262 is required for PITPβ targeting to Golgi membranes.

Introduction

Because the discovery that a phosphatidylinositol transfer protein (PITP) plays an essential role in regulating the interface between lipid metabolism and membrane trafficking from the yeast trans-Golgi network (TGN; Bankaitis *et al.*, 1990; Cleves *et al.*, 1991a; Cleves *et al.*, 1991b), it has become increasingly clear that lipid metabolism regulates many individual trafficking steps throughout the secretory pathway (Cleves *et al.*, 1991a; De Camilli *et al.*, 1996; Simonsen *et al.*, 2001). In vivo studies demonstrate PITPs either control the efficiency at which trafficking reactions occur (Bankaitis *et al.*, 1989; Bankaitis *et al.*, 1990; Cleves *et al.*, 1991b; Kearns *et al.*, 1997) or impart spatial organization to these reactions (Lopez *et al.*, 1994; Nakase *et al.*, 2001; Vincent *et al.*, 2005). PITPs do so by coupling their ability to bind and/or transfer specific lipids to the coordination of lipid metabolic pathways with specific membrane trafficking steps (see (Phillips *et al.*, 2006). In vitro reconstitution of various membrane trafficking or receptor-coupled signaling reactions also identify involvements for PITPs in these events ((Hay and Martin, 1993; Ohashi *et al.*, 1995; Cunningham *et al.*, 1996; Jones *et al.*, 1998).

The available evidence indicates confident assignment of function for any individual PITP requires in vivo studies with model genetic systems. The reconstituted systems that show PITP dependence are remarkably promiscuous from the perspective of source of PITP. This is amply demonstrated by the stoichiometric interchangeability of yeast and mammalian PITPs in such reconstitutions (Ohashi *et al.*, 1995; Cunningham *et al.*, 1996; Jones *et al.*, 1998), even though these PITPs exhibit unrelated structural folds (Sha *et al.*, 1998; Yoder *et al.*, 2001; Tilley *et al.*, 2004). By contrast, in vivo studies show even very closely related PITPs play nonredundant functions in cells (Li *et al.*, 2000; Alb *et al.*, 2002; Alb *et al.*, 2003; Routt and Bankaitis, 2004; Vincent *et al.*, 2005).

Mammalian cells express three soluble PITPs. PITPα and PITPβ share 77 and 95% primary sequence identity and similarity, respectively, and are encoded by distinct genes. The third, rdgBβ, is considerably more diverged and remains largely unstudied (Fullwood *et al.*, 1999). The shared homologies notwithstanding, PITPα and PITPβ are functionally distinct (Alb *et al.*, 2002; Alb *et al.*, 2003). In this regard, PITPα binds PtdIns and PtdCho, whereas PITPβ binds both those phospholipids and, in addition, sphingomyelin (SM; de Vries *et al.*, 1995). Moreover, recombinant PITPα and PITPβ localize to distinct compartments, the former to the cytosol and nucleus and the latter to the cytosol and a perinuclear compartment that is likely the Golgi complex (de Vries *et al.*, 1995; De Vries *et al.*, 1996; van Tiel *et al.*, 2002). The relationship between the distinct biochemical properties of these two PITP isoforms and localization and function (if any) remain to be determined.

Herein, we report that endogenous PITPβ (and a novel spliceoform thereof) localizes predominantly to TGN membranes and that localization is specified by a

functionally redundant set of three short C-terminal motifs. These motifs are collectively insufficient to target a naive reporter to Golgi membranes, but cooperate with a $W_{202}W_{203}$ motif to generate an efficient TGN-targeting module. We also show that the phospholipid-bound status of PITPβ does not contribute to its association with the TGN. Finally, in contrast to a previous claim (van Tiel *et al.*, 2002), our data indicate that neither localization of PITPβ nor its novel spliceoform to Golgi membranes is obligately regulated by conventional protein kinase C (PKC)-mediated phosphorylation of residue serine 262.

Materials and Methods

Mammalian Cell Culture and Transfections

Murine embryonic fibroblasts (MEFs) were derived from E16.5 wild-type and *PITPα*$^{-/-}$ embryos as previously described (Alb *et al.*, 2003). The mammalian cell lines used in this study were cultured in DMEM containing 10% fetal bovine serum, 1 U/ml penicillin G, 100 μg/ml streptomycin, and 4.2 μl β-mercaptoethanol (for 500 ml of complete medium). Cultures were incubated at 37°C and in 5% CO2.

COS-7 cells were transfected using Lipofectamine Plus reagent (Invitrogen, Carlsbad, CA). Briefly, 24 h before transfection the cells were plated at 50–60% confluency in six-well plates containing glass coverslips. DNA (1.5–2 μg) was reconstituted in 100 μl of OptiMEM (Invitrogen), mixed with 2 μl of Plus reagent, and incubated at room temperature for 15 min. In a separate microcentrifuge tube, 3 μl of Lipofectamine was diluted in 100 μl of OptiMEM for each transfection. After 15 min, the solutions were mixed and then incubated for 15 min at 25°C. Cells were washed twice

with OptiMEM and incubated at 37°C with DNA mixture in 1 ml OptiMEM for 3 h. Subsequently, 4 ml of complete medium was added, and cells were cultured for 18–24 h before processing for immunocytochemistry. MEFs were transfected using the Amaxa (Cologne, Germany) nucleofector following the manufacturer's directions.

Antibody Reagents

PITP antibodies used in this study included: a PITPβ isoform–specific rabbit polyclonal antibody directed against the C-terminal 25 amino acid of PITPβ (generous gift from Bruce Hamilton), a PITPα isoform–specific chicken polyclonal antibody directed against the last 15 amino acids of PITPα (Alb *et al.*, 2002), and the NT-PITP-antibody rabbit polyclonal immunoglobulin (Ig) raised against the N-terminus of PITPα and that recognizes both PITPα and PITPβ (generous gift of Prof. George Helmkamp, Jr.).

The following primary antibodies were used: a monoclonal antibody directed against actin (Chemicon, Temecula, CA), sheep polyclonal anti-TGN38 Ig (Serotec), monoclonal anti-GM130 antibodies (BD Bioscience, San Diego, CA), and murine monoclonal anti-giantin Ig (generous gift from Dr. Hans Peter Hauri, Switzerland). Secondary antibodies used included: Alexa fluorescein isothiocyanate 488 (Molecular Probes, Eugene, OR), Cy5-conjugated anti-mouse and fluorescein isothiocyanate–conjugated anti-mouse (Jackson ImmunoResearch, West Grove, PA), and goat anti-rabbit, goat anti-mouse, or goat anti-chicken horseradish peroxidase (HRP)-conjugated antibodies (Jackson ImmunoResearch).

Immunocytochemistry

Cells were cultured on glass coverslips. Cells were fixed for 15 min with 3.7% formaldehyde in phosphate-buffered saline (PBS), permeabilized in 0.2% Triton X-100 in PBS for 4 min, rinsed once in PBS, and then preincubated for 30 min in blocking buffer (2% BSA in PBS). Permeabilized cells were subsequently incubated with suitable primary antibody appropriately diluted in blocking buffer for 1 h at room temperature, rinsed four times 5 min with PBS, and then incubated with the secondary antibodies appropriately diluted in blocking buffer for 1 h. Cells were rinsed four times in PBS, and coverslips were mounted onto glass slides and examined in a Leica SP2 Laser Scanning Confocal Microscope (Leica, Deerfield, IL). Images were processed with the use of Adobe Photoshop 6.0 (Adobe Systems, Mountain View, CA).

In classifying PITP localization profiles as "Golgi", two major criteria were applied. First, for to score a profile as Golgi the appropriate query profile (GFP or PITP) must exhibit obvious and predominant colocalization with a Golgi marker (TGN38 or GM130). Second, the Golgi component of the query profile must be the strongest signal recorded in the cell being scored. Failure to satisfy both these criteria resulted in a non-Golgi score. Fixed and stained samples were blinded before scoring to control for investigator bias.

Pharmacological Challenge

PITPα–/– MEFs were grown on glass coverslips to subconfluency and intoxicated with chelerethryne chloride (0.66 μM; Sigma, St. Louis, MO) or G109203X (10 nM; Sigma) for appropriate times. PKC activity in MEFs was also stimulated by exposure of cells grown on coverslips to PMA (100 nM, Sigma) for 15 min in serum-free medium. Cells were subsequently fixed for PITPβ immunostaining as described above. Cell-free

extracts were prepared for parallel-treated cultures and processed for immunoblot analysis as described below.

SDS-PAGE and Immunoblotting

Cultures were rinsed with ice-cold PBS and scraped into lysis buffer (20 mM Tris-HCL, pH 7.4, 150 mM NaCl, 2 mM EDTA, 10 mM NaF, 1% Triton 1 mM orthovanadate supplemented with a cocktail of protease inhibitors (Complete; Roche, Indianapolis, IN). For preparation of cell-free extracts, cells (grown to confluency in a 100-mm dish) were incubated with 700 µl of lysis buffer at 4°C for 10 min and then scraped with a rubber policeman into microcentrifuge tubes. After centrifugation at 14,000 x *g* for 10 min, the supernatant was mixed in Laemmli sample buffer and heated for 5 min at 95°C. Samples were resolved by SDS-PAGE (10%) and transferred to nitrocellulose (Millipore, Billerica, MA). Membranes were blocked overnight at 4°C in TBST (5% dry nonfat milk in 0.05% Tween 20 in Tris-buffered saline) and then incubated for 3 h at room temperature with the appropriate primary antibodies diluted in TBST. Membranes were rinsed four times for 5 min each with TBST and then incubated with the appropriate HRP-conjugated secondary antibody for 1 h, and washed four times for 5 min each with TBST. Blots were developed on x-ray film (Eastman Kodak, Rochester, NY) using the enhanced chemiluminescence (ECL) Western blotting detection reagent (Amersham, Arlington Heights, IL).

Generation of PITPα-GFP and PITPβ-GFP cDNAs

PCR primers for rat-PITPα and rat-PITPβ cDNA sequences were flanked on the 5' end with the restriction enzyme site HindIII and on the 3' end with the restriction enzyme site BamHI. The HindIII-BamHI PCR fragments were cloned into the pEGFP-C1 plasmid

(Clontech, Palo Alto, CA). Yeast plasmids harboring PITPα and PITPβ cDNAs (Skinner *et al.*, 1993) were used as templates in the PCR reactions used for generating the appropriate DNA fragments for cloning. The resulting plasmids were designated pRE772 (PITPβ-GFP) and pRE774 (PITPα-GFP). Primer sequences used are available from the authors by request.

Yeast Complementation Assay

Wild-type and mutant PITPβ or PITPβ-GFP cDNAs, as appropriate, were cloned into the multicopy yeast URA3 vector YEplac195 such that the cDNA was expressed either under control of the powerful constitutive *PGK* promoter or the constitutively expressed but weaker *SEC14* promoter. This expression vector was transformed into the *sec14-1^{ts}* yeast strain (CTY 1-1A, MAT**a** *ura3-52 his3Δ200, lys2-810 sec14-1^{ts}*; (Cleves *et al.*, 1991b) using the lithium acetate method of Ito *et al.* (1983). As matched controls, isogenic vectors with either no insert or with *SEC14* or *PITPβ* cDNA inserts were also transformed into the *sec14-1^{ts}* yeast host strain. Transformants were selected and cultured in uracil-free glucose minimal medium (Sherman, 1983). Five OD_{600} equivalents of each strain were resuspended in 200 µl Tris-EDTA buffer and serially diluted 10-fold in Tris-EDTA buffer. An aliquot (5 µl) of each dilution was spotted on duplicate YPD agar plates. One plate was incubated at the 30°C (a permissive temperature for *sec14-1^{ts}* mutants) to report unrestrained growth and viability. The companion plate was incubated at 37°C (normally a restrictive temperature for *sec14-1^{ts}* mutants) to assess phenotypic rescue of sec14-1ts.

Phospholipid-Transfer Assays

Assays were performed using cytosol prepared from the sec14 Δcki1 host strain CTY303 expressing the desired PITP as described previously (Kearns *et al.*, 1998; Phillips *et al.*, 1999; Li *et al.*, 2000; Vincent *et al.*, 2005). Cytosol fractions generated from CTY303 variants expressing Sec14p (positive control) or no PITP (negative control) were generated and assayed in parallel with those fractions containing PITPα, PITPβ, or PITPβ variants.

Site-directed Mutagenesis

The QuickChange kit (Stratagene, La Jolla, CA) was used. Sequences of the various mutagenic primers used are available from the authors by request. All mutant versions generated were verified by nucleotide sequence analysis.

Results

Endogenous PITPβ Localizes to the Mammalian Golgi Complex

Previous experiments suggesting a Golgi localization of PITPβ in mammalian cells relied on microinjection of purified fluorophore-modified protein into cells (De Vries *et al.*, 1996) or creation of stable cell lines that overexpress PITPβ (van Tiel *et al.*, 2002). As a result, several key questions regarding PITPβ localization remain. First, it remains to be demonstrated whether endogenous PITPβ is genuinely a Golgi membrane–associated protein. Second, the precise distribution of PITPβ within the Golgi stack also remains to be determined.

Specific localization of endogenous PITPβ was complicated by our observation that antibodies generated against the extreme C-terminal 15- and 25-residue peptides of these proteins, although facile for distinguishing PITPα from PITPβ by immunoblotting, are not satisfactory for immunofluorescence experiments (unpublished data). To

circumvent this issue, we used polyclonal antibodies raised against amino-terminal sequences conserved between PITPα and PITPβ. These antibodies (NT-PITP-antibody) are suitable for immunofluorescence but are not specific reagents in that these recognize both PITPα and PITPβ isoforms in immunoblotting experiments. The specificity issue notwithstanding, we inspected the endogenous PITP immunofluorescence staining profiles obtained with NT-PITP-antibody in an array of cell lines. Swiss 3T3 fibroblasts exhibited a strong perinuclear staining of what appears to be the Golgi apparatus and a diffuse signal in the cytoplasm and the nuclear matrix (Figure 1A). The PITP profiles obtained with Swiss 3T3 cells and NT-PITP-antibody as reporter were typical. Very similar results were also obtained with a variety of other cell lines including astrocytes, primary neurons, and COS-7, HeLa, and HEK293 cells. That the perinuclear PITP staining identifies the Golgi complex is indicated by the coincidence of this profile with that obtained for the cis-Golgi marker GM130 (Figure 1A). As the NT-PITP-antibody immunofluorescence profiles collected with immortalized cell lines represent the sum of endogenous PITPβ and PITPα distribution, and previous studies indicate PITPα localizes to the cytoplasm and nuclear matrix (De Vries *et al.*, 1996), these various localization profiles suggest that endogenous PITPβ targets to Golgi membranes in a variety of cell types.

To visualize endogenous PITPβ in isolation from PITPα, we used NT-PITP-antibody as PITP detector and took advantage of PITPα nullizygous primary cell lines that we had previously generated. The nullizygous MEFs are well suited for these experiments as these cells are phenotypically indistinguishable from wild-type MEFs and retain unadulterated levels of endogenous PITPβ (Alb *et al.*, 2002; Alb *et al.*, 2003). As

shown in Figure 1B, NT-PITP-antibody decorates an elaborate ribbonlike perinuclear structure in these PITPα–/– MEFs, and this structure is also stained by the cis-Golgi marker GM130. The GM130 and presumptive PITPβ staining profiles are very similar in form, but are not coincident. These data indicate that PITPβ does not localize to cis-Golgi membranes but, rather, localizes to a distinct subcompartment of the Golgi complex (see below). Very little staining of the cytoplasm or nucleus is observed, and staining of the lacelike ER is also evident. These staining profiles were absent when naive preimmune serum was substituted for NT-PITP-antibody in these experiments.

To confirm localization of the known PITPβ, we constructed a PITPβ-GFP chimera, where GFP was fused to the C-terminus of PITPβ. The activity of the PITPβ-GFP chimera was established with a yeast phenotypic rescue assay. This assay capitalizes on previous demonstrations that high-level expression of mammalian PITPs in yeast rescues the growth and secretory defects associated with inactivation of the essential yeast PITP Sec14p (Skinner *et al.*, 1993; Tanaka and Hosaka, 1994). This rescue is dependent on robust PtdIns-binding/transfer by the heterologous mammalian PITP (Alb *et al.*, 1995). As shown in Figure 1C, a sec14-1ts yeast strain carrying an ectopic copy of the wild-type SEC14 gene grows robustly at 37°C. By contrast, the isogenic sec14-1ts strain fails to grow at all at 37°C, i.e., the restrictive temperature at which the thermolabile sec14-1ts gene product is inactive. Expression of PITPβ-GFP restored robust growth to the sec14-1ts yeast mutant at the restrictive 37°C temperature.

The functional PITPβ-GFP was expressed in MEFs and the distribution of the chimera was monitored. These localization experiments confirm an unambiguous affinity

of PITPβ-GFP for Golgi membranes in MEFs (Figure 1D) and also in COS-7 cells (see below).

PITPβ Selectively Associates with the TGN

Although both Golgi and ER membranes harbor pools of PITPβ, Golgi localization predominates and how PITPβ targets to the Golgi membrane system is the focus of this study. To more precisely assign the Golgi subcompartment of residence for endogenous PITPβ, we performed a series of double-label immunofluorescence experiments. In these experiments, NT-PITP-antibody was used in combination with compatible antibodies raised against markers for specific Golgi compartments. These markers included GM130 for cis-Golgi, giantin for cis- and medial-Golgi, and TGN38 for the TGN. PITPα nullizygous MEFs were used to ensure specific detection of endogenous forms of PITPβ.

As shown in Figures 2, A and B, endogenous PITPβ exhibits little coincidence of staining with the cis-Golgi marker GM130, or the medial-Golgi marker giantin, even though the general profiles for PITPβ and these markers are very similar. Endogenous PITPβ species exhibit a higher degree of colocalization with the trans-Golgi membrane marker TGN38, however (Figure 2C). The predominant localization of PITPβ to TGN membranes is emphasized in a stereo reconstruction of the MEF Golgi apparatus generated from triple-label experiments monitoring PITP, giantin, and TGN38 (Supplemental Video, Figure S1). The rotating image distinguishes giantin staining from the yellow staining that reports colocalization of TGN38 and PITPβ. We infer from these experiments that PITPβ targets predominantly to the trans-aspect of the Golgi stack in MEFs.

During the course of these studies, we noted the existence in the NCBI Protein Database of an uncharacterized PITPβ spliceoform (referred to as PITPβ^{QGQR}, as opposed to canonical spliceoform that we refer to as PITPβ) that is invisible to our PITPβ-specific antibodies in immunoblot experiments (murine form, accession number AAH34676; rat form, AAH61538; human form, AAH31427). This spliceoform is detected by the NT-PITP-antibody, however, and the PITPβ localization profiles described in Figure 2 represent the sum of the PITPβ and PITPβ^{QGQR} profiles (these two spliceoforms are both expressed in MEFs; unpublished data). Defined GFP-chimeras permit localization of each spliceoform in isolation, however. As further described below, we show that both PITPβ-GFP and PITPβ^{QGQR}-GFP reporters target efficiently to similar (albeit not identical) Golgi subcompartments.

PITPβ C-terminal Motifs Necessary for TGN Targeting

The distinctive localization profiles for PITPβ and PITPα are remarkable in light of the high degree of primary sequence identity shared by these PITPs. To map the determinants specifying targeting of PITPβ to the mammalian TGN in an unbiased manner, we constructed a reciprocal series of PITPβ/PITPα hybrid proteins in the context of a functional PITP-GFP chimera. The functional status of key chimeras was confirmed in the heterologous yeast sec14-1ts phenotypic rescue assay (Skinner *et al.*, 1993); described above and in Figure 1C). All chimeras generated were active in the yeast phenotypic rescue assay and were expressed both in PITPα–/– MEFs and in COS-7 cells. The respective intracellular distributions were imaged and quantified for both cell types. In describing the results of the mapping experiments, we present data obtained with MEFs and report the COS-7 data in Supplemental Materials.

The C-terminal 28 PITPβ residues are both necessary for PITPβ targeting to Golgi membranes and are sufficient to efficiently redirect PITPα to that location (Figure 3A). The results were robust because the incidence of Golgi targeting in cells was >90% for PITPβ and the PITPα/β chimera and <5% for PITPα and the PITPβ/α chimera. Representative images for each chimera are shown in Figure 3B. In the imaging experiments reported herein, we typically identify the Golgi region by surveying the cis-Golgi marker GM130 but confirmed that assignment by costaining with the pan-Golgi marker wheat germ agglutinin and, for key reporter/mutant constructs, by costaining for TGN38 (see below).

Alignment of the PITPβ and PITPα C-terminal primary sequences identifies three motifs of greatest divergence between these isoforms. We refer to these motifs as BOX1, BOX2, and BOX3 (Figure 3C). Mutagenesis experiments, where each individual BOX region from PITPα was substituted for the corresponding BOX region of PITPβ, demonstrated that PITPβ^{KQE}, PITPβ^{QDPK}, and PITPβ^{MTD} all exhibited efficiencies of Golgi localization similar to those recorded for the PITPβ control (Figure 3, C and D). Thus, no single BOX motif is essential for PITPβ targeting to Golgi membranes. We also observed that swap of any two of the BOX domains from PITPα into the PITPβ context did not compromise association of PITPβ with TGN membranes (Figure 3, C and D). These data indicate that the presence of any single PITPβ motif is sufficient for maintenance of PITPβ localization to the Golgi complex. Parallel analyses of the localization properties of each chimera were also conducted in COS-7 cells with essentially identical results (Supplemental Materials, Figure S2).

PITPβ C-terminal Motifs Sufficient for Targeting PITPα to Golgi Membranes

To address the dual criteria of necessity and sufficiency, we tested whether any BOX residues sufficient for PITPβ localization to the TGN were capable of redirecting PITPα to the same. To this end, PITPβ BOX1 or BOX3 residues were incorporated into the context of an otherwise wild-type PITPα. The localization profiles of both constructs ($PITP\alpha^{QET}$ and $PITP\alpha^{TSA}$) fully recapitulated the nuclear and cytoplasmic distribution of the PITPα control (Figure 4A). Thus, neither BOX1 nor BOX3 has an assignable targeting function on its own in the context of PITPα. However, BOX2 residues, although dispensable for PITPβ targeting to the Golgi complex, increased the efficiency with which an otherwise wild-type PITPα reporter associates with Golgi membranes. That construct ($PITP\alpha^{KGSR}$) was scored as targeting to Golgi membranes in 51% of the transfected cells analyzed. Although this level of targeting is not as robust as that observed with the PITPβ positive control (>90%), it is substantial when compared with the basal association of the PITPα control with the Golgi complex (ca. 5%; Figure 4A).

When multiple PITPβ BOX motifs were swapped into the PITPα context, an essentially complete redirection of a PITPα reporter to the TGN was observed. Combinatorial incorporation of PITPβ BOX1 and BOX2 residues, BOX1 and BOX3 residues, or BOX2 and BOX3 residues into the PITPα context yielded chimeras that efficiently targeted to Golgi membranes (Figures 4, A and B). For reasons detailed below, we were particularly interested in any role BOX2 or its individual residues may play in the localization of PITPβ to the TGN. In that regard, the dispensability of BOX2 residues for PITPβ Golgi targeting was further emphasized in a swap of BOX2 from PITPα for the PITPβ BOX2 in the context of a PITPα chimera that harbors the C-terminal 28 PITPβ residues. This $PITP\alpha^{QET\text{-}TSA}$ chimera is composed entirely of PITPα primary sequence,

save 24 of 28 C-terminal residues where the PITPα BOX2 motif is substituted for that of PITPβ. Yet, PITPα$^{QET\text{-}TSA}$ retains its capacity to target to Golgi membranes (Figures 4, A and B). Again, these conclusions were confirmed when these same chimeras were expressed in COS-7 cells and the corresponding localization profiles were scored (Supplemental Materials, Figure S3). The data indicate that the combination of any two of the PITPβ BOX motifs is sufficient to generate a robust Golgi localization signal in the context of PITPα.

PITPβ Ser262 Is Nonessential for Golgi Localization

The dispensability of BOX2 for PITPβ localization to TGN membranes was counter to the findings of (van Tiel *et al.*, 2002), who reported that phosphorylation of a BOX2 residue (S_{262}) is essential for PITPβ targeting to Golgi membranes. Yet, our demonstration that swap of PITPβ BOX2 residues significantly improved PITPα targeting to Golgi membranes (i.e., the PITPα^{KGSR} construct; Figure 4A) is consistent with a more substantial role for BOX2 in Golgi targeting. To investigate these paradoxical findings in more detail, we analyzed the involvement of S_{262} itself in PITPβ localization. Consistent with the results of the BOX2 chimera experiments, PITPβ^{S262A}, PITPβ^{S262D}, PITPβ^{S262E}, and PITPβ^{S262P} all targeted to Golgi membranes as efficiently as the PITPβ control (Figure 4C). These results were recapitulated in the context of COS-7 cells (Supplemental Figures and Supplemental Table S1).

To determine whether an analogous phosphorylation may be sufficient to redirect PITPα to Golgi membranes, we incorporated phosphomimetic amino acids at the corresponding P_{263} residue of PITPα to generate the PITPα^{P263D} and PITPα^{P263E} mutants. The ability of each to associate with MEF TGN membranes was then assessed. Neither

PITPα^{P263D} nor PITPα^{P263E} targeted to Golgi membranes any more efficiently than the PITPα control (Figure 4D). We repeated these analyses in COS-7 cells. Again, neither incorporation of the $P_{263}S$ missense substitution, nor $P_{263}E$, into the context of PITPα-GFP had any major effect on the intracellular distribution of the chimera (Supplemental Materials, Supplemental Table S1).

A Novel PITPβ Isoform with Altered BOX2 Residues Targets to the TGN

All of the experiments described above rely on mutagenesis of canonical PITPβ. The novel murine PITPβ spliceoform described above (PITPβ^{QGQR}) differs from canonical PITP β predominantly in BOX2 (Figure 4E). Interestingly, S_{262} of canonical PITPβ is Q_{262} in PITPβ^{QGQR}. PCR assays indicate both PITPβ and PITPβ^{QGQR} are expressed in PITPα–/– MEFs at approximately equal levels.

Localization experiments using GFP-tagged forms show PITPβ^{QGQR}, like PITPβ, associates with MEF Golgi membranes (Figure 4E). These results are consistent with data indicating S_{262} is nonessential for efficient targeting of PITPβ species to that compartment. PITPβ^{QGQR} displays a single nonconserved serine residue (S_{259}) in the region of divergence, but the $S_{259}A$ mutation has no effect on targeting of a PITPβ^{QGQR}-GFP chimera to TGN membranes (Figure 4E). These data lead us to form two conclusions in addition to S_{262} dispensability for PITPβ targeting to Golgi. First, S_{259} does not offer an alternative phosphorylation site required for PITPβ^{QGQR} association with Golgi membranes. Second, mammalian cells can express more than one PITPβ species in cells but, in this case, both PITPβ and PITPβ^{QGQR} isoforms home to Golgi membranes. Comparison of the localization profiles of PITPβ-GFP and PITPβ^{QGQR}-GFP chimeras indicates both target to the TGN, although PITPβ^{QGQR}-GFP also exhibits partial

colocalization with the medial-Golgi marker mannosidase II (Supplemental Materials, Figure S4, A and B). PITPβ^{QGQR}-GFP also appears to target more efficiently to cis-Golgi membranes than does PITPβ-GFP (Supplemental Materials, Figure S4C). Thus, PITPβ^{QGQR} may represent more of a pan-Golgi PITPβ than the canonical PITPβ.

PITPβ Targeting to Golgi Membranes Is Independent of PtdIns- or SM-Transfer Activity

As described in detail below, the C-terminal 28 PITPβ residues are sufficient to redirect PITPα to Golgi membranes but are insufficient to target a naive protein to this intracellular location. These data suggest that multiple localization signals may be involved in localizing PITPβ to the TGN and that a subset of these determinants likely resides in the PITP domain itself. As PITP domains represent specific lipid-binding modules, PITPβ lipid-binding properties themselves could potentially define components of a combinatorial targeting signal.

To test this possibility, we took advantage of mutant PITPβ derivatives with selective defects in the loading/transfer of defined phospholipid substrates. Given that PITPβ is distinguished from PITPα in its ability to bind SM in addition to PtdIns and PtdCho, one attractive possibility is that SM loading contributes to the affinity of PITPβ for Golgi membranes. Data obtained from three independent lines of experimentation demonstrate that SM-loading and Golgi targeting are not strictly coupled. First, wholesale swap of the PITPα C-terminal 28 residues into the context of PITPβ leads to a PITP chimera that fails to associate with the Golgi complex (see Figure 3, A and B above). Yet, this PITPβ/α chimera exhibits robust SM transfer in vitro (Figure 5A). Second, reciprocal swap of the PITPβ C-terminal 28 residues into the context of PITPα results in

a hybrid PITPα/β that efficiently targets to the Golgi complex (see Figure 3, A and B above). This PITPα/β chimera, while elaborating both PtdIns- and PtdCho- transfer activity, exhibits no detectable SM-loading/transfer activity in vitro (Figure 5A). Third, substitution of only two amino acids in PITPα to the cognate PITPβ residues is sufficient to confer robust SM-transfer activity to PITPα (PITPα^{LF221,225IL}; Figure 5A). Reciprocally, conversion of those cognate PITPβ residues to the corresponding PITPα residues strongly and specifically compromises the SM-transfer activity of PITPβ (PITPβ^{IL220,224LF}; Figure 5A). In neither case does modulation of SM-loading/transfer affect PtdIns- or PtdCho-transfer activity or PITP localization. PITPβ^{IL220,224LF} fully retains the ability to target efficiently to Golgi membranes, whereas PITPα^{LF221,225IL} does not (Figure 5B).

To probe the involvement of PtdIns loading in targeting of PITPβ to the TGN, we took advantage of mutants specifically defective in PtdIns-binding/transfer activity. PITPα residue T59 is essential for PtdIns-binding/transfer, but plays no role in PtdCho-binding/transfer (Alb *et al.*, 1995). The selective effects of the mutant translated to the PITPβ context as biochemical analyses confirmed that the corresponding PITPβ mutant (PITPβ^{T58D}) retains high levels of both PtdCho- and SM-transfer activity in the absence of measurable PtdIns-transfer activity (unpublished data). We constructed the PITPβ^{T58D}-GFP chimera and assessed its subcellular distribution in PITPα–/– MEFs. Imaging experiments show ca. 90% of the cells expressing PITPβ^{T58D}-GFP exhibited robust Golgi staining profiles, a score recapitulating that of the PITPβ control (Figure 5C). When the experiment was performed in COS-7 cells, PITPβ^{T58D}-GFP assumed an obvious Golgi

localization in 91% of the 99 expressing cells imaged (90 Golgi/9 non-Golgi profiles). Thus, PtdIns-loading/transfer does not contribute to PITPβ targeting to Golgi membranes.

Uncoupling of Phospholipid-Transfer Activity from PITPβ Targeting to Golgi Membranes

Although neither PtdIns- or SM-loading/transfer activity are required for PITPβ association with the TGN, a combination of phospholipid-loading/transfer activities could contribute to such targeting. We therefore tested whether residue Ser165 is required for targeting of PITPβ to the Golgi complex. This residue lies in the PITP regulatory loop (Yoder *et al.*, 2001). The side-chain status of this residue is functionally important because incorporation of either alanine or glutamate at this position abolishes all PITPα phospholipid-transfer activities (van Tiel *et al.*, 2000).

The PITPβ^{S165A} mutant was generated and its biochemical properties were assayed in vitro. As reported by (van Tiel *et al.*, 2000) for PITPα^{S166A}, we too find PITPβ^{S165A} exhibited no measurable PtdIns-, PtdCho-, or SM-transfer activity, even though full-length PITPβ was readily detected in the cytosolic fractions by immunoblot (unpublished data). The S_{165}A missense substitution had no effect on PITPβ localization when assayed in PITPα$^{-/-}$ MEFs. PITPβ^{S165A}-GFP was targeted as efficiently to Golgi membranes as the PITPβ-GFP control (Figure 5D). Because PITPβ^{S165A} exhibits no detectable phospholipid-transfer activity, PITPβ^{S165A}-GFP association with Golgi membranes is independent of phospholipid-transfer activity.

We also expressed PITPβ^{S165,262A}-GFP in PITPα–/– MEFs and assessed the ability of this double mutant to target to TGN membranes. This experiment was motivated by the demonstration that PITPα residue S_{166} and PITPβ residue S_{165} are minor PKC

phosphorylation sites (van Tiel *et al.*, 2000; van Tiel *et al.*, 2002). PITPβ^{S165,262A} is therefore devoid of the PKC phosphorylation sites for which there is any evidence of use. Yet, PITPβ^{S165,262A}-GFP homes to TGN membranes in PITPα –/– MEFs (Figure 5D). These data provide further support for our conclusion that PKC-mediated phosphorylation of PITPβ (at least on the presently known S_{165} and S_{262} sites) does not play an essential role in localization of this protein to mammalian TGN membranes.

A WW Motif Common to PITPα and PITPβ Contributes to Association of PITPβ with TGN Membranes

PITPα occupied with either PtdCho or PtdIns crystallizes as a dimer, and the dimerization interface is defined by two small hydrophobic motifs displayed on exposed loops of the PITP fold (Figure 6A; Yoder *et al.*, 2001; Tilley *et al.*, 2004). These two motifs are represented by $_{72}$FVRML$_{76}$ and $W_{203}W_{204}$ of PITPα and $_{71}$FVRMI$_{75}$ and $W_{202}W_{203}$ of PITPβ, respectively, and both are suggested to play critical roles in mediating membrane binding by PITPα (Schouten *et al.*, 2002; Tilley *et al.*, 2004). To test whether $_{71}$FVRMI$_{75}$ or $W_{202}W_{203}$ contribute to localization of PITPβ to the murine TGN, we mutagenized these motifs in the context of a PITPβ-GFP reporter and analyzed localization of the corresponding reporters in PITPα–/– MEFs. The comprehensive data are quantified in Figure 6B, and representative imaging profiles for the corresponding mutant PITPβ forms are given in Figure 6C.

Consistent with the view that the WW motif contributes to membrane binding, the PITPβ^{WW202,203AA}-GFP chimera failed to associate stably with PITPα–/– MEF TGN membranes. By contrast, PITPβ^{MI74,75AA}-GFP retained near wild-type efficiencies for TGN targeting (Figure 6, B and C). Although there is a consistent diminution in TGN

association for the PITPβ^{MI74,75AA}-GFP chimera, the defect is minor. Essentially the same results were obtained with PITPβ^{F71A}-GFP and PITPβ^{VR72,73AA}-GFP chimeras. By contrast, the individual W_{202} and W_{203} residues each play important roles in localization of PITPβ, as evidenced by the obvious defects in PITPβ^{W202A}-GFP and PITPβ^{W203A}-GFP association with MEF TGN membranes (Figure 6B).

Previous data obtained from PtdIns loading assays performed with permeabilized cells indicated PITPα^{WW202,203AA} is strongly defective in PtdIns loading and is incompetent for the membrane interaction step of a phospholipid-transfer reaction (Tilley *et al.*, 2004). We obtained two lines of evidence that are not congruent with this conclusion, at least in the PITPβ context. First, biochemical assays for phospholipid-transfer activity demonstrate PITPβ^{MI74,75AA} and PITPβ^{WW202,203AA} exhibit significant levels of PtdIns-, PtdCho-, and SM-transfer activity in vitro (Figure 7A). Second, we again took advantage of the yeast phenotypic rescue assay described above to independently assess whether the phospholipid-binding/transfer activities of the double mutant PITPs were strongly compromised. The results from that rescue assay also support the conclusion that both PITPβ^{MI74,75AA} and PITPβ^{WW202,203AA} are substantially functional proteins. As shown in Figure 7B, a wild-type yeast strain grows robustly at 30 and 37°C. By contrast, an isogenic sec14-1ts strain grows only at the permissive temperature of 30°C and not at all at the restrictive temperature of 37°C, i.e., the temperature at which the thermolabile sec14-1ts gene product is inactive. PITPβ expression from either a strong constitutive promoter (pPGK) or a weaker constitutive promoter (pSEC14) restored essentially wild-type growth properties to the sec14-1ts yeast mutant. Similarly, expression of either PITPβ^{MI74,75AA} or PITPβ^{WW202,203AA} from the

pPGK driver also supported efficient rescue of sec14-1ts-associated growth defects at 37°C (Figure 7B). Rescue mediated by both mutant PITPβ forms was also recorded when the mutant proteins were expressed from the weaker pSEC14 promoter, although quality of rescue was diminished slightly under those conditions for PITPβ^{WW202,203AA} (Figure 7B).

Taken together, the data indicate neither PITPβ^{MI74,75AA} nor PITPβ^{WW202,203AA} exhibit dramatic defects in phospholipid-transfer activity and phospholipid loading. Because these various double mutant PITPs retain phospholipid-transfer activity, the PITP fold must remain unperturbed in the double mutants. We conclude that the TGN localization defects associated with mutation of $W_{202}W_{203}$ cannot be simply ascribed to a wholesale inability of PITPβ to interact with membranes.

PITPβ Motifs Sufficient for Redirection of GFP to the TGN

The collective data suggest it is the combination of weak membrane targeting/association signals defined by the C-terminal BOX residues and the $W_{202}W_{203}$ motif that specifies PITPβ association with TGN membranes. To test this prediction we fused the C-terminal 35 and 71 residues of PITPβ to the GFP C-terminus. The former chimera (GFP-PITPβ$^{237–271}$) elaborates all three of the C-terminal BOX motifs, is predicted to preserve the C-terminal PITPβ helix, but lacks both the $W_{202}W_{203}$ motif and obviously lacks an intact PITP fold. The latter chimera (GFP-PITPβ$^{201–271}$) elaborates both $W_{202}W_{203}$ and the three BOX motifs, is predicted to maintain the ultimate two PITPβ helices, but lacks an intact PITP fold. The chimeras were expressed in PITPα−/− MEFs and their respective intracellular distributions were determined.

As expected, the GFP control distributes to the cytoplasm and nuclear matrix and fails to associate with Golgi membranes as evidenced by its lack of colocalization with the TGN marker TGN38 (Figure 8). This profile was recapitulated for the GFP-PITPβ$^{237–271}$ chimera that harbors all three of the C-terminal BOX motifs but no $W_{202}W_{203}$ motif. By contrast, GFP-PITPβ$^{201–271}$ targeted efficiently to PITPα−/− MEF TGN as demonstrated by its colocalization with TGN38-positive structures (Figure 8). Some 85% of the cells showed coincident localization of GFP-PITPβ$^{201–271}$ with the TGN. Thus, linking the PITPβ $W_{202}W_{203}$ motif with the three BOX motifs generated a targeting module that satisfies the dual criteria of necessity and sufficiency for specific association with TGN membranes.

PITPβ Association with TGN Membranes and Action of PKCs

The evidence reported herein is incongruent with the claim that PITPβ association with the Golgi complex depends on conventional PKC-mediated phosphorylation of S_{262} (van Tiel *et al.*, 2002). We therefore investigated what effect inactivation of conventional PKCs has on localization of PITPβ to the TGN. As a first approach, we applied a blunt pharmacological strategy. PITPα$^{-/-}$ MEFs were intoxicated with two different inhibitors of conventional PKCs, and PITPβ distribution of was monitored at various times postchallenge. Neither GF109203X nor chelerythrine chloride intoxication had any effect, at any time, on the association of PITPβ with the MEF TGN (Figures 9, A and B). The efficacy of pharmacological challenge in inhibiting PKC activity was confirmed by monitoring phospho-MARCKS upon inhibitor challenge (Figure 9C).

In the pharmacological challenge experiments we used the NT-PITP-antibody as reporter. Thus, we were unable to distinguish between PITPβ and PITPβ^{QGQR} in those

experiments. We therefore repeated these experiments using a PITP-GFP reporter and arrived at the same conclusions. PITPβ-GFP localization to the MEF TGN was resistant to challenge with GF109203X or chelerythrine chloride under the same conditions described in Figure 9C. Some 72% of mock-challenged MEFs exhibited a TGN profile for PITPβ-GFP (136/188 cells), and similar results were obtained upon MEF intoxication with GF109203X (78%; 192/247 cells) or chelerythrine chloride (85%; 109/129 cells).

In a second approach, we derived MEFs from embryos individually nullizygous for either the nonconventional PKCδ or PKCε isoforms. Both of these isoforms localize to the mammalian Golgi complex (Lehel *et al.*, 1995; Storz *et al.*, 2004) and therefore represent reasonable candidate PKCs for which PITPβ is a physiological substrate. Again, localization to the murine Golgi of endogenous PITPβ species was unimpressed by genetic ablation of the PKCε or the PKCδ isoform (see Supplemental Materials, Figure S5A). Although we concur with (van Tiel *et al.*, 2002) that PITPβ can be phosphorylated by PKCs in vivo (i.e., PMA stimulates phosphorylation of endogenous PITPβ), we believe this effect is likely mediated through PKCδ because PMA challenge has no obvious effect on PITPβ phosphorylation status in PKCδ$^{-/-}$ MEFs (see Supplemental Materials, Figure S5B). Given that the Golgi-associated PKCδ plays no obligate role in targeting PITPβ to the TGN, we suggest PMA-stimulated phosphorylation of PITPβ reflects elevated PKCδ activity evoking an adventitious phosphorylation of vicinal proteins on Golgi membranes.

Discussion

Herein, we identify endogenous PITPβ as a peripheral protein of mammalian TGN (and ER) membranes and describe a mechanism for PITPβ localization to those

membranes. This mechanism involves four elements that define two distinct categories of targeting information. The first consists of three functionally redundant motifs that reside in the PITPβ C-terminal 28 residues. The second is represented by a $W_{202}W_{203}$ motif required for PITPβ association with TGN membranes. We posit these two sets of elements cooperate to localize PITPβ to the mammalian TGN. The cooperative contribution of both sets of elements generates a modular targeting code both necessary and sufficient for specific homing of proteins to the TGN.

How is specificity of targeting determined? The three motifs embedded in the C-terminal 28 PITPβ residues represent the most logical candidates for specificity elements. The rationale is threefold. First, each motif defines a region of primary sequence divergence between PITPβ and PITPα. Second, the presence of at least one element is necessary to preserve PITPβ localization to the TGN. Third, transplantation of any two motifs into PITPα efficiently redirects this protein to the TGN. Thus, the three C-terminal elements satisfy the dual criteria of necessity and sufficiency for specifying localization of a PITP reporter to TGN membranes. Whether the C-terminal specificity elements engage a proteinaceous receptor or recognize some lipid platform unique to the TGN remains an open question. However, we find PITPβ association with Golgi membranes is sensitive to brefeldin A, indicating a dependence on a functional ARF (or ARL) GTPase cycle.

We suggest the $W_{202}W_{203}$ motif contributes to PITPβ association with TGN membranes by providing a nonspecific and low-affinity membrane-binding site. Our demonstration that PITPβ association with TGN membranes is compromised by mutations of the $W_{202}W_{203}$ motif supports this view. The concept is also consistent with

structural data indicating $W_{202}W_{203}$ lies on a loop oriented on the same face of the PITPβ as the mouth of the phospholipid-binding pocket (Yoder *et al.*, 2001; Tilley *et al.*, 2004). The $W_{202}W_{203}$ motif does not confer specificity of membrane binding because this element is common to both PITPα and PITPβ, and these PITPs exhibit distinct localization profiles.

Although the idea that $W_{202}W_{203}$ functions in a nonspecific and low-affinity membrane-binding reaction has its justification, other data do not readily conform to such a model. Alanine scanning mutagenesis indicates this motif has no major role in PITPβ phospholipid-transfer activity or loading with a phospholipid substrate. It could be argued this result is inconsistent with a nonspecific membrane-binding function for $W_{202}W_{203}$. We do not favor this interpretation because the phospholipid-transfer assays and yeast phenotypic rescue assay that we employ as functional tests are biased in favor of transient membrane associations. Such assays likely minimize the importance of a stabilization of membrane-binding function for $W_{202}W_{203}$.

The various phospholipid loading properties of PITPβ do not contribute in any obvious way to its association with the TGN. Of particular interest is the case of SM-binding/transfer because this property suggested an attractive mechanism for the specific homing of PITPβ to Golgi membranes. This mechanism was based on the dual arguments that PITPβ is distinguished from PITPα by its ability to load with SM and that the major site of SM synthesis in mammalian cells is the Golgi complex (Futerman *et al.*, 1990; Bankaitis, 2002). The fact that the TGN-targeting mechanism does not survey the phospholipid-bound state of PITPβ also has implications for models invoking a delivery function for PITPβ in supply of TGN membranes with PtdIns (e.g., to support TGN

phosphoinositide pools). Other PITPs likely help execute such functions (Litvak *et al.*, 2005).

Our data indicate a concerted action of specific and general membrane-binding elements in the targeting of PITPβ to the TGN. We find the targeting process is not obligately coupled to PITPβ phosphorylation of residue S_{262} by conventional PKCs or at least two nonconventional PKC isoforms. That conclusion is supported by both PKCδ$^{-/-}$ and PKCε$^{-/-}$ MEF data, and the general resistance of PITPβ TGN association to challenge of cells with inhibitors of conventional PKCs. Moreover, PITPβ TGN localization signals accommodate an array of side chains at residue S_{262}—indicating neither S_{262} itself, nor its phosphorylation, is an essential component of PITPβ TGN-targeting information. The fact that combined mutagenesis to alanine of PITPβ residues S_{262} and S_{165} (a minor PKC phosphorylation site in vitro) has no effect on PITPβ localization further emphasizes this point. We expect these general findings will hold equally true for the novel PITPβ^{QGQR} spliceoform.

Our collective results are comprehensively at odds with the report of (van Tiel *et al.*, 2002), who claim that phosphorylation of residue S_{262} is required for Golgi membrane localization of PITPβ. Can these conflicting conclusions be reconciled? (van Tiel *et al.*, 2002) utilized stable NIH3T3 cell lines that overproduce PITPβ for their studies. One formal possibility is that the visible pool of PITPβ in those stable cell lines behaves differently from the endogenous pool. We do not favor this interpretation because the PITPβ-GFP chimera we used consistently localized to TGN membranes with the same fidelity as endogenous PITPβ. Also, because van Tiel *et al*. were clearly monitoring PITPβ, and not PITPβ^{QGQR}, the discrepancies cannot be ascribed to spliceoform issues.

The possibility that NIH3T3 cells used by van Tiel *et al*. behave differently than MEFs or COS-7 cells cannot be formally excluded, although the absolute efficiencies of PITP-GFP targeting to the TGN in MEFs and COS-7 cells were consistently similar.

The (van Tiel *et al.*, 2002) report suggests several areas of experimentation that leave room for ambiguity of interpretation. First, the parameters of what constitutes a Golgi profile in their studies were not defined by the use of known Golgi markers, and no quantification of the imaging data was presented. Second, there was no description of controls for monitoring what effect pharmacological inhibition of conventional PKCs has on Golgi organization in their cell lines. Perturbation of Golgi organization may complicate interpretation of PITPβ localization data. Third, the scope of the mutagenesis from which van Tiel *et al*. reached their conclusions was limited to a single mutant ($PITP\beta^{S262A}$). The issue of sufficiency of S_{262} phosphorylation for PITP targeting to Golgi membranes was not addressed. Finally, the arguments that PITPβ residue S_{262} represents a major in vivo phosphorylation site are based on in vitro schemes using recombinant proteins (van Tiel *et al.*, 2002). Direct identification of phosphorylation sites in endogenous PITPβ is required to resolve this important issue.

A remarkable facet of the biological activities of PITPs is the dedication with which these proteins couple to specific physiological functions (Routt and Bankaitis, 2004; Phillips *et al.*, 2006). The example of PITPα and PITPβ is clear testimony to this effect as these closely related PITP isoforms assume radically different localization profiles and are functionally nonredundant. Our finding that murine cells can express what are likely two biochemically indistinguishable PITPβ spliceoforms, and yet localize both to similar regions of the Golgi stack, suggests that even finer functional distinctions

may yet exist. Our analyses of how PITPβ targets to specific Golgi subcompartments gives us the ability to interchange, in a rational and directed way, either the localization, or the phospholipid-binding properties, or both, of PITPα and of defined PITPβ spliceoforms. This facility permits direct experimental address, in the mouse, of whether the distinct biological activities of these proteins are strictly a function of protein localization or whether differential phospholipid-binding properties also contribute to function.

Acknowledgments

We thank Con Beckers and Doug Cyr for helpful discussions and insightful criticisms throughout this work, and the assistance of Michael Chua and Jan Sinyshyn of the Michael Hooker Microscopy Core (UNC) is acknowledged. Bruce Hamilton (UCSD), Hans-Peter Hauri (Basel), and George Helmkamp, Jr. generously donated antibodies for this study. Oligonucleotide primer synthesis and DNA sequence analyses were performed via the Lineberger Comprehensive Cancer Center Genome Analysis and Nucleic Acids Core facility. This work was supported by National Institutes of Health (NIH) Grants NS37723 and NS42651 awarded to V.A.B. K.E.I. was supported by a Cell and Molecular Biology Training Grant from the NIH (T32 GM08581), and R.P.H.H. was supported in part by a North Atlantic Treaty Organization Science Fellowship of the Netherlands Organization for Scientific Research (NWO).

Figures

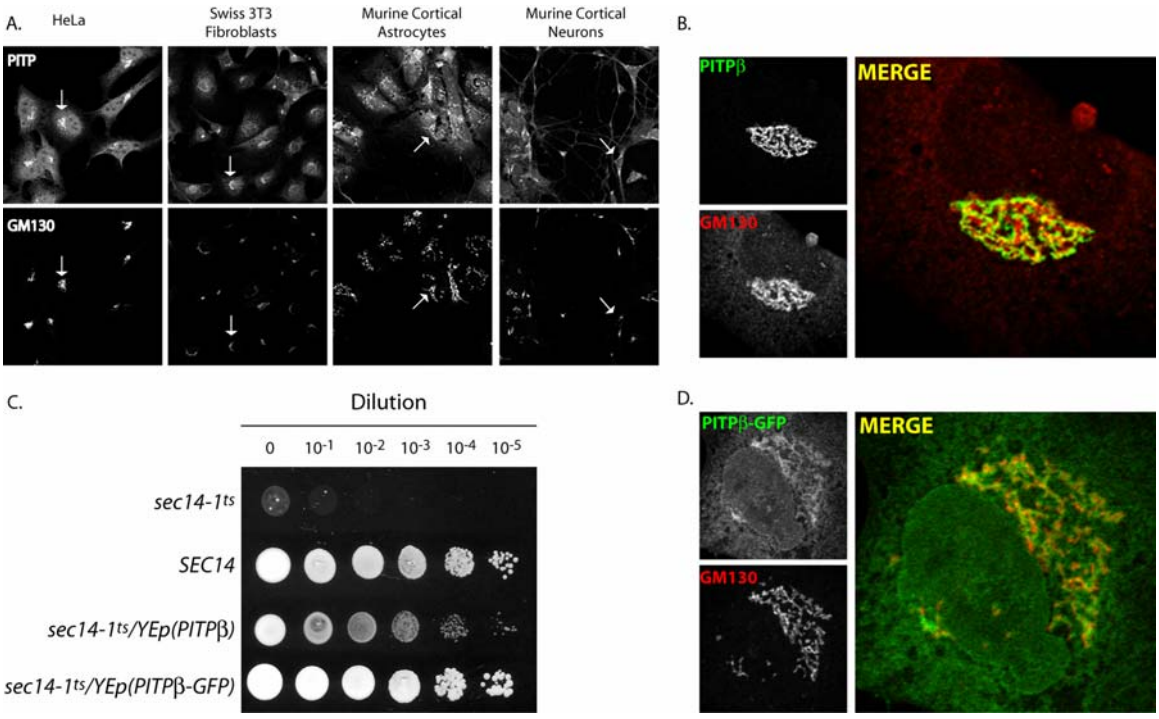

Figure 2.1: Endogenous PITP localization profiles. (A) Fixed and permeabilized cells of the indicated cell type were stained with a PITP antibody that detects PITPα and PITPβ and antibodies directed against the Golgi marker GM130. The PITP (top panels) and GM130 profiles (bottom panels) are shown. Arrows indicate one example of the clear colocalization of an endogenous PITP with Golgi membranes for each cell type and orient the remaining Golgi profiles in the matched panels. (B) PITPα$^{-/-}$ MEFs were fixed and decorated with primary antibodies directed against PITP antigen or the *cis*-Golgi marker GM130. Representative individual profiles for endogenous PITPβ and GM130 are shown in the left panels, as indicated, and the merged profile is depicted in the right panel. (C) PITPβ-GFP chimera is a functional protein. Serial 10-fold dilutions of isogenic sets of a *sec14-1*^{ts} strain, derivatives of that strain carrying a high-copy plasmid (YEp) driving expression of either PITPβ, PITPβ-GFP, or a wild-type *SEC14* gene (as indicated) were spotted onto YPD agar and incubated at 37°C for 48 h. The 37°C

condition, although permissive for growth of wild-type yeast, is restrictive for growth of *sec14-1*^{ts} yeast mutants. This *sec14-1*^{ts} growth defect is rescued by expression of either PITPβ or the PITPβ-GFP chimera, indicative of preservation of PITPβ activity in the PITPβ-GFP chimera. Strains used: CTY1-1A (*sec14-1*^{ts}), and CTY1-1A transformed with YEp(*SEC14*), YEp(*PITPβ*), and YEp(*PITPβ-GFP*), respectively. The respective PITPβ genes were driven by the strong and constitutively expressed yeast *PGK* promoter. (D) PITPβ-GFP faithfully targets to the Golgi complex. PITPα nullizygous MEFs were transfected with a PITPβ-GFP expression plasmid, fixed, and decorated with primary antibodies directed against GFP antigen and antibodies directed against GM130, as indicated. Representative individual profiles for PITPβ-GFP and GM130 are shown in the left panels, and the merged profile is depicted in the right panel.

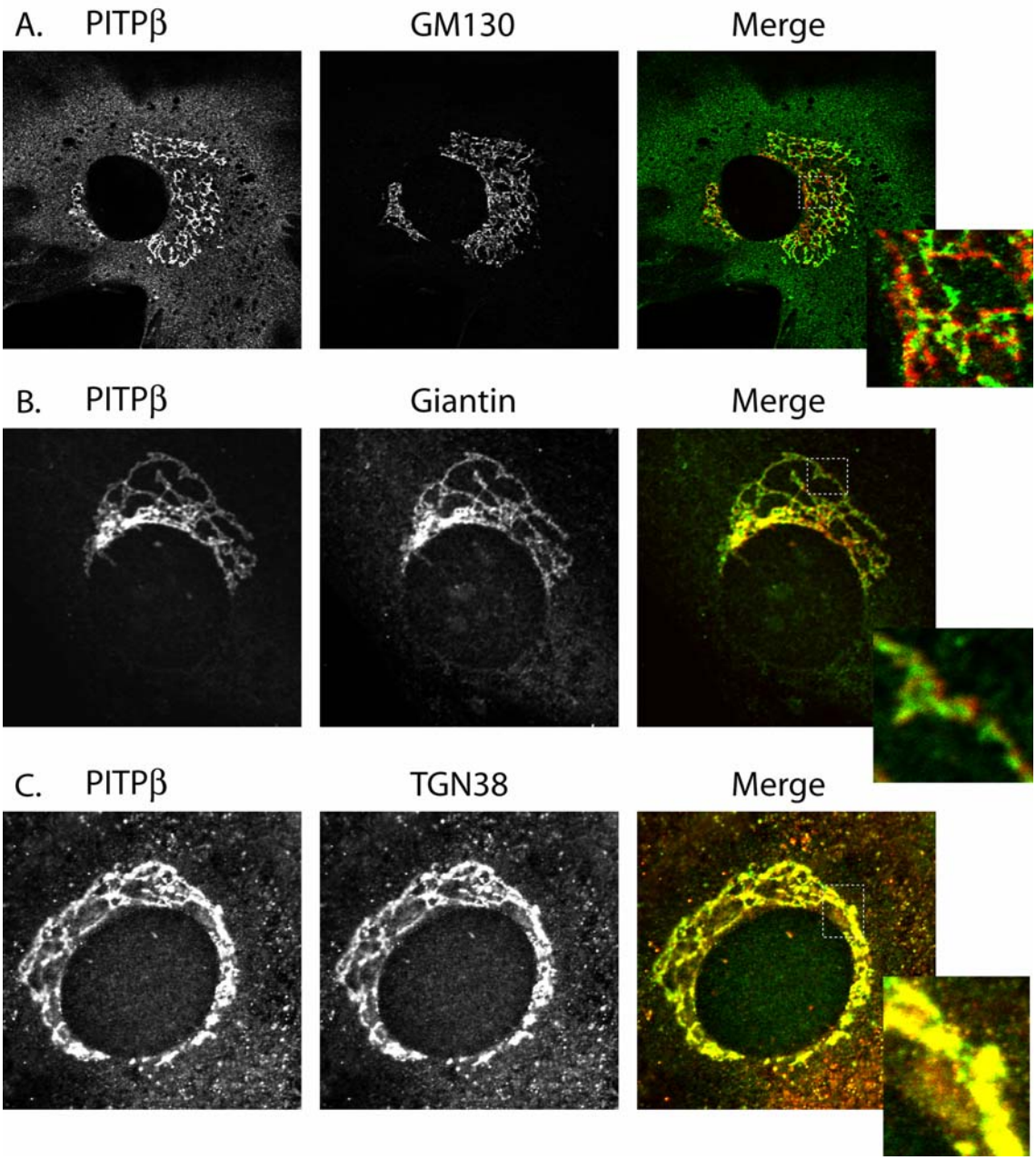

Figure 2.2: PITPβ localizes specifically to TGN membranes. PITPα nullizygous MEFs were fixed and decorated with primary antibodies directed against PITP antigen (rabbit polyclonal NT-PITP-antibody) and antibodies directed against either the *cis*-Golgi marker GM130 (A), the medial-Golgi marker giantin (B), or the *trans*-Golgi marker TGN38 (C). The individual and merged profiles are identified at the top. The respective

insets represent a higher magnification of the boxed region of the corresponding merged profile for purposes of enhanced detail.

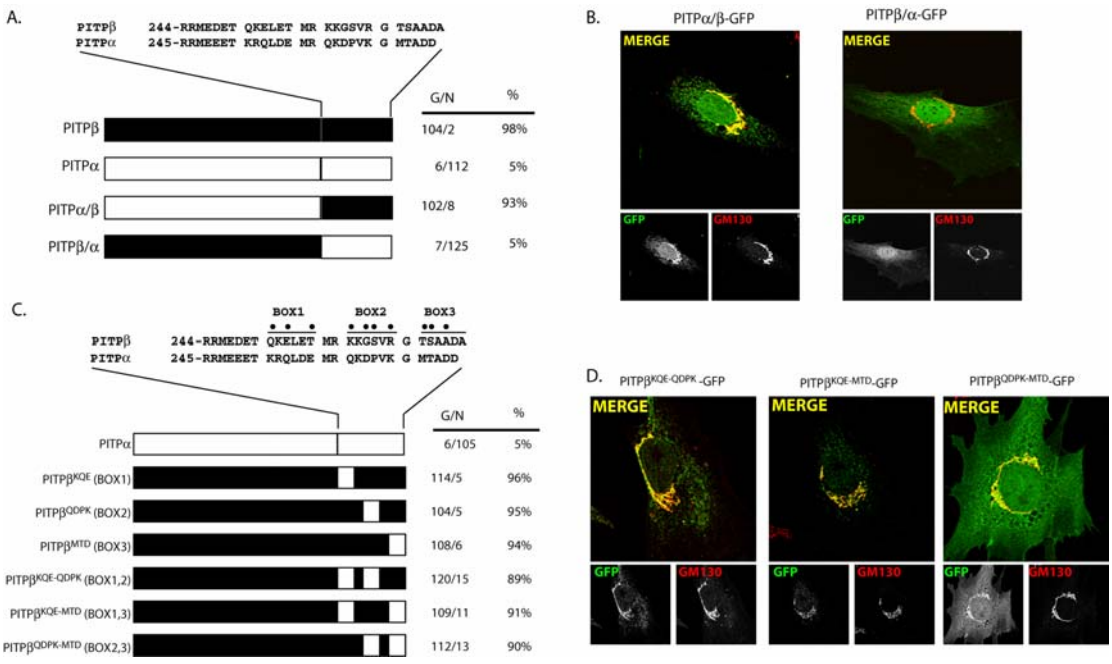

Figure 2.3: C-terminal PITPβ localization elements necessary for TGN association. (A) Alignment of the C-terminal 28 residues of PITPβ with the corresponding region of PITPα is given. Schematic illustrations of PITPα, PITPβ, and each of the reciprocal C-terminal swaps are depicted at bottom. At right, for each corresponding PITP version is given the number of imaged cells that exhibited a Golgi (G) or non-Golgi (N) immunofluorescence profile when that construct was expressed in MEFs as a PITP-GFP chimera and visualized along with the GM130 marker. The percentage of imaged cells with Golgi profiles is also given. (B) Imaging of PITPs with exchanged C-terminal regions. Representative localization profiles for PITPα/β-GFP and PITPβ/α-GFP when expressed in PITPα$^{-/-}$ MEFs are shown. Individual PITP-GFP and GM130 profiles are presented in the bottom panels underneath the corresponding merged profile. (C) Swap of divergent BOX motifs from PITPα into the context of PITPβ. The BOX motifs are defined at top, and the most divergent residues within each are highlighted (●). The series

of hybrid PITPs analyzed is illustrated and each swap is further defined at left by identification of which PITPα residues were introduced to generate the swap. Quantification of PITPα$^{-/-}$ MEFs expressing each individual hybrid with respect to number of cells displaying Golgi (G) or non-Golgi (N) localization profile, along with percentages of cells displaying Golgi localization, is also given. (D) Representative images of PITPα$^{-/-}$ MEFs individually expressing each of the three PITPβ-GFP chimeras where two of the three BOX motifs were mutagenized to PITPα versions. The identities of the swaps are indicated at top. Individual PITP-GFP and GM130 profiles are presented in the bottom panels underneath the corresponding merged profile.

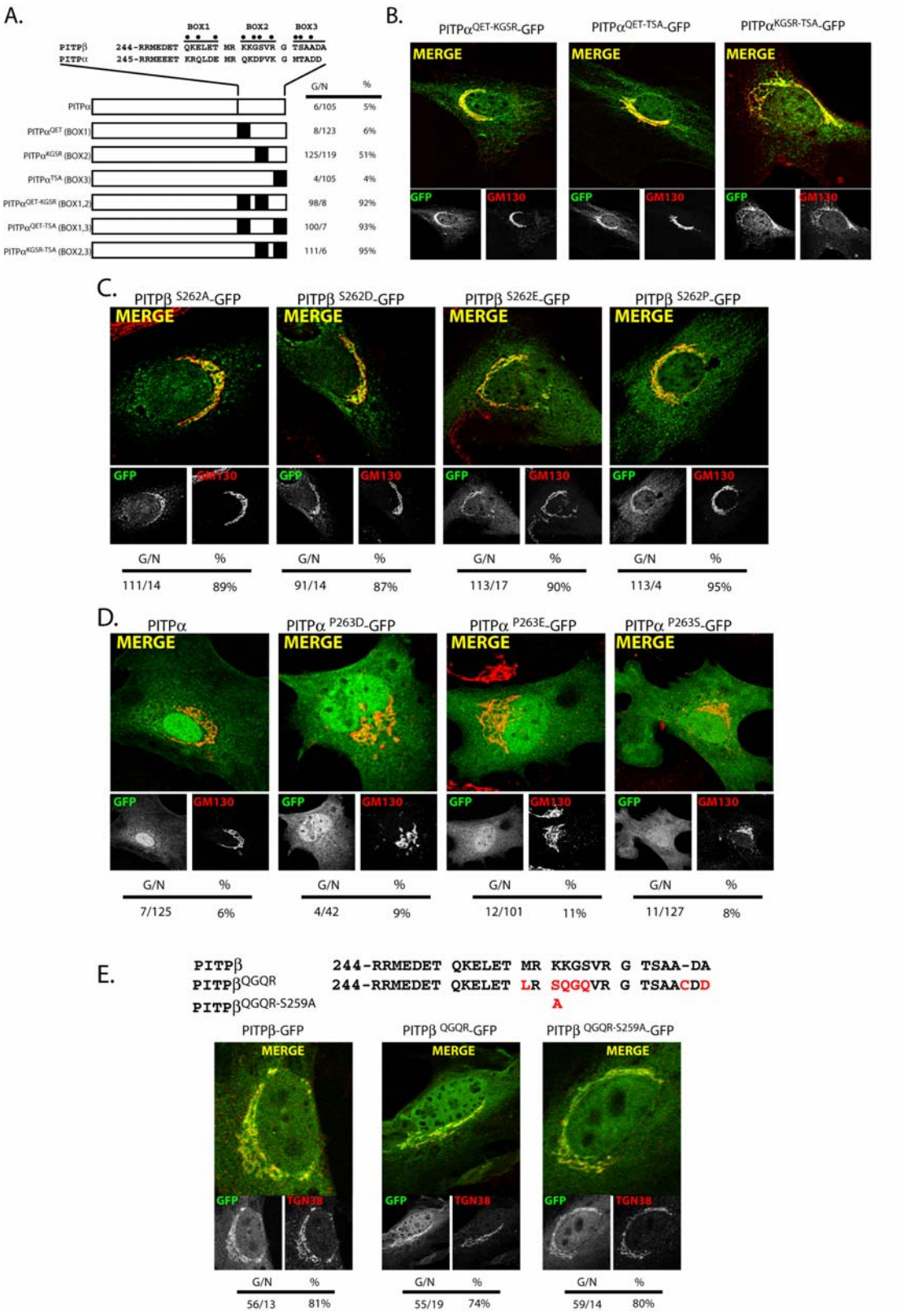
A.
BOX1
BOX2
BOX3
PITPβ 244-RRMEDET QKELET MR KKGSVR G TSAADA
PITPα 245-RRMEEET KRQLDE MR QKDPVK G MTADD
G/N %
PITPα 6/105 5%
PITPα^QET (BOX1) 8/123 6%
PITPα^KGSR (BOX2) 125/119 51%
PITPα^TSA (BOX3) 4/105 4%
PITPα^QET-KGSR (BOX1,2) 98/8 92%
PITPα^QET-TSA (BOX1,3) 100/7 93%
PITPα^KGSR-TSA (BOX2,3) 111/6 95%
B.
PITPα^QET-KGSR-GFP
PITPα^QET-TSA-GFP
PITPα^KGSR-TSA-GFP
MERGE
GFP
GM130
C.
PITPβ S262A-GFP
PITPβ S262D-GFP
PITPβ S262E-GFP
PITPβ S262P-GFP
MERGE
GFP
GM130
G/N % 111/14 89%
G/N % 91/14 87%
G/N % 113/17 90%
G/N % 113/4 95%
D.
PITPα
PITPα P263D-GFP
PITPα P263E-GFP
PITPα P263S-GFP
MERGE
GFP
GM130
G/N % 7/125 6%
G/N % 4/42 9%
G/N % 12/101 11%
G/N % 11/127 8%
E.
PITPβ 244-RRMEDET QKELET MR KKGSVR G TSAA-DA
PITPβ^QGQR 244-RRMEDET QKELET LR SQGQVR G TSAACDD
PITPβ^QGQR-S259A A
PITPβ-GFP
PITPβ QGQR-GFP
PITPβ QGQR-S259A-GFP
MERGE
GFP
TGN38
G/N % 56/13 81%
G/N % 55/19 74%
G/N % 59/14 80%

Figure 2.4: (preceding page) C-terminal PITPβ localization elements sufficient for redirecting PITPα to TGN membranes. (A) Swap of divergent BOX motifs from PITPβ into the context of PITPα. The BOX motifs are defined at the top, and the most divergent residues within each are highlighted (●). The series of hybrid PITPs is illustrated and each swap is further defined at left by identification of which PITPβ residues were introduced to generate the swap. Quantification of PITPα$^{-/-}$ MEFs expressing each individual hybrid with respect to number of cells displaying Golgi (G) or non-Golgi (N) localization profile, along with percentages of cells displaying Golgi localization, is also given. Representative images of PITPα$^{-/-}$ MEFs individually expressing: (B) each of the three PITPα-GFP chimeras where two of the three BOX motifs were mutagenized to PITPβ versions. The identities of the swaps are indicated at top. Individual PITP-GFP and GM130 profiles are presented in the bottom panels underneath the corresponding merged profile. (C) Each of the three PITPβ-GFP chimeras where residue S_{262} is mutagenized to A, D, E, or P as indicated. Individual PITPβ^{S262}-GFP and GM130 profiles are presented in the bottom panels underneath the corresponding merged profile. (D) Each of the three PITPα-GFP chimeras where residue P_{263} is mutagenized to S (the corresponding PITPβ residue) or the phosphomimetic residues D or E as indicated at top. Individual PITPα^{P263}-GFP and GM130 profiles are presented in the bottom panels underneath the corresponding merged profile. (E) The C-terminal 28 residues of PITPβ and the novel PITPβ^{QGQR} spliceoform are aligned at top, and the BOX motifs are identified. Differences in primary sequence are highlighted in red. The position of the S_{259}A mutation in PITPβ^{QGQR} is also indicated. Representative profiles for the corresponding GFP chimeras and GM130 are shown, as are the merged

profiles. In B–E quantification of number of cells displaying Golgi (G) or non-Golgi (N) localization profile, along with percentages of cells displaying Golgi localization, is given.

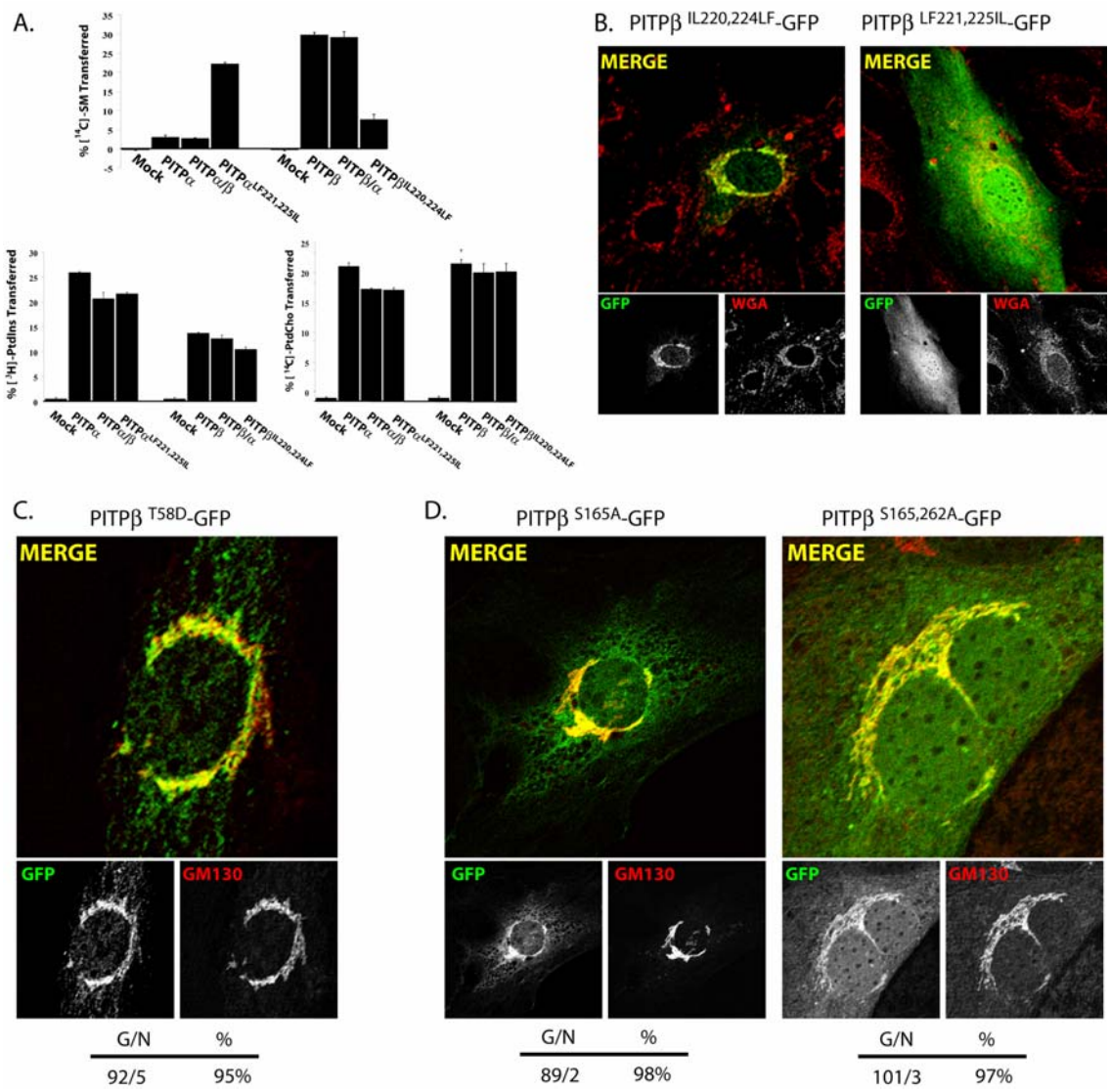

Figure 2.5: PITPβ localization to TGN membranes is independent of phospholipid loading. (A) Phospholipid-transfer properties of select PITP chimeras. Abilities of each individual PITP or PITP chimera to transfer [^{14}C]-SM, [^{3}H]PtdIns, or [^{14}C]PtdCho (as indicated) was determined in cytosol fractions prepared from yeast strain CTY303 (*sec14*Δ *cki1*Δ) expressing recombinant versions of the respective PITPs (Phillips *et al*., 1999; Li *et al*., 2000). CTY303/YEp(*URA3*) cytosol was prepared and used as negative control. Activity is represented as the percentage of total input radiolabeled phospholipid transferred from donor membranes to unlabeled acceptor membranes during the course of

the experiment. Assay blanks represented addition of buffer alone to the transfer assay reactions, and these background values were subtracted from the other measurements. Values represent the averages of triplicate determinations from a representative experiment, and at least three independent experiments were performed. In the experiment shown, input phospholipid-transfer substrate was 19,850 cpm [^{14}C]SM; 21,050 cpm [^{3}H]PtdIns; 21,250 cpm [^{14}C]PtdCho. Background values for these respective transfer assays were 700, 315, and 820 cpm. A representative image of PITPα$^{-/-}$ MEFs expressing a (B) PITPβ^{IL220,224LF}-GFP or a PITPα^{LF221,225IL}-GFP chimera. Cells were imaged for GFP and the pan-Golgi marker wheat germ agglutinin (WGA), as indicated. Corresponding merged profiles are shown. (C) PITPβ^{T58D}-GFP chimera. PITPβ^{T58D}-GFP and GM130 profiles are presented in the bottom panels underneath the corresponding merged profile. (D) PITPβ^{S165A}-GFP or a PITPβ^{S165,262A}-GFP chimera. Cells were imaged for GFP and GM130, as indicated. Corresponding merged profiles are shown. For C and D, quantification of number of cells displaying Golgi (G) or non-Golgi (N) localization profiles, along with the percentages of cells displaying Golgi localization, are given for each construct at the bottom of the corresponding panel set.

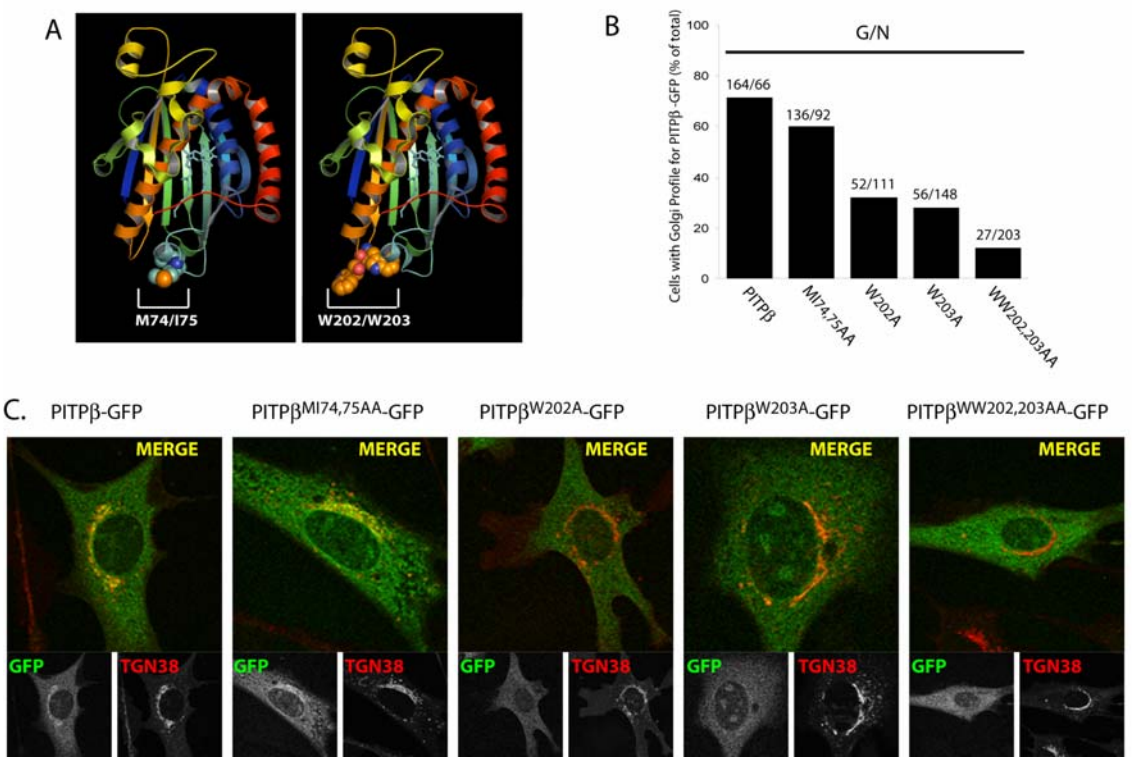

Figure 2.6: General PITP elements required for PITPβ localization to TGN membranes. (A) Ribbon diagram of the PtdIns-bound PITPα crystal structure with space-fill renditions of the $M_{74}I_{75}$ and $W_{202}W_{203}$ side-chains, as indicated. (B) Quantification of percentage of transfected PITPα$^{-/-}$ MEFs displaying Golgi localization profiles for each PITPβ-GFP construct (identified at bottom). The ratio of number of cells imaged with clear Golgi profiles (G) for the indicated PITPβ-GFP chimera to the number of cells imaged for that chimera that show a non-Golgi profile (N) is given above each corresponding bar. (C) Representative images of PITPα$^{-/-}$ MEFs expressing the indicated PITPβ-GFP chimeras. The localization profiles for the indicated PITPβ-GFP (bottom left panels), corresponding TGN38 (bottom right panels), and merged profiles (top panels) are presented.

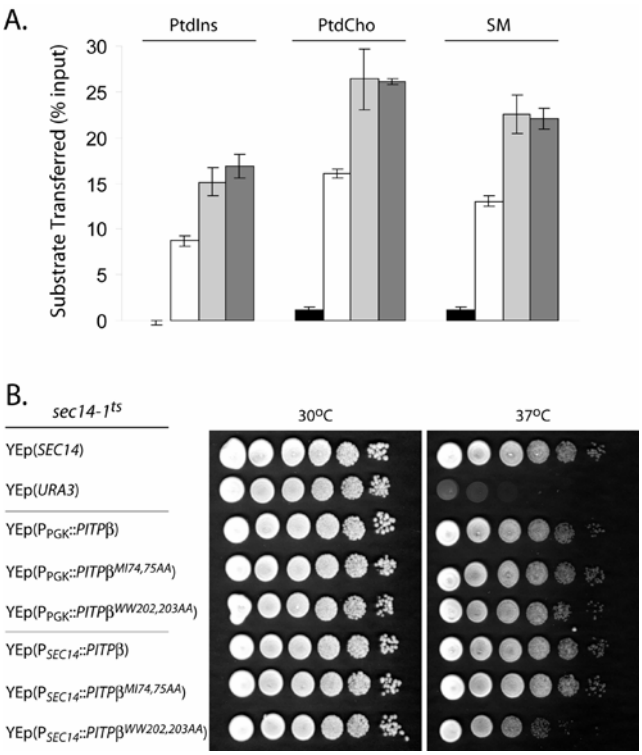

Figure 2.7: Properties of PITPβ^{W202W203} interaction with membranes. (A) Phospholipid-transfer assays. Abilities of each individual PITP to transfer [^{3}H]PtdIns, [^{14}C]PtdCho, or [^{14}C]-SM, (indicated at top) was determined in cytosol fractions prepared from yeast strain CTY303 (*sec14*Δ *cki1*Δ) expressing the negative control gene *URA3* (black bars), or recombinant versions of the respective PITPs (PITPβ, white bars; PITPβ^{MI74,75AA}, hatched bars; PITPβ^{WW202,203AA}, stippled bars). Activity is represented as the percentage of total input radiolabeled phospholipid transferred from donor membranes to unlabeled acceptor membranes during the course of the experiment. Values represent the averages of triplicate determinations from a representative experiment, and at least three independent experiments were performed. Assay blanks represented addition of buffer alone to the transfer assay reactions, and corresponding background values were subtracted from the other measurements. In this set of assays, input substrate was 14,792 cpm [^{3}H]PtdIns; 27,940 cpm [^{14}C]PtdCho; 22,216 cpm

[^{14}C]SM, respectively. Background values were 295, 485, and 236 cpm for each respective assay. (B) PITPβ ^{WW202,203AA} mutants preserve function as assayed in yeast. Serial 10-fold dilutions of isogenic sets of a *sec14-1*^{ts} strain, derivatives of that strain carrying a high-copy plasmid (YEp) driving expression of either PITPβ, PITPβ-^{WW202,203AA}, PITPβ-^{MI74,75AA}, or a wild-type *SEC14* gene (as indicated) were spotted onto YPD agar and incubated at 37°C for 48 h. Strains used were CTY1-1A (*sec14-1*^{ts}), and CTY1-1A transformed with YEp(*SEC14*), YEp(*PITPβ*), YEp(PITPβ-^{MI74,75AA}), and YEp(*PITPβ*^{WW202,203AA}), respectively. The PITPβ genes were driven by the strong and constitutively expressed yeast *PGK* promoter (P_{PGK}) or the weaker constitutively expressed *SEC14* promoter (P_{SEC14}), as indicated.

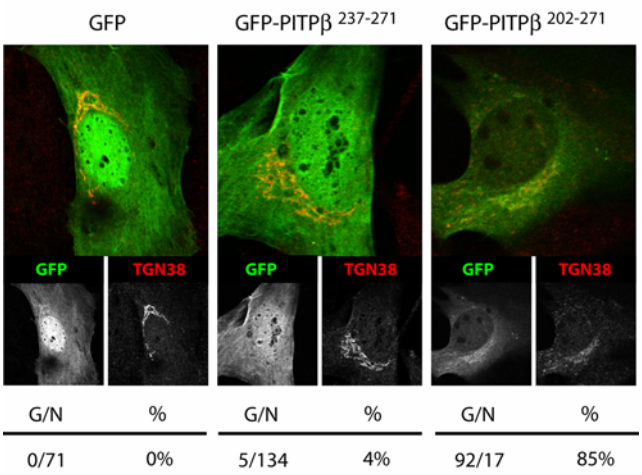

Figure 2.8: $W_{202}W_{203}$ and C-terminal BOX motifs in TGN targeting. Representative profiles for a GFP control, the GFP-PITPβ$^{237–271}$ chimera, and the GFP-PITPβ$^{201–271}$ chimera are shown. Quantification of transfected PITPα$^{-/-}$ MEFs displaying Golgi localization profiles for each GFP-PITPβ construct is given at bottom as the ratio of number of cells imaged with clear Golgi profiles for the indicated GFP-PITPβ chimera to the total number of cells imaged for that chimera.

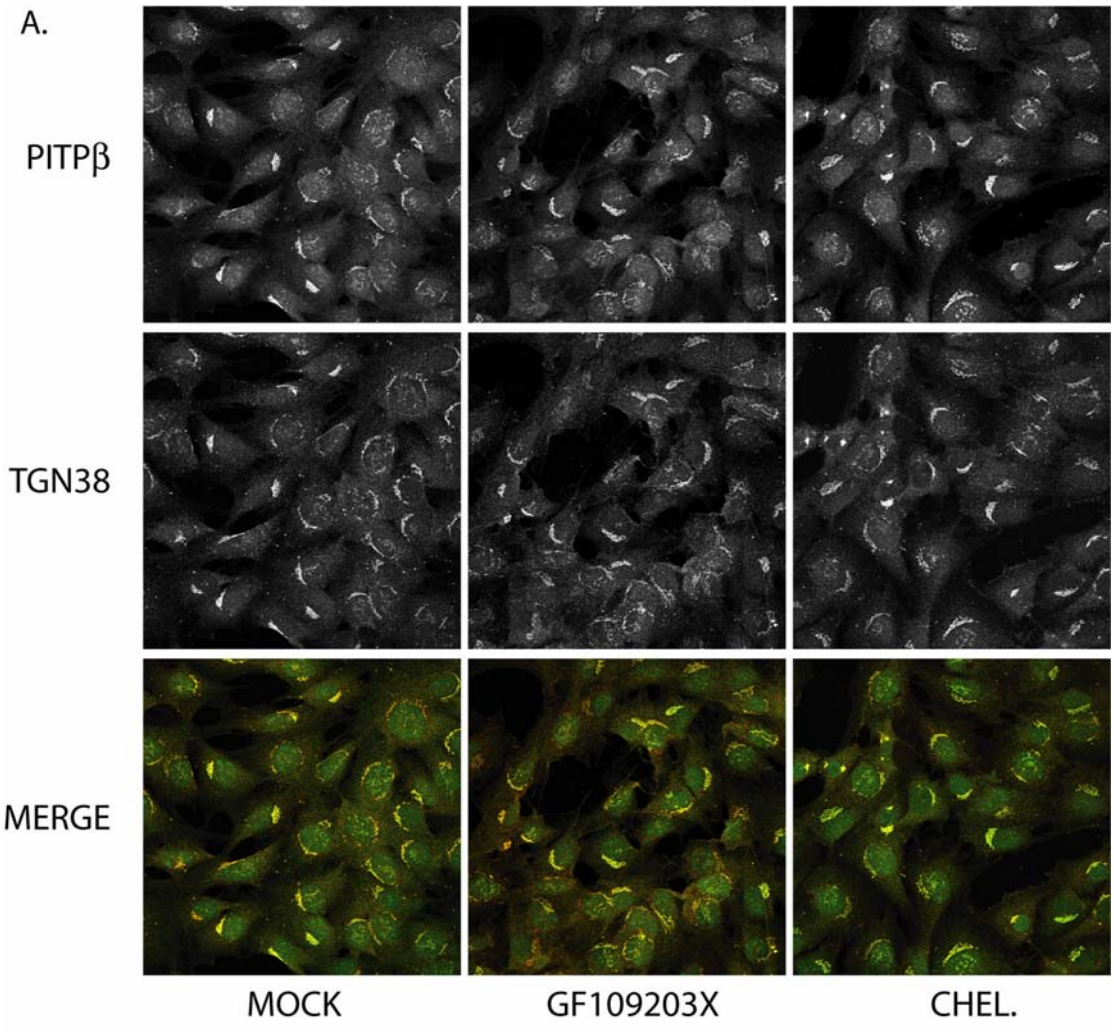
A.
PITPβ
TGN38
MERGE
MOCK
GF109203X
CHEL.

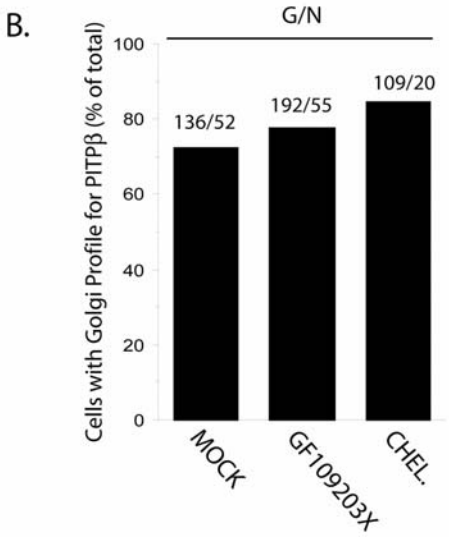
B.
G/N
Cells with Golgi Profile for PITPβ (% of total)
100
80
60
40
20
0
136/52
192/55
109/20
MOCK
GF109203X
CHEL.

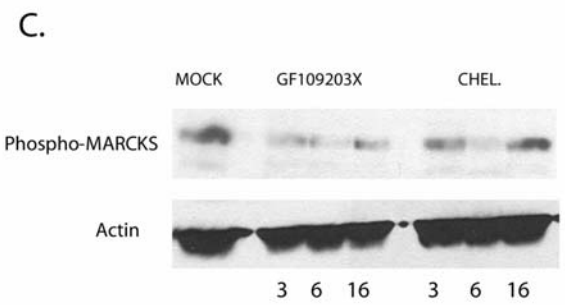
C.
MOCK
GF109203X
CHEL.
Phospho-MARCKS
Actin
3 6 16 3 6 16

Figure 2.9: (preceding page) PITPβ localization and protein kinases C. (A) Profiles (individual and merged) for endogenous PITPβ and TGN38 in PITPα$^{-/-}$ MEFs challenged with no inhibitor (MOCK), GF109203X (10 nM), or chelerythrine chloride (CHEL., 660 nM). The profiles shown at 6 h after challenge but are representative for what was observed at 3 and 16 h postchallenge as well. (B) Quantification of the imaging data presented in A. Number of cells imaged with clear Golgi profiles as a function of total number of cells imaged for each condition are indicated above each corresponding bar. (C) PITPα$^{-/-}$ MEFs were challenged with no inhibitor (MOCK) or GF109203X (10 nM) or chelerythrine chloride (CHEL., 660 nM) for the indicated times. Cell-free lysates were prepared, resolved by SDS-PAGE and blotted to nitrocellulose, and blots were decorated with antibodies specific for phospho-MARCKs (a PKC substrate) and actin (loading control). Antibodies used detect MARCKS phosphorylated at $Ser_{159}Ser_{163}$ (Santa Cruz).

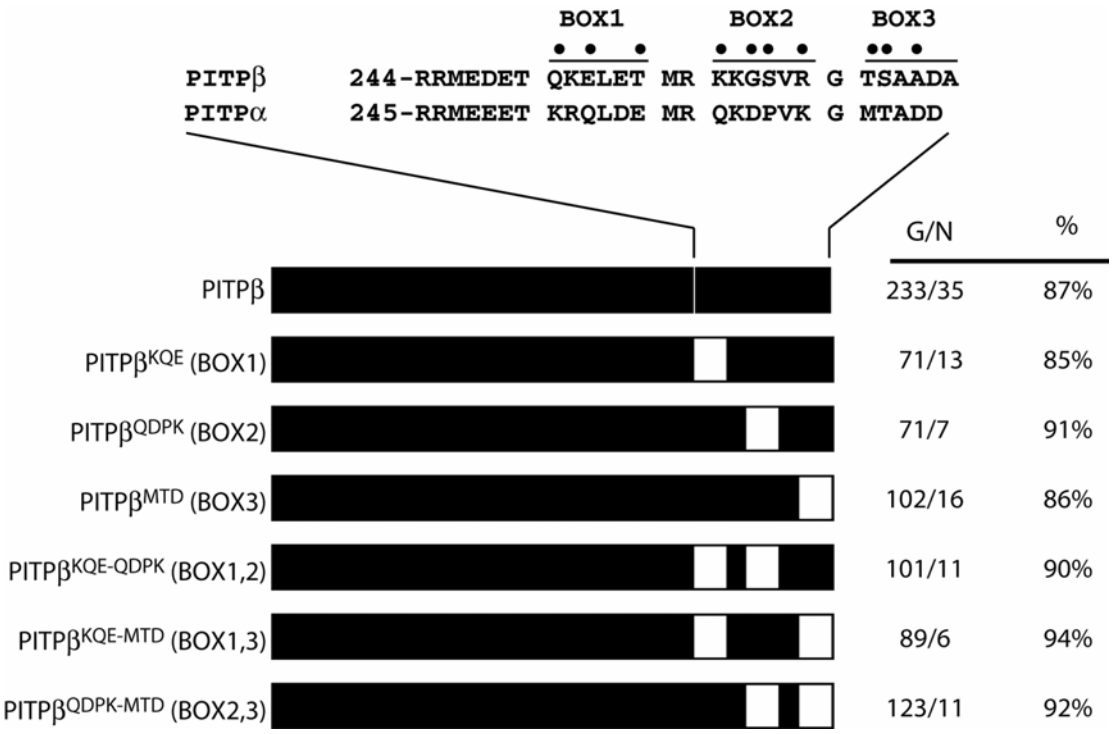

Figure 2.10 (Supplemental Figure 2) -C-terminal PITPβ localization elements necessary for TGN association. Alignment of the C-terminal 28 residues of PITPβ with the corresponding region of PITPα is given. The BOX motifs are shown at top. The most divergent residues within each are highlighted (•). Schematic illustrations of PITPα, PITPβ and each of the reciprocal C-terminal swaps are depicted at bottom. At right, for each corresponding PITP version, is given the number of imaged cells that exhibited a Golgi (G) or non-Golgi (N) immunofluorescence profile when that construct was expressed in COS-7 cells as a PITP-GFP chimera and visualized along with the GM130 marker. The percentage of imaged cells with Golgi profiles is also given.

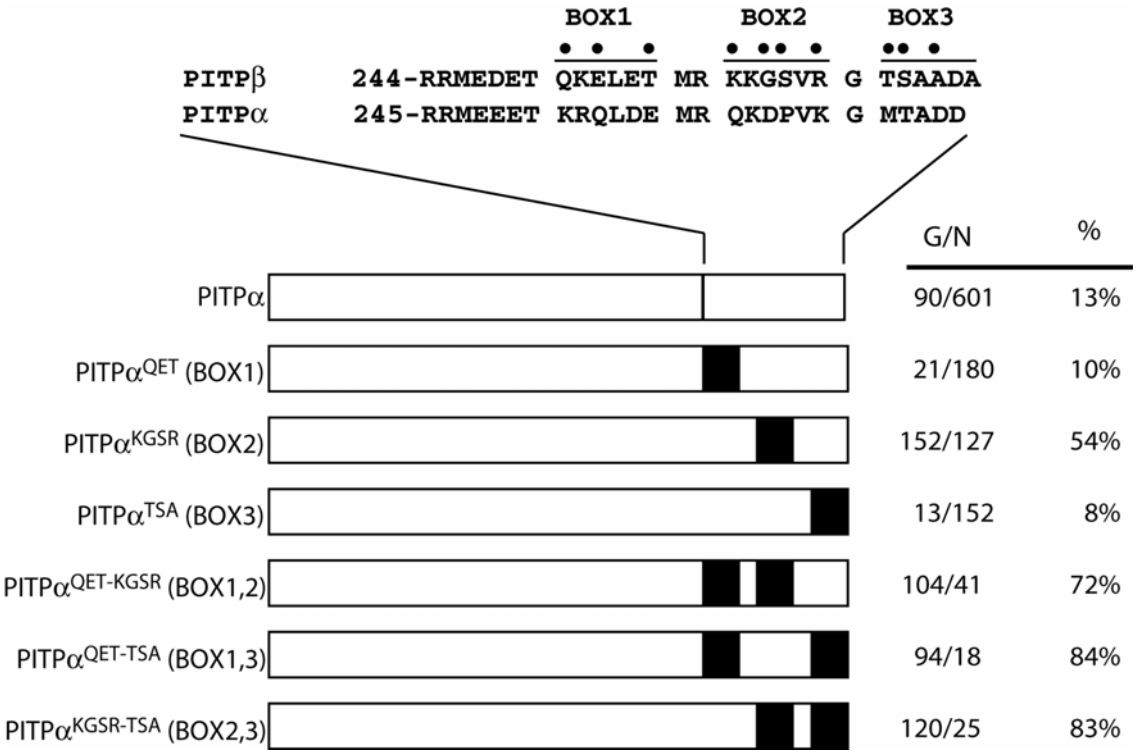

Figure 2.11 (Supplemental Figure 3) - C-terminal PITPβ localization elements sufficient for redirecting PITPα to TGN membranes. Swap series of divergent BOX motifs from PITPβ into the context of PITPα is shown. The most divergent residues within each are highlighted (•). The series of hybrid PITPs is illustrated and each swap is further defined at left by identification of which PITPβ residues were introduced to generate the swap. Quantification of COS-7 cells expressing each individual hybrid with respect to number of cells displaying Golgi (G) or non-Golgi (N) localization profile, along with percentages of cells displaying Golgi localization, is also given.

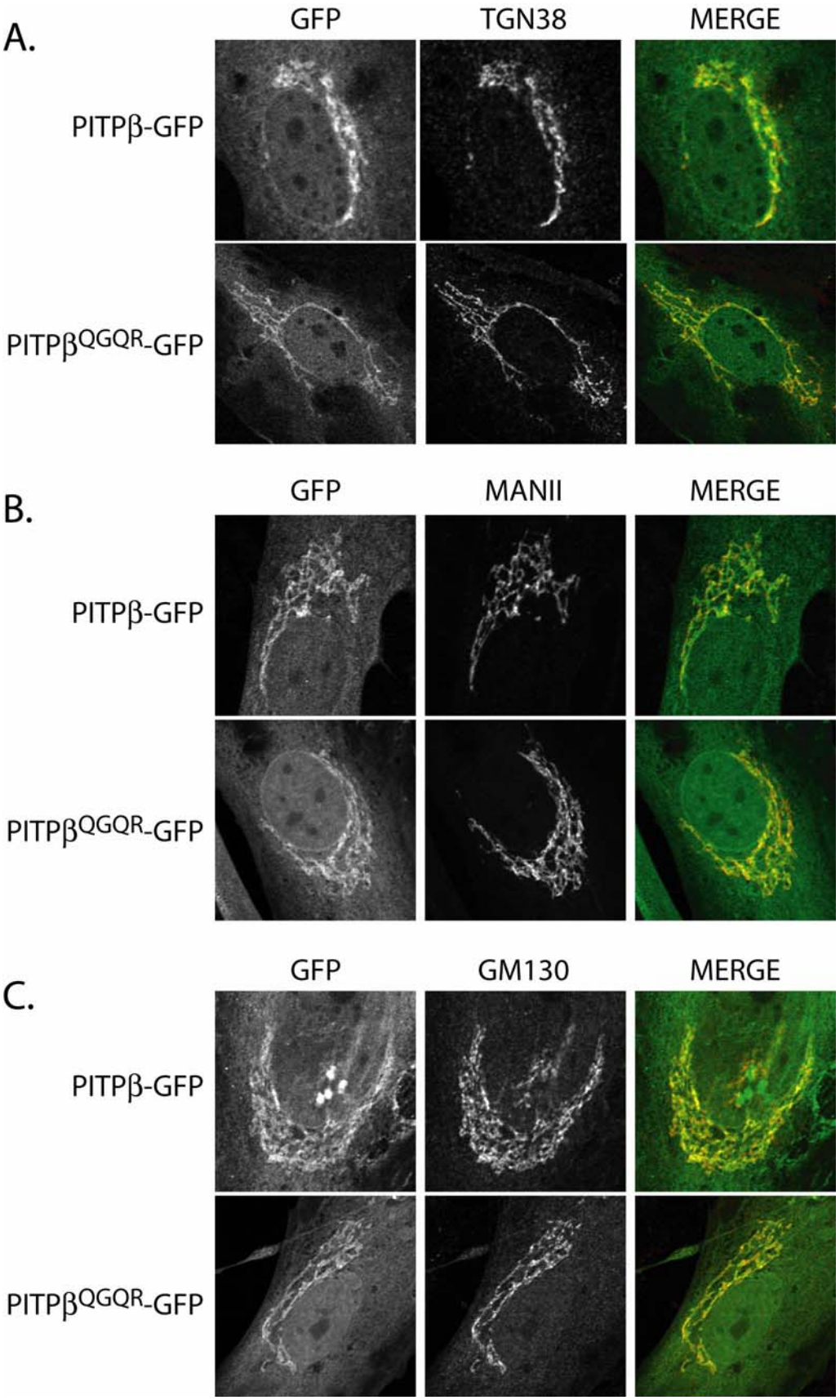
A.
GFP
TGN38
MERGE
PITPβ-GFP
PITPβQGQR-GFP
B.
GFP
MANII
MERGE
PITPβ-GFP
PITPβQGQR-GFP
C.
GFP
GM130
MERGE
PITPβ-GFP
PITPβQGQR-GFP

Figure 2.12 (Supplemental Figure 4; preceding page) - Comparison of PITPβ and PITPβQGQR localization in MEFs. PITPα nullizygous MEFs expressing PITPβ-GFP or PITPβ QGQR-GFP were fixed and decorated with primary antibodies directed against either the trans-Golgi marker TGN38 (A), the medial-Golgi marker mannosidase II (B) , or the cis-Golgi marker GM130 (C) . GFP-chimera localization was followed by intrinsic GFP fluorescence. The individual and merged profiles are identified.

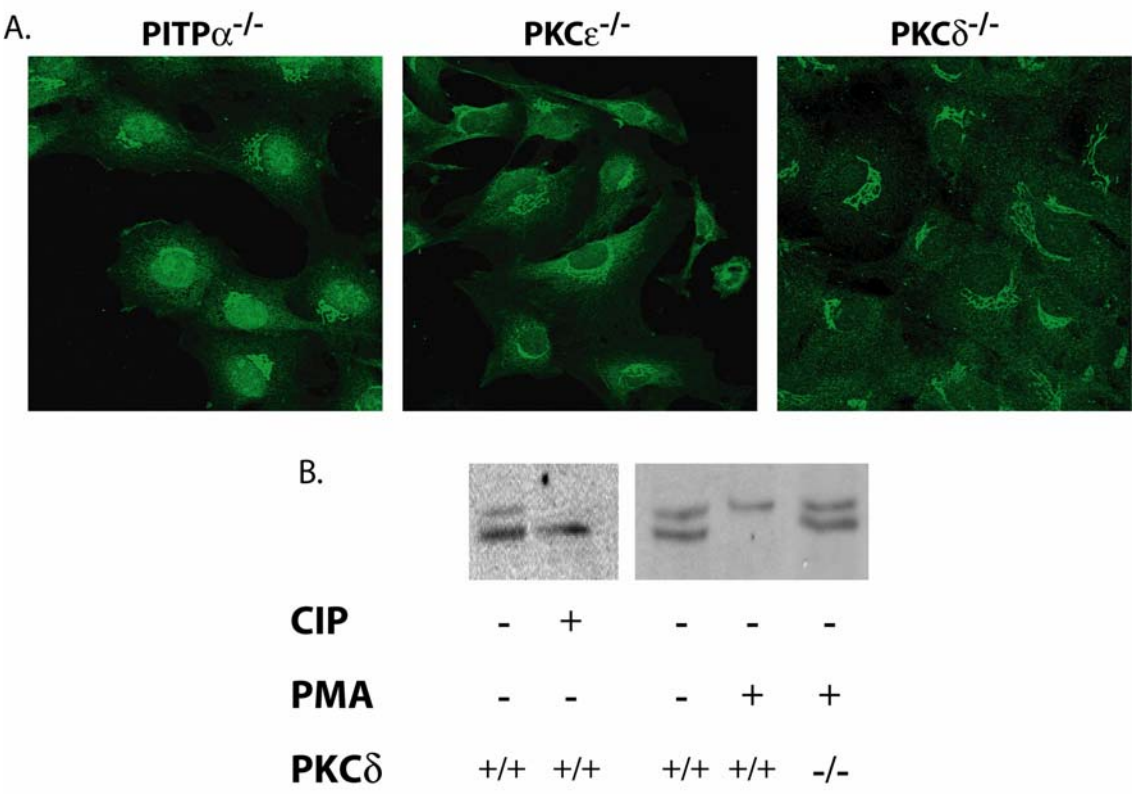

Figure 2.13 (Supplemental Figure 5) - PITPβ localization in PKCδ-/- MEFs. (A) Endogenous PITPβ profile of E16.5 PITPα-/- PKCε-/-, and PKCδ-/- MEFs, as indicated. The NT-PITP serum was employed in these experiments, and the PITPα-/- MEFs represent the positive control. In all cases essentially all cells exhibited a robust Golgi profile for endogenous PITPβ species. (B) PMA-induced phosphorylation of PITPβ is ablated in PKCδ-/- MEFs. Cell-free extracts from MEFs of indicated PKCδ genotype were generated, resolved by SDS-PAGE, transferred to nitrocellulose and developed with PITPβ-specific antibodies (PITPβ QGQR is not detected) and an ECL scheme. Instances where cells were treated with PMA (100nM; 15 min), or extracts were incubated with calf-intestine phosphatase (CIP), are identified at bottom. MEF PKCδ genotypes for each condition are also identified. PITPβ is a phosphoprotein as indicated by the collapse of the PITPβ doublet to the lower apparent molecular mass form upon treatment of lysates

with CIP, and by the complete conversion of the PITPβ doublet to the higher apparent molecular mass form by treatment of cells with PMA. This PMA effect is not observed in PKCδ-/- MEFs, although the PITPβ doublet is maintained.

	G/N	%
PITPβ	233/35	87%
PITPα	90/511	13%
PITPβ^{S262A}	181/38	79%
PITPβ^{S262D}	162/41	80%
PITPβ^{S262E}	102/22	71%
PITPβ^{S262P}	330/42	88%
PITPα^{P263S}	164/614	21%
PITPα^{P263E}	156/567	22%

Table 2.1 (Supplemental Table 1) - Summary of effect of missense substitutions on PITP localization in COS-7 cells. Quantification of COS-7 cells expressing each indicated mutant form of PITPβ-GFP and PITPα-GFP with respect to number of cells displaying Golgi (G) or non-Golgi (N) localization profile. Corresponding percentages of cells displaying Golgi localization is also given.

References

Alb, J.G., Jr., Cortese, J.D., Phillips, S.E., Albin, R.L., Nagy, T.R., Hamilton, B.A., and Bankaitis, V.A. (2003). Mice lacking phosphatidylinositol transfer protein-alpha exhibit spinocerebellar degeneration, intestinal and hepatic steatosis, and hypoglycemia. J Biol Chem *278*, 33501-33518.

Alb, J.G., Jr., Gedvilaite, A., Cartee, R.T., Skinner, H.B., and Bankaitis, V.A. (1995). Mutant rat phosphatidylinositol/phosphatidylcholine transfer proteins specifically defective in phosphatidylinositol transfer: implications for the regulation of phospholipid transfer activity. Proc Natl Acad Sci U S A *92*, 8826-8830.

Alb, J.G., Jr., Phillips, S.E., Rostand, K., Cui, X., Pinxteren, J., Cotlin, L., Manning, T., Guo, S., York, J.D., Sontheimer, H., Collawn, J.F., and Bankaitis, V.A. (2002). Genetic ablation of phosphatidylinositol transfer protein function in murine embryonic stem cells. Mol Biol Cell *13*, 739-754.

Bankaitis, V.A. (2002). Cell biology. Slick recruitment to the Golgi. Science *295*, 290-291.

Bankaitis, V.A., Aitken, J.R., Cleves, A.E., and Dowhan, W. (1990). An essential role for a phospholipid transfer protein in yeast Golgi function. Nature *347*, 561-562.

Bankaitis, V.A., Malehorn, D.E., Emr, S.D., and Greene, R. (1989). The Saccharomyces cerevisiae SEC14 gene encodes a cytosolic factor that is required for transport of secretory proteins from the yeast Golgi complex. J Cell Biol *108*, 1271-1281.

Cleves, A., McGee, T., and Bankaitis, V. (1991a). Phospholipid transfer proteins: a biological debut. Trends Cell Biol *1*, 30-34.

Cleves, A.E., McGee, T.P., Whitters, E.A., Champion, K.M., Aitken, J.R., Dowhan, W., Goebl, M., and Bankaitis, V.A. (1991b). Mutations in the CDP-choline pathway for phospholipid biosynthesis bypass the requirement for an essential phospholipid transfer protein. Cell *64*, 789-800.

Cunningham, E., Tan, S.K., Swigart, P., Hsuan, J., Bankaitis, V., and Cockcroft, S. (1996). The yeast and mammalian isoforms of phosphatidylinositol transfer protein can all restore phospholipase C-mediated inositol lipid signaling in cytosol-depleted RBL-2H3 and HL-60 cells. Proc Natl Acad Sci U S A *93*, 6589-6593.

De Camilli, P., Emr, S.D., McPherson, P.S., and Novick, P. (1996). Phosphoinositides as regulators in membrane traffic. Science *271*, 1533-1539.

de Vries, K.J., Heinrichs, A.A., Cunningham, E., Brunink, F., Westerman, J., Somerharju, P.J., Cockcroft, S., Wirtz, K.W., and Snoek, G.T. (1995). An isoform of the

phosphatidylinositol-transfer protein transfers sphingomyelin and is associated with the Golgi system. Biochem J *310 (Pt 2)*, 643-649.

De Vries, K.J., Westerman, J., Bastiaens, P.I., Jovin, T.M., Wirtz, K.W., and Snoek, G.T. (1996). Fluorescently labeled phosphatidylinositol transfer protein isoforms (alpha and beta), microinjected into fetal bovine heart endothelial cells, are targeted to distinct intracellular sites. Exp Cell Res *227*, 33-39.

Fullwood, Y., dos Santos, M., and Hsuan, J.J. (1999). Cloning and characterization of a novel human phosphatidylinositol transfer protein, rdgBbeta. J Biol Chem *274*, 31553-31558.

Futerman, A.H., Stieger, B., Hubbard, A.L., and Pagano, R.E. (1990). Sphingomyelin synthesis in rat liver occurs predominantly at the cis and medial cisternae of the Golgi apparatus. J Biol Chem *265*, 8650-8657.

Hay, J.C., and Martin, T.F. (1993). Phosphatidylinositol transfer protein required for ATP-dependent priming of Ca(2+)-activated secretion. Nature *366*, 572-575.

Ito, H., Fukuda, Y., Murata, K., and Kimura, A. (1983). Transformation of intact yeast cells treated with alkali cations. J. Bacteriol. *153*, 163-168.

Jones, S.M., Alb, J.G., Jr., Phillips, S.E., Bankaitis, V.A., and Howell, K.E. (1998). A phosphatidylinositol 3-kinase and phosphatidylinositol transfer protein act synergistically in formation of constitutive transport vesicles from the trans-Golgi network. J Biol Chem *273*, 10349-10354.

Kearns, B.G., McGee, T.P., Mayinger, P., Gedvilaite, A., Phillips, S.E., Kagiwada, S., and Bankaitis, V.A. (1997). Essential role for diacylglycerol in protein transport from the yeast Golgi complex. Nature *387*, 101-105.

Kearns, M.A., Monks, D.E., Fang, M., Rivas, M.P., Courtney, P.D., Chen, J., Prestwich, G.D., Theibert, A.B., Dewey, R.E., and Bankaitis, V.A. (1998). Novel developmentally regulated phosphoinositide binding proteins from soybean whose expression bypasses the requirement for an essential phosphatidylinositol transfer protein in yeast. Embo J *17*, 4004-4017.

Lehel, C., Olah, Z., Jakab, G., and Anderson, W.B. (1995). Protein kinase C epsilon is localized to the Golgi via its zinc-finger domain and modulates Golgi function. Proc Natl Acad Sci U S A *92*, 1406-1410.

Li, X., Routt, S.M., Xie, Z., Cui, X., Fang, M., Kearns, M.A., Bard, M., Kirsch, D.R., and Bankaitis, V.A. (2000). Identification of a novel family of nonclassic yeast phosphatidylinositol transfer proteins whose function modulates phospholipase D activity and Sec14p-independent cell growth. Mol Biol Cell *11*, 1989-2005.

Litvak, V., Dahan, N., Ramachandran, S., Sabanay, H., and Lev, S. (2005). Maintenance of the diacylglycerol level in the Golgi apparatus by the Nir2 protein is critical for Golgi secretory function. Nat Cell Biol *7*, 225-234.

Lopez, M.C., Nicaud, J.M., Skinner, H.B., Vergnolle, C., Kader, J.C., Bankaitis, V.A., and Gaillardin, C. (1994). A phosphatidylinositol/phosphatidylcholine transfer protein is required for differentiation of the dimorphic yeast Yarrowia lipolytica from the yeast to the mycelial form. J Cell Biol *125*, 113-127.

Nakase, Y., Nakamura, T., Hirata, A., Routt, S.M., Skinner, H.B., Bankaitis, V.A., and Shimoda, C. (2001). The Schizosaccharomyces pombe spo20(+) gene encoding a homologue of Saccharomyces cerevisiae Sec14 plays an important role in forespore membrane formation. Mol Biol Cell *12*, 901-917.

Ohashi, M., Jan de Vries, K., Frank, R., Snoek, G., Bankaitis, V., Wirtz, K., and Huttner, W.B. (1995). A role for phosphatidylinositol transfer protein in secretory vesicle formation. Nature *377*, 544-547.

Phillips, S.E., Sha, B., Topalof, L., Xie, Z., Alb, J.G., Klenchin, V.A., Swigart, P., Cockcroft, S., Martin, T.F., Luo, M., and Bankaitis, V.A. (1999). Yeast Sec14p deficient in phosphatidylinositol transfer activity is functional in vivo. Mol Cell *4*, 187-197.

Phillips, S.E., Vincent, P., Rizzieri, K.E., Schaaf, G., Bankaitis, V.A., and Gaucher, E.A. (2006). The diverse biological functions of phosphatidylinositol transfer proteins in eukaryotes. Crit Rev Biochem Mol Biol *41*, 21-49.

Routt, S.M., and Bankaitis, V.A. (2004). Biological functions of phosphatidylinositol transfer proteins. Biochem Cell Biol *82*, 254-262.

Schouten, A., Agianian, B., Westerman, J., Kroon, J., Wirtz, K.W., and Gros, P. (2002). Structure of apo-phosphatidylinositol transfer protein alpha provides insight into membrane association. Embo J *21*, 2117-2121.

Sha, B., Phillips, S.E., Bankaitis, V.A., and Luo, M. (1998). Crystal structure of the Saccharomyces cerevisiae phosphatidylinositol-transfer protein. Nature *391*, 506-510.

Sherman, F.F.G.R., Hicks J. B. (1983). Methods in Yeast Genetics. Cold Spring Harbor Laboratory Press: Cold Spring Harbor, NY.

Simonsen, A., Wurmser, A.E., Emr, S.D., and Stenmark, H. (2001). The role of phosphoinositides in membrane transport. Curr Opin Cell Biol *13*, 485-492.

Skinner, H.B., Alb, J.G., Jr., Whitters, E.A., Helmkamp, G.M., Jr., and Bankaitis, V.A. (1993). Phospholipid transfer activity is relevant to but not sufficient for the essential function of the yeast SEC14 gene product. Embo J *12*, 4775-4784.

Storz, P., Doppler, H., and Toker, A. (2004). Protein kinase Cdelta selectively regulates protein kinase D-dependent activation of NF-kappaB in oxidative stress signaling. Mol Cell Biol *24*, 2614-2626.

Tanaka, S., and Hosaka, K. (1994). Cloning of a cDNA encoding a second phosphatidylinositol transfer protein of rat brain by complementation of the yeast sec14 mutation. J Biochem *115*, 981-984.

Tilley, S.J., Skippen, A., Murray-Rust, J., Swigart, P.M., Stewart, A., Morgan, C.P., Cockcroft, S., and McDonald, N.Q. (2004). Structure-function analysis of human [corrected] phosphatidylinositol transfer protein alpha bound to phosphatidylinositol. Structure *12*, 317-326.

van Tiel, C.M., Westerman, J., Paasman, M., Wirtz, K.W., and Snoek, G.T. (2000). The protein kinase C-dependent phosphorylation of serine 166 is controlled by the phospholipid species bound to the phosphatidylinositol transfer protein alpha. J Biol Chem *275*, 21532-21538.

van Tiel, C.M., Westerman, J., Paasman, M.A., Hoebens, M.M., Wirtz, K.W., and Snoek, G.T. (2002). The Golgi localization of phosphatidylinositol transfer protein beta requires the protein kinase C-dependent phosphorylation of serine 262 and is essential for maintaining plasma membrane sphingomyelin levels. J Biol Chem *277*, 22447-22452.

Vincent, P., Chua, M., Nogue, F., Fairbrother, A., Mekeel, H., Xu, Y., Allen, N., Bibikova, T.N., Gilroy, S., and Bankaitis, V.A. (2005). A Sec14p-nodulin domain phosphatidylinositol transfer protein polarizes membrane growth of Arabidopsis thaliana root hairs. J Cell Biol *168*, 801-812.

Yoder, M.D., Thomas, L.M., Tremblay, J.M., Oliver, R.L., Yarbrough, L.R., and Helmkamp, G.M., Jr. (2001). Structure of a multifunctional protein. Mammalian phosphatidylinositol transfer protein complexed with phosphatidylcholine. J Biol Chem *276*, 9246-9252.

Chapter 3

siRNA mediated knockdown of PITPβ

Abstract

Phosphatidylinositol transfer proteins (PITPs) are a family of proteins that act at the interface of lipid metabolism and membrane trafficking. Some members of the family act in specialized cell types, while others are required for general cell maintenance. In mammals, the closely related PITPs PITPα and PITPβ are known to have distinct functions, and knockout mouse studies have revealed roles for PITPα in brain, intestine, and liver function. The cellular role for PITPβ, however, is not known. Attempts to make PITPβ knockout mice have been unsuccessful, suggesting that PITPβ is an essential protein. In this chapter, I used siRNA-mediated gene silencing to address the role of PITPβ in human cell lines. Treatment of HeLa or HEK293 cells resulted in a 40-70% reduction in PITPβ RNA levels, and the reduction in PITPβ RNA levels was accompanied by a disorganization of the Golgi network. Though PITPβ localizes specifically to the trans-Golgi network, the Golgi disorganization manifested itself at all levels of the Golgi. Changes in Golgi morphology are often associated with trafficking defects, so we assessed the anterograde and retrograde trafficking in PITPβ siRNA-treated cells. Anterograde trafficking, as measured by a glycosaminoglycan labeling assay, was delayed, but retrograde trafficking was unaffected in PITPβ siRNA-treated cells. The siRNA-mediated knockdown of PITPβ reveals a cellular function for PITPβ,

and provides a system to better understand the critical features and mechanism of action of the protein.

Introduction

Protein trafficking through the ER and Golgi of cells is a coordinated process regulated by a number of proteins and lipids. Proteins such as SNAREs, Rabs, and ARFs recruit cargo and promote vesicle curvature. Lipids such as diacylglycerol (DAG) and phosphoinositides play crucial roles in both the physical aspect of vesicle formation and in protein recruitment. DAG is a conical lipid that promotes vesicle budding and recruits Golgi signaling proteins (Baron and Malhotra, 2002; Dries *et al.*, 2007). PtdIns(4)P is enriched in the Golgi, and is required for both the activity of the ARF-GEFs such as the yeast Gcs1 (Yanagisawa *et al.*, 2002), and the recruitment of proteins necessary for vesicle formation and cargo assembly (D'Angelo *et al.*, 2008).

Phosphatidylinositol (PtdIns)/phosphatidylcholine (PtdCho) transfer proteins (PITPs) stand at the interface of phosphoinositide signaling and membrane trafficking and are defined by their *in vitro* ability to transfer PtdCho and PtdIns between membrane bilayers in an energy independent fashion. *In vivo* they possess diverse yet unique trafficking roles. Some PITPs are required for the function of very specialized cell types. For example, the plant PITP AtSfh1 regulates PtdIns(4,5)P_2 homeostasis in growing root hairs by establishing tip-localized PtdIns(4,5)P_2 landmarks, and is required to allow polarized trafficking in these cells. Loss of AtSfh1 leads to a loss of polarity as indicated by a breakdown of tip-localized Ca^{2+}-influx, a dramatic rearrangement of the cytoskeleton and short, sometimes multi-tipped root hairs (Vincent *et al.*, 2005). The Drosophila RdgB protein, which contains an essential PITP domain, is necessary for

proper termination of the light response in the eye (Milligan *et al.*, 1997). The importance of the PITP domain is emphasized by the fact that the PITP domain alone can rescue the retinal degeneration phenotype.

Other PITPs are required for cellular survival and thus carry important house keeping functions, such as regulation of Golgi lipids. Sec14, the major yeast PITP, is required for the formation of secretory vesicles at the *trans*-Golgi network (TGN) through regulation of PtdIns(4)P and DAG and it regulates turnover of complex sphingolipids in endosomes (Cleves *et al.*, 1991; Kearns *et al.*, 1997; Nemoto *et al.*, 2000; Mousley *et al.*, 2008; Schaaf *et al.*, 2008). Phospholipid-bound structures that were recently solved at high resolution suggest that Sec14 regulates phosphoinositide homeostasis by mediating a lipid exchange reaction of PtdIns versus PtdCho at the TGN (and potentially other) membranes. Functional studies indicate that during this exchange reaction, Sec14 renders PtdIns a better substrate for phosphorylation by a PtdIns 4-OH kinase and thereby overcomes an intrinsic substrate unavailability of membrane-bound PtdIns to PtdIns-kinases (Schaaf *et al.*, 2008). This model of Sec14 as a platform for lipid exchange is very much in agreement with a model of PITPs as nanoreactors (Ile *et al.*, 2006), where nanoreactors are defined as platforms that integrate diverse phospholipid signaling pathways and present a defined lipid pool. In the case of Sec14, the nanoreactor presents Golgi-localized PtdIns to a downstream lipid-modifying enzyme. An important aspect of the nanoreactor concept is that the integration of a phospholipid signaling event and the presentation of a specific phospholipid to a phospholipid metabolic enzyme results in an organized assembly of phospholipid product as suggested

by the presence of specific lipid-binding domains in addition to the PITP domain in multidomain PITPs (Ile et al., 2006).

Interestingly, besides the Sec14 proteins, metazoan genomes encode non-sequence related PITPs with *in vitro* properties that are almost identical to Sec14 (proteins). Mammals express five metazoan PITPs with yet largely unidentified cellular functions (Phillips *et al.*, 2006). One member of this family, the membrane bound PITP Nir2, was proposed to have orthologous functions to Sec14 and is also required for regulation of DAG levels via the PC synthesis pathway and Golgi trafficking (Litvak *et al.*, 2005). PITPα, a soluble representative of this family, is found in the cytosol and nucleus of the cell and is not required for cell survival, though nullizygous PITPα mice die by two weeks past birth (Alb *et al.*, 2003).

Another soluble PITP, PITPβ, is understudied, yet what is known suggests that the protein plays a critical role in cells (Alb *et al.*, 2002). PITPβ is localized to the trans-Golgi network and, in addition to the *in vitro* transfer functions for PtdIns and PtdCho, PITPβ can transfer sphingomyelin (SM). In the present study we aimed to understand the cellular function of PITPβ as a prototype of soluble metazoan PITPs and potential key player in membrane trafficking. Because of its TGN localization and potential housekeeping role in cells, we hypothesized that PITPβ would be required for membrane trafficking to or from the TGN, and addressed this question by siRNA-mediated knockdown of PITPβ. We demonstrate that PITPβ is required for cell survival. The loss of PITPβ causes a dispersal of the Golgi network, although Golgi associated proteins remain associated with the dispersed Golgi. At the EM level, the Golgi phenotype manifests as swollen Golgi stacks, suggesting the accumulation of cargo. A trafficking

delay in PITPβ-depleted cells was demonstrated by the delayed secretion of pulse labeled glycans. These discoveries report a new layers of complexity on how trafficking from the Golgi might be regulated in metazoan cells.

Materials and Methods

Cell culture and siRNA treatment

siRNA studies were performed in HeLa, HEK293ad, or immortalized mouse embryo fibroblast (iMEF) cells grown in DMEM supplemented with 10% FBS, 100 μg/ml penicillin, and 100 μg/ml streptomycin. Three siRNAs against the human PITPβ were designed and synthesized by Ambion (Austin, TX). The sequences of the sense strands of these siRNAs are:

siRNA #1: 5' GCAUUAUUCCAGUCAGUCAtt 3'

siRNA #2: 5' GCUAGUAAGAAUGAGACUGtt 3'

siRNA #3: 5' CCAGACUUGGGAACAUUAGtt 3'

The antisense strands were complementary to the uppercase portion of the siRNA listed above, with an additional two nucleotide overhang at the 3' end.

Four siRNAs against the mouse PITPβ were designed and synthesized by Dharmacon (Thermo Scientific). The target sequence of these siRNAs are:

mouse siRNA #1: 5' GCAGAACAAUUGUAACGAA 3'

mouse siRNA #2: 5' CUACAAAGCUGAUGAAGAC 3'

mouse siRNA #3: 5' UAAGAAGGGUUCCGUCCGA 3'

mouse siRNA #4: 5' CAUUGCAGAUCGAAGUCAA 3'

siRNA treatment of cells was performed according to the protocol for the Lipofectamine 2000 reagent (Invitrogen, Carlsbad, CA). Cells were plated at

approximately 70% confluence in 24 well plates the day before siRNA transfection. On the day of transfection, 1 μL of Lipofectamine 2000 was added to a tube containing 50 μL OptiMEM, and 1.5 μL of 20 μM siRNA was added to another aliquot of 50 μL OptiMEM. After 5 minutes, these tubes were mixed and incubated at room temperature for 30 minutes. Cells were washed once in OptiMEM and the Lipofectamine/siRNA mixture was added, along with an additional 100 μL OptiMEM. After 6-8 hours, the media was changed to complete DMEM media.

Brefeldin A (BFA) treatment was performed 2 days after siRNA treatment by replacing the culture media with complete media plus 10 μg/mL BFA for the indicated times. Following BFA treatment, cells were immediately washed, fixed, and stained as described below.

Immunofluorescence

After treatment with siRNA, cells were prepared for immunofluoresence as follows. First, cells were fixed in 3.7% formaldehyde for 12 minutes. Cells were then permeabilized with 0.2% Triton X-100 for 4 minutes, washed, and blocked with 2% BSA in PBS. Primary antibody was diluted into 2% BSA/PBS at the following dilutions: gm130- 1:400, TGN46- 1:200, COPII- 1:200, Orp9- 1:2000. DAPI and appropriate fluorescent-conjugated secondary antibodies were ordered from Invitrogen and used at 1:1000.

Cells were imaged on an inverted confocal microscope (model 510 meta; Carl Zeiss MicroImaging, Inc.; 63× C-Apochromat 1.2 oil immersion lens). Images were processed using the Adobe Photoshop CS2 software.

Protein trafficking assays

Glycosaminoglycan release assays were performed as described in Litvak et al (Litvak *et al.*, 2005). Briefly, control or PITPβ siRNA-treated cells were washed in buffer A (125 mM NaCl, 5 mM KCl, 5.6 mM glucose, 20 mM Hepes-NaOH, pH7.2, 1.8 mM $CaCl_2$, and 1.8 mM MgCl) and incubated with 1 mM xyloside in buffer A for 15 minutes at 37ºC. Cells were labeled with ^{35}S sulfate (80 μCi/mL) for 5 minutes at 37ºC, washed with serum-free DMEM, and incubated (chased) with cold medium for various periods of time. The cell media was collected and centrifuged at 12,000 x g for 10 minutes to remove cells and debris. To lyse the cells, the monolayers were treated with 0.1M NaOH for 1 hour at 37ºC. Glycosaminoglycans were precipitated from cells and cell media by incubation with 0.6% condroitin sulphate and 1% cetylpyridinium chloride for 12 hours at room temperature. Samples were spun down at 3000 x g and pellets were washed twice in 1% cetylpyridinium chloride in 20 mM NaCl. Pellets were dissolved in 2M NaCl and counted in a scintillation counter. The data is expressed as the ratio of the 35S-glycosamines in the supernatant to the total 35S-glycosamines (cell pellet plus supernatant).

EM

Mock and PITPβ siRNA-treated cells were washed, trypsinized, and centrifuged, and the pellets were washed 3 x 10 minutes in 3% glutaraldehyde in sodium cacodylate buffer (0.1M sodium cacodylate, 2mM CaCl2, pH 7.4). The cells were fixed by a 1 hour incubation in 1% OsO4 in sodium cacodylate buffer. The cell pellet was washed 3 x 10 min in sodium cacodylate buffer and incubated for 30 minutes in the dark in 2% uranylacetate/50% ethanol. Sequential dehydration was performed by 10 minute washes in increasing ethanol concentrations (50%, 70%, 80%, 90%, 95%, 100%). After

dehydration, pellets were incubated for 30 minutes with acetone, 1 hour with 1:1 acetone/Polybed 812 (Polysciences Inc., Warrington, PA), and 24 hours with Polybed 812. Pellets were then transferred to fresh Polybed 812 and baked at 60ºC for 48 hours.

Sections were cut by an ultramicrotome, placed on 100 μm copper grids, and counterstained with Reynold's Lead Citrate (8 mM $Pb(NO_3)_2$, 0.12 M sodium citrate, 0.16 M NaOH). Sections were examined at 80kV on an FEI Tecnai 12 electron microscope TEM and images were captured using Gatan micrograph 3.9.3 software.

Cloning of lipid sensors

A lipid sensor for PI levels was described previously (Liu *et al.*, 2008). A DAG sensor was constructed by cloning the cysteine rich domain (CRD) of PKD (aas 1-355) (Rey and Rozengurt, 2001) into pEGFP-C2 using a forward XhoI primer and a reverse HindIII primer.

Results

siRNAs reduce PITPβ levels in human and mouse cell lines

Previous studies of PITPβ in mouse have indicated a clear role for the protein in embryonic development: matings of PITPβ heterozygous mice yielded no live homozygous knockouts (Alb *et al.*, 2002). Indirect results in ES cells suggested an essential housekeeping role of PITPβ (Alb *et al.*, 2002). However, currently there is nothing known about the specific function of PITPβ in mammalian cells. To study the function of PITPβ in mammalian cells, we used siRNA to knock down gene expression.

Three siRNAs against human PITPβ were designed by the Ambion algorithm and targeted exons 8, 3 and 6 (by siRNA #1, 2, and 3, respectively). As an initial test of the

efficacy of the siRNAs, RT-PCR was performed on siRNA-treated HEK293Ad and HeLa cells. Cells were treated with mock or PITPβ siRNA, and RNA was collected about 52 hours after treatment. In both HeLa and HEK293Ad, all three siRNAs were capable of significantly reducing PITPβ levels, knocking down RNA levels of PITPβ by about 40 to 70 % (Figure 1a).

As an additional model for PITPβ knockdown, siRNAs were designed against the mouse PITPβ. The siRNAs targeted different exons than the human siRNAs (exons 4/5, 8, 11, and 7 for siRNA 1-4 respectively). The mouse siRNAs were tested in immortalized mouse embryo fibroblasts (iMEFs) using the same conditions used for the human siRNA. RT-PCR of siRNA-treated iMEFs showed that the siRNAs did not reduce PITPβ mRNA levels as effectively as the human system, however one of the four siRNAs (mouse siRNA #4) did reduce PITPβ levels by about 30-40 % (Figure 1a). The reduced efficacy of the siRNAs could be due to the siRNA sequences being less effective against PITPβ, or the iMEFs could be less responsive than the human cell lines to siRNA treatment.

Because the siRNAs were more effective in human cell types, we focused on HeLa and HEK293Ad cells, and examined the effect of the siRNAs on protein levels by Western blot. Protein was collected 52 hours after siRNA treatment, separated by SDS-PAGE, and transferred to nitrocellulose by western transfer. The nitrocellulose blot was probed with a PITPβ antibody and a GAPDH antibody for normalization. PITPβ protein levels were found to be reduced by about 50% relative to GAPDH in HeLa cells that had been treated with either mock or PITPβ siRNA #1, #2, or #3 (Figure 1b). Thus, the treatment with siRNAs leads to a decrease in both mRNA and protein levels of PITPβ.

Loss of PITPβ leads to cell death

Previous studies using mouse as a model suggested that PITPβ could be an essential housekeeping protein (Alb *et al.*, 2002). Therefore, we first assessed whether reduction in PITPβ levels affected cell survival. Identification of live cells within a cell population can be determined using trypan blue exclusion, as only dead cells can be stained with the dye. Using this method, live cells were counted after siRNA treatment. Significant cell death was observed at 2 days after treatment, and few cells survived to 3 days after siRNA (Figure 1c), corroborating previous studies suggesting that PITPβ has an essential activity in mammalian cells.

Cells with reduced PITPβ levels have dispersed Golgi structures

PITPs in several different species have essential roles and are localized at the Golgi network, including the yeast protein Sec14p (Bankaitis *et al.*, 1989), the Drosophila protein vib (giotto) (Gatt and Glover, 2006; Giansanti *et al.*, 2006), and the mammalian protein Nir2 (Litvak *et al.*, 2005). All of these proteins are thought to be essential for regulating phospholipid homeostasis at membrane sites that are competent for the formation of secretory vesicles. Disregulation of lipids at the Golgi often leads to Golgi morphological changes and trafficking defects. Thus, we hypothesized that PITPβ could also play a role in regulation of Golgi phospholipids and trafficking. As an initial test of whether PITPβ might have an effect on Golgi function, the Golgi morphology was examined in PITPβ siRNA-treated cells.

Since PITPβ is localized to the trans-Golgi network (TGN), the TGN was examined for morphological changes by immunofluorescence. Initial studies were performed with siRNA #2, which had the greatest effect on RNA levels in HEK293Ad

and HeLa cells (Figure 1a). Staining with the TGN marker TGN46 showed that, while mock siRNA-treated cells often had a small, compact Golgi, the PITPβ siRNA #2-treated cells had a more dispersed or "relaxed" trans-Golgi. This phenotype was seen in both HeLa cells, and, more dramatically, in HEK293Ad (Figure 2a).

The Golgi is composed of *cis*, *medial* and *trans* stacks that are decorated with distinct proteins. A defect in the *trans*-Golgi stack is not necessarily seen in the *cis* or *medial* Golgi. Therefore, we examined whether the defect was specific to the trans-Golgi, or whether other Golgi compartments were affected. Staining of the cells with the cis-Golgi marker gm130 revealed that the cis-Golgi, like the trans-Golgi, was more dispersed in PITPβ siRNA-treated cells. The cis-Golgi marker continued to localize in very close proximity with the trans-Golgi marker in cells with a dispersed Golgi, indicating that Golgi stacks themselves are not disrupted. Thus, despite the fact that PITPβ is localized to the trans-Golgi, the loss of PITPβ affects the morphology of all levels of the Golgi stack.

As a quantitative assessment of the Golgi phenotype, the Golgi dispersal phenotype upon PITPβ knockdown was scored. HeLa cells were treated with mock and PITPβ siRNAs, fixed, and stained with Golgi (anti-gm130) and nuclear (DAPI) markers. Images from slides of mock and PITPβ siRNA-treated cells were taken at random, and the images were blinded. Cells in each image were classified as having a "tight", "moderately dispersed", or "severely dispersed" Golgi. For each siRNA condition, at least 245 cells were counted.

The clear effect of PITPβ on the Golgi was evident from the compiled cell counts. For siRNA #2, which had the greatest effect on mRNA levels, we also saw the most

dramatic increase in "severely dispersed" Golgi, and a concomitant decrease in cells with "compact" Golgi apparati. In HEK293Ad cells, the altered Golgi morphology was seen with all three PITPβ siRNAs, while in HeLa cells, only siRNAs #2 and #3 caused the increase in dispersed Golgi in agreement with a somewhat attenuated effect of siRNA #1 on mRNA levels in these cells. The effect of the siRNAs was much stronger in HEK293Ad, suggesting that these cells are more sensitive to loss of PITPβ or that silencing was more effective (Figure 2b).

The Golgi phenotype was also examined in iMEFs treated with the mouse siRNAs. The dispersed Golgi phenotype was seen only with mouse siRNA #4, and as expected by the weaker reduction in PITPβ levels, the phenotype was also much less severe than in the human cell types. These results indicate that the phenotype is not cell, species, or siRNA-specific. Further, the correlation between level of PITPβ message reduction and severity of phenotype supports a dose-dependent role for PITPβ in maintaining the integrity of the Golgi.

The Golgi morphology changes seen by immunofluorescence indicated a role of PITPβ in Golgi organization. The Golgi organizational defect was further characterized by ultra thin section electron microscopy. The Golgi apparatus in wild type cells is easily identified by its proximity to the nucleus and its distinctive cisternal stacks. The mock siRNA-treated cells had Golgi apparati that appeared normal, but in the PITPβ siRNA-treated cells, the Golgi were distended. Consistent with the immunofluorescence, the distension occurred at the cis, medial, and trans levels of the Golgi (Figure 2c).

Transport from TGN is delayed in PITPβ-depleted cells

Golgi defects seen by immunofluorescence and EM, particularly the swollen cisternae, are generally hallmarks of a block or delay in protein transport that results in cargo buildup in the Golgi, (Liljedahl *et al.*, 2001; Godi *et al.*, 2004; Litvak *et al.*, 2005). Bulk transport through the Golgi was assessed by tracking the secretion of labeled glycosaminoglycans. Mock and PITPβ siRNA-treated cells were incubated with xyloside, a glycosaminoglycan acceptor and pulsed with ^{35}S-sulphate which will be incorporated into the glycosaminoglycan modifications. Trafficking is measured at various time points after chase with unlabeled sulphate. At 20 minutes of chase, PITPβ siRNA –treated cells exhibited more than a 2-fold decrease in the release of labeled glycosaminoglycans. In contrast, after 40 minutes of chase, mock and PITPβ siRNA-treated cells had equivalent amounts of released glycosaminoglycans (Figure 3). The trafficking delay (albeit not complete block in trafficking) caused by knockdown of PITPβ could indicate that alternative mechanisms compensate for the lack of PITPβ. Alternatively, since knockdown of PITPβ was not complete in our experiments, the delay could simply reflect the reduction, but not complete ablation, of PITPβ. A third possibility is that the delay in secretion could be a secondary effect of a retrograde trafficking problem.

PITPβ-depleted cells maintain normal retrograde trafficking

Brefeldin A (BFA) is a fungal metabolite that inhibits secretion and leads to the collapse of the Golgi into the ER. It acts by stabilizing an ARF/GDP/ARF-GEF complex thus preventing ARF activation and coat recruitment (Peyroche *et al.*, 1999). We addressed the question of whether PITPβ-depleted cells were deficient in retrograde

trafficking by studying the rate at which the Golgi was reabsorbed into the ER upon treatment with BFA.

Two days after transfection, PITPβ and mock siRNA-treated cells were subjected to BFA intoxication for various time points. Cells were then fixed and stained with gm130. By 5 minutes after treatment, both PITPβ and mock siRNA cells showed a more disperse Golgi. Because the Golgi network in PITPβ cells is more disperse to begin with, the dispersal in PITPβ siRNA-treated cells was more severe than mock after the 5 minute BFA treatment. By 15 minutes, the Golgi collapse was complete under both siRNA conditions, with no tight perinuclear Golgi networks visible in mock or PITPβ siRNA-treated cells. The similar rate of Golgi dispersal/collapse indicates that there is no large scale defect in retrograde trafficking.

Lipid sensor membrane association is unchanged in PITPβ siRNA-treated cells

Analyses in other organisms reveal that PITPs play important roles in integrating phospholipid signaling events and regulating phospholipid homeostasis. The ability of PITPβ to bind phospholipids, its association with the trans-Golgi network, and its critical role in protein trafficking suggest that PITPβ could be regulating phospholipids at the TGN in order to promote membrane trafficking. Two lipids that play known roles in protein trafficking from the Golgi are DAG and PtdIns(4)P. DAG recruits protein kinase D (PKD), a protein which is required for proper fission of vesicles from the TGN (Liljedahl *et al.*, 2001; Baron and Malhotra, 2002). In addition, PKD also promotes the recruitment of PtdIns 4-OH kinase IIIβ, which catalyzes the conversion of PtdIns to PtdIns(4)P (Hausser *et al.*, 2005; Hausser *et al.*, 2006). PtdIns(4)P promotes transport from the Golgi through the recruitment of coat adapters, such as AP1 and epsins, and

other lipid modifying proteins such as CERT and OSBP (reviewed in (D'Angelo *et al.*, 2008).

Fluorescently tagged lipid sensors were used as a first means of detecting whether lipid levels were altered in the TGN of cells where PITPβ levels were reduced. The cysteine rich domain (CRD) region of PKD1 mediates its interaction with DAG (Rey and Rozengurt, 2001; Baron and Malhotra, 2002), thus a fluorescently tagged PKD CRD domain was used as a DAG sensor. The sensor was expressed in cells treated with either mock or PITPβ specific siRNA, and the cells were fixed and stained with a Golgi marker. Images of the stained cells show that, while the Golgi was relaxed in PITPβ siRNA-treated cells, the GFP-PKD-CRD sensor was still associated with the relaxed Golgi (Figure 4).

The PtdIns(4)P sensor is based on a similar principal as the DAG sensor. The FAPP1 and FAPP2 proteins have been shown to bind to PtdIns(4)P by its PH domain (Godi *et al.*, 2004). Furthermore, this chimera has successfully been shown to function as a bona fide PtdIns(4)P sensor (Godi *et al.*, 2004). An mCherry-tagged FAPP1 PH domain (Liu *et al.*, 2008) was transfected into HeLa cells treated with mock or PITPβ siRNA. As with the DAG sensor, the FAPP1-PH localized to the Golgi in both mock and PITPβ siRNA-treated cells (Figure 4).

Discussion

In this chapter, I've demonstrated a role for PITPβ in maintaining the structure and anterograde trafficking function of the Golgi. siRNA-mediated knockdown of PITPβ in human cell lines leads to a dispersed Golgi that is disrupted at all levels, and ultimately cell death. Anterograde trafficking defects through the TGN are revealed by

glycosoaminoglycan pulse chase assays, and these changes are not accompanied by delays in retrograde trafficking.

As discussed previously, there are several PITPs with critical roles in Golgi trafficking. Most notably, both Sec14p and Nir2 modulate DAG levels through the regulation of PtdCho levels (Skinner *et al.*, 1995; Litvak *et al.*, 2005; Xie *et al.*, 2005). Sec14p also regulates PtdIns4P levels, but Nir2's role in PtdIns-4P regulation is less clear (Peretti *et al.*, 2008).

Both DAG and PtdIns4P are attractive targets of regulation for PITPβ. Cells treated with siRNA against Nir2 (which reduces DAG levels) or siRNA against PtdIns-4 kinase IIα (which reduces PtdIns-4P) exhibit many of the same phenotypes as the PITPβ siRNA-treated cells, including the dispersed Golgi and the transport defects (Wang *et al.*, 2003; Litvak *et al.*, 2005). Expression of PtdIns4-P or DAG sensors in PITPβ or mock siRNA-treated cells showed no major defects in Golgi association of these markers. However, because the lipid levels are likely well in excess of what the sensors can detect, the sensors may not be sensitive enough to detect several fold changes in lipid levels. Rescue experiments (described below), and introduction of short chain lipids could help us to determine if lipid deficiencies lead to the Golgi and trafficking defects seen in PITPβ siRNA cells.

One possibility for how PITPβ could function comes from studies of Sec14p. Sec14p function requires both PtdIns and PtdCho activity to reside on the same molecule, leading to the hypothesis that the exchange of lipids is required for their modification. The presentation function of Sec14 (along with findings from plant PITPs) led to the proposal of PITPs as nanoreactors – molecules that couple lipid binding subunits with

lipid modification enzymes. This nanoreactor concept could well be extended to PITPβ, where PITPβ would act with PtdIns-4(OH) kinase or SM synthase as a nanoreactor, with the ultimate result of secretion promotion. PITPβ could require the exchange of any combination of PtdIns, PtdCho, and SM for modification of any of these lipids.

A key way to address whether PITPβ is a nanoreactor and which lipids it acts on will be to examine which properties of PITPβ are essential for its function. We have mutants that affect the PtdIns and SM binding ability and the Golgi localization of PITPβ, but unfortunately, it has so far proven impossible to rescue the phenotypes of PITPβ siRNA-treated cells with wild type PITPβ. Development of a system where wild type PITPβ fully rescues the siRNA phenotypes will open the door to a greater understanding of PITPβ function.

Figures

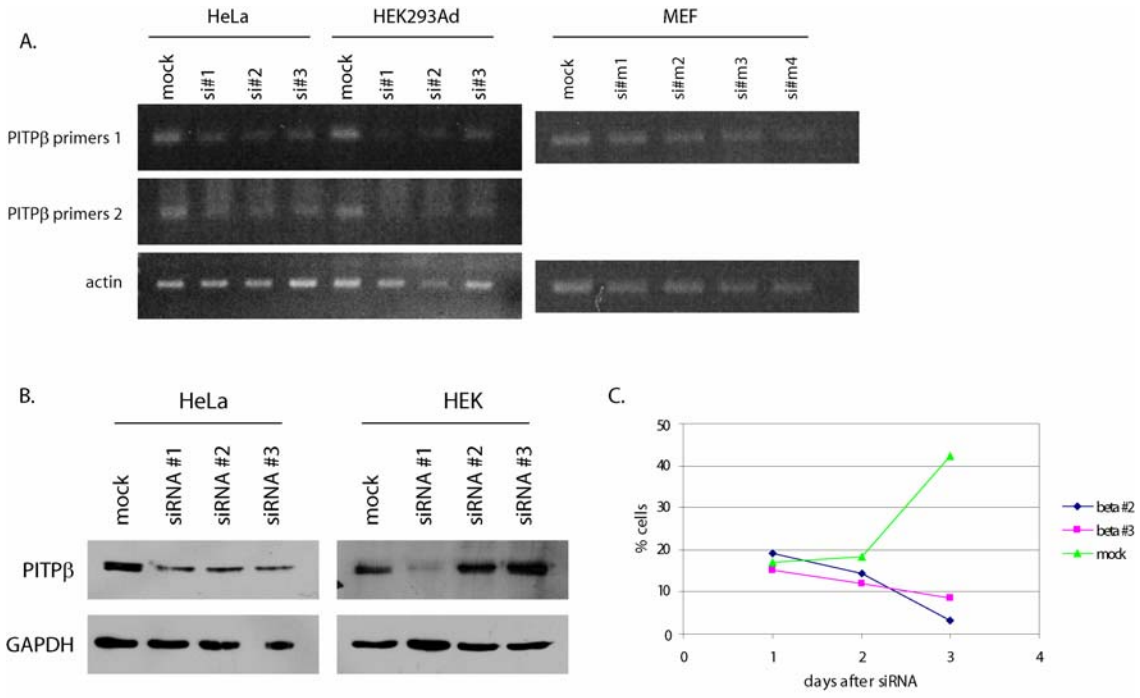

Figure 3.1: Several PITPβ siRNAs are capable of reducing PITPβ levels in mammalian cells. A) RT-PCR was performed on RNA was extracted from mock and PITPβ siRNA-treated cells. Levels of PITPβ were assessed by PCR amplification using primers for PITPβ and actin (for normalization). B) Protein lysates were collected from mock or PITPβ si-RNA treated cells at 52 hours after siRNA treatment. Lysates were separated by SDS-PAGE, transferred to nitrocellulose, and probed with PITPβ or GAPDH antibodies. C) Reduction of PITPβ levels leads to cell death. HeLa cells were treated with mock or PITPβ siRNAs, and at 1, 2, or 3 days after siRNA treatment, and viable cells were identified by their ability to exclude trypan blue dye.

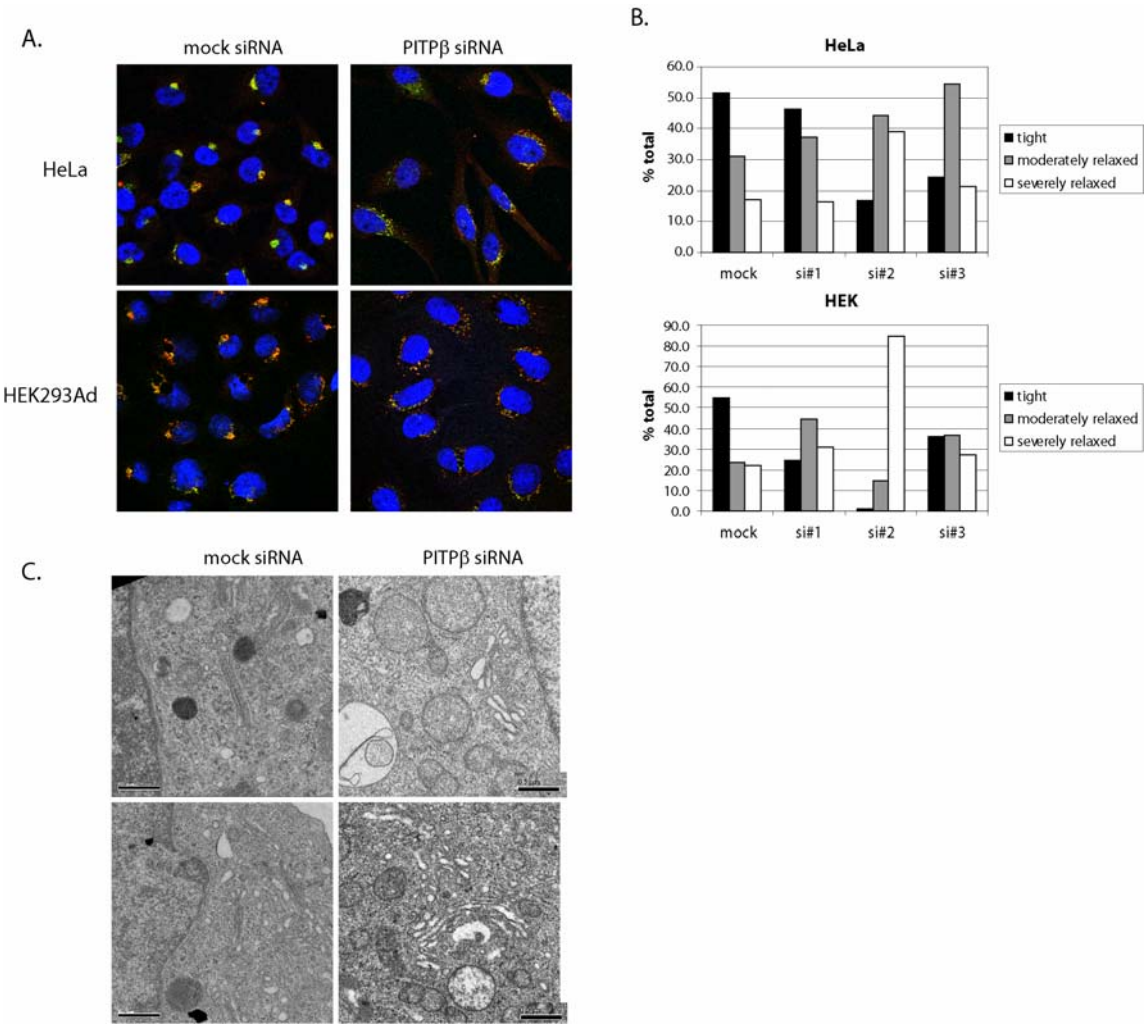

Figure 3.2: Reduced PITPβ levels lead to changes in pan-Golgi morphology. A) HEK and HeLa cells were treated with a negative control ("mock") siRNA or PITPβ siRNA #2. Two days after siRNA treatment, cells were fixed, permeabilized, and stained with markers for the nucleus (DAPI), trans-Golgi (TGN46; red), and cis-Golgi (gm130; green). Representative images are shown. B) The effects of siRNA on HEK293Ad and HeLa cells were quantified. HEK293Ad and HeLa cells were treated with mock and human PITPβ siRNA #1-3, fixed two days after siRNA treatment, and stained as described in (A). Images of each treatment and cell type were blinded, and the cells in each image were scored for Golgi morphology. Data is from 3 separate experiments are

shown and at least 245 cells were counted for each condition. C) Mock siRNA and PITPβ siRNA #2 treated HeLa cells were fixed and prepared for transmission electron microscopy at 2 days after siRNA treatment. Two representative images for each condition are shown. The scale bar corresponds to 0.5 μm.

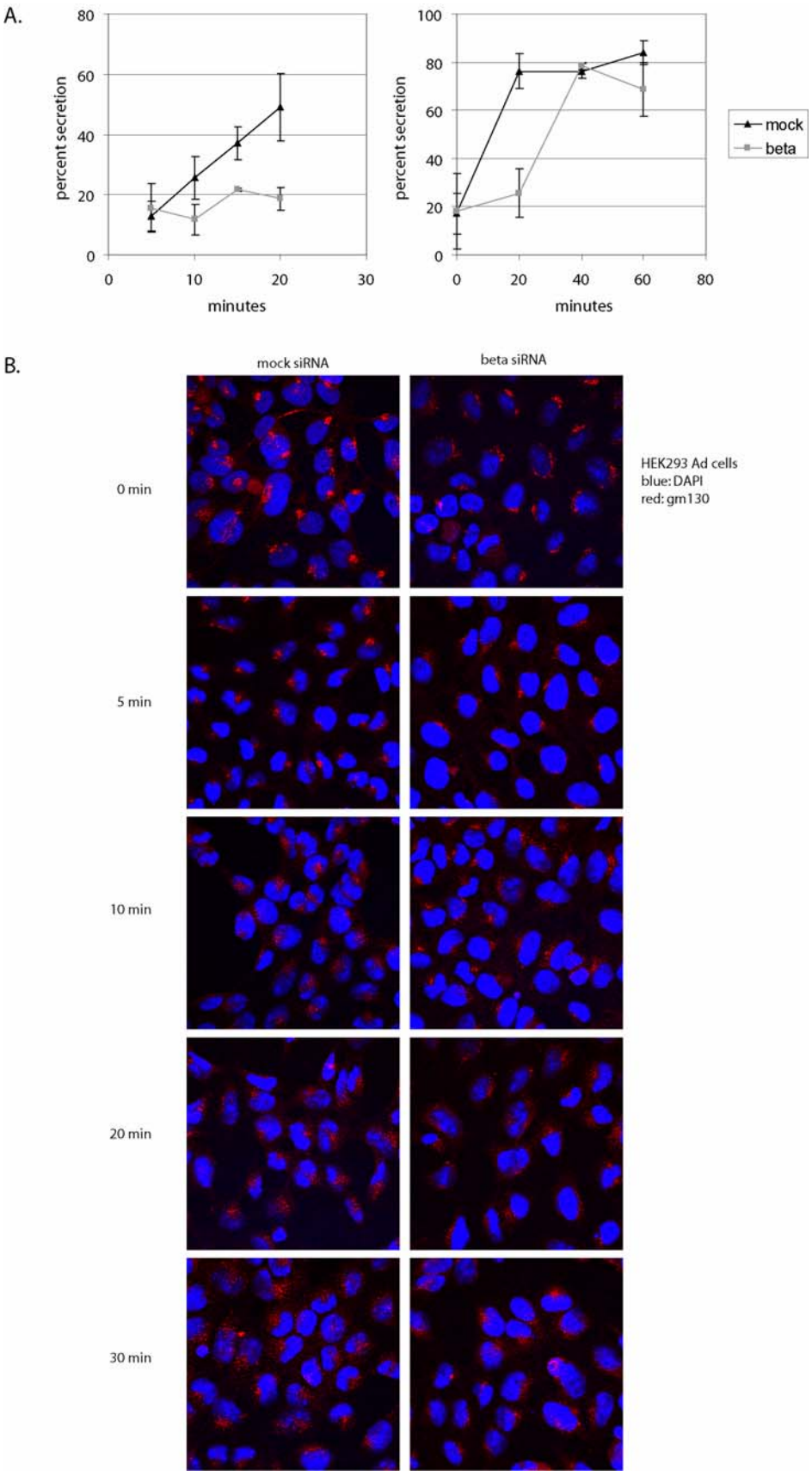
A.
percent secretion
minutes
mock
beta
B.
mock siRNA
beta siRNA
0 min
5 min
10 min
20 min
30 min
HEK293 Ad cells
blue: DAPI
red: gm130

Figure 3.3 (preceding page): Trafficking through the trans-Golgi is delayed in PITPβ-depleted cells. Bulk traffic through the Golgi is measured by a glycosaminoglycan release assay. Cells were treated with mock or PITPβ siRNA, incubated with xyloside, pulse labeled with ^{35}S, and chased with cold media for different periods of time. Glycosaminoglycans were precipitated from cells and media, and counted. The data is expressed as the percent secretion (counts in the supernatant divided by total counts). The assay was performed three times, and the displayed data is from two representative experiments performed in triplicate.

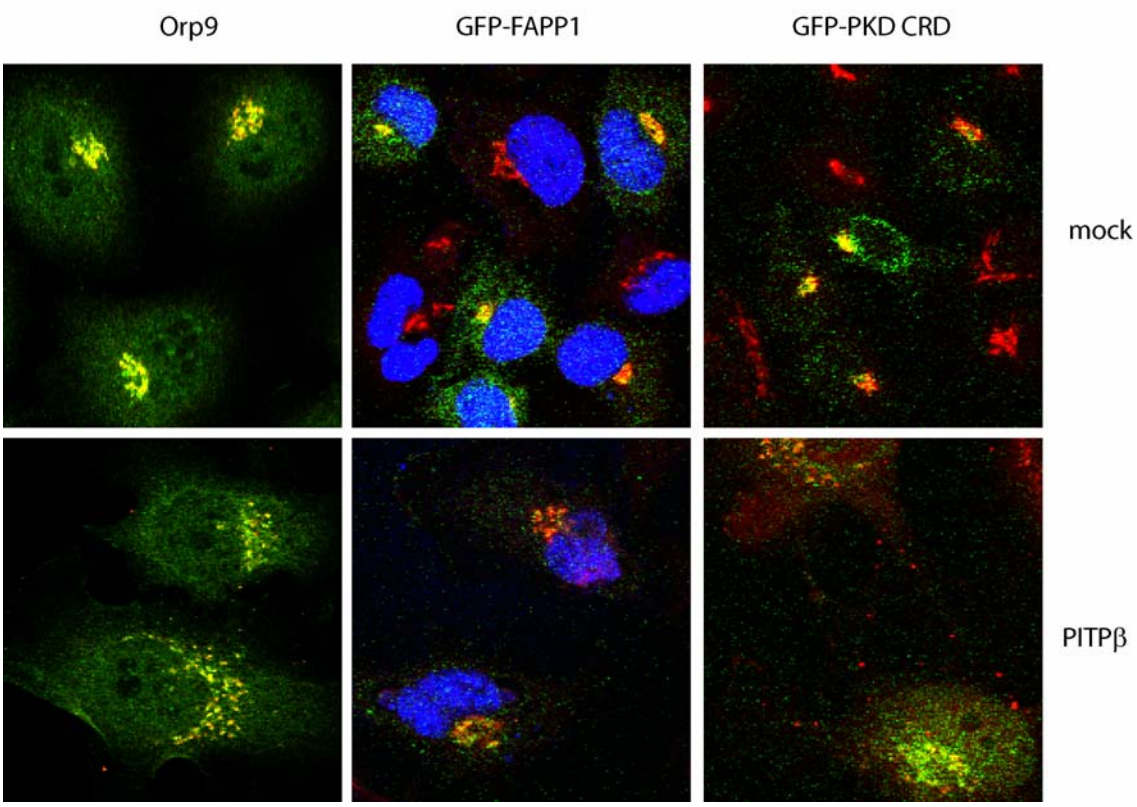

Figure 3.4: The localization of lipid binding proteins is unaffected in PITPβ siRNA-treated cells. HeLa cells were treated with mock siRNA or PITPβ siRNA #2 and transfected with appropriate lipid sensor encoding plasmids at 6 hours after the start of siRNA treatment. Two days after siRNA treatment, cells were fixed, permeabilized, and stained with gm130 (red), and for the left panel, also anti-Orp9 (kind gift of Neale Ridgway, Dalhousie University). Representative merged images are shown.

References

Alb, J.G., Jr., Cortese, J.D., Phillips, S.E., Albin, R.L., Nagy, T.R., Hamilton, B.A., and Bankaitis, V.A. (2003). Mice lacking phosphatidylinositol transfer protein-alpha exhibit spinocerebellar degeneration, intestinal and hepatic steatosis, and hypoglycemia. J Biol Chem *278*, 33501-33518.

Alb, J.G., Jr., Phillips, S.E., Rostand, K., Cui, X., Pinxteren, J., Cotlin, L., Manning, T., Guo, S., York, J.D., Sontheimer, H., Collawn, J.F., and Bankaitis, V.A. (2002). Genetic ablation of phosphatidylinositol transfer protein function in murine embryonic stem cells. Mol Biol Cell *13*, 739-754.

Bankaitis, V.A., Malehorn, D.E., Emr, S.D., and Greene, R. (1989). The Saccharomyces cerevisiae SEC14 gene encodes a cytosolic factor that is required for transport of secretory proteins from the yeast Golgi complex. J Cell Biol *108*, 1271-1281.

Baron, C.L., and Malhotra, V. (2002). Role of diacylglycerol in PKD recruitment to the TGN and protein transport to the plasma membrane. Science *295*, 325-328.

Cleves, A.E., McGee, T.P., Whitters, E.A., Champion, K.M., Aitken, J.R., Dowhan, W., Goebl, M., and Bankaitis, V.A. (1991). Mutations in the CDP-choline pathway for phospholipid biosynthesis bypass the requirement for an essential phospholipid transfer protein. Cell *64*, 789-800.

D'Angelo, G., Vicinanza, M., Di Campli, A., and De Matteis, M.A. (2008). The multiple roles of PtdIns(4)P -- not just the precursor of PtdIns(4,5)P2. J Cell Sci *121*, 1955-1963.

Dries, D.R., Gallegos, L.L., and Newton, A.C. (2007). A Single Residue in the C1 Domain Sensitizes Novel Protein Kinase C Isoforms to Cellular Diacylglycerol Production
10.1074/jbc.C600268200. J. Biol. Chem. *282*, 826-830.

Gatt, M.K., and Glover, D.M. (2006). The Drosophila phosphatidylinositol transfer protein encoded by vibrator is essential to maintain cleavage-furrow ingression in cytokinesis. J Cell Sci *119*, 2225-2235.

Giansanti, M.G., Bonaccorsi, S., Kurek, R., Farkas, R.M., Dimitri, P., Fuller, M.T., and Gatti, M. (2006). The class I PITP giotto is required for Drosophila cytokinesis. Curr Biol *16*, 195-201.

Godi, A., Di Campli, A., Konstantakopoulos, A., Di Tullio, G., Alessi, D.R., Kular, G.S., Daniele, T., Marra, P., Lucocq, J.M., and De Matteis, M.A. (2004). FAPPs control Golgi-to-cell-surface membrane traffic by binding to ARF and PtdIns(4)P. Nat Cell Biol *6*, 393-404.

Hausser, A., Link, G., Hoene, M., Russo, C., Selchow, O., and Pfizenmaier, K. (2006). Phospho-specific binding of 14-3-3 proteins to phosphatidylinositol 4-kinase III beta protects from dephosphorylation and stabilizes lipid kinase activity. J Cell Sci *119*, 3613-3621.

Hausser, A., Storz, P., Martens, S., Link, G., Toker, A., and Pfizenmaier, K. (2005). Protein kinase D regulates vesicular transport by phosphorylating and activating phosphatidylinositol-4 kinase IIIbeta at the Golgi complex. Nat Cell Biol *7*, 880-886.

Ile, K.E., Schaaf, G., and Bankaitis, V.A. (2006). Phosphatidylinositol transfer proteins and cellular nanoreactors for lipid signaling. Nat Chem Biol *2*, 576-583.

Kearns, B.G., McGee, T.P., Mayinger, P., Gedvilaite, A., Phillips, S.E., Kagiwada, S., and Bankaitis, V.A. (1997). Essential role for diacylglycerol in protein transport from the yeast Golgi complex *387*, 101-105.

Liljedahl, M., Maeda, Y., Colanzi, A., Ayala, I., Van Lint, J., and Malhotra, V. (2001). Protein kinase D regulates the fission of cell surface destined transport carriers from the trans-Golgi network. Cell *104*, 409-420.

Litvak, V., Dahan, N., Ramachandran, S., Sabanay, H., and Lev, S. (2005). Maintenance of the diacylglycerol level in the Golgi apparatus by the Nir2 protein is critical for Golgi secretory function. Nat Cell Biol *7*, 225-234.

Liu, Y., Boukhelifa, M., Tribble, E., Morin-Kensicki, E., Uetrecht, A., Bear, J.E., and Bankaitis, V.A. (2008). The Sac1 phosphoinositide phosphatase regulates Golgi membrane morphology and mitotic spindle organization in mammals. Mol Biol Cell *19*, 3080-3096.

Milligan, S.C., Alb, J.G., Jr., Elagina, R.B., Bankaitis, V.A., and Hyde, D.R. (1997). The phosphatidylinositol transfer protein domain of Drosophila retinal degeneration B protein is essential for photoreceptor cell survival and recovery from light stimulation. J Cell Biol *139*, 351-363.

Mousley, C.J., Tyeryar, K., Ile, K.E., Schaaf, G., Brost, R.L., Boone, C., Guan, X., Wenk, M.R., and Bankaitis, V.A. (2008). Trans-Golgi network and endosome dynamics connect ceramide homeostasis with regulation of the unfolded protein response and TOR signaling in yeast. Mol Biol Cell *19*, 4785-4803.

Nemoto, Y., Kearns, B.G., Wenk, M.R., Chen, H., Mori, K., Alb, J.G., Jr., De Camilli, P., and Bankaitis, V.A. (2000). Functional characterization of a mammalian Sac1 and mutants exhibiting substrate-specific defects in phosphoinositide phosphatase activity. J Biol Chem *275*, 34293-34305.

Peretti, D., Dahan, N., Shimoni, E., Hirschberg, K., and Lev, S. (2008). Coordinated lipid transfer between the endoplasmic reticulum and the Golgi complex requires the VAP proteins and is essential for Golgi-mediated transport. Mol Biol Cell *19*, 3871-3884.

Peyroche, A., Antonny, B., Robineau, S., Acker, J., Cherfils, J., and Jackson, C.L. (1999). Brefeldin A acts to stabilize an abortive ARF-GDP-Sec7 domain protein complex: involvement of specific residues of the Sec7 domain. Mol Cell *3*, 275-285.

Phillips, S.E., Ile, K.E., Boukhelifa, M., Huijbregts, R.P., and Bankaitis, V.A. (2006). Specific and nonspecific membrane-binding determinants cooperate in targeting phosphatidylinositol transfer protein beta-isoform to the mammalian trans-Golgi network. Mol Biol Cell *17*, 2498-2512.

Rey, O., and Rozengurt, E. (2001). Protein kinase D interacts with Golgi via its cysteine-rich domain. Biochem Biophys Res Commun *287*, 21-26.

Schaaf, G., Ortlund, E.A., Tyeryar, K.R., Mousley, C.J., Ile, K.E., Garrett, T.A., Ren, J., Woolls, M.J., Raetz, C.R., Redinbo, M.R., and Bankaitis, V.A. (2008). Functional anatomy of phospholipid binding and regulation of phosphoinositide homeostasis by proteins of the sec14 superfamily. Mol Cell *29*, 191-206.

Skinner, H.B., McGee, T.P., McMaster, C.R., Fry, M.R., Bell, R.M., and Bankaitis, V.A. (1995). The Saccharomyces cerevisiae phosphatidylinositol-transfer protein effects a ligand-dependent inhibition of choline-phosphate cytidylyltransferase activity. Proc Natl Acad Sci U S A *92*, 112-116.

Vincent, P., Chua, M., Nogue, F., Fairbrother, A., Mekeel, H., Xu, Y., Allen, N., Bibikova, T.N., Gilroy, S., and Bankaitis, V.A. (2005). A Sec14p-nodulin domain phosphatidylinositol transfer protein polarizes membrane growth of Arabidopsis thaliana root hairs. J Cell Biol *168*, 801-812.

Wang, Y.J., Wang, J., Sun, H.Q., Martinez, M., Sun, Y.X., Macia, E., Kirchhausen, T., Albanesi, J.P., Roth, M.G., and Yin, H.L. (2003). Phosphatidylinositol 4 phosphate regulates targeting of clathrin adaptor AP-1 complexes to the Golgi. Cell *114*, 299-310.

Xie, Y., Ding, Y.Q., Hong, Y., Feng, Z., Navarre, S., Xi, C.X., Zhu, X.J., Wang, C.L., Ackerman, S.L., Kozlowski, D., Mei, L., and Xiong, W.C. (2005). Phosphatidylinositol transfer protein-alpha in netrin-1-induced PLC signalling and neurite outgrowth. Nat Cell Biol *7*, 1124-1132.

Yanagisawa, L.L., Marchena, J., Xie, Z., Li, X., Poon, P.P., Singer, R.A., Johnston, G.C., Randazzo, P.A., and Bankaitis, V.A. (2002). Activity of specific lipid-regulated ADP ribosylation factor-GTPase-activating proteins is required for Sec14p-dependent Golgi secretory function in yeast. Mol Biol Cell *13*, 2193-2206.

Chapter 4 - Phosphatidylinositol Transfer Protein Beta is Required for Structural Integrity of Double Cone Cell Outer Segments in Developing Zebrafish

Abstract

Phosphatidylinositol transfer proteins (PITPs) in yeast coordinate lipid metabolism with the execution of specific membrane trafficking pathways in eukaryotic cells. While there is some evidence that the structurally unrelated metazoan-specific PITPs (mPITPs) may also be involved in membrane trafficking in higher cells, the mPITPs remain an under-investigated class of proteins. Not only is it unclear what biological activities mPITPs discharge, the mechanisms by which these proteins function are also not understood. The soluble class 1 mPITPs include the PITPα and PITPβ isoforms and, of these, the β-isoforms are particularly poorly characterized. Herein, we report use of zebrafish as model vertebrate for the study of class 1 mPITP (and particularly PITPβ) biological function. Zebrafish express PITPα and PITPβ-isoforms and a novel PITPβ-like isoform (DrPITPγ). DrPITPβ expression is particularly robust in double cone cells of the zebrafish retina, and functional interference experiments demonstrate the two DrPITPβ spliceoforms are collectively and specifically required for biogenesis/maintenance of the outer segments of double cone photoreceptor cells in developing retina. By contrast, reduced DrPITPα activity is essential for successful execution of early developmental programs. This study reports the initial characterization of the zebrafish class 1 mPITP family, and the first functional analysis of PITPβ function in a vertebrate.

Introduction

The functional compartmentalization of membrane surfaces is an essential feature of the strategies by which eukaryotic cells organize both signaling inputs and outputs. Lateral organizations of lipids within membranes represent central principles for such a biochemical compartmentalization, and a number of different lipid species are involved in facilitating such organization. Sphingomyelin (SM), cholesterol and other sphingolipids exhibit physical partitioning properties critical for formation of lateral heterogeneities (lipid rafts) that exert a broad spectrum of biological effects (Rajendran and Simons, 2005). Phosphoinositides (PIPs), the phosphorylated versions of phosphatidylinositol (PtdIns), are also major components of membrane signaling systems (Berridge and Irvine, 1989; Majerus, 1992; Fruman *et al.*, 1998; Strahl and Thorner, 2007). The involvement of PIPs takes on multiple forms, including roles as precursors for generation of soluble and lipid second messengers (e.g. inositol phosphates and diacylglycerol, respectively; Nishizuka, 1995; Rhee, 2001), and as binding platforms for the recruitment of proteins to appropriate membrane locations(Hurley and Meyer, 2001; Lemmon, 2003). The utility of PIPs as binding platforms for the appropriate spatial and temporal recruitment of signaling proteins is, in part, a function of the chemical diversities of PIP headgroups -- diversities encoded by the number and the positional arrangement of phosphates that decorate the inositol headgroup (Irvine and Schell, 2001). From the perspective of PIPs as binding platforms, further diversification of PIP-centric biological outcomes is realized by coincidence detection mechanisms that couple the chemical identity of a particular PIP with a second protein or lipid binding activity (Ile *et al.*, 2006).

A newly described coincidence detection mechanism for functional specification of PIP signaling involves Sec14-like PtdIns-transfer proteins (PITPs). Whereas PITPs have been

historically interpreted as carrier proteins that mobilize individual lipid molecules (PtdIns and phosphatidylcholine; PtdCho) between membrane bilayers in cells (Hsuan and Cockcroft, 2001), this view rests solely on an operational in vitro definition of uncertain physiological significance (Helmkamp *et al.*, 1974; Wirtz, 1991). Indeed, evidence from Sec14-like PITPs argues strongly for a lipid sensor role for these proteins that is coupled to substrate presentation functions required for sufficient PtdIns kinase activity in vivo. The coupling of sensor/presentation activities is realized via heterotypic lipid exchange cycles that allow Sec14-like PITPs to impose an instructive regulation of PtdIns kinases – a level of control that cues activation of lipid kinases to specific metabolic inputs (Schaaf *et al.*, 2008). This mechanism is conceptually summarized as Sec14-like PITPs serving as nanoreactors for PIP synthesis (Ile *et al.*, 2006). Structure-based predictive bioinformatics suggest Sec14-like proteins link divergent territories of the lipid metabolome to PIP signaling in eukaryotic cells (Ryan *et al.*, 2007; Schaaf et al., 2008).

Whereas Sec14 is an ancient and exclusively eukaryotic structural unit (Phillips *et al.*, 2006b), expression of a second comprehensively unrelated group of PITPs is essentially restricted to the *Metazoa* (mPITPs; Phillips et al,, 2006b) – with *Dictyostelium* presenting an enigmatic exception (Swigart *et al.*, 2000). Such an evolutionary restriction identifies these mPITPs as signatures of the most complex eukaryotes. Whether mPITPs fulfill a sensor/presentor function resembling that of Sec14-like PITPs, or whether these function altogether differently remains an open question. Indeed, little is confidently known regarding their biological functions. The mPITPs fall into the categories of small cytosolic class 1 versions and the large tightly membrane-bound class 2 proteins (Fullwood *et al.*, 1999). Our studies focus on the class 1 mPITPs of which there are three in mammals: PITPα, PITPβ and RdgBα (Dickeson *et al.*, 1989; Tanaka and Hosaka, 1994; Fullwood *et al.*, 1999). The α and β isoforms

share ca. 77% primary sequence identity, but assume different localization profiles in cells and exhibit biochemical differences in their phospholipid binding/transfer properties (Phillips *et al.*, 2006a). RdgBα is only ca 42% identical to PITPα and PITPβ and remains uncharacterized (Lu *et al.*, 2001). Whereas *Pitpα*$^{0/0}$ mice have been generated (these develop to birth but suffer from complex pathologies that result in neonatal death; Alb *et al.*, 2003), essentially nothing is known regarding PITPβ function. Attempts to generate PITPβ-nullizygous mice, or cell lines, have thus far failed (Alb *et al.*, 2002). The negative data suggest PITPβ executes essential housekeeping functions and, given the striking localization of PITPβ to the mammalian trans-Golgi complex, such functions are likely executed at the level of the Golgi complex (Phillips *et al.*, 2006a).

To address the issue of class 1 mPITP (and particularly PITPβ) biological function more readily, we employed the experimentally tractable zebrafish (*Danio rerio*) as model vertebrate. Zebrafish express a set of mPITPs resembling that found in mammals with the addition of a unique DrPITPβ-like isoform designated DrPITPγ. Functional interference experiments demonstrate DrPITPβ dysfunction evokes specific defects in biogenesis/maintenance of the outer segments of double cone photoreceptor cells in developing retina. These defects are associated with altered status of a retinal-specific arrestin (Arr3L) in double cone cells, although reduced Arr3L activity does not evoke reciprocal effects; i.e. loss of DrPITPβ, structural derangements in double cone cells, or compromised structural integrity of double cone outer segments. We propose DrPITPβ is required for optimal activity of the robust membrane trafficking system required for photoreceptor outer segment biogenesis and maintenance. Finally, in contrast to the specific developmental defects scored in DrPITPβ morphants, DrPITPα insufficiencies result in early developmental failure. The collective data describe the initial description of the zebrafish class 1 mPITP family, and document the first functional analysis of a PITPβ in a vertebrate.

Materials and Methods

Zebrafish.

Zebrafish were raised in either the University of Notre Dame Fish Facility or the UNC Zebrafish Aquaculture Core Facility. The strains used were AB and AB/Tu from the University of Oregon.

Polyclonal antibody production and purification.

The entire coding region of DrPITPβ was amplified using Pfu polymerase (Stratagene) with forward and reverse primers 5'- **GAATTC**GATGGTGCTCATCAAGGA -3' and 5'- **CTC GAG**TGCCTCATTGTTCGTGAGC -3', respectively. The PCR product was cloned into pCRScript (Stratagene) and ultimately subcloned into the pET23b prokaryotic expression vector (Novagen) at the EcoRI and XhoI sites (corresponding sites in the primers are indicated in bold) so that the recombinant protein could be produced with a His_8-tag. Correctness of the *DrPITPβi2* cDNA subcloned in pET23b was confirmed by nucleotide sequence analysis of the entire cDNA region. The fusion protein was expressed according to the manufacturer's protocol (Novagen), analyzed by Coomassie-stained SDS-PAGE, and purified by electroelution from gel slices(Vihtelic *et al.*, 1993). Rabbits were immunized using 100 μg purified fusion protein per injection. An affinity column was generated by coupling purified PBS-dialyzed DrPITPβi2 fusion protein (AminoLink Plus; Pierce) to Sepharose beads using neutral coupling buffer (0.1 M sodium phosphate, 0.15 M NaCl [pH 7.2]). Antibodies were immunopurified using this affinity column using methods previously described (Vihtelic *et al.*, 1999). The pan-PITP antibody is a rabbit polyclonal immunoglobulin that detects the N-terminal 1/3 of mammalian PITPα and PITPβ (a kind gift from Drs. George Helmkamp Jr. and Lynn Yarbrough, University of Kansas Med. Ctr.).

Zebrafish PITPβ and rat PITPβ yeast expression vectors.

Saccharomyces cerevisiae strains employed include CTY1-1A (MATa *ura3-52 lys2-801 his3Δ200 sec14-1^{ts}*), CTY1079 (MATa *ura3-52 lys2-801 his3Δ200 sec14-1^{ts} spo14Δ*), and CTY303 (MATa *ura3-52 his3Δ200 sec14Δ cki1::HIS3*). Zebrafish cDNA was generated by reverse transcription (kit and protocol from Invitrogen, Carlsbad, CA) from RNA collected from 6 days past fertilization (dpf) zebrafish. DrPITPα, DrPITPβi1, DrPITPβi2, and DrPITPγ cDNAs were amplified by PCR from total cDNA using primers clamped with *XhoI* and *SacII* restriction sites (Supplementary Table S1). Rat PITPβ was also amplified by PCR using oligonucleotides clamped with *XhoI* and *SacII*. The corresponding PCR products were verified by nucleotide sequence analysis and subcloned into the *XhoI* and *SacII* restriction sites of yeast episomal vector pDR195 to allow expression in yeast under control of the powerful and constitutive PMA promoter (Rentsch *et al.*, 1995).

Phosphoinositide analysis

Yeast cells were grown in minimal media, and mid-logorithmic growth phase cultures were labeled overnight with 20 μCi/mL of 3H-inositol. After a 3 hour heat shock at 37ºC, labeling was terminated by addition of 5% TCA (final). The pellet was washed twice in water and disrupted in 4.5% perchloric acid. The solution was neutralized by addition of EDTA pH 8.0, and lipids were extracted with ethanol:water:diethyl ether:1-butanol (15:15:5:1). Lipids were dried down, resuspended in chloroform, and run on TLC using a chloroform: MeOH: water: ammonium hydroxide (9.6:8:1.4:1) solution.

Phenotypic rescue experiments in yeast.

Yeast strains were grown to saturation overnight in liquid uracil-free minimal medium or complex YPD medium at 26°C with shaking. Culture densities were subsequently adjusted to a 25 OD_{600}, and normalized cultures were serially diluted into YPD liquid medium to generate the desired-fold dilution series for each culture. A 5 μl aliquot of each culture dilution series was spotted in an ordered array onto a dried YPD agar plate. The YPD plates were subsequently incubated at 37°C for 24 hr and cell growth in each spot was recorded.

Phospholipid transfer assays.

Phospholipid transfer assays were performed as described (Kearns *et al.*, 1998; Phillips *et al.*, 1999; Li *et al.*, 2000; Yanagisawa *et al.*, 2002). Briefly, yeast strain CTY303, which is devoid of measurable endogenous PtdIns-, PtdCho- and SM-transfer activities, was transformed with episomal pDR195 (negative control), or derivatives harboring *rPITPβ*, *DrPITPβ* (i1 and i2), or *DrPITPγ*. The CTY303 derivative strains were grown to saturation and harvested. Cell pellets were resuspended in spheroplast buffer (1.1 M sorbitol, 10 mM Tris-HCl [pH 7.5]), and cells disrupted by vigorous vortexing with glass beads (0.5 mm; Sigma). Broken cell extracts were clarified by serial centrifugation at 1,000 g and 100,000 g, and the 100,000g supernatant fractions were clarified by filtration through 0.45 μM diameter pore membranes (Millipore). PtdIns- and PtdCho- transfer assays using clarified yeast cytosol were performed as described(Aitken *et al.*, 1990). [1,2-^{3}H]-Inositol, [^{14}C]-PtdCho and [^{14}C]-SM were from American Radiolabeled Chemicals, Inc. All other phospholipids were from Avanti Polar Lipids (Alabaster, AL). SM-transfer assays were performed in the same manner as PtdCho-transfer assays with the modification that [^{14}C]-SM was incorporated into donor liposomes.

Protein preparation.

Yeast CTY303 derivatives carrying vectors driving expression of zebrafish and rat PITP cDNAs were cultured overnight in uracil-deficient media. Culture aliquots (5ml) were collected by centrifugation, and the yeast pellets were washed 1X with water and 2X with acetone. Pellets were subsequently air dried, resuspended in Laemmli buffer and disrupted by vortexing with glass beads (three one minute bursts of vortexing, with one minute on ice between bursts). The glass beads were pelleted and the supernatant (yeast protein lysate) was collected and boiled prior to resolution by SDS-PAGE. Resolved proteins were transferred to nitrocellulose and individually decorated with either anti-DrPITPβ or pan-PITP immunoglobulin, respectively.

Heterologous expression in mammalian cells.

Expression and immunofluorescence localization of DrPITPβi1, DrPITPβi2, or DrPITPγ in mammalian cells was performed as described (Phillips *et al.*, 2006a). COS7 cells (grown in DMEM supplemented with 10% FBS and 1% penicillin/1% streptomycin) were transfected using FuGene (Roche Applied Science, Indianapolis, IN), as recommended by the manufacturer.

Frozen section and whole-mount immunolocalization.

Cryosections of adult *albino* zebrafish eye were prepared as described (Barthel and Raymond, 1990; Vihtelic *et al.*, 1999). Harvested eyes were fixed with 4.0% paraformaldehyde/5.0% sucrose in PBS [pH 7.4] at 25°C for 1 hr, embedded in OCT (Sakura Finetek), and sectioned using a cryostat. Stored cryosections (12 μm) were warmed to room temperature (RT), air-dried, and rehydrated in TBS (pH 7.5). Sections were blocked with TBS/5% normal goat serum at RT

for 60 min, and incubated with primary antisera diluted in TBS/5% normal goat serum/0.1% Triton X-100 at RT overnight. Primary antibodies were decorated with Cy3- (1:500; Jackson ImmunoResearch) or AF488-conjugated (1:500; Molecular Probes) secondary antibodies. Negative controls included omission of primary antibody and labeling with pre-immune serum. For whole-mount labeling, adult retinas were fixed with 4% paraformaldehyde/5% sucrose/PBS at RT for 4 hrs, rinsed in TBS and water (5 min each), plunged into acetone at –20°C for 5 min, and serially transferred to water and TBS (Vihtelic and Hyde, 2000).

For frozen section labeling, embryos were dechorionated using Pronase (1 mg/ml), rinsed in water, and fixed in 4% paraformaldehyde/5% sucrose/PBS at room temperature for 20 min. Fixed embryos were washed in 5% sucrose/PBS, incubated in 30% sucrose/PBS at 4°C overnight, and frozen in OCT. Embryos for whole-mount labeling were fixed at 25°C for 20 min, washed in TBS, post-fixed in methanol (5 min, -20°C), and washed in TBS. Tissues were blocked with TBS/5% normal goat serum/1% DMSO/0.1% Triton X-100 overnight at 4°C. Retinas and embryos were incubated in diluted primary antibody overnight or for 48 hours, respectively. Antibody staining profiles were developed by washing in several changes of blocking buffer (4 hrs total), and incubation with secondary antibodies overnight at 4°C.

In situ hybridization

Nucleotide probes for *DrPITPβ* and *DrPITPγ* expression were generated by amplification of the corresponding cDNAs using the appropriate yeast expression vectors (see above) as templates. The probe cDNAs were subcloned into pGEM Easy-T® (Promega, Madison, WI) in both orientations to create sense and antisense probes. Vectors were linearized and transcribed using

MAXIscript (Ambion, Austin, Texas) and T7 polymerase. In situ hybridizations were performed using standard methods (http://zfin.org/zf_info/zfbook/chapt9/9.82.html) and 28 hpf embryos.

Morpholino injections

Morpholinos designed for specific inhibition of *DrPITP* translation were from Gene Tools, LLC (Philomath, OR) and had the following sequences: Standard negative control, 5' – CCTCTTACC TCAGTTACAATTTATA – 3'; PITPβMO1, 5'- ACGATATTCCTTGATGAGCACCATC – 3'; PITPβMO2, 5'- TTGATGAGCACCATCTTCTTTCCAC –3'; and PITPβMO5-M, 5'- ACCA TATTCGTTCATGACCACGATC – 3'; PITPα MO1, 5'- CATGTTATCTCCTTTGCCGCCCC GT-3'; PITPα 5mm, 5'- CATCTTATGTGCTTTCCCCCCCCGT-3'; Arr3L MO1, 5' – TCTTCT TGTAAACTTTGTCAGCCAT – 3'; Arr3L 5mm, 5'- TCTTGTTCTAAAGTTTCTCACCCAT - 3'. All morpholinos were labeled with lissamine at their 3' ends. Morpholinos were suspended in water to a final concentration of 0.5 mM, and ca. 5 nL was injected into the yolk of 1-4 cell embryos. At 24 hpf, larvae were examined for lissamine fluorescence as indicator of morpholino uptake. Larvae failing to present lissamine staining were discarded. Lissamine-positive larvae were incubated at 28ºC until 72 hpf.

Zpr1 immunoblotting and immunoprecipitation

Adult eyes were disrupted in homogenization buffer (20 mM Tris, pH 7.4, 150 mM NaCl, 4 mM $MgCl_2$, 2 mM EDTA, and 0.2% Triton X-100) supplemented with a protease inhibitor cocktail (Complete, Roche Applied Science, Indianapolis, IN). Insoluble material was sedimented by centrifugation at 16,000 *g*. Laemmli buffer was added to the supernatants, and each sample was denatured by heating at 60°C for 15 minutes. The denatured homogenates were resolved by

SDS-PAGE, protein species were transferred to nitrocellulose, and the blots were subsequently developed using the zpr1 monoclonal antibody at a 1:500 dilution.

Immunoprecipitations were performed by homogenizing adult eye tissue as described above for the immunoblotting experiments. After the low speed spin, the supernatant was collected and cleared with protein A Sepharose beads for 30 minutes. The beads were pelleted, the supernatant was collected, and the cleared supernatant was supplemented with fresh Sepharose A beads and zpr1 antibody (1:10 dilution). The mixture was incubated overnight at 4ºC with continuous agitation. The beads were pelleted, washed with lysis buffer and, after the final wash, the beads were resuspended in sample buffer. Controls lacking either antibody or eye homogenate were performed in parallel. All samples were resolved by SDS-PAGE, stained with blue-silver (Morgan *et al.*, 2006), and the single visible polypeptide band was excised and submitted for mass spectrometry analysis at the UNC Michael Hooker Proteomics Center.

Genes encoding candidate zpr1 antigens were recovered from an adult zebrafish retinal cDNA library prepared by reverse transcription (Superscript First Strand Synthesis System, Invitrogen) of RNA template isolated from adult zebrafish eyes (Trizol; Invitrogen, Carlsbad, CA). ORFs encoding candidate proteins identified by mass spectrometry (arrestin 3-like and β-actin) were amplified from the cDNA library by PCR. Primers were designed from sequences deposited in NCBI Entrez Nucleotide (arrestin 3 like: BC076177; β-actin: BC063950) and were clamped with *NotI* in the forward primer and *XhoI* in the reverse primer. The relevant coding sequence of interest was subcloned into pET28 with an N-terminal His_8 epitope tag. Identities of subclones were verified by nucleotide sequence analysis.

pET28/Arrestin 3-like, pET28/actin, pET28 were transformed into BL21-CodonPlus (DE3)-RIL competent cells (Stratagene, La Jolla, CA). The plasmid-bearing *E. coli* strains were

cultured to mid-logarithmic growth phase in LB media supplemented with 25 μg/mL kanamycin and 25 μg/mL chloramphenicol and protein expression was induced with IPTG (200μM final concentration). Bacterial cells were subsequently harvested by centrifugation, resuspended in lysis buffer (300 mM NaCl, 50 mM sodium phosphate, pH 7.5), and lysed by three bursts of sonication (10 seconds each). Debris was removed by centrifugation, the supernatant was collected, and individual proteins were resolved by SDS-PAGE. Resolved proteins were transferred to nitrocellulose and probed with antibodies directed against zpr1 (Zebrafish International Resource Center, Eugene, OR) and actin (Chemicon, Temecula, CA), respectively.

Thin section electron microscopy and histology.

Three days after fertilization and morpholino injection, zebrafish larvae were fixed overnight at 4ºC in 2% formaldehyde/2.5% glutaraldehyde/100 mM cacodylate, washed 3 times in 100 mM cacodylate and three times in water. The larvae were dehydrated by a series of ethanol washes from 50% to 100% ethanol, a wash in 1:1 xylene/EtOH, and incubation in 100% xylene. Larvae were transferred to embedding media by incubation in a 1:1 xylene/polybed 812, 1:2 xylene/polybed 812, and 100% polybed 812 series. The polybed 812 embedded samples were baked in molds for two days at 60ºC. Thin sections were stained with alcoholic uranyl acetate and Reynold's lead citrate, and visualized at 80kV on an FEI Tecnai 12 electron microscope. Images were captured using Gatan micrograph 3.9.3 software. For histological analyses, 3 μM sections were cut and stained with 1:1 methylene blue:Azure II.

Results

The zebrafish cohort of class 1 PITPs.

While a presumptive zebrafish PITPα orthologue has been identified (Xie *et al.*, 2005), no reports are available for zebrafish PITPβ. A protein annotated as homologous to mammalian PITPβ is present in both the ZFIN and NCBI databases (reference numbers ZDB-GENE-040426-895 and NM_200920). The zebrafish *PITPβ* gene (*DrPITPβ*), and its inferred gene product, corresponds in sequence and genomic organization most closely to what we refer to as the mammalian "alternative spliceoform" – as opposed to the "canonical spliceoform" (Phillips *et al.*, 2006a). Examination of EST and genomic sequences (NCBI UniGene website) reveal that *DrPITPβ* resides on chromosome 10 in the genomic region spanning nucleotides 42,255,368 through 42,284,830. Moreover, *DrPITPβ* undergoes the same exon-skipping splicing events exhibited by the mammalian *PITPβ* transcript (Morgan *et al.*, 2006; Phillips *et al.*, 2006a), and two *DrPITPβ* mRNA spliceoforms are expressed. These *DrPITPβ* spliceoforms are herein designated in a fashion consistent with the nomenclature of the mammalian spliceoforms. That is, the *DrPITPβ* identified in the database corresponds to DrPITPβi2 as it is the cognate of the mammalian *PITPβ* alternative spliceoform. The *DrPITPβ* spliceoform that corresponds to the canonical mammalian *PITPβ* spliceoform is designated DrPITPβi1.

Search of the ZFIN database with the RnPITPβ primary sequence as query identified another closely-related, yet previously unidentified, PITPβ-like gene on chromosome 3 spanning nucleotides 13,898,735 through 13,918,905. The corresponding primary mRNA transcript consists of 11 exons and, when spliced, is predicted to encode a 271 amino acid protein. The presence of ESTs indicates this gene is transcribed and is unlikely to represent a pseudogene. We refer to this gene as DrPITPγ (reference numbers: ZDB-GENE-040426-2791, NM_213443).

The coding regions of DrPITPβi1 and DrPITPγ share 73% nucleotide sequence identity, and the inferred gene products share 78% identity at the primary sequence level (Figure 1A). As detailed information regarding physiological functions of PITPβ in vertebrates remains uncharacterized, herein we focus primarily on analyzing physiological roles of the zebrafish PITPβ-like isoforms.

Zebrafish PITPβ-like proteins exhibit PtdIns/PtdCho/SM transfer activities in vitro.

A heterologous phenotypic rescue assay was used to determine whether the zebrafish PITPβ or PITPγ exhibited functional properties consistent with PITPs. This assay is based on previous demonstrations that high-level expression of rodent PITPα or PITPβ (RnPITPβ) rescues the growth and secretory defects associated with thermosensitive versions of Sec14 -- the major PITP of yeast (Skinner *et al.*, 1993; Tanaka and Hosaka, 1994). To this end, a *sec14-1*^{ts} mutant yeast strain was transformed with yeast episomal plasmids driving constitutive expression of either RnPITPβ (positive control), of DrPITPβ spliceoforms 1 or 2, or DrPITPγ. The ability of these individual plasmids to rescue growth of the *sec14-1*^{ts} mutant at restrictive temperatures (37°C) was then assessed. The positive control strain expressing the canonical mammalian PITPβ (*RnPITPβ*) grew well under these conditions, as expected (Tanaka and Hosaka, 1994). The spot inocula representing 10^{0} to 10^{-3} dilutions of the original culture exhibited robust growth, while the 10^{-4} spot dilution revealed the growth of single colonies within the inoculated area (Figure 1B). The *sec14-1*^{ts} negative control strain carrying vector alone was inviable at 37°C as indicated by its failure to exhibit visible growth in any of the spot inocula. Plasmids driving individual expression of DrPITPβ isoforms 1 or 2, or DrPITPγ, also restored robust growth of the into the *sec14-1*^{ts} mutant at 37°C (Figure 1B). These data clearly demonstrate that all three zebrafish PITPβ-like proteins exhibit functional properties of PITPs.

We tested whether the zebrafish PITPβ-like proteins exhibit intrinsic phospholipid transfer activities with the biochemical signatures of PITPβs. In a manner similar to the phenotypic rescue experiments described above, DrPITPβ isoforms 1 and 2 and DrPITPγ were individually expressed in the *cki1 sec14Δ* yeast strain CTY303, a yeast strain that lacks measurable endogenous PtdIns- or PtdCho-transfer activity and permits facile detection of phospholipid transfer activities of heterologous PITPs (Cleves *et al.*, 1991; Skinner *et al.*, 1993; Kearns *et al.*, 1998; Li *et al.*, 2000). Cytosol was prepared from the appropriate *cki1 sec14Δ* derivative strains and was assayed for PtdIns-, PtdCho- and SM-transfer activities.

As expected, 2 mg of cytosol prepared from the CTY303 vector-only control strain failed to present any significant PtdIns-, PtdCho- or SM-transfer activity (Figure 1C). Cytosol containing RnPITPβ (the positive control) strain exhibited robust transfer activities for all three phospholipid substrates (Figure 1C). Incorporation of 2 mg of RnPITPβ cytosol into the assay resulted in the in vitro transfer of approximately 16%, 8% and 8% of the total input [^{3}H]-PtdIns, [^{14}C]-PtdCho and [^{14}C]-SM from donor to acceptor membranes, respectively. Similarly, cytosol fractions containing DrPITPβi1 or DrPITPβi2 also exhibited comparable levels of transfer activity for all three phospholipid substrates relative to rPITPβ control cytosol (Figure 1C). While DrPITPγ cytosol also presented robust PtdIns- and PtdCho-transfer activities, SM-transfer activity was significantly lower than the activities measured for the mammalian PITPβ or for DrPITPβi1 and DrPITPβi2. Nevertheless, the measured activities were still significantly above background. Given the similar magnitudes of PtdIns- and PtdCho-transfer activities in DrPITPγ cytosol relative to DrPITPβi1 or DrPITPβi2 cytosol, these biochemical data suggest DrPITPγ exhibits inferior SM-transfer activity. These results, while not allowing direct comparisons of specific activities for PtdIns-, PtdCho- and SM-transfer between rPITPβ and the zebrafish PITPβ-

like proteins, nevertheless demonstrate that all three of these zebrafish PITPs harbor intrinsic biochemical signatures of PITPβs.

Mammalian PITPα and PITPβs are further distinguished by their intracellular localization – mammalian PITPβ isoforms target to TGN membranes whereas PITPα localizes to nuclear/cytosolic compartments(de Vries *et al.*, 1995; De Vries *et al.*, 1996; Phillips *et al.*, 2006a). By this criterion, the three zebrafish PITPβ-like proteins also score as PITPβs, rather than PITPαs. DrPITPβi1, DrPITPβi2 and DrPITPγ chimeras bearing C-terminal GFP tags distributed to Golgi membranes when expressed in mammalian cells -- as did the control rPITPβ-GFP reporter (Figure 1D). DrPITPγ-GFP, however, was distributed more broadly than DrPITPβi1- and DrPITPβi2-GFP. This zebrafish-specific PITPβ co-localized with both Golgi and ER markers (Figure 1D). These three localization patterns stand in clear contrast with the localization profile of the DrPITPα which, in agreement with previous reports, exhibited a predominantly a cytosolic/nuclear distribution (Figure 1D).

Zebrafish PITPβ isoforms stimulate phosphoinositide synthesis in yeast.

We exploited the yeast system to assess whether DrPITPβi1, DrPITPβi2 and DrPITPγ are able to stimulate activity of a PtdIns 4-OH kinase in its native environment. Using a previously reported strategy (Phillips *et al.*, 1999; Schaaf *et al.*, 2008), we took advantage of yeast strains ablated for Sac1 PtdIns-4-P phosphatase activity to this end. Yeast defective in Sac1 activity present a ca. 10-fold accumulation of PtdIns-4-P relative to isogenic wild-type strains (Guo *et al.*, 1999; Rivas *et al.*, 1999), this accumulation is entirely attributable to the activity of a single PtdIns 4-OH kinase in yeast (Stt4; (Nemoto *et al.*, 2000; Foti *et al.*, 2001)). The magnitude of this dramatic accumulation is reduced by 50% upon inactivation of the major yeast PITP Sec14 (Figure 2;

(Phillips *et al.*, 1999; Rivas *et al.*, 1999; Schaaf *et al.*, 2008)). The 2.5-fold effect on PtdIns-4-P accumulation under conditions of Sec14 insufficiency permits assessment of the ability of a heterologous PITP to stimulate PtdIns-4-P synthesis by the Stt4 PtdIns 4-OH kinase. Reconstitution of *sec14-1^{ts} sac1* yeast with DrPITPβi1, DrPITPβi2 and DrPITPγ fully rescued the depressed Stt4 activity of the control *sec14-1^{ts} sac1* strain (Figure 2).

Similar results were obtained when these assays were performed in yeast *sec14-1^{ts} sac1* strains expressing mammalian PITPα and PITPβ. In both cases, reconstitution of a *sec14-1^{ts} sac1* strain with the mammalian PITP resulted in a ca. 2.5-fold stimulation of Stt4 activity. This effect was abolished by incorporating a T→D missense substitution for T_{59} and T_{58} of PITPα and PITPβ, respectively. PITPα^{T59D} and PITPβ^{T58D} are each selectively inactivated for PtdIns binding/transfer without compromise of PtdCho- or, in the case of PITPβ, SM-binding/transfer activity (Alb et al., 1995; Phillips et al., 2006). Thus, vertebrate class 1 PITPs are generally able to stimulate activity of the yeast Stt4 PtdIns 4-OH kinase in its endogenous setting.

Spatial and developmental expression of DrPITPβ and DrPITPγ.

RT-PCR was used as readout for zebrafish PITPβ-like gene expression during development (i.e. at 6 and 24 hour hpf, at 6 dpf, and in adult fish). As shown in Figure 3A, both *DrPITPβ* and *DrPITPγ* transcripts were readily detected at all four stages. Both *DrPITPβi1* and *DrPITPγ* mRNAs were robustly expressed by 24 hpf and, in both cases, these levels were maintained into adulthood. *DrPITPβi2* mRNA exhibited a more delayed time course for appearance as robust levels were induced at some point between the 24hpf and 3dpf developmental stages. These data indicate that the *DrPITPβ* mRNA splicing program which produces the mRNA for the canonical DrPITPβi1 predominates at the early stages of development, and the exon-skipping splicing

strategy that generates the mRNA for the alternative DrPITPβi2 spliceoform is engaged later. A more detailed profile was obtained by whole-mount in situ hybridization. Both *DrPITPβ* and *DrPITPγ* presented a ubiquitous expression profile throughout the 28 hpf embryo, and *DrPITPβ* expression was particularly robust in the eye (Figure 3B). As to spliceoform specificity, we find both DrPITPβi1 and DrPITPβi2 are expressed in the eye, with DrPITPβi2 exhibiting higher expression (Supplementary Figure S1). In the experiments described below, all readouts employed fail to distinguish between these two spliceoforms, and all subsequent manipulations affect both. As a result, we henceforth refer to these two proteins collectively as DrPITPβ.

Characterization of a DrPITPβ-specific polyclonal antibody.

To more precisely determine the pattern of DrPITPβ expression in adult retina, polyclonal antibodies were raised against purified recombinant DrPITPβi2. The specificity of the affinity-purified antibodies was tested in several ways. First, immunoblotting experiments probing yeast lysates expressing DrPITPβi1, DrPITPβi2 or DrPITPγ demonstrated the DrPITPβ polyclonal antibodies readily detect both DrPITPβi1 and DrPITPβi2, but detect DrPITPγ only very poorly (Figure 3C). Moreover, these same experiments demonstrated DrPITPα does not immunoreact with the anti-DrPITPβ serum at all. A pan-PITP antibody detected all isoforms in these same lysates (Figure 3C). Second, the immunopurified antibodies detect a protein with an apparent molecular mass of ca. 35 kDa in zebrafish retinal extracts (Figure 3C), an apparent mass in reasonable agreement with the 32 kDa calculated from the DrPITPβi1 and DrPITPβi2 primary sequences. When zebrafish retinal extracts were probed with pan-PITP antibodies which detect mammalian PITPα and PITPβ isoforms (Skinner *et al.*, 1993; Alb *et al.*, 1995), one 35 kDa immunoreactive species was detected (Figure 3C). This species exhibited the same mobility by

SDS-PAGE as the DrPITPβi1 and DrPITPβi2 polypeptides. These data demonstrate the affinity-purified anti-DrPITPβ antibodies specifically report DrPITPβi1/DrPITPβi2 without significant interference from DrPITPγ or DrPITPα.

DrPITPβ expression in adult zebrafish retina is restricted to photoreceptor cells.

Like other vertebrates, the zebrafish retina is composed of six neuronal cell types whose cell bodies are arranged into three nuclear layers. These nuclear layers are clearly separated from each other by two sharply defined synaptic (plexiform) layers. The photoreceptors, which consist of the rod and cone cells, form synapses in the outer plexiform layer (OPL) with second order neurons of the inner nuclear layer (INL). Zebrafish possess three different cone cell types: the short single, long single and the double cone cells. Each double cone cell is comprised of a long and short member and, whilst these members are fused along most of their lengths, these maintain individual cell structures such as outer segments and synaptic pedicles. In vertical retinal sections, the rod outer segments are most proximal and are adjacent to the pigmented epithelium, while the various cone cell types reside in a layer between the elongated rod outer segments and the more distally located rod nuclei of the outer nuclear layer (ONL). Each cone cell type assumes a signature morphology and location within the cone cell layer. Proceeding from the ONL proximally towards the rod outer segment layer, the short single cones, long single cones and double cone cells are each localized in distinct and identifiable rows.

Immunolocalization of DrPITPβ in frozen sections of adult zebrafish retina revealed expression is restricted to the photoreceptor layer with the most intense labeling localized to the OPL (Figures 4A and B). To determine if the DrPITPβ profile corresponded to rod or cone photoreceptors, rhodopsin immuno-labeling was performed to mark the rod outer segments

(ROS). In frozen sections dual-labeled for rhodopsin and DrPITPβ, the DrPITPβ-positive cells (including their relatively short triangular outer segments) were positioned distal to the ROS layer (Figure 4C). These data assign DrPITPβ expression to cone photoreceptor cells (Figure 4C). Because the most intense DrPITPβ staining in the retina was associated with the OPL, we examined the preparations in greater detail to determine whether DrPITPβ expression was most highly concentrated in the photoreceptor synaptic terminals, or whether it was localized in the proximal processes of INL cells (e.g. in bipolar or horizontal cells). Dual-label experiments, using α-tubulin as a marker to define structural organization of the OPL-proximal and -distal extents of the plexiform layer, clearly identified DrPITPβ-labeled processes as cone cell synaptic pedicles. The staining profiles were inconsistent with labeling of the smaller rod spherules. These DrPITPβ-labeled processes were intimately associated with the proximal α-tubulin-positive structures, which likely represent bipolar cell dendrites (Figure 4D). Even at this resolution, invaginating α-tubulin-stained processes were occasionally observed to be partially surrounded by DrPITPβ-stained pedicles (data not shown).

The cone photoreceptor localization of DrPITPβ was examined at higher resolution (Figure 4E). Similar to the dual-labeled retina in vertical section (Figures 4C and D), the most intense DrPITPβ labeling was associated with expansive photoreceptor terminals (Figure 4E). Furthermore, the faint outer segment signal was restricted to a single row of cone cells, whose outer segments were located adjacent to the ROS layer. This arrangement is consistent with that of double cone cells. We failed to detect DrPITPβ staining in either the long or the short single cone outer segments, although these cell structures were plainly visible within the plane of the sections. The small number of DrPITPβ-labeled cone pedicles, relative to the total number of cone cells in this section, corresponded to the number of labeled outer segments.

DrPITPβ is primarily expressed in double cone photoreceptor cells.

The outer segment and synaptic pedicle-labeling patterns both suggest DrPITPβ expression is restricted to a single cone cell type – most likely double cone cells. To more precisely assign the identity of the DrPITPβ-expressing cone cells, monoclonal antibody (mAb) zpr-1 was used as specific double cone cell label. MAb zpr-1 decorates an uncharacterized antigen associated with the plasma membrane of double cone cells (termed zpr-1 or Fret43), but not the other photoreceptor types (Larison and Bremiller, 1990) (Figure 4F). Dual-labeling of frozen retinal sections with mAb zpr-1 and affinity-purified anti-DrPITPβ serum yielded extensively overlapping signals that were most apparent in the region of the synaptic pedicles (Figure 4G, arrowheads). These profiles strongly suggest DrPITPβ expression is primarily confined to the double cone cells. We further examined the co-localization of zpr-1 and DrPITPβ in retinal whole-mount preparations (Figure 5). At the edge of the retinal tissue, dissociated photoreceptors were observed in vertical profile (Figure 5, Panels A-C). In every case that a double cone cell was identified by zpr-1 staining (Figure 5B), that cell also expressed DrPITPβ (Figure 5, Panels A and C).

When viewed from a tangential perspective, zebrafish cone cells are uniquely arrayed in a crystalline-like mosaic whose pattern is repeated across the entire retina. In this arrangement, the short and long single cones alternate within single rows. These rows alternate, in turn, with rows composed exclusively of double cone cells. The rod photoreceptors randomly fill in the spaces between the regularly arranged cone cells. Focusing at the level of the photoreceptor cell synaptic termini, zpr-1 and DrPITPβ both reside in cells arranged in repeating rows (Figure 5, Panels D-F). Merge of the images reveals complete correspondence between zpr-1 and

DrPITPβ-containing cells (Figure 5F). When viewed from this focal perspective, it was apparent that each labeled pedicle actually consisted of the fused pedicles of the two members of the double cone cell pair. Closer inspection revealed that, in some instances, the zpr-1 and DrPITPβ profiles overlapped in the terminal of a single member of a double cone cell pair. These results confirm DrPITPβ is primarily expressed in double cone cells, and is not highly expressed in short- or long- single cone cells. The data further suggest that, at least in some cases, DrPITPβ expression is restricted to one member of the double cone pair. Finally, no unambiguous DrPITPβ expression was detected in double cone pair outer segments in these sections (data not shown). These data suggest DrPITPβ is enriched in synaptic pedicles, but it remains formally possible that a minor DrPITPβ pool also associates with outer segments

DrPITPβ insufficiencies result in loss of double cone cell outer segments.

The specific expression profile in the zebrafish retina suggests DrPITPβ executes developmental or phototransduction activities in double cone cells. To this end, the consequences of DrPITPβ insufficiency on double cone function were determined. Two DrPITPβ morpholinos were employed in these studies (MO1 and MO2; see Materials and Methods). Efficacy was determined by injection of each morpholino into 1-4 cell zebrafish zygotes, lysates were subsequently prepared from 3 dpf larvae, and DrPITPβ levels were quantified by SDS-PAGE and immunoblotting. Both MO1 and MO2 injection strongly reduced DrPITPβ expression relative to uninjected controls (Figure 6A). These reductions were not recorded when either of two independent negative control morpholinos were injected – one a scrambled morpholino from GeneTools (Philomath, OR) and the second an MO1-like morpholino with 5 mismatches

(MO5-M) (Figure 6A). The sequences for the negative control morpholinos are detailed in the Materials and Methods.

Embryos injected with DrPITPβ MO1 or MO2 and the negative control MOs were examined for morbidity and morphological deficiencies. No differences were recorded in the viabilities of MO1 or MO2-injected morphants at 3 dpf relative to negative controls. There were also no dramatic developmental or morphological defects/delays in DrPITPβ morphants relative to controls in that time window (data not shown). That MO1 and MO2 injection effectively compromised DrPITPβ expression in retina was evident in examination of retinal cryosections of 3dpf larvae. DrPITPβ immunostaining was strongly reduced in DrPITPβ morphants, relative to controls (Figure 6B). In keeping with the specific DrPITPβ retinal expression profiles, no derangements in the expression or organization of single cone cell and rod cell opsins (blue opsin and rhodopsin, respectively) were observed in DrPITPβ morphant larvae (Supplementary Figure 2). Those data indicate DrPITPβ insufficiencies fail to obviously affect development of those photoreceptor cell types that do not express this protein.

DrPITPβ insuffiencies were accompanied by strong reductions in staining of double cone cells by mAb zpr-1, however. The majority of DrPITPβ morphant larvae presented faint or undetectable zpr-1 staining, while negative control larvae all exhibited moderate to strong zpr-1 staining (Figure 6B). With $\geq$ 14 larvae analyzed for each morpholino injected, 60% of the uninjected and 72% of the MO5-M mismatch control retinas presented strong zpr-1 expression. By contrast, only 21% of the MO1 and MO2 retinas showed strong zpr-1 expression. The retinal cryosections were also probed for green opsin -- an independent double cone marker. In contrast to the case of zpr-1, green opsin staining was unaffected in DrPITPβ morphants (Figure 6C). With at least 10 morphants examined, 82% and 90% of MO1 and MO2 injected larvae presented

robust green opsin staining, respectively. This is compared to 93% and 81% of the unchallenged larvae and those insulted with the 5 mismatch control MO, respectively. These data indicate that not all double cone cell markers are affected in the face of reduced DrPITPβ expression.

A decrement in one double cone cell marker, but not another, might reflect a developmental defect or delay. To address this possibility, the status of Müller glial cells was examined using glutamine synthase as marker. Müller cell development precedes that of double cone cells, and these glial cells protect and nourish retinal cells (Bringmann *et al.*, 2006). Glutamine synthase expression was unaffected in the either MO1- or MO2-derived DrPITPβ morphants (90% and 100% present glutamine synthase staining, respectively) as indicated by comparisons of the morphant staining profiles to those presented by uninjected or MO5-M injected controls (83% and 100%, respectively) (Figure 6D). These data suggest no general delay in retinal development under conditions of reduced DrPITPβ expression.

DrPITPβ-deficient double cone cells present outer segment defects.

Consistent with the developmental marker experiments, histological analyses of DrPITPβ and control morphant eyes reported no major anatomical abnormalities in DrPITPβ morphant retinae (6 larvae from each morphant or control class were analyzed). Since the majority of ONL cells at 3 dpf are cone cells, significant double cone cell loss was expected to manifest itself in large reductions in numbers of nuclei. IMF staining of nuclei reported no obvious change in numbers of nuclei in DrPITPβ morphant ONL, however. Histological examinations did reveal a modest disorganization of the ONL in DrPITPβ morphants compared to controls. Specifically, the distances between the RPE and the nuclei of ONL exhibited greater variation in DrPITPβ

morphants compared to controls, and organization of the ONL cells was less regular (Figure 7A). These modest structural abnormalities diagnosed more subtle double cone cell defects.

Ultra-thin-section electron microscopy (EM) was used to examine double cone cell morphology in more detail in DrPITPβ morphants at 3 dpf. Multiple sections (>25) and at least four morphant and control larvae were examined in these analyses. The EM images consistently reported a significant decrement in the numbers of properly assembled outer segments in DrPITPβ morphants, as opposed to control embryos where these were easily identified (Figure 7B). Using the signature triangular outer segment morphology as hallmark for double cone cells, these photoreceptor cells were clearly recognized in 96% of the thin sections derived from retinas of embryos injected with the MO5-M control, while identifiable double cone cells were scored in only 20% and 24% of MO1- and MO2-injected DrPITPβ morphant sections, respectively (Figure 7B). We note that the double cone cell outer segment deficiencies in morphant larvae disappeared by 5 dpf, at which time morphant retinas were indistinguishable from controls and DrPITPβ protein expression was restored to normal levels (data not shown). These data indicate that outer segment defects associated with DrPITPβ insufficiencies are corrected upon DrPITPβ resupply. Collectively, the EM and histology data suggest DrPITPβ morphants produce properly fated double cone cells which present structurally compromised outer segments during the window of time that DrPITPβ levels are below functional threshold.

Impaired outer segment biogenesis/maintenance is expected to manifest itself in a compromised phototransduction. To that end, the electrophysiological response of morphant and control larvae to red light was measured. The technical demands of the electrophysiological experiment require use of 5 dpf larvae, however, and no significant differences in the photo-responses of morphant vs control retinas were recorded (Supplementary Figure S3). As the

outer segment derangements that accompany DrPITPβ insufficiencies are not apparent at this stage, the data do not address functionality of the structurally impaired outer segments under conditions of DrPITPβ deficit. However, these experiments do demonstrate that the delay in biogenesis of morphologically normal outer segments in fish recovering from DrPITPβ deficiencies does not compromise the ultimate production of functional outer segments.

zpr-1 antigen is retinal arrestin 3-like protein.

The specific loss of zpr-1 staining in DrPITPβ morphant double cone cells is striking given there are no perturbations in expression of other photoreceptor cell markers. These data suggest a functional linkage between DrPITPβ and zpr-1, thereby emphasizing the need to identify the uncharacterized zpr-1 antigen. To this end, mAb zpr-1 was used as affinity reagent to purify its cognate ligand from zebrafish retina and to subsequently determine its molecular identity. Immunoblotting experiments demonstrate mAb zpr-1 recognizes a single ca 45 kDa protein in lysates of adult zebrafish retina (Figure 8A). Similarly, mAb zpr-1 immunoprecipitates a single 45 kDa species from the same tissue. The immunoprecipitation was specific given the fact that recovery of that species was dependent on both mAb zpr-1 and retinal homogenate (Figure 8B). The purified species was excised from the gel and subjected to MALDI-TOF mass spectrometry. Two candidate proteins were identified – the 39.5 kDa *Danio rerio* arrestin 3-like (Arr3L) and the 41.5 kDa *Danio rerio* β-actin. The candidates were assigned with high confidence from 20 and 17 individual peptide matches, respectively (Supplementary Table S2).

That Arr3L is a retinal-specific arrestin made it an attractive candidate for the zpr-1 antigen. To assign zpr-1 molecular identity, Arr3L and zebrafish β-actin polypeptides were individually produced in *E. coli* using a pET28 protein expression vector (see Materials and

Methods). Immunoblotting experiments with mAb zpr-1 demonstrated an immunoreactive species of the expected molecular mass in bacterial lysates containing Arr3L (Figure 8C). No mAB zpr-1 immunoreactive species were detected in lysates prepared from vector-only controls, nor from bacteria expressing zebrafish β-actin. In the latter case, anti-actin serum readily detected the expressed recombinant actin polyppetide. With regard to arrestin specificity, mAb zpr-1 failed to detect the closely-related arrestin Arr3, nor was there detectable immunoreactivity of mAb zpr-1 with recombinant zebrafish Sag and Zgc:66109 retinal arrestins, or with the ubiquitously expressed Arr2b arrestin (Supplementary Figure S4).

Independent confirmation that zpr-1 antigen is indeed Arr3L was obtained from experiments where Arr3L expression was specifically targeted by morpholino-mediated silencing. Injection of embryos with an Arr3L-directed morpholino exerted no obvious developmental effects (data not shown), but such challenge eliminated staining of double cone cells in morphant larvae by mAb zpr-1. This effect was not recapitulated in unchallenged embryos, or in embryos insulted with the cognate 5-mismatch control morpholino. Moreover, in contrast to the reciprocal case where DrPITPβ morphants were strongly impaired for zpr1-immunostaining (see above), Arr3L morphant retinas supported robust expression of both green opsin and DrPITPβ -- as was also apparent in retinas culled from uninjected embryos, or embryos challenged with the 5-mismatch morpholino (Figure 8D). Futhermore, the green opsin and DrPITPβ staining profiles in morphant vs control retinas were very similar – suggesting loss of Arr3L function does not evoke general defects in retinal ultrastructure. Finally, the retinal phenotypes associated with Arr3L- and DrPITPβ deficiencies were different in one other important respect. Whereas DrPITPβ insufficiencies impair double cone cell development (as assessed by monitoring of outer segment ultrastructure), Arr3L morphant retinas presented well-

formed outer segments (Figure 8E). These data argue that outer segments deficits in DrPITPβ morphants do not derive from Arr3L dysfunction. Rather, structural impairments of outer segments and altered Arr3L (zpr-1) status are consequences of reduced DrPITPβ activity.

Arr3L transcription in DrPITPβ morphants.

The phenotypes associated with DrPITPβ deficiency -- reduced Arr3L and defective double cone cell outer segment morphology -- potentially diagnose any of several defects. Double cone outer segments may fail to form correctly, or may not be effectively maintained in DrPITPβ morphants. Since Arr3L engages light-activated opsins in outer segments, derangement of these structures could promote Arr3L degradation. Alternatively, DrPITPβ morphants may exhibit partial defects in double cone cell lineage determination with accompanying defects in transcriptional programming. In such case, transcription of *ARR3L*, and of genes encoding other factors that contribute to outer segment biogenesis or maintenance, might be compromised.

To distinguish between these general possibilities, *ARR3L* mRNA levels in DrPITPβ morphants were compared to those of uninjected embryos, or embryos injected with the MO5-M control morpholino. Total RNA was isolated from embryos injected with DrPITPβ morphlinos. Because morpholino efficacy varies from morphant to morphant, RNA was prepared from three independent sets of morphants. Each set included larvae derived from embryos injected with DrPITPβ-directed morpholinos MO1 and MO2, from embryos injected with the five mismatch control morpholino, and from uninjected embryos. RT-PCR analyses estimated relative *ARR3L* mRNA levels. In all cases, the RT-PCR assay scored similar levels of *ARR3L* mRNA in MO1- and MO2-derived DrPITPβ morphants relative to the mismatch morpholino and uninjected negative controls (Figure 8F). These data indicate Arr3L transcription is not impaired in

DrPITPβ-deficient double cone cells – further supporting the conclusion that the structurally compromised double cone cells of DrPITPβ morphants are properly fated.

DrPITPα morphants arrest early in development.

The rather subtle developmental phenotypes associated with DrPITPβ morphants raised the question of whether the DrPITPγ and DrPITPα isoforms discharge more significant developmental functions in zebrafish. Embryos injected with morpholinos directed against DrPITPγ failed to present significant increases in morbidity, or obvious morphological or developmental deficiencies (data not shown). The lack of a suitable DrPITPγ -specific antibody with which to independently assess DrPITPγ protein levels in the presumptive morphants precludes confident interpretation of these negative data. By contrast, interference with DrPITPα expression levied an early developmental arrest in the interval between 80% epiboly through the bud stage (8-10 hpf) (Figure 9A). Until the point of arrest, DrPITPα morphants followed developmental trajectories that were indistinguishable from those of embryos insulted with the mismatch control morpholino (Figure 9A). DrPITPα morphants remained in an apparent state of terminal developmental arrest for 24 hpf without exhibiting obvious signs of degeneration or structural decay normally associated with loss of viability. By 48 hpf, however, the unambiguous indicators diagnostic of morbidity were on display in all morphants (Figure 9B).

Discussion

Herein, we describe the initial characterization of the zebrafish class 1 mPITP family, and document the first functional analysis of a PITPβ in a vertebrate system. We report zebrafish express a set of mPITPs that recapitulates the cohort found in mammals – i.e. a DrPITPα and two directly paralogous spliceoforms of DrPITPβ. Zebrafish also express a unique DrPITPβ-like isoform not found in mammals which we designate DrPITPγ. Biochemical characterization of each individual protein species confirms their identification as PITPβs. Functional interference experiments, while uninformative for DrPITPγ, demonstrate collective DrPITPβ spliceoform function is not essential for general zebrafish development. Rather, the DrPITPβs are specifically required for photoreceptor outer segment biogenesis/maintenance in the double cone cells of developing retina. Moreover, DrPITPβ insufficiencies result in altered status of the retina-specific arrestin Arr3L in double cone cells. The specific developmental defects levied by reduced DrPITPβ function are in stark contrast to the consequences of diminished DrPITPα function. DrPITPα insufficiencies lead to early developmental failure and, ultimately, loss of viability of the terminally arrested embryo. The collective data demonstrate DrPITPβ and DrPITPα isoforms discharge distinct developmental functions in zebrafish. While DrPITPα is required for progression through early embryonic development, we propose DrPITPβ supports the high capacity membrane trafficking pathway required for outer segment biogenesis and maintenance in double cone photoreceptor cells.

The panel of zebrafish class 1 PITPβs

Zebrafish express a DrPITPα and three class 1 mPITPs with properties characteristic of PITPβ isoforms. Two of these proteins represent DrPITPβ spliceoforms that correspond to the

'canonical'and 'non-canonical' PITPβ spliceoforms that differ only in their extreme C-terminal sequences (Morgan *et al.*, 2006; Phillips *et al.*, 2006a). The zebrafish cognates are DrPITPβi2 and DrPITPβi1, respectively. Using the canonical mPITPβ (DrPITPβi1) sequence as standard, the exon-skipping event that distinguishes these spliceoforms affects a window defined by the last fifteen residues of the canonical mPITPβ. The alternative splicing event introduces five amino-acid substitutions into that region and incorporates one additional residue (Phillips *et al.*, 2006a). In addition to the 'canonical' and 'non-canonical' DrPITPβ sliceoforms, zebrafish express a novel isoform (DrPITPγ) from a distinct structural gene highly homologous to the *DrPITPβ* structural gene at the nucleotide level. DrPITPγ also shares a high degree of primary sequence with DrPITPβ spliceoforms.

A battery of functional data identifies DrPITPβi1, DrPITPβi2 and DrPITPγ as PITPs of the β-isoform class. First, each individual protein exhibits unambiguous PtdIns-, PtdCho- and SM-transfer activities in vitro. Of the three, DrPITPγ harbors the least robust SM-transfer activity, but this activity is nonetheless significant. Second, heterologous expression of each individual protein in yeast with a functionally thermosensitive PITP (the *sec14-1*^{ts} gene product) phenotypically rescues the conditional growth defects associated with the *sec14-1*^{ts} lesion. Third, the phenotypic rescue of the *sec14-1*^{ts} mutation by DrPITPβi1, DrPITPβi2 and DrPITPγ is accompanied by restoration of stimulated PtdIns-4-phosphate synthesis by the Stt4 PtdIns 4-OH kinase – thereby establishing these particular class 1 mPITPs as functional potentiators of PtdIns kinase activity. That PtdIns-binding is essential for vertebrate class 1 PITP α- and β- isoforms to stimulate PtdIns kinase is amply demonstrated by the inability of mutants specifically impaired for PtdIns-binding/transfer, to effect such a stimulation. While potentiation of PtdIns kinases is a

consistent feature of PITPs, the heterologous context of the result has important implications for mechanisms of class 1 mPITP function (see below).

DrPITPβ and double cone cell development

DrPITPβ and DrPITPγ isoforms exhibit similar temporal expression profiles. In situ hybridization experiments, although reporting a ubiquitous spatial expression profile for the DrPITPβs and DrPITPγ, score particularly robust DrPITPβ expression in the developing eye. Of the two DrPITPβ spliceoforms, the 'non-canonical' DrPITPβi2 is the more highly expressed in that organ. Moreover, the alternative splicing program that generates DrPITPβi2 engages later in development than the one which produces the 'canonical' DrPITPβi1. As we have yet to demonstrate a clear functional distinction between the two DrPITPβ spliceoforms, it remains unclear why a splicing program switch is engaged in this manner. The functional significance of enhanced DrPITPβi2 expression in retina, relative to that of DrPITPβi1, is also not obvious. This enhancement may simply reflect an idiosyncracy of the larger splicing properties of the tissue -- rather than a specific requirement for DrPITPβi2 vs DrPITPβi1 activity in retina.

Restriction of DrPITPβ expression to double cone cells, where the protein(s) distribute predominantly to the synaptic pedicles, is striking. Functional interference data are congruent with the DrPITPβ expression profile. While DrPITPβ morphants progress through larger developmental processes normally, morphologically recognizable double cone cells do not form in these animals. All available data suggest double cone cells are fated correctly (green opsin, a specific marker for double cone cells, is produced in morphant retinas), but these photoreceptor cells present structural derangements associated with impaired biogenesis/maintenance of outer

segments. These defects are associated with loss of immunoreactivity of double cone cells with the previously uncharacterized zpr-1 antigen – another specific marker for double cone cells.

Herein, zpr-1 is identified as Arr3L, and the linkage between DrPITPβ dysfunction, defective outer segment morphology in double cone photoreceptor cells, and altered status of a double cone cell-specific arrestin, is a compelling one. Transcription of the *ARR3L* gene is not compromised in DrPITPβ morphants, and we believe it most likely that Arr3L is destabilized in DrPITPβ-insufficient retina. Because the detection method employs a monoclonal antibody, other possibilities cannot be excluded – e.g. an altered Arr3L modification profile that interferes with mAb zpr-1 immunoreactivity, or altered Arr3L regulation at the translational level. Regardless, the developmental photoreceptor cell defects associated with DrPITPβ insufficiencies are reversible. DrPITPβ recovery reconstitutes the retina with morphologically normal and functional double cone cells. Moreover, the relationship between DrPITPβ and Arr3L expression is not reciprocal. Arr3L morphants do not present loss of DrPITPβ expression in the retina, nor do these result in structurally compromised double cone outer segments.

Vertebrate rod and cone cell outer segments are composed of an extensive assembly of intricate membraneous discs/lamellae subject to a vigorous course of continuous self-renewal (Bok and Young, 1972; Young, 1974). As such, the outer segment establishment/maintenance program relies on a high capacity membrane trafficking system which renders it exquisitely sensitive to perturbations in membrane trafficking. Localization of mPITPβ isoforms to the trans-Golgi network, and the abilities of DrPITPβ isoforms to localize to mammalian Golgi membranes in heterologous expression studies, suggests a potential mechanism for how diminution of DrPITPβ activity evokes structural derangement of outer segments. DrPITPβ insufficiencies may subtly compromise Golgi function in double cone cells and evoke significant

defects in opsin transport from that organelle. Reduced incorporation of material into the outer segment via biosynthetic trafficking is expected to result in outer segment loss if membrane protein turnover in those structures is sustained at normal rates (Figure 10). In mammalian rod cells, the SARA FYVE domain adaptor protein responds to PtdIns-3-P cues, and cooperates with the syntaxin 3 t-SNARE, to drive a vesicle fusion process required for outer segment membrane disc formation and maintenance of outer segment integrity (Chuang *et al.*, 2007). Given the ability of DrPITPβs to potentiate the activities of PtdIns kinases, one attractive scenario is DrPITPβs support an analogous PtdIns-3-P/SARA-dependent pathway in zebrafish double cone cells. In that regard, we note an uncharacterized ORF annotated as encoding a zebrafish SARA homolog is present in both the ZFIN and NCBI databases (ZFYVE9; reference numbers ZDB-GENE-030131-1426 and CAN88231, respectively; resides on chromosome 2 in the genomic region spanning nucleotides 14,608,532-14,643,375).

While this model has its attractive features, it is not directly congruent with the primary localization of DrPITPβ to the synaptic pedicle. The pool of Golgi membranes most proximal to the outer segment lies within the double cone cell inner segment. One possibility is a minor pool of DrPITPβ does indeed reside in the inner segment, and is associated with Golgi membranes in that locale, or is transiently associated with the outer segments themselves, but that the steady-state DrPITPβ distribution is more concentrated (and more easily detected) in the synaptic pedicle. A second possibility is DrPITPβ is sequestered from the inner segment and plays no direct role in double cone Golgi function there. Rather, DrPITPβ may indirectly coordinate lipid-derived signaling inputs in the synaptic pedicle with inner segment membrane dynamics (Fig. 10). It is a reasonable proposition that the expensive outer segment biogenesis/renewal processes would somehow be coordinated with the synaptic activity of the double cone cell.

Functional diversification of class1 DrPITPβ and DrPITPα isoforms

The data report unexpectedly limited developmental functions for zebrafish DrPITPβs. What level of functional redundancy exists between the various DrPITP isoforms? From the perspective of DrPITPγ, no clear resolution to this question presents itself at this time. DrPITPα and the DrPITPβ spliceoforms are functionally distinct, however. The retina developmental phenotypes associated with DrPITPβ insufficiencies are manifest without overt interference with DrPITPα function. Reciprocally, interference with DrPITPα activity results in an early and terminal developmental arrest in the face of DrPITPβ and DrPITPγ expression. Taken together, the data are consistent with a growing body of evidence to indicate that the biological activities of individual PITPs are functionally specialized. In that regard, it will be of considerable interest to determine the basis of developmental failure in DrPITPα morphants. It also deserves special emphasis that the terminal phenotypes associated with class 1 mPITPα insufficiencies are dramatically different in mice as compared to zebrafish. In contrast to the catastrophic early developmental failure observed in DrPITPα morphants, the cognate mouse nullizygotes develop to birth, and are born alive at Mendelian frequencies as anatomically correct neonates, but expire shortly thereafter (Alb *et al.*, 2003). Thus, the results reported herein only demonstrate that DrPITPα and DrPITPβ discharge very different functions during zebrafish development, but also that vertebrates utilize diverse biological strategies for the employ of paralogous class1 PITPs.

Mechanistic implications for class1 PITP function in metazoans

Finally, whatever the biological coupling may be for any individual class 1 mPITP, it is a common theme that these proteins interface with PtdIns kinases. The data reported herein

provide new information pertinent to the mechanisms by which class 1 mPITPs potentiate PtdIns kinase activities. Do class 1 mPITPs execute this stimulation via roles as bona fide transfer proteins (Wirtz, 1991), or do these proteins serve as nanoreactors in the fashion proposed for the Sec14-like PITPs (Ile *et al.*, 2006)? It is currently presumed that class 1 mPITPs are carrier proteins that supply membranes engaged in PIP signaling with PtdIns so that the signaling circuit can be recharged (Hsuan and Cockcroft, 2001). This PtdIns supply model posits mPITP-dependent transport of PtdIns from its site of synthesis in the ER to the signaling membrane, and that forward PtdIns flow is counterbalanced by back-transfer of PtdCho to close a vectorial phospholipid transfer loop. There is no evidence to support such a vectorial transfer pathway in vivo, and the model poses the additional difficulty that it is effectively impossible to disprove. One distinction between PtdIns-supply and nanoreactor models, however, is that PtdIns surfeit is predicted to abolish requirements for mPITP-mediated PtdIns-supply mechanisms for stimulating PtdIns kinases. By contrast, nanoreactor mechanisms for mPITP-mediated potentiation of PtdIns-kinases should be apparent under conditions of PtdIns excess. That DrPITPs and mammalian class 1 mPITPs enhance PtdIns kinase activity in yeast (i.e. an organism whose bulk membrane PtdIns load is ca. 25% of total glycerophospholipid by mass; McGee et al., 1994) indicates class 1 PITPs can operate in nanoreactor mode. Whether class 1 mPITPs do so in their native setting is obviously more difficult to discern, and no final conclusion can yet be reached regarding this matter. Nevertheless, the principle is established. The remarkable fact that vertebrate mPITPs evolved separately from yeast PITPs, yet can still productively stimulate yeast PtdIns kinase activities, demonstrates no privileged interaction is required between the PITP and the kinase for stimulation. It now remains to decipher the larger developmental signaling pathways that interface with DrPITPβs and DrPITPα in zebrafish.

Figure legends

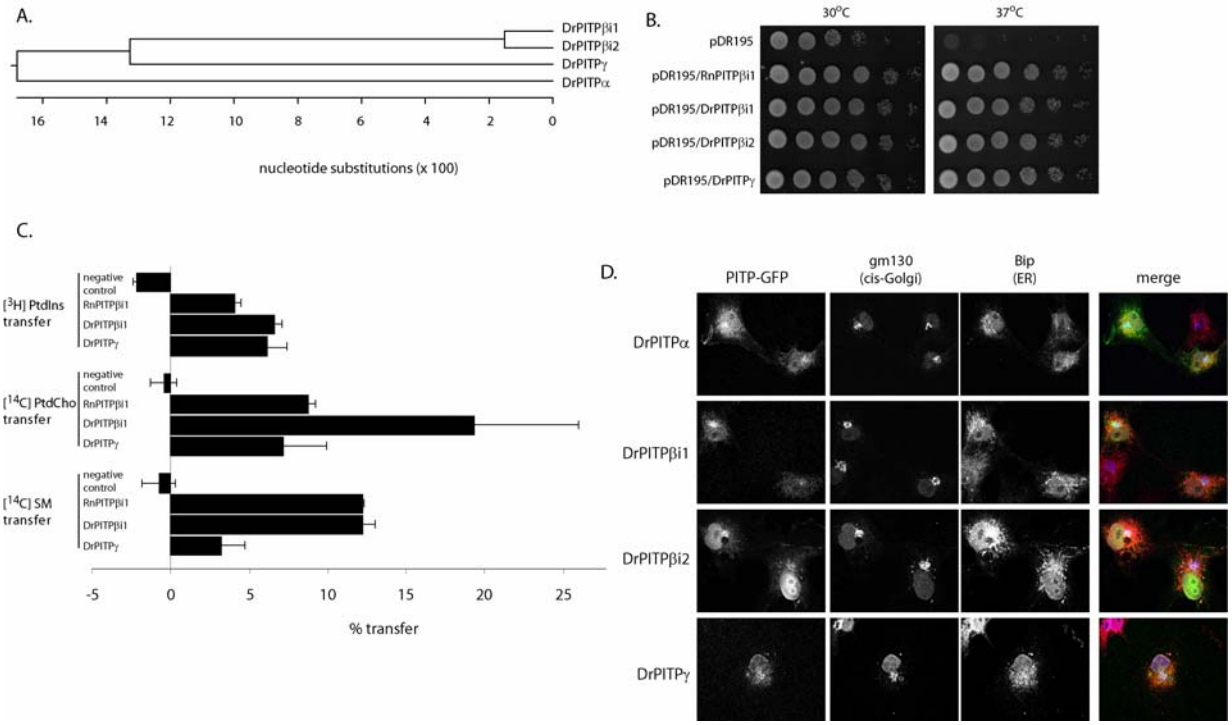

Figure 4.1. DrPITPβ and DrPITPγ isoforms. **A)** A ClustalW phylogenetic grouping of presumptive zebrafish DrPITPα, DrPITPβi1, and DrPITPγ is shown. DrPITPγ scores as a PITPβ isoform. **B)** Zebrafish PITP cDNAs were subcloned into the multicopy yeast *URA3* expression vector pDR195 where heterologous PITP gene expression is driven by a powerful constitutive promoter. Each individual expression construct was transformed into the yeast strain CTY-1-1A (*ura3-52, sec14-1^{ts}*). Ten-fold dilution series were prepared from saturated liquid cultures normalized to similar cell densities and dilution spotted onto rich YPD solid media in parallel. One set of YPD plates was incubated for 48 hours at 30º (permissive for *sec14-1^{ts}*) and 37ºC (restrictive for *sec14-1^{ts}*). Both DrPITPβ isoforms and DrPITPγ phenotypically rescued growth of the *sec14-1^{ts}* yeast strain at 37ºC. **C)** In vitro lipid transfer activities of presumptive zebrafish PITPβ-like proteins. Transfer assays score mobilization of radiolabeled PtdIns, PtdCho, or SM

substrate between distinct membrane bilayer systems. Clarified cytosol prepared from yeast strain CTY303 (*sec14Δ cki1*) expressing each protein of interest served as protein source. Cytosol from CTY303 carrying an empty vector served as a negative control, while corresponding cytosol containing rat PITPβi1 was included as a positive control. The data shown is a single transfer assay, performed in triplicate that is representative of at least three independent experiments. The phospholipid-transfer substrate inputs for these assays were: 21,799 cpm [^{3}H]PtdIns; 13,426 cpm [^{14}C]PtdCho; 12,645 cpm [^{14}C]SM;. Background values (buffer control) for these respective transfer assays were 1324, 1404 and 1038 cpm. **D)** Localization of zebrafish PITPβ-like isoforms in mammalian cells. COS7 cells expressing GFP-tagged versions of zebrafish PITPs were fixed, permeabilized, and stained with antibodies that detect the cis-Golgi (gm130; blue) and the ER (BiP; red). Representative profiles for GFP expression or antibody staining are shown in the left panels, and the merged images are shown in the right panel.

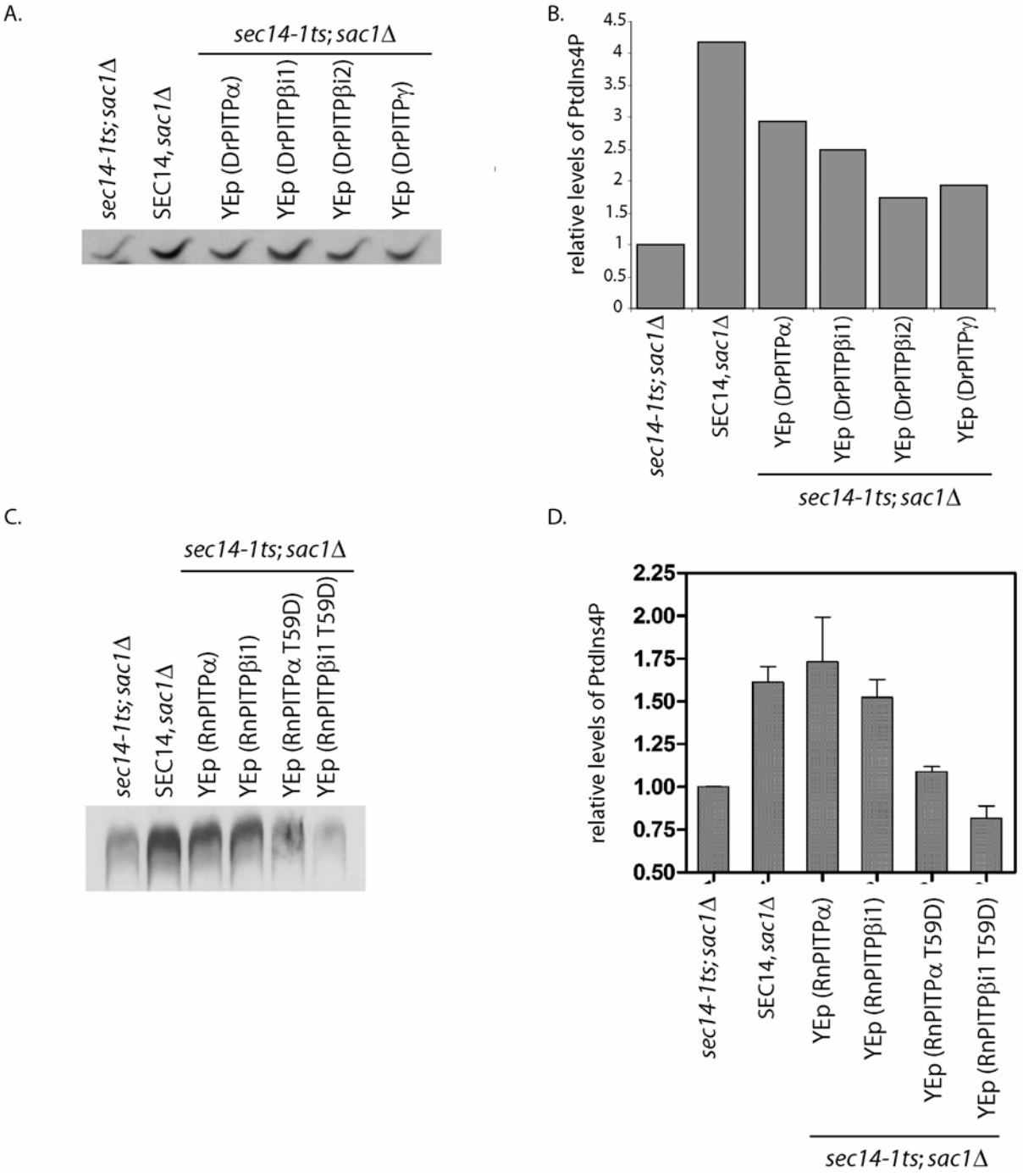

Figure 4.2. PI synthesis in yeast (in progress) (A) Isogenic yeast strains (sec14-1ts Δsac1) expressing empty vector (pDR195), pDR195 (Sec14), and the zebrafish PITPs (A; DrPITPα, DrPITPβi1, DrPITPβi2, and DrPITPγ) or the mammalian PITPs (C; RnPITPα and RnPITPβ and T59D mutants) were labeled to steady-state with ^{3}H-inositol. After a 3 hour shift to 37ºC, lipids

were extracted, separated by 1 dimensional thin layer chromatography, and quantified by densitometry (B, D).

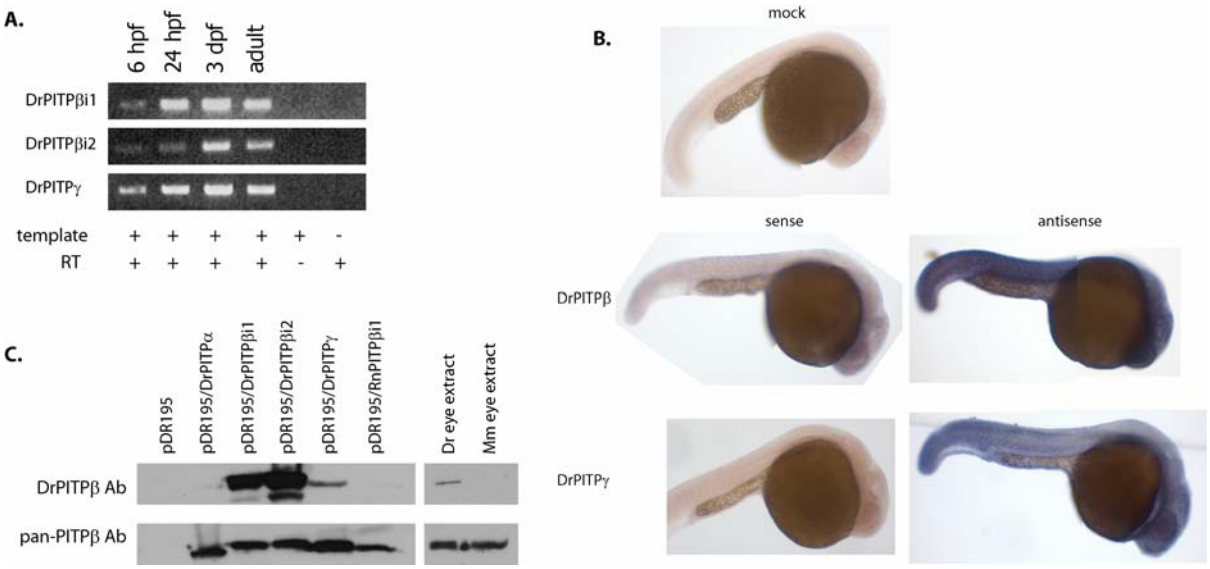

Figure 4.3. Temporal and spatial expression of DrPITPβ and DrPITPγ. **A)** DrPITPβ and DrPITPγ are expressed at all ages tested. RNA was collected from zebrafish at 6 and 24 hours past fertilization (hpf), 6 days past fertilization (dpf), and from adult fish. The RNA was reverse transcribed, and the respective cDNAs (template) amplified using primers directed against *DrPITPβ*, *DrPITPγ*, and actin sequences. The amplified cDNAs reflect relative mRNA abundance in each sample, and amplification of products was both dependent on template and reverse transcriptase (RT). **B)** In situ staining of *DrPITPβ* and *DrPITPγ* expression profiles. In situ hybridization analyses were performed on 28 hpf fish using specific antisense probes for *DrPITPβ* and *DrPITPγ* mRNAs, respectively. Sense probes were used as negative controls, as were "mock" controls where probe was omitted. Both *DrPITPβ* and *DrPITPγ* were expressed in a wide range of tissues throughout the adult fish, and *DrPITPβ* is most highly expressed in the eye. **C)** Characterization of DrPITPβ antibody. Individual DrPITPs were expressed in yeast, lysates were prepared, resolved by SDS-PAGE, transferred to nitrocellulose, and probed with either anti-DrPITPβ serum (top panel) or a control pan-PITP antibody (bottom panel) as indicated. To detect total PITPs in the eye, a blot with the same samples was probed with the

NT1/3 pan PITP antibody. This blot indicates that at least 2 species of PITP are expressed in the zebrafish eye. Protein extracts from zebrafish (Dr) or murine (Mm) eyes were also probed with these respective antibodies.

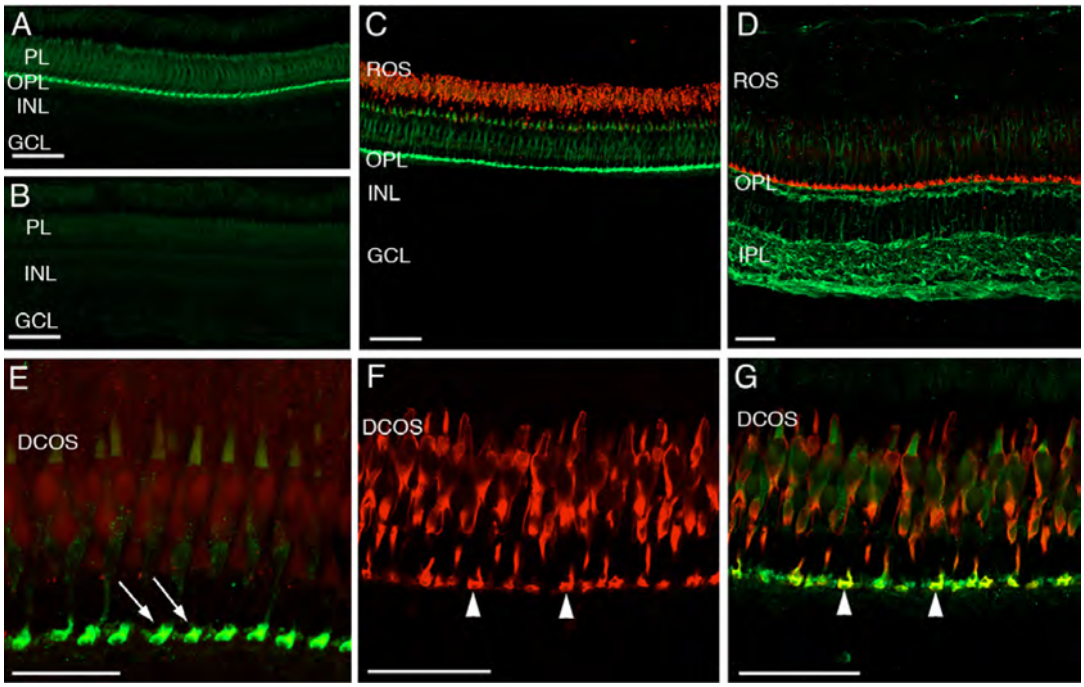

Figure 4.4. DrPITPβ immunolocalization in the adult zebrafish retina. Panel A depicts an adult retina cryosection labeled with the anti-DrPITPβ immunoglobulin. The labeling is confined to the photoreceptor layer (PL) and the outer plexiform layer (OPL). Panel B represents a negative control section labeled with pre-immune serum. Panel C shows a double-label experiment using where profiles of DrPITPβ (green; anti-DrPITPβ antibodies) and the zpr-1 marker (red; mAb zpr-3; labels the rod outer segments -- ROS) are visualized. Panel D represents a double-label image showing staining profiles for DrPITPβ (red) and α-tubulin (green). Panel E is a high magnification image of a DrPITPβ staining profile revealing the intense signal in the photoreceptor synaptic pedicles (arrows) in the OPL. Panel F highlights the zpr-1 staining profile (visualized via the mAb zpr-1 antibody), which specifically marks double cone cells. Panel G is a merged double-label image comparing DrPITPβ (green) and zpr-1 staining profiles (red). The data shown in panels F and G show were from frozen retinal sections. Arrowheads in Panels F and G point to the double-labeled cone cell synaptic pedicles. Abbreviations: PL,

photoreceptor layer; INL, inner nuclear layer; GCL, ganglion cell layer; ROS, rod outer segments; OPL, outer plexiform layer; IPL, inner plexiform layer; DCOS, double cone cell outer segments. Scale bars are 50 μm in all panels except Panel E (25 μm).

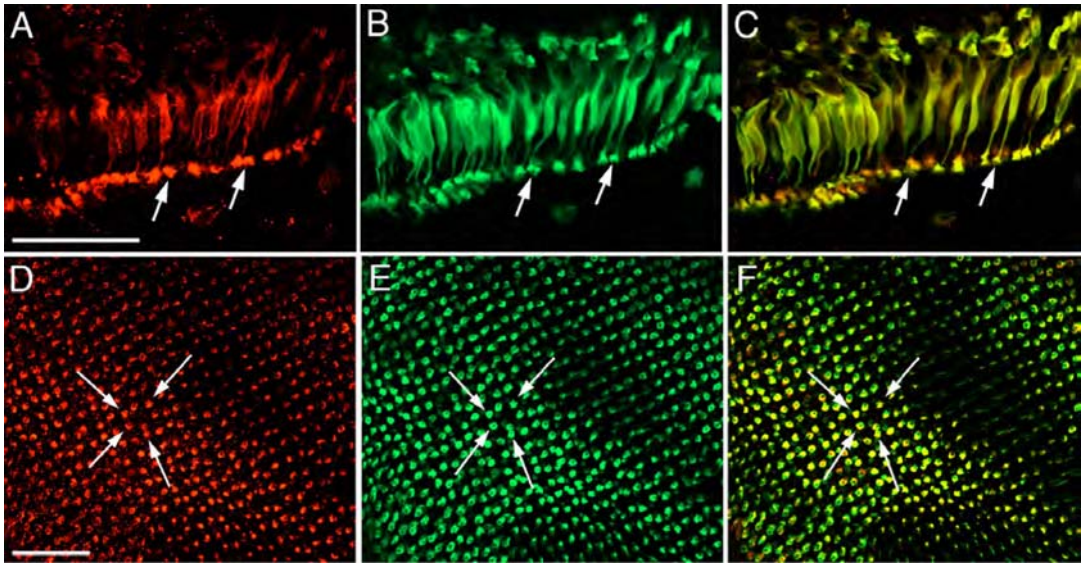

Figure 4.5. DrPITPβ and the double cone cell-specific zpr-1 antigen co-localize in adult retina. Panels A-C depict dissociated double cone cells labeled both with anti-DrPITPβ serum and mAb zpr-1. Panel A shows the DrPITPβ profile, Panel B the zpr-1 profile, and Panel C is a merged image. Arrows identify double cone cell synaptic pedicles. Panels D-F show DrPITPβ and zpr-1 staining profiles in retinal wholemounts at the level of cone cell synaptic pedicles. Panel D depicts the DrPITPβ profile, Panel E the zpr-1 (i.e. double cone cell) profile, and Panel F the merge. Arrows highlight the same individual labeled cone pedicles in each panel. There is perfect correspondence between DrPITPβ and zpr-1 signals at the level of double cone cell synaptic terminals. Scale bars -- 50 μm.

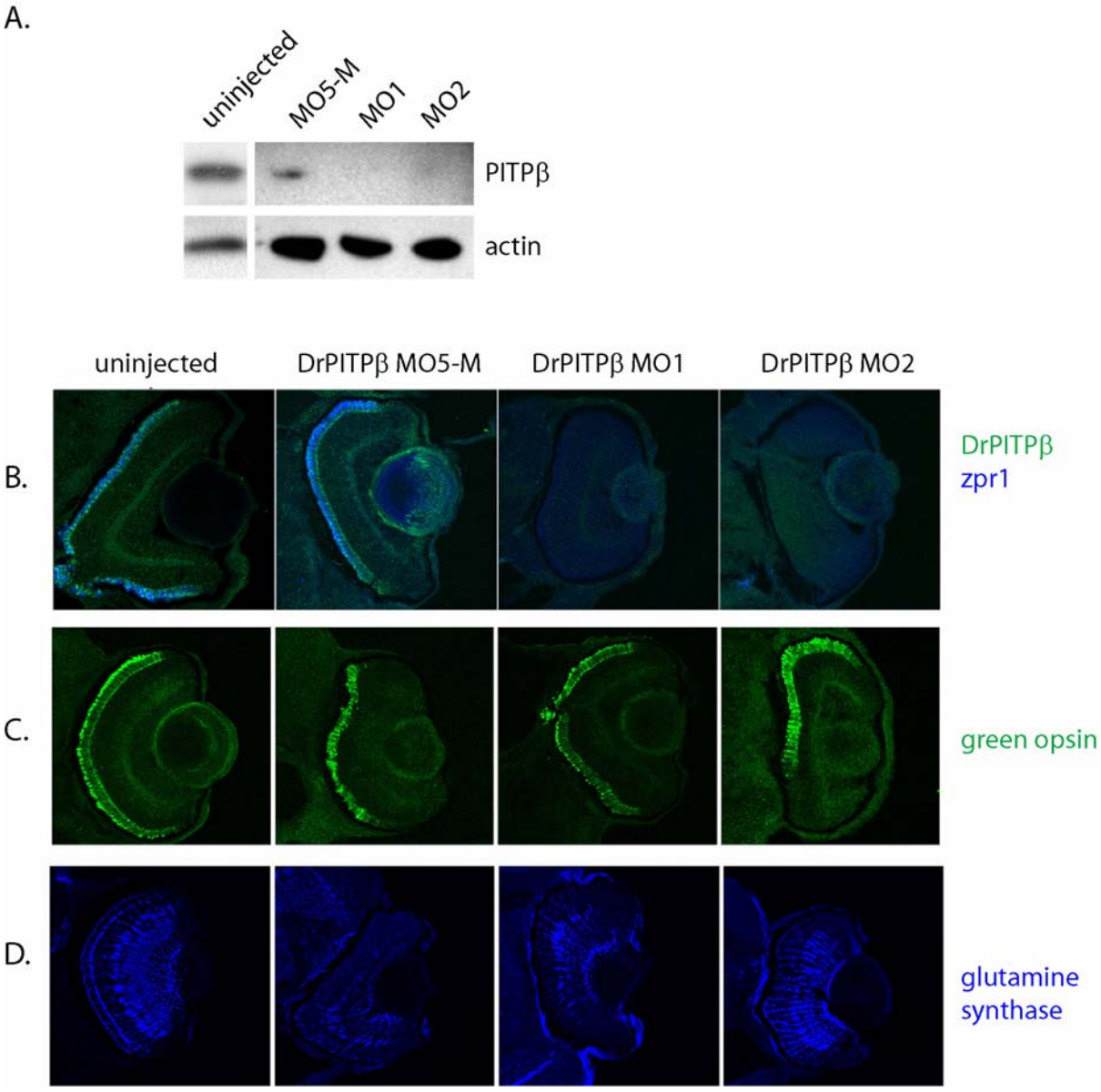

Figure 4.6. Reduced DrPITPβ expression results in loss of zpr1-staining. **A)** Morpholinos (DrPITPβ -directed morpholinos 1 and 2, a 5 mismatch control version of βMO1, and a non-specific negative control) were injected into 1-4 cell stage embryos. Three days after fertilization, embryos were disrupted, solubilized in sample buffer, proteins resolved by SDS-PAGE, and transferred to nitrocellulose. Blots probed with anti-DrPITPβ immunoglobulin reveal that βMO1 and βMO2, but not the controls, depress DrPITPβ protein levels. **B-D)**

Morphants were fixed at 3 dpf, embedded in OCT, and sectioned. Sections containing retina were stained for **B)** DrPITPβ and zpr1 antigen, **C)** green opsin, or **D)** glutamine synthase.

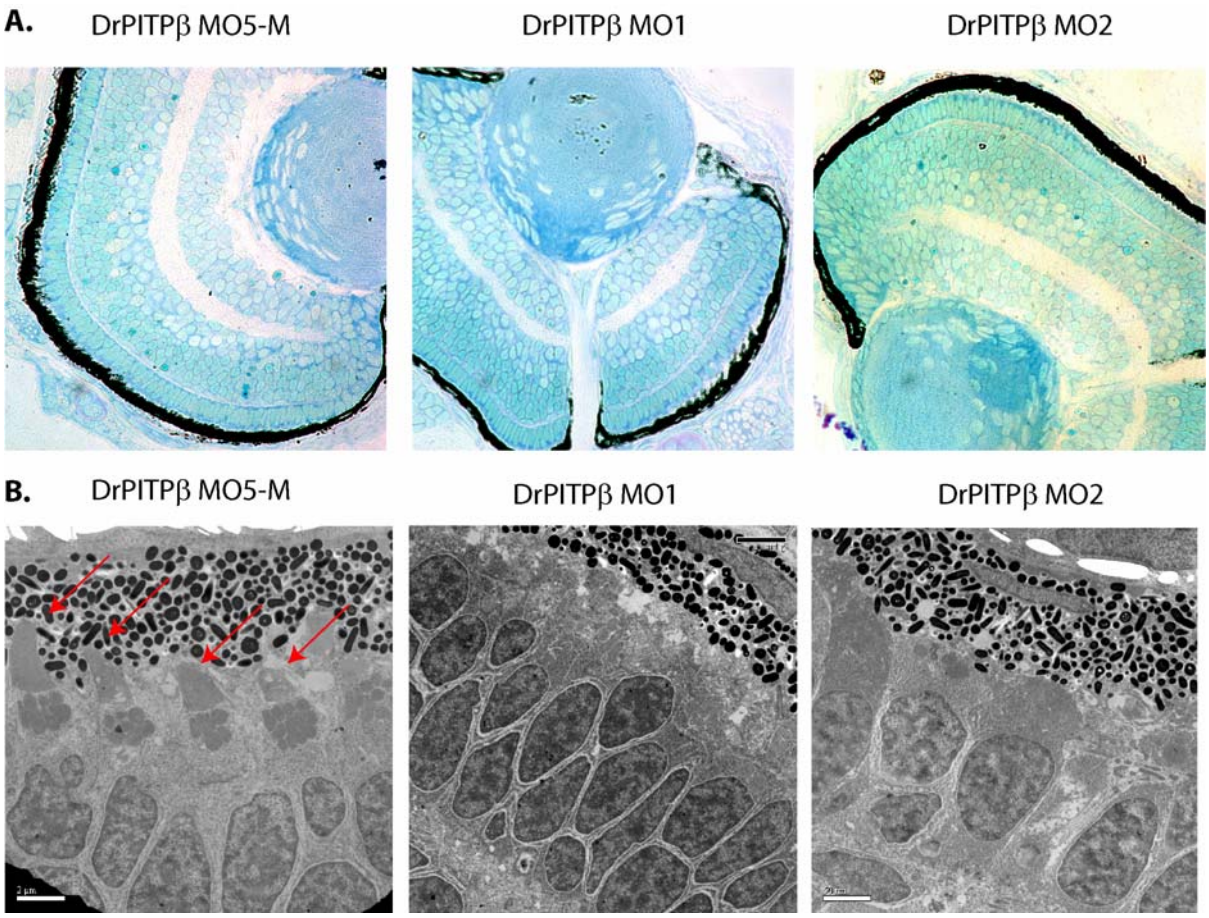

Figure 4.7. DrPITPβ morphants present double cone cell structural defects. **A)** Control and DrPITPβ morphants (3dpf) were fixed and dehydrated. After embedding in Polybed 812 resin, 3µm sections were cut and stained with 1:1 methylene blue:Azure II. No gross structural defects are observed in morphant eye sections relative to control. **B)** Ultrathin sections were stained with uranyl acetate and lead citrate, and visualized by electron microscopy. Outer cone cells are clearly recognized in the control by their well-formed and distinctive outer-segments (indicated by red arrows). These structures are absent, or otherwise unrecognizable, in morphant retina.

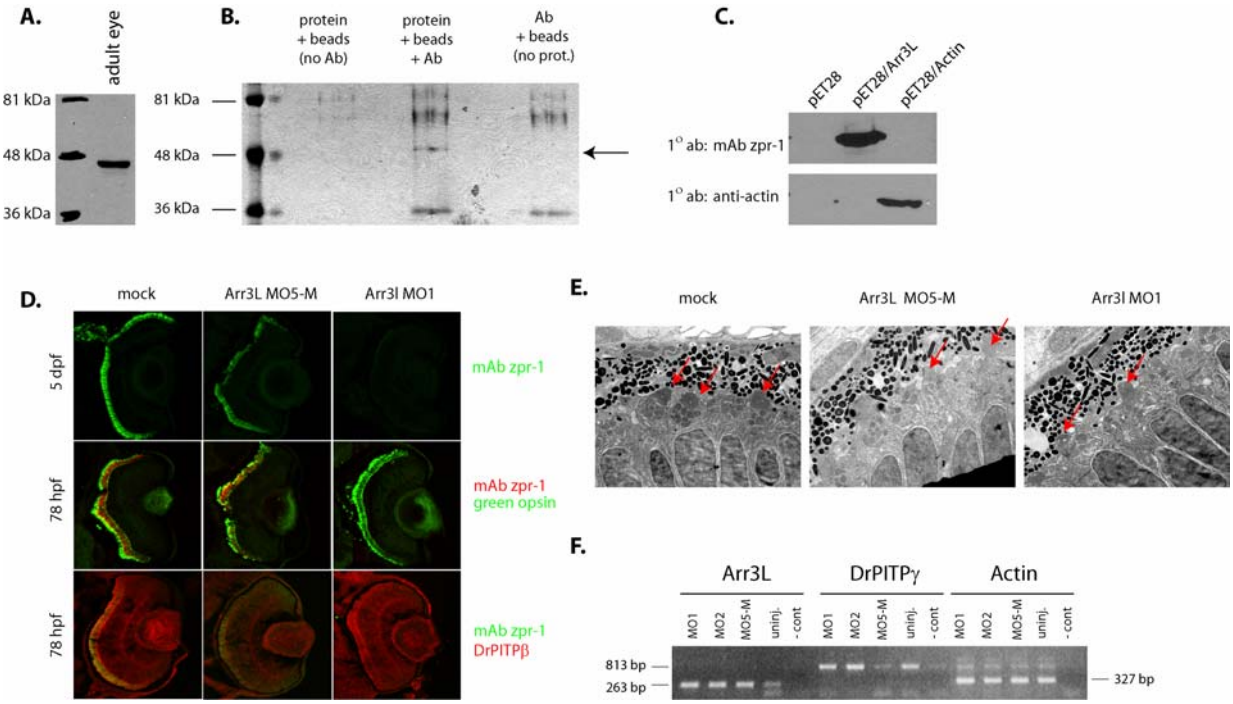

Figure 4.8. Identification of zpr1 antigen as arrestin-3-like. **A)** mAb zpr1 detects a ~50 kDa antigen in the adult zebrafish eye. Lysate of adult zebrafish eye was fractionated by SDS-PAGE, the resolved species transferred to nitrocellulose, and zpr-1 antigen identified by immunoblotting with mAb zpr1. **B)** A 50 kDa species is immunoprecipitated from adult zebrafish eye lysates. The lysates were precleared by incubation with protein A beads and re-incubated with mAb zpr1 and protein A beads. Proteins bound to the beads were resolved by SDS-PAGE. Two controls were included: sample without lysate, and sample without mAb zpr1. The species indicated with an arrow was uniquely recovered from the complete incubation, and was excised for identification by mass spectrometry. **C)** The previously uncharacterized zpr1 antigen is arrestin 3-like. Open reading frames of the two candidates for zpr1 antigen identified by MALDI-TOF mass spectrometry, β-actin and arrestin-like 3, were subcloned into pET28, and expressed in bacteria. Clarified lysates prepared from bacteria expressing each individual protein were resolved by SDS-PAGE, transferred to nitrocellulose, and blotted with mAb zpr1 or anti-actin immunoglobulin as indicated. Lysates prepared from bacteria carrying the pET28 vector alone

served as negative control. **D)** Arr3L morphants present reduced Arr3L immunoreactivity without affecting DrPITPβ expression. Embryos (1-4 cell stage) injected with morpholino against Arr3L, or the corresponding 5 mismatch control morpholino (MO5-M), were examined at 3 dpf for Arr3L, green opsin, and DrPITPβ staining. **E)** Arr3L morphants present normal outer segment morphologies. Morpholino-injected embryos were fixed and prepared for ultra-thin section electron microscopy. Sections from at least 3 fish were examined and representative images are shown. Outer segments are indicated with a red arrow. **F)** *ARR3L* gene expression is not impaired in DrPITPβ morphants. Embryos were injected with morpholinos against DrPITPβ (DrPITPβ MO1 and MO2) or corresponding negative controls (MO5-M and non-specific negative control). RNA was collected by Trizol extraction from 3 of each of the morphant categories, RNA was reverse-transcribed, and PCR amplification of the resulting cDNA was performed using primers specific for *ARR3L* sequences. *DrPITPγ* and *Dr-actin* sequences were amplified as normalization controls. For all primer sets, a water control ("-cont") was included. A representative morphant data set is shown.

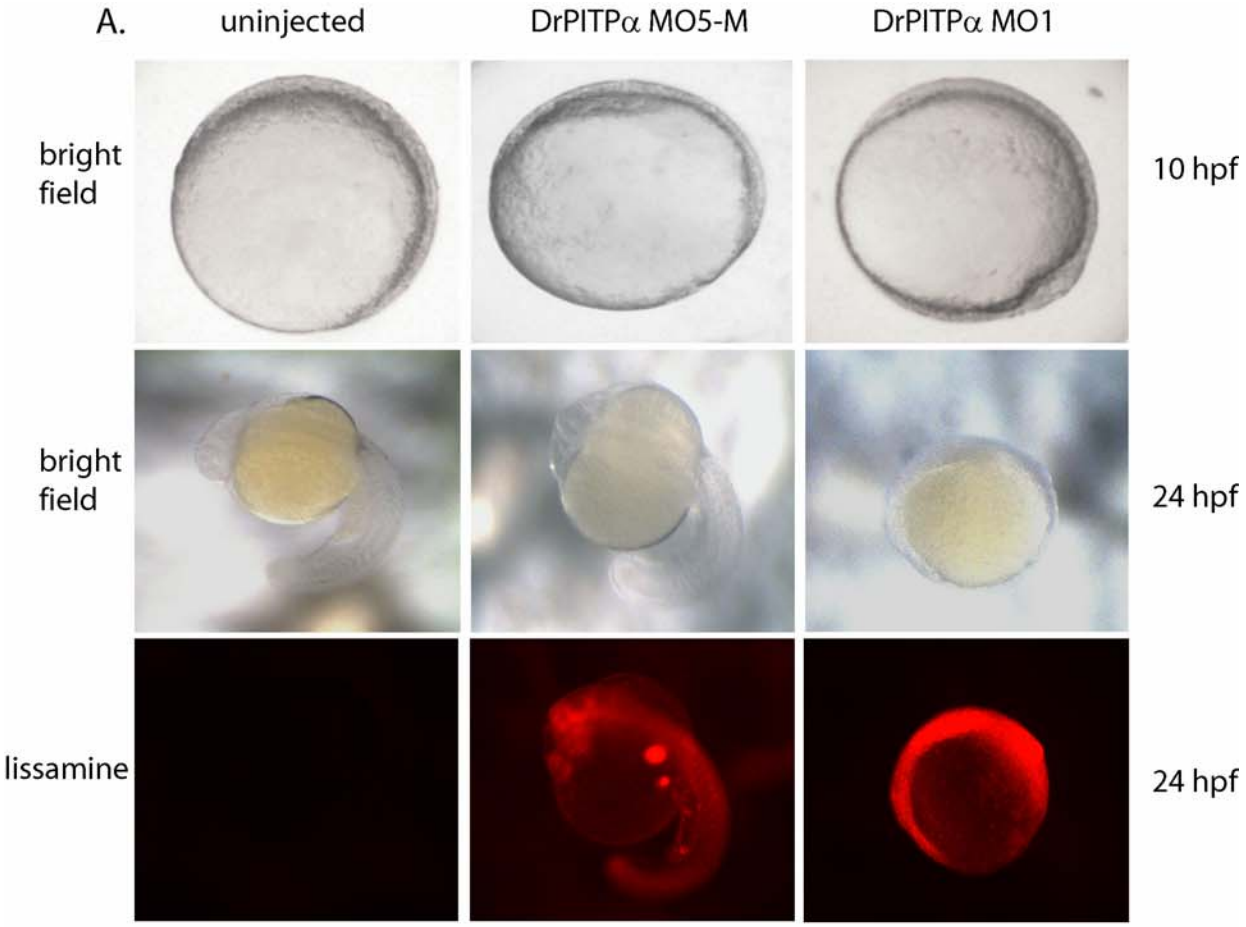
A.
uninjected
DrPITPα MO5-M
DrPITPα MO1
bright field
10 hpf
bright field
24 hpf
lissamine
24 hpf

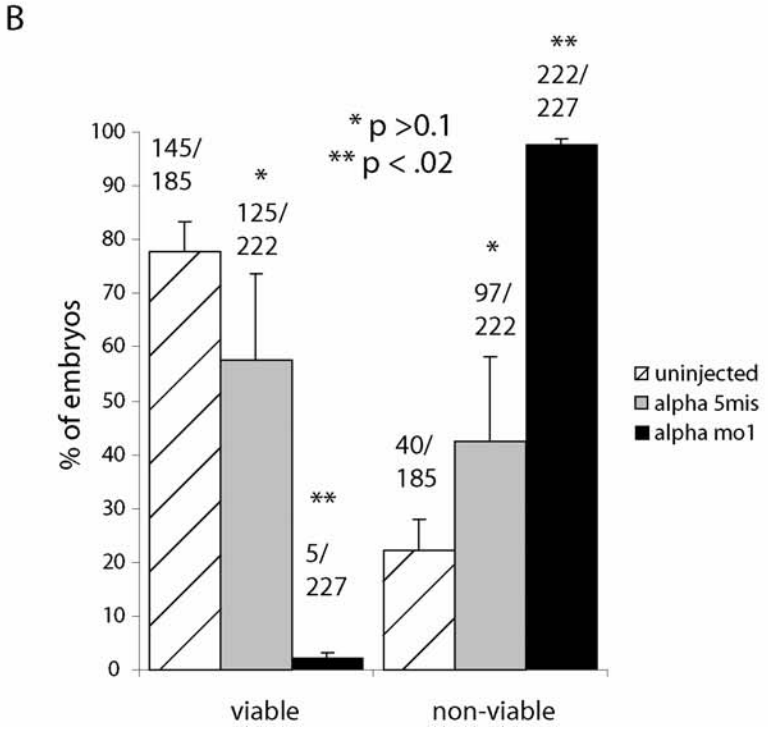
B
* p >0.1
** p < .02
145/ 185
*
125/ 222
**
5/ 227
40/ 185
*
97/ 222
**
222/ 227
% of embryos
100
90
80
70
60
50
40
30
20
10
0
viable
non-viable
uninjected
alpha 5mis
alpha mo1

Figure 4.9. DrPITPα morphants fail at an early stage of development. **A)** Zebrafish embryos were injected with DrPITPα-directed (DrPITPα MO1) or corresponding 5 mismatch control (DrPITPα MO5-M) morpholinos at the 1-4 cell stage, and brightfield images were taken at the indicated hpf. At 24 hours, images were also taken in the red fluorescence channel to identify embryos containing the lissamine-tagged morpholino. **B)** At 48 hours past fertilization, control and morpholino injected embryos were classified as viable or inviable based on visual inspection. Data are from three independent experiments, and p-values relative to the uninjected control are indicated (* $p>0.1$; ** $p<0.02$).

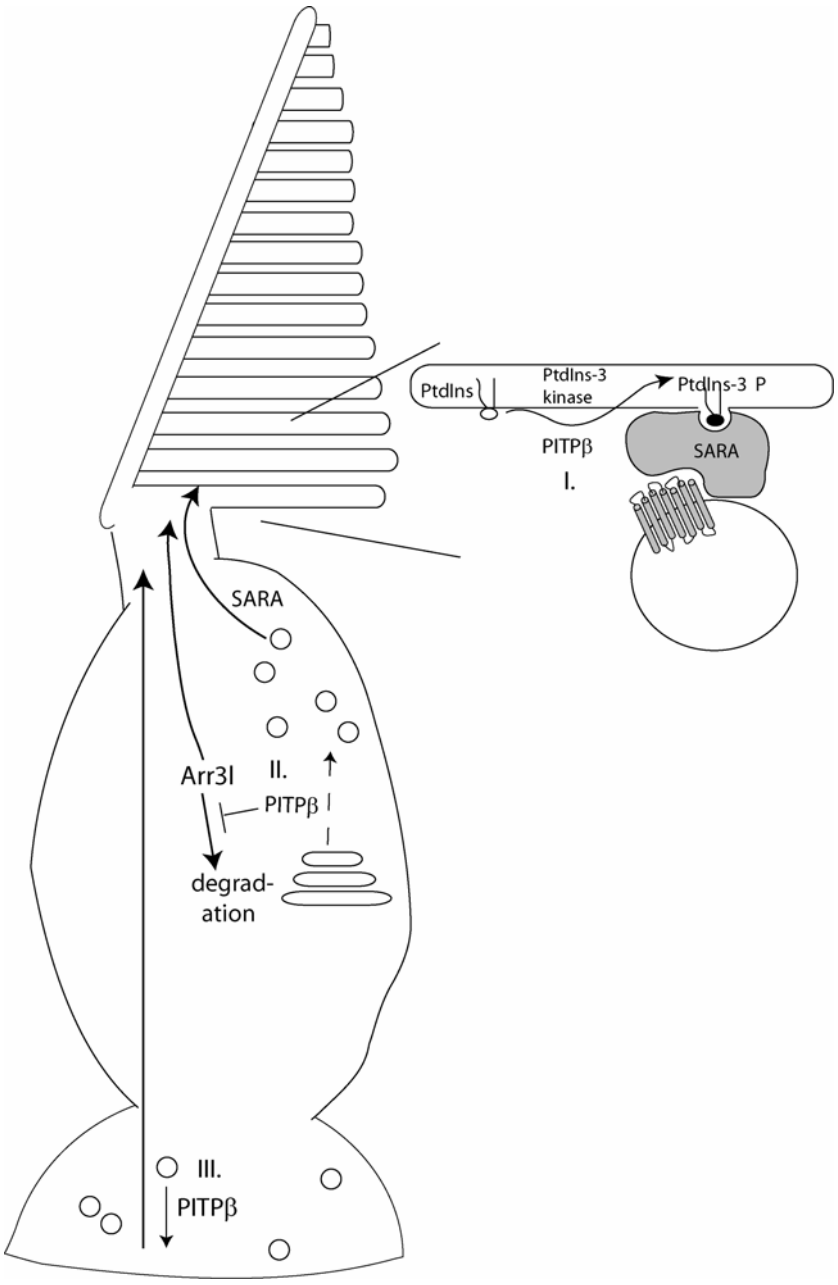

Figure 4.10. DrPITPβ function in double cone cell outer segment biogenesis and maintenance. **(I)** DrPITPβ cooperates with a PtdIns 3-OH kinase to promote PtdIns-3-phosphate production on the outer segment. PtdIns-3-phosphate serves as a landmark on the outer segment membrane that facilitates SARA-regulated docking and fusion of opsin-containing vesicles to the outer segment (acceptor compartment). **(II)** DrPITPβ cooperates with what would likely be a PtdIns 4-OH kinase, at the level of the double cone cell Golgi complex, to promote formation of opsin-

containing vesicles that will ultimately fuse to outer segment discs in a SARA-regulated manner. **(III)** DrPITPβ regulates signaling in the synaptic pedicle and the robustness of this signaling is transduced from the synaptic pedicle to outer segments. In this model, DrPITPβ may promote formation/fusion of synaptic vesicles and, in the absence of proper synaptic signaling, the outer segment of the cone cell is not maintained. In all three scenarios, Arr3L protein stability is suggested to be dependent on its association with functional outer segments.

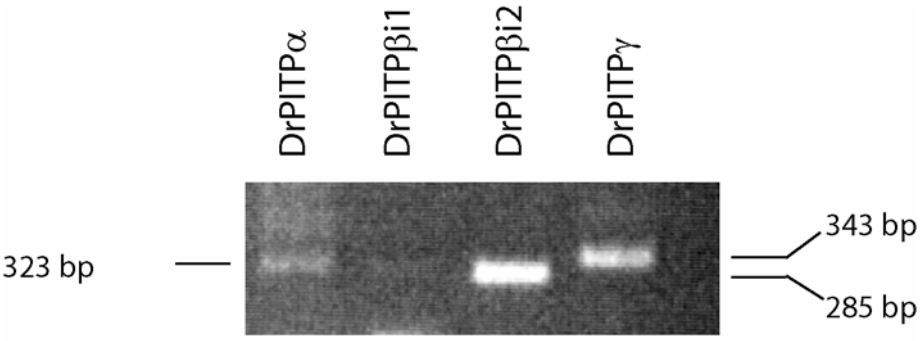

Supplementary Figure S1 (Figure 4.11) – All PITP isoforms are expressed in the adult zebrafish eye. Total RNA was extracted from an adult zebrafish eye, and reverse transcribed into cDNA. PCR amplification was performed with primers specific for *DrPITPα*, *DrPITPβi1*, *DrPITPβi2* or *DrPITPγ* sequences.

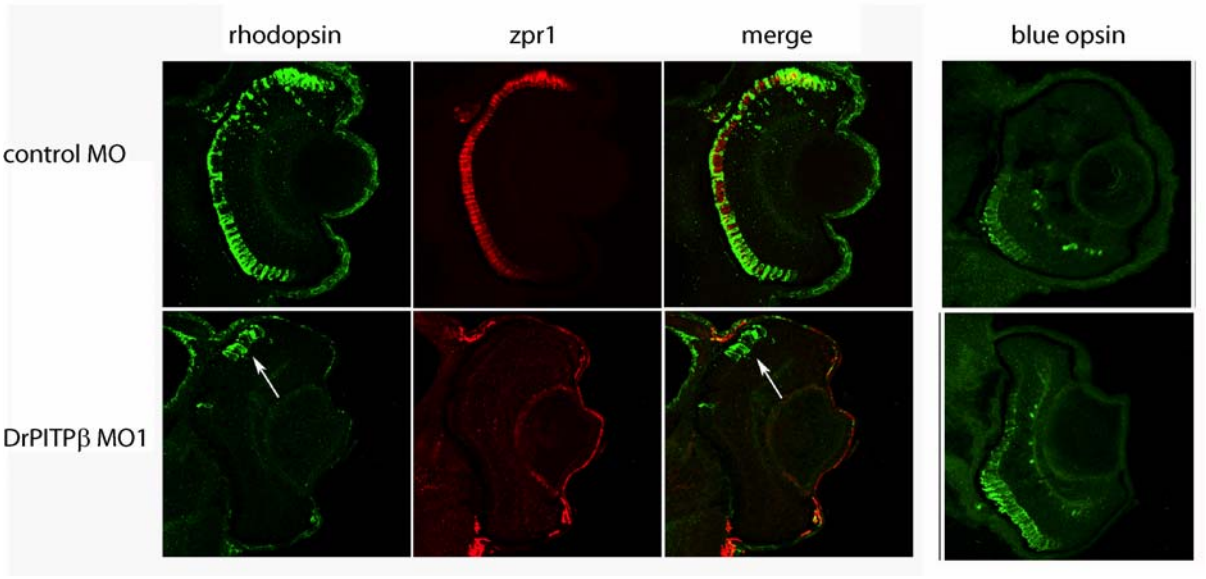

Supplementary Figure S2 (Figure 4.12) – Blue opsin and rhodopsin expression are unaffected in DrPITPβ morphants. Zebrafish embryos injected with negative control morpholino or *DrPITPβ* MO1 were fixed, embedded, and cryosectioned at 3 dpf. Sections through the center of the retina were stained for zpr1 and the rod cell opsin (rhodopsin) (left panels), or the single cone cell marker blue opsin (right panel). Blue opsin and rhodopsin staining are present in both control and morphant eye sections, while mAb zpr1-staining is seen only in the control.

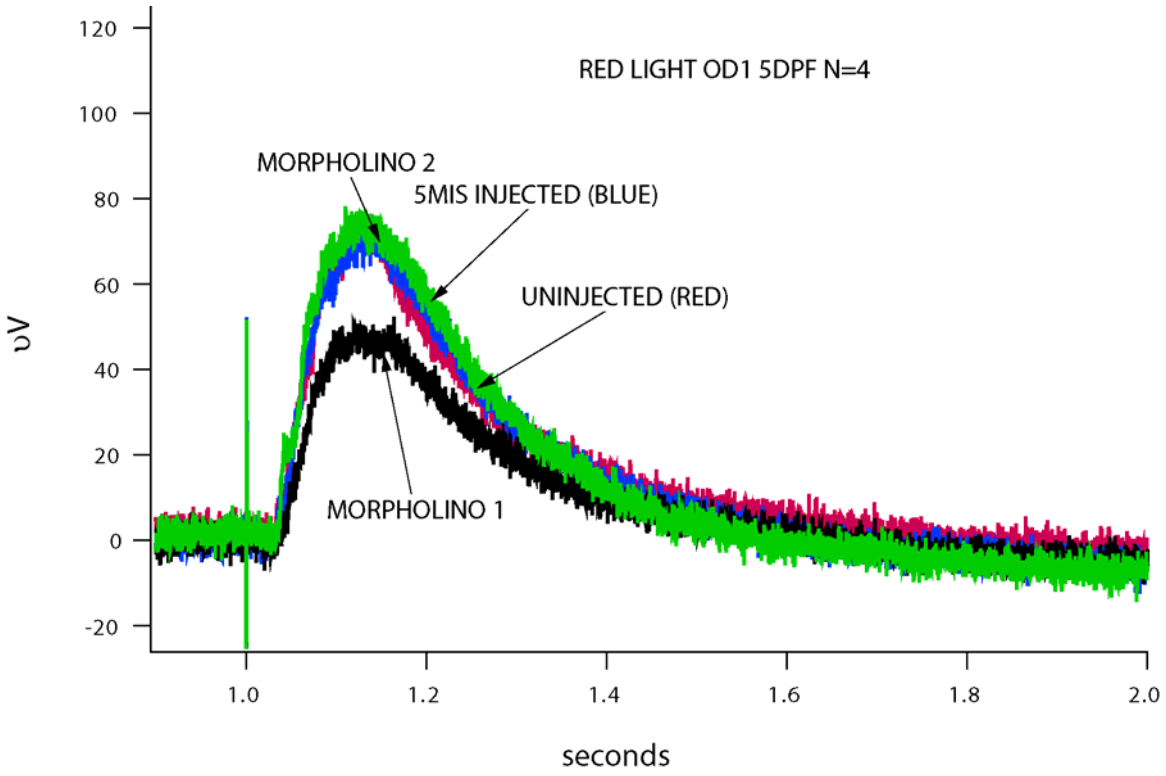

Supplementary Figure S3 (Figure 4.13) – At 5dpf, DrPITPβ morphants display no defects in electroretinograms (ERGs) measuring their response to light. Zebrafish embryos were injected at the 1-4 cell stage with control or DrPITPβ morpholinos, and the ERG was performed at 5 dpf. Following a flash of light, recordings from all of the fish indicated a rapid response ("b-wave") of similar magnitudes followed by a recovery to baseline. Data are representative of at least 10 ERGs performed on 2 sets of morphants.

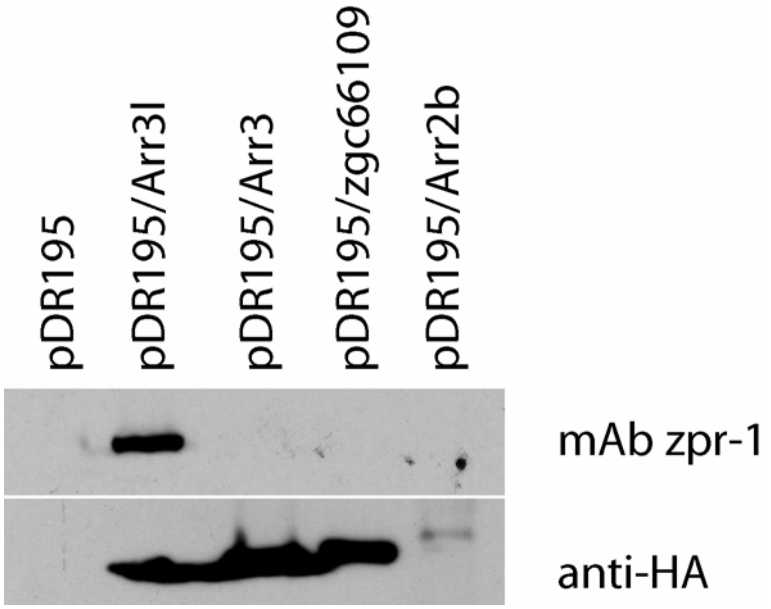

Supplementary Figure S4 (Figure 4.14) – MAb zpr1 only detects Arr3L, and not other retinal and ubiquitously expressed arrestins. The open reading frame of *ARR3L* and five additional zebrafish arrestins were PCR amplified from an adult zebrafish cDNA library with primers also encoding an HA epitope-tag. The PCR products were subcloned into a yeast expression vector (pDR195) and transformed into yeast. Lysates were prepared from the resulting yeast strains, lysate proteins were separated by SDS-PAGE, transferred to nitrocellulose, and probed with mAb zpr-1 and anti-HA. Though all of the arrestins were expressed (as detected by the HA antibody), only Arr3L was detected by mAb zpr1.

primer name	sequence (5' to 3')
PITPalpha XhoI for	AAACTCGAGATGTTGATAAAGGAGTTTCG
PITPalpha SacII rev	AAACCGCGGTCATTCATCTGCGGCAGACATCCC
PITPbeta XhoI for	AAACTCGAGATGGTGCTCATCAAGGAATATCG
PITPbeta i1 SacII rev	AAACCGCGGCTACTCTTCAGATGCTGTTGTGCCTC
PITPbeta i2 SacII rev	AAACCGCGGTCATTGTTCGTGAGCAGCACTGG
PITPgamma XhoI for	AAACTCGAGATGGTACTCATCAAGCAATACCAGG
PITPgamma SacII rev	AAACCGCGGCTAGTCCTCGCCCGCTTTCATCCC

Supplementary Table S1 – Primers used to amplify zebrafish PITP structural genes.

Sample (Band/ Spot)	Well	office use only	Protein Name	Species	Database Accession ID [1]	MW (Da)	Peptide Count [2]	MS & MS/MS Score [3]	Peptide sequenced Ion Score [4]	Scoring threshold [5]
1		1	Arrestin 3, retinal (X-arrestin), like.- Brachydanio rerio	Danio rerio	Q6DH07_BRARE	39475.5	20	574	440	55
			BC063950 NID: - Danio rerio	Danio rerio	AAH63950	41739.7	17	535	419	55

NOTE: Please note that the observed peptides may match more than one protein from a given database. In cases where more than one protein matches the same peptides, only the highest scoring protein is reported.

1 = For the protein sequence search this ID at "http://www.ncbi.nlm.nih.gov", change search parameter to "Protein"
If the protein isn't found at NCBI try searching the MSDB database found at http://csc-fserve.hh.med.ic.ac.uk/msdb.html then Clink on Link: "Searching MSDB" and enter the Database Accession # (listed in the table) as the "P code"

2 = Number of peptides that match the theoretical digest of the primary protein identified.

3 = Score of the quality of the peptide-mass fingerprint match and the quality of the MS/MS peptide fragment ion matches (if MS/MS data was generated).

4 = Score of the quality of MS/MS peptide fragment ion matches only (if MS/MS data was generated).

5 = Significant score threshold. An "MS & MS/MS score" above this value indicates a significant identification ($p<0.05$) for the given database.

Supplementary Table S2 – MALDI-TOF mass spectrometry of mAb-zpr1 ligand. The gel-purified polypeptide species specifically precipitated from the adult zebrafish eye by mAb zpr-1 (Figure 8) was submitted for analysis by mass spectrometry. Two proteins were identified from tryptic digests of the submitted sample, and the summary analytical report is shown.

References

Aitken, J.F., van Heusden, G.P., Temkin, M., and Dowhan, W. (1990). The gene encoding the phosphatidylinositol transfer protein is essential for cell growth. J Biol Chem *265*, 4711-4717.

Alb, J.G., Jr., Cortese, J.D., Phillips, S.E., Albin, R.L., Nagy, T.R., Hamilton, B.A., and Bankaitis, V.A. (2003). Mice lacking phosphatidylinositol transfer protein-alpha exhibit spinocerebellar degeneration, intestinal and hepatic steatosis, and hypoglycemia. J Biol Chem *278*, 33501-33518.

Alb, J.G., Jr., Gedvilaite, A., Cartee, R.T., Skinner, H.B., and Bankaitis, V.A. (1995). Mutant rat phosphatidylinositol/phosphatidylcholine transfer proteins specifically defective in phosphatidylinositol transfer: implications for the regulation of phospholipid transfer activity. Proc Natl Acad Sci U S A *92*, 8826-8830.

Alb, J.G., Jr., Phillips, S.E., Rostand, K., Cui, X., Pinxteren, J., Cotlin, L., Manning, T., Guo, S., York, J.D., Sontheimer, H., Collawn, J.F., and Bankaitis, V.A. (2002). Genetic ablation of phosphatidylinositol transfer protein function in murine embryonic stem cells. Mol Biol Cell *13*, 739-754.

Barthel, L.K., and Raymond, P.A. (1990). Improved method for obtaining 3-microns cryosections for immunocytochemistry. J Histochem Cytochem *38*, 1383-1388.
Berridge, M.J., and Irvine, R.F. (1989). Inositol phosphates and cell signalling. Nature *341*, 197-205.

Bok, D., and Young, R.W. (1972). The renewal of diffusely distributed protein in the outer segments of rods and cones. Vision Res *12*, 161-168.

Bringmann, A., Pannicke, T., Grosche, J., Francke, M., Wiedemann, P., Skatchkov, S.N., Osborne, N.N., and Reichenbach, A. (2006). Muller cells in the healthy and diseased retina. Prog. Retin. Eye Res. *25*, 397-424.

Chuang, J.Z., Zhao, Y., and Sung, C.H. (2007). SARA-regulated vesicular targeting underlies formation of the light-sensing organelle in mammalian rods. Cell *130*, 535-547.

Cleves, A.E., McGee, T.P., Whitters, E.A., Champion, K.M., Aitken, J.R., Dowhan, W., Goebl, M., and Bankaitis, V.A. (1991). Mutations in the CDP-choline pathway for phospholipid biosynthesis bypass the requirement for an essential phospholipid transfer protein. Cell *64*, 789-800.

de Vries, K.J., Heinrichs, A.A., Cunningham, E., Brunink, F., Westerman, J., Somerharju, P.J., Cockcroft, S., Wirtz, K.W., and Snoek, G.T. (1995). An isoform of the phosphatidylinositol-transfer protein transfers sphingomyelin and is associated with the Golgi system. Biochem J *310 (Pt 2)*, 643-649.

De Vries, K.J., Westerman, J., Bastiaens, P.I., Jovin, T.M., Wirtz, K.W., and Snoek, G.T. (1996). Fluorescently labeled phosphatidylinositol transfer protein isoforms (alpha and beta), microinjected into fetal bovine heart endothelial cells, are targeted to distinct intracellular sites. Exp Cell Res *227*, 33-39.

Dickeson, S.K., Lim, C.N., Schuyler, G.T., Dalton, T.P., Helmkamp, G.M., Jr., and Yarbrough, L.R. (1989). Isolation and sequence of cDNA clones encoding rat phosphatidylinositol transfer protein. J Biol Chem *264*, 16557-16564.

Foti, M., Audhya, A., and Emr, S.D. (2001). Sac1 lipid phosphatase and Stt4 phosphatidylinositol 4-kinase regulate a pool of phosphatidylinositol 4-phosphate that functions in the control of the actin cytoskeleton and vacuole morphology. Mol Biol Cell *12*, 2396-2411.

Fruman, D.A., Meyers, R.E., and Cantley, L.C. (1998). Phosphoinositide kinases. Annu Rev Biochem *67*, 481-507.

Fullwood, Y., dos Santos, M., and Hsuan, J.J. (1999). Cloning and characterization of a novel human phosphatidylinositol transfer protein, rdgBbeta. J Biol Chem *274*, 31553-31558.

Guo, S., Stolz, L.E., Lemrow, S.M., and York, J.D. (1999). SAC1-like domains of yeast SAC1, INP52, and INP53 and of human synaptojanin encode polyphosphoinositide phosphatases. J Biol Chem *274*, 12990-12995.

Helmkamp, G.M., Jr., Harvey, M.S., Wirtz, K.W., and Van Deenen, L.L. (1974). Phospholipid exchange between membranes. Purification of bovine brain proteins that preferentially catalyze the transfer of phosphatidylinositol. J Biol Chem *249*, 6382-6389.

Hsuan, J., and Cockcroft, S. (2001). The PITP family of phosphatidylinositol transfer proteins. Genome Biol *2*, REVIEWS3011.

Hurley, J.H., and Meyer, T. (2001). Subcellular targeting by membrane lipids. Curr Opin Cell Biol *13*, 146-152.

Ile, K.E., Schaaf, G., and Bankaitis, V.A. (2006). Phosphatidylinositol transfer proteins and cellular nanoreactors for lipid signaling. Nat Chem Biol *2*, 576-583.

Irvine, R.F., and Schell, M.J. (2001). Back in the water: the return of the inositol phosphates. Nat Rev Mol Cell Biol *2*, 327-338.

Jones, S.M., Alb, J.G., Jr., Phillips, S.E., Bankaitis, V.A., and Howell, K.E. (1998). A phosphatidylinositol 3-kinase and phosphatidylinositol transfer protein act synergistically in formation of constitutive transport vesicles from the trans-Golgi network. J Biol Chem *273*, 10349-10354.

Kearns, M.A., Monks, D.E., Fang, M., Rivas, M.P., Courtney, P.D., Chen, J., Prestwich, G.D.,

Theibert, A.B., Dewey, R.E., and Bankaitis, V.A. (1998). Novel developmentally regulated phosphoinositide binding proteins from soybean whose expression bypasses the requirement for an essential phosphatidylinositol transfer protein in yeast. Embo J *17*, 4004-4017.

Larison, K.D., and Bremiller, R. (1990). Early onset of phenotype and cell patterning in the embryonic zebrafish retina. Development *109*, 567-576.

Lemmon, M.A. (2003). Phosphoinositide recognition domains. Traffic *4*, 201-213.

Li, X., Routt, S.M., Xie, Z., Cui, X., Fang, M., Kearns, M.A., Bard, M., Kirsch, D.R., and Bankaitis, V.A. (2000). Identification of a novel family of nonclassic yeast phosphatidylinositol transfer proteins whose function modulates phospholipase D activity and Sec14p-independent cell growth. Mol Biol Cell *11*, 1989-2005.

Lu, C., Peng, Y.W., Shang, J., Pawlyk, B.S., Yu, F., and Li, T. (2001). The mammalian retinal degeneration B2 gene is not required for photoreceptor function and survival. Neuroscience *107*, 35-41.

Majerus, P.W. (1992). Inositol phosphate biochemistry. Annu Rev Biochem *61*, 225-250.

McGee, T.P., H.B. Skinner, E.A. Whitters, S.A. Henry, and **V.A. Bankaitis**. 1994. A phosphatidylinositol transfer protein controls the phosphatidylcholine content of yeast Golgi membranes. J.Cell Biol. *124*, 273-287.

Morgan, C.P., Allen-Baume, V., Radulovic, M., Li, M., Skippen, A., and Cockcroft, S. (2006). Differential expression of a C-terminal splice variant of phosphatidylinositol transfer protein beta lacking the constitutive-phosphorylated Ser262 that localizes to the Golgi compartment. Biochem J *398*, 411-421.

Nemoto, Y., Kearns, B.G., Wenk, M.R., Chen, H., Mori, K., Alb, J.G., Jr., De Camilli, P., and Bankaitis, V.A. (2000). Functional characterization of a mammalian Sac1 and mutants exhibiting substrate-specific defects in phosphoinositide phosphatase activity. J Biol Chem *275*, 34293-34305.

Nishizuka, Y. (1995). Protein kinase C and lipid signaling for sustained cellular responses. Faseb J *9*, 484-496.

Phillips, S.E., Ile, K.E., Boukhelifa, M., Huijbregts, R.P., and Bankaitis, V.A. (2006a). Specific and nonspecific membrane-binding determinants cooperate in targeting phosphatidylinositol transfer protein beta-isoform to the mammalian trans-Golgi network. Mol Biol Cell *17*, 2498-2512.

Phillips, S.E., Sha, B., Topalof, L., Xie, Z., Alb, J.G., Klenchin, V.A., Swigart, P., Cockcroft, S., Martin, T.F., Luo, M., and Bankaitis, V.A. (1999). Yeast Sec14p deficient in phosphatidylinositol transfer activity is functional in vivo. Mol Cell *4*, 187-197.

Phillips, S.E., Vincent, P., Rizzieri, K.E., Schaaf, G., Bankaitis, V.A., and Gaucher, E.A. (2006b). The diverse biological functions of phosphatidylinositol transfer proteins in eukaryotes. Crit Rev Biochem Mol Biol *41*, 21-49.

Rajendran, L., and Simons, K. (2005). Lipid rafts and membrane dynamics. J Cell Sci *118*, 1099-1102.

Rentsch, D., Laloi, M., Rouhara, I., Schmelzer, E., Delrot, S., and Frommer, W.B. (1995). NTR1 encodes a high affinity oligopeptide transporter in Arabidopsis. FEBS Lett *370*, 264-268.

Rhee, S.G. (2001). Regulation of phosphoinositide-specific phospholipase C. Annu Rev Biochem *70*, 281-312.

Rivas, M.P., Kearns, B.G., Xie, Z., Guo, S., Sekar, M.C., Hosaka, K., Kagiwada, S., York, J.D., and Bankaitis, V.A. (1999). Pleiotropic alterations in lipid metabolism in yeast sac1 mutants: relationship to "bypass Sec14p" and inositol auxotrophy. Mol Biol Cell *10*, 2235-2250.

Ryan, M.M., Temple, B.R., Phillips, S.E., and Bankaitis, V.A. (2007). Conformational dynamics of the major yeast phosphatidylinositol transfer protein sec14p: insight into the mechanisms of phospholipid exchange and diseases of sec14p-like protein deficiencies. Mol Biol Cell *18*, 1928-1942.

Schaaf, G., Ortlund, E.A., Tyeryar, K.R., Mousley, C.J., Ile, K.E., Garrett, T.A., Ren, J., Woolls, M.J., Raetz, C.R., Redinbo, M.R., and Bankaitis, V.A. (2008). Functional anatomy of phospholipid binding and regulation of phosphoinositide homeostasis by proteins of the Sec14 superfamily. Mol Cell *29*, 191-206.

Skinner, H.B., Alb, J.G., Jr., Whitters, E.A., Helmkamp, G.M., Jr., and Bankaitis, V.A. (1993). Phospholipid transfer activity is relevant to but not sufficient for the essential function of the yeast SEC14 gene product. EMBO J *12*, 4775-4784.

Strahl, T., and Thorner, J. (2007). Synthesis and function of membrane phosphoinositides in budding yeast, Saccharomyces cerevisiae. Biochim Biophys Acta *1771*, 353-404.

Swigart, P., Insall, R., Wilkins, A., and Cockcroft, S. (2000). Purification and cloning of phosphatidylinositol transfer proteins from Dictyostelium discoideum: homologues of both mammalian PITPs and Saccharomyces cerevisiae sec14p are found in the same cell. Biochem J *347 Pt 3*, 837-843.

Tanaka, S., and Hosaka, K. (1994). Cloning of a cDNA encoding a second phosphatidylinositol transfer protein of rat brain by complementation of the yeast sec14 mutation. J Biochem *115*, 981-984.

Vihtelic, T.S., Doro, C.J., and Hyde, D.R. (1999). Cloning and characterization of six zebrafish

photoreceptor opsin cDNAs and immunolocalization of their corresponding proteins. Vis Neurosci *16*, 571-585.

Vihtelic, T.S., Goebl, M., Milligan, S., O'Tousa, J.E., and Hyde, D.R. (1993). Localization of Drosophila retinal degeneration B, a membrane-associated phosphatidylinositol transfer protein. J Cell Biol *122*, 1013-1022.

Vihtelic, T.S., and Hyde, D.R. (2000). Light-induced rod and cone cell death and regeneration in the adult albino zebrafish (Danio rerio) retina. J Neurobiol *44*, 289-307.

Wirtz, K.W. (1991). Phospholipid transfer proteins. Annu Rev Biochem *60*, 73-99.

Xie, Y., Ding, Y.Q., Hong, Y., Feng, Z., Navarre, S., Xi, C.X., Zhu, X.J., Wang, C.L., Ackerman, S.L., Kozlowski, D., Mei, L., and Xiong, W.C. (2005). Phosphatidylinositol transfer protein-alpha in netrin-1-induced PLC signalling and neurite outgrowth. Nat Cell Biol *7*, 1124-1132.

Yanagisawa, L.L., Marchena, J., Xie, Z., Li, X., Poon, P.P., Singer, R.A., Johnston, G.C., Randazzo, P.A., and Bankaitis, V.A. (2002). Activity of specific lipid-regulated ADP ribosylation factor-GTPase-activating proteins is required for Sec14p-dependent Golgi secretory function in yeast. Mol Biol Cell *13*, 2193-2206.

Young, R.W. (1974). Biogenesis and renewal of visual cell outer segment membranes. Experimental Eye Research *18*, 215-223.

Chapter 5 - Discussion

In the present work I addressed two main questions: 1) What is the function of metazoan PITPs and PITPβ in particular? 2) What distinguishes PITPβ from PITPα? In this discussion, I will review my findings and present areas for further study.

Distinction between PITPα and PITPβ in mammals

In Chapter 2, I addressed several factors that distinguish mammalian PITPα from PITPβ. We were able to show that PITPβ localizes primarily to the trans-Golgi network (TGN) and that its localization is independent of the phospholipid-bound state of PITPβ. The question remains, however, of which features are essential for the unique properties of the molecule. Based on known properties of PITPα and PITPβ, we hypothesized that either localization or binding of sphingolmyelin (SM) are the distinguishing features of PITPβ. SM is the major sphingolipid in mammals and is synthesized at the TGN from ceramide and phosphatidylcholine by sphingomyelin synthase. A PITPβ loss of function system is necessary to test the importance of these features.

PITPβ in mammalian cells

We have found that, in mammalian cells, PITPβ plays a role in maintaining the structure and anterograde trafficking function of the Golgi. The reduction of PITPβ levels by siRNA ultimately leads to cell death. The Golgi and trafficking phenotypes, along with known properties of PITPβ lead us to propose that PITPβ regulates lipid levels in the Golgi. What role might PITPβ play in Golgi lipid regulation?

With our recent development of an siRNA-mediated knockdown system for PITPβ in human cell lines (chapter 3), we are now in a unique position to address the role of PITPβ at the Golgi and in lipid regulation through the following questions: i) Are the individual phospholipid binding/ transfer activities and in particular the sphingomyelin (SM) transfer/binding activity essential properties of PITPβ? To this end, we have generated PtdIns binding mutants that still retain their ability to bind PtdCho/SM and SM binding mutants that retain their ability to bind PtdIns and PtdCho (Chapter 2, Alb *et al.*, 1995; Tilley *et al.*, 2004). ii) If both SM and PtdIns binding activities are individually required for PITPβ function, we can investigate whether SM and PtdIns lipid binding properties have to reside in *cis* in order to reconstitute a functional PITPβ. iii) How important is Golgi localization of PITPβ in order to rescue Golgi morphological defects and trafficking defects associated with lack of PITPβ? The outcome of these questions will help us to understand the molecular mechanism by which PITPβ and metazoan PITPs in general might execute biological function.

A requirement for lipid binding activities in *cis* (e.g. SM and PtdIns) would suggest that, similar to Sec14, PITPβ mediates a lipid exchange reaction in which one of the exchanged lipids becomes a better substrate for a downstream lipid-modifying enzyme. In the case of Sec14, an absolute requirement for binding of PtdIns and PtdCho in *cis* and cumulative evidence that Sec14 genetically interacts with PtdIns 4-OH kinases and is required for the biosynthesis of PtdIns(4)P led to a model in which PtdIns is presented to a PtdIns 4-OH kinase during an exchange reaction with PtdCho (Schaaf *et al.*, 2008).

With regard to the function of PITPβ, we can only speculate at this point. Could PITPβ function in a similar manner to Sec14? Is exchange of PtdIns with PtdCho or SM a prerequisite to make PtdIns vulnerable for PtdIns 4-OH kinase attack? Structurally, the PITPs and Sec14 molecules are distinct, and it would seem that PITPβ does not share the same mechanism of action with Sec14. PtdIns, PtdCho, and SM bind in essentially the same site of the PITP molecules, unlike the distinct headgroup binding sites in Sec14. However, structural considerations - lipid close to the protein surface (as in the case of Sec14) versus deep ligand or different lipids with almost identical atomic coordination, as in the case of PtdIns, PtdCho and SM in PITPs, have limited significance as long as exchange intermediates and the topology of the exchange reaction remain unknown. In addition, functional data in yeast indicate that, like Sec14, PITPs increase PtdIns(4)P levels, suggesting a potential role of PITPs to present PtdIns to a PtdIns 4-OH kinase, at least in heterologous systems (Chapter 4).

If PITPβ did have the lipid presentation mechanism of Sec14, likely presentation scenarios could either be that PITPβ presents PtdIns to PtdIns kinases like Sec14, or it presents PtdCho to SM synthase during a PL exchange reaction ultimately regulating DAG levels. Presentation of SM to the SM synthase would decrease DAG levels and increase PtdCho levels, which is inconsistent with the functional data indicating a role for PITPβ in allowing trafficking from the Golgi, though of course this function cannot yet be ruled out.

In order to fully investigate the presentation scenario proposed above, we would need to develop a PtdCho binding mutant of PITPβ. Because the PtdIns and PtdCho headgroups bind at the same site of the PITP molecule and the PtdIns headgroup is larger,

it has so far been impossible to identify a PtdCho binding mutant. Rescue experiments with the PtdIns and SM will still give important insight into the functions of these molecules. For example, if both PtdIns binding/transfer and SM binding/transfer activities are individual required for PITPβ function, but, unlike Sec14 these binding activities can be combined in *trans* (e.g. by co-expression of different PL-binding mutants) to reconstitute a functional PITPβ, this result would be more indicative of an *in vivo* transfer role of PITPβ where vectorial transfer of substrate is required for biological function. An example for this reaction mechanism has been described for the ceramide transfer protein CERT (Hanada *et al.*, 2003). In this latter case, vectorial transfer of ceramide from the ER to the Golgi to deliver the substrate for the SM-synthase is an essential property of the protein (Hanada *et al.*, 2009).

Future experiments to test whether the phenotypes in PITPβ siRNA-treated cells could be attributed to changes in lipid levels could be done by increasing levels of relevant lipids (through addition of membrane-permeable short chain lipids) to see if the Golgi phenotypes are rescued. If increasing lipid levels rescued effects due to loss of PITPβ, a more direct role for PITPβ in presenting lipid could be tested in biochemical assays. A PtdIns-kinase assay has been established in our lab (Schaaf *et al.*, 2008), and this assay or a similar assay with purified sphingomyelin synthase could be performed. SM-synthase performs the interconversion of PtdCho and ceramide with SM and DAG, so purified sphingomyelin synthase would be used to look at modification of either SM or PtdCho.

Alternatively, alterations in lipid composition of PITPβ siRNA- treated cells could be analyzed. Experiments with lipid sensors did not show large scale changes in

lipid levels, but changes below the detection limits of the sensors could still affect trafficking. Direct measurements of lipid composition of subcellular compartments would be helpful, however Golgi-membranes cannot be easily isolated without introducing artifacts during lipid extraction. Measuring total cell lipid extracts might hide potentially significant alterations in Golgi PL composition. A potential breakthrough in this regard might come from recent advances in immunoisolation procedures for recovery of specific membrane compartments combined with a novel quantitative shotgun lipidomics approach by improved mass-spectrometric techniques (Klemm *et al.*, 2009).

Rescue of loss of PITPβ-associated phenotypes

A prerequisite to investigate the functional activity of mutant proteins is a functional rescue experiment in PITPβ siRNA-treated cells. First attempts to establish this rescue system failed. Potential reasons for the difficulties to rescue siRNA-treated cells are that the levels of the rescue protein are too high or too low. Varying levels of expression have been tested, but perhaps all were outside the correct range. Additionally, PITPβ may require specific control of its expression not provided by plasmid rescue. The total cDNA of PITPβ (with 5' and 3' UTR) is currently being cloned, with hopes that the UTRs will provide the additional level of expression regulation. The cell culture/siRNA system may not be the ideal system for rescue experiments, if, for example, the siRNAs interfere with proper expression of the rescue plasmids. An additional weakness of the siRNA system is that not every cell has the same level of PITPβ knockdown, making it difficult to assess both phenotypes and rescue. With these

limitations in mind, the mouse system may be a better system to both see phenotypes and perform rescue.

The conditional knockout (or "floxed") PITPβ mice or ES cells are an ideal system to address PITPβ function. In Appendix A, I describe the construction of a vector where critical exons of PITPβ are flanked by loxP sites. In the presence of the cre molecule, the DNA sequence between the loxP sites is excised by site-specific recombination. The advantage of this system over the siRNA system is that PITPβ expression can be completely and irreversibly removed, and we can study what happens in a true "loss of function" situation. In addition, because of the different mechanism and level of loss of PITPβ expression, rescue experiments may be more easily performed.

PITPα and PITPβ in zebrafish

Since the rescue experiments of PITPβ siRNA-treated cells proved to be difficult and are still in an somewhat initial state, we investigated PITP function in zebrafish, which has the advantages of a well established, effective method of reducing protein expression (morpholinos), and easy detection of early developmental defects.

We found that DrPITPβ expression is particularly strong in double cone cells of the zebrafish retina, and that the two DrPITPβ spliceoforms are collectively required for the biogenesis or maintenance of the outer segments of double cone photoreceptor cells in the developing retina. Reduction of PITPβ levels by morpholino (MO) injection has no effect on the survival or gross morphology of the fish up to 3 dpf. Effects are seen in the eye, but, based on the ubiquitous expression of PITPβ as shown by in situ hybridization, it seems possible that other organ systems might be affected as well. In contrast, a minimal level of DrPITPα activity is essential for successful execution of

early developmental programs. Zebrafish treated with PITPα MO arrest at ~10-12 hpf, and die by 48 hpf. Unlike MmPITPβ, DrPITPα does not appear to be required for cell survival, since cells survive and divide for the initial stages of development. In addition to PITPα and PITPβ homologues, zebrafish have an additional member of the soluble PITP cohort, which we've termed PITPγ. So far, the function of DrPITPγ is unknown, though we hypothesize that it could perform the housekeeping function performed in mammals by MmPITPβ.

Despite the similar lipid transfer properties of zebrafish and mammalian PITPα/β orthologue pairs, PITPα and PITPβ orthologues in zebrafish have very different functions than their mammalian counterparts, which suggests that functional differences between PITPα and PITPβ may depend on more than just localization and SM binding ability. Further proof that biochemical properties and localization may not define the function of the PITPs comes from the identification of PITPγ, a novel PITP with the same properties of PITPβ. Though its function has not yet been shown, PITPγ is unlikely to share the same specific function of PITPβ.

Using zebrafish to understand PITPs

The ablation of PITPs in zebrafish provides unique loss of function phenotypes, and a new way to understand PITPs. The early arrest phenotype of PITPα morphants is particularly interesting. At the point of arrest, a number of key events are occurring in the development of the animal, including neural tube and tail bud formation. Is PITPα involved in either of these events? To answer this question, the expression patterns of a number of developmental markers should be determined. Key markers would be flh, a transcription factor involved in neural tube closure (Talbot *et al.*, 1995); ntl, which is

required for both neural tube closure and tail formation; ph2α which is expressed at the time and site of tail bud formation (Komoike *et al.*, 2005), and myoD, to determine if somites have begun to form (Pownall *et al.*, 2002).

The expression patterns of PITPα mRNA (http://zfin.org/cgi-bin/webdriver?MIval=aa-fxallfigures.apg&OID=ZDB-PUB-040907-1&fxallfig_probe_zdb_id=ZDB-CDNA-040425-1670) at later stages are consistent with sites of PITPα function in mouse (e.g. brain and intestine). One possibility is that DrPITPα has similar roles to MmPITPα in adult fish, but has an additional role in a developmental process. I propose to test this hypothesis by injecting a small dose of zebrafish PITPα mRNA (with silent mutations to make it resistant to the morpholino) along with the morpholino. mRNA is generally degraded more quickly than a morpholino, thus the net effect would be an early "burst" of PITPα expression, followed by PITPα null conditions. This experiment could give an initial idea of what processes/tissue systems PITPα is required for once the stage of the initial arrest is passed.

Our findings are somewhat at odds with a work published by the Xiong group showing that PITPα morpholino injection leads to axon guidance defects. Our results show that zebrafish injected with standard doses of PITPα morpholino do not survive to the stage indicated by (Xie *et al.*, 2005). However, this discrepancy might be simply explained by a dose dependent effect of MO application. In our hands, zebrafish embryos that receive low doses of PITPα morpholino can survive for longer periods of time, and we hypothesize that these were the conditions that were employed in the work mentioned above. If this is indeed the case, the finding would be consistent with recent

work carried out in mouse, where even 50-80% reduction of PITPα levels leads to neuronal phenotypes (Hamilton *et al.*, 1997; Alb *et al.*, 2003), M. Boukhelifa, unpublished data).

The function of PITPγ remains an open and intriguing question. Since MmPITPβ is essential in mammalian cells, and neither MmPITPα nor MmPITPβ are essential in zebrafish, we hypothesize that PITPγ could be essential in zebrafish. Alternatively, another molecule (perhaps another less closely related member of the PITP family) might perform the function of the mammalian PITPβ in zebrafish. We have attempted to study the function of PITPγ by morpholino knockdown. However, our results (lack of any phenotype) are difficult to interpret since we cannot assess knockdown efficiency (data not shown). In future experiments, we would like to address the problem of assessing knockdown in one of two ways. A splice site morpholino, which prevents proper splicing, and thus proper expression of a gene, could be employed, since efficiency of splice site morpholinos can be determined by RT-PCR. Alternatively, a PITPγ-specific antibody could be generated. These antibodies could not only be used to investigate efficiency of the MO knockdown by western blot analyses but also (dependent on the quality of the antibody) to study the subcellular localization within zebrafish cells.

If loss of PITPγ has an early embryonic lethal phenotype, it could serve as a good system to test rescue of PITP function in zebrafish. In contrast, the PITPβ morphant is not ideal for rescue experiments since injected (resistant) mRNAs will likely degrade by the time the eye phenotype is seen. A PITP morphant with an early phenotype could be used to determine the essential functions of the PITP by employing localization mutants, PL-binding mutants and chimeras.

DrPITPβ in the zebrafish eye, like the MmPITPα in the mammalian intestine is an example of PITP function in a specialized system. Interestingly, PITPs in the eye, the intestine, and the brain all function in polarized cell types with high membrane turnover requirements, suggesting a common function or mechanisms for the mammalian PITPα and the zebrafish PITPβ.

Further studies of PITPβ in the zebrafish eye are complicated by the fact that morpholinos are only effective in the first several days of development, and the eye is difficult to study at this age. To better understand the phenotype of PITPβ, and whether any other organs are affected, it would be useful to get or make a PITPβ knockout line. Libraries of zebrafish with viral insertions that can disrupt genes have been developed by Znomics (Portland, Oregon). Several lines with insertions in the PITPβ gene are available. Even though insertions could only be identified in introns and promoter regions, they may be sufficient to disrupt gene expression. If gene expression is indeed substantially reduced in these lines, we can not only investigate the effect of reduced PITPβ on the maintenance of the outer segments of double cone photoreceptor cells, but also ask whether these cells can develop at all in the absence of PITPβ. Any potential impairment of cone cell formation or development could also be further investigated by electrophysiology, and we can confirm (or refute) whether the loss of double cone cells leads to a decreased electrophysiological response, as we would predict.

Alb, J.G., Jr., Cortese, J.D., Phillips, S.E., Albin, R.L., Nagy, T.R., Hamilton, B.A., and Bankaitis, V.A. (2003). Mice lacking phosphatidylinositol transfer protein-alpha exhibit spinocerebellar degeneration, intestinal and hepatic steatosis, and hypoglycemia. J Biol Chem *278*, 33501-33518.

Alb, J.G., Jr., Gedvilaite, A., Cartee, R.T., Skinner, H.B., and Bankaitis, V.A. (1995). Mutant rat phosphatidylinositol/phosphatidylcholine transfer proteins specifically defective in phosphatidylinositol transfer: implications for the regulation of phospholipid transfer activity. Proc Natl Acad Sci U S A *92*, 8826-8830.

Hamilton, B.A., Smith, D.J., Mueller, K.L., Kerrebrock, A.W., Bronson, R.T., van Berkel, V., Daly, M.J., Kruglyak, L., Reeve, M.P., Nemhauser, J.L., Hawkins, T.L., Rubin, E.M., and Lander, E.S. (1997). The vibrator mutation causes neurodegeneration via reduced expression of PITP alpha: positional complementation cloning and extragenic suppression. Neuron *18*, 711-722.

Hanada, K., Kumagai, K., Tomishige, N., and Yamaji, T. (2009). CERT-mediated trafficking of ceramide. Biochim Biophys Acta *1791*, 684-691.

Hanada, K., Kumagai, K., Yasuda, S., Miura, Y., Kawano, M., Fukasawa, M., and Nishijima, M. (2003). Molecular machinery for non-vesicular trafficking of ceramide. Nature *426*, 803-809.

Klemm, R.W., Ejsing, C.S., Surma, M.A., Kaiser, H.J., Gerl, M.J., Sampaio, J.L., de Robillard, Q., Ferguson, C., Proszynski, T.J., Shevchenko, A., and Simons, K. (2009). Segregation of sphingolipids and sterols during formation of secretory vesicles at the trans-Golgi network. J Cell Biol *185*, 601-612.

Komoike, Y., Kawamura, A., Shindo, N., Sato, C., Satoh, J., Shiurba, R., and Higashinakagawa, T. (2005). Zebrafish Polycomb group gene ph2alpha is required for epiboly and tailbud formation acting downstream of FGF signaling. Biochem Biophys Res Commun *328*, 858-866.

Pownall, M.E., Gustafsson, M.K., and Emerson, C.P. (2002). MYOGENIC REGULATORY FACTORS AND THE SPECIFICATION OF MUSCLE PROGENITORS IN VERTEBRATE EMBRYOS doi:10.1146/annurev.cellbio.18.012502.105758. Annual Review of Cell and Developmental Biology *18*, 747-783.

Schaaf, G., Ortlund, E.A., Tyeryar, K.R., Mousley, C.J., Ile, K.E., Garrett, T.A., Ren, J., Woolls, M.J., Raetz, C.R., Redinbo, M.R., and Bankaitis, V.A. (2008). Functional anatomy of phospholipid binding and regulation of phosphoinositide homeostasis by proteins of the sec14 superfamily. Mol Cell *29*, 191-206.

Talbot, W.S., Trevarrow, B., Halpern, M.E., Melby, A.E., Farr, G., Postlethwait, J.H., Jowett, T., Kimmel, C.B., and Kimelman, D. (1995). A homeobox gene essential for zebrafish notochord development. Nature *378*, 150-157.

Tilley, S.J., Skippen, A., Murray-Rust, J., Swigart, P.M., Stewart, A., Morgan, C.P., Cockcroft, S., and McDonald, N.Q. (2004). Structure-function analysis of human

[corrected] phosphatidylinositol transfer protein alpha bound to phosphatidylinositol. Structure *12*, 317-326.

Xie, Y., Ding, Y.Q., Hong, Y., Feng, Z., Navarre, S., Xi, C.X., Zhu, X.J., Wang, C.L., Ackerman, S.L., Kozlowski, D., Mei, L., and Xiong, W.C. (2005). Phosphatidylinositol transfer protein-alpha in netrin-1-induced PLC signalling and neurite outgrowth. Nat Cell Biol *7*, 1124-1132.

Appendix A: Mouse models of PITPβ

Part I: Gene trap mouse

Materials and Methods

Cell culture

The following gene trap ES cells were ordered from the Sanger Institute for Genomic Research (SIGTR): AG0287, CD0139, AR0037, and AQ0491. Gene trap and unmodified ES cells were cultured as described previously (Alb *et al.*, 2002) in DMEM supplemented with 50 μg/mL Penn-Strep, 2 mM L-glutamine, 15% FBS, 1 mM sodium pyruvate, 1X non-essential amino acids, LIF, and β-mercaptoethanol.

Gene trap cassette localization

Genomic DNA and cDNA were prepared from 60 mm dishes of ES cell line using the Qiagen AllPrep DNA/RNA mini kit. PCR to determine the trapped exon was performed on gene trap ES cell cDNA with the βgeo1 reverse primer, and forward primers in exons 3-9 (sequences in Table m1). The intronic insertion site of the gene trap was identified using the βgeo2 reverse primer and forward primers in intron 7 (relevant primer sequences shown in Table m1). The PCR product of the i710500f and βgeo2 reverse primers was sequenced to find the exact site of insertion.

Injection of ES cells and identification of gene trap mice

ES cell injection was performed by the University of North Carolina Animal Models Core. The AR0037 ES cell line was injected into E3.5 C57BL/6 embryos, which were implanted into pseudopregnant females. Chimeric male progeny were mated to wild type females to identify males capable of germ line transmission.

Results

Three gene trap ES cell lines target to intron 7

Though previous studies indicated that PITPβ was required for normal development, the knockout line was not ideal for screening embryos, and we have not been able to stage a careful analysis of the age of lethality. Identifying the exact stage of lethality is critically important to our understanding of PITPβ's function. Very early embryonic lethality would suggest a housekeeping role for PITPβ, while mid-gestation lethality would indicate a specific developmental role for PITPβ. I therefore attempted to create a new, easily screenable knockout model for PITPβ.

Several companies and institutions have generated libraries of knockout mice using a method developed by Zambrowicz et al and Wiles et al (Zambrowicz *et al.*, 1998; Wiles *et al.*, 2000). In this method a DNA cassette is electroporated into ES cells and will randomly incorporate into the genome. The cassette contains a splice acceptor site, a neomycin resistance gene and a β-gal expression gene, followed by a transcription termination site. In cells where the cassette inserts into an intron, the splice acceptor site diverts normal splicing, preventing expression of the wild type protein. Instead, cells express a neomycin resistance gene and β-gal, permitting the screening of cells with a gene diverting insertion. Reverse sequencing from the gene trap identifies the gene that is "trapped" by the insertion. In addition to providing a "ready to use" knockout mouse model, these mice can be used to study expression patterns of a gene, since β-gal is expressed under the gene's promoter.

A search of the Sanger Institute Gene Trap Resource online database of available gene trap lines (http://www.sanger.ac.uk/PostGenomics/genetrap/) with PITPβ sequence found 5 lines reported to trap in PITPβ (search performed in August 2005). One of these

lines with a reported insertion in intron 1 (line RRC161 from Bay Genomics) had been previously analyzed in the lab. Despite a clear insertion site in intron 1 in the RRC161 line, and consistent splice diversion in ES cells, the gene trap did not divert splicing in mice (Phillips, unpublished data). Thus, this line cannot be used to create a knockout mouse model. Of the remaining four lines, sequencing results on the SIGTR website indicated that the gene trap was after exon 6 for one line (CD0139) and after exon 7 for the other three lines (AG0287, AR0037, and AQ0491). We ordered all four lines in order to confirm the site of gene trap insertion and choose the best line for our experiments.

We first checked the ES cell cDNA to confirm that the splice trap interrupted the PITPβ gene. The cell lines were expanded, and cDNA was prepared from a plate of the cells. Using the 100f and 200f forward primers in exons 3 and 4 of PITPβ and a reverse primer in the gene trap, I amplified a clear band from three of the four ES cell lines (AG0287, CD0139, and AR0037). PCR amplification from line AQ0491 cDNA using the 100f and 200f primers did not yield product, indicating that the gene trap does not fall in PITPβ (data not shown). Thus, this line was not studied further.

We then performed PCR analysis to confirm that the insertion diverts splicing after the reported exon. PCR amplification with primer 400f from exon 7 of PITPβ yeilded product for all three lines, but primers 500f and 600f, from exon 8 and exon 9, respectively, do not yield product (Figure m1). The gene trap in line CD0139 had previously been reported to fall in intron 6, but the PCR results indicate that the trap falls in intron 7. This inconsistency was likely a consequence of poor sequencing on the SIGTR website where exon 7 was not detected.

Since the gene trap insertion lines allow expression of exons of a gene before the insertion site, we investigated whether the three exon 7 trapping lines would be suitable knockout models. We examined which portion of PITPβ would be expressed in the three lines trapping after exon 7, and found that Exons 1-7 of PITPβ express 152 amino acids of the protein. Based on previously published crystal structures(Yoder *et al.*, 2001; Vordtriede *et al.*, 2005), this fragment would not be expected to form a complete lipid binding pocket. Thus, we expect that an intron 7 gene trap insertion would act as a knockout.

Determination of the intronic location of gene trap in AR0037

It is necessary to identify the intronic site of the gene trap insertion in order to design a genomic DNA (gDNA) PCR screen that can efficiently identify gene trap heterozygous mice. gDNA was prepared from the three PITPβ splice trap lines, and screened by PCR using reverse primers in the gene trap and forward primers in intron 7. Forward primers were designed at every 1-1.5 kb in the first 11.5 kb of the 21.7 kb intron 7. Only one line had the gene trap inserted within the first 11.5 kb: AR0037 (Figure m1). Forward primers i7 8500f, i7 9500f and i7 10500f but not i7 11500f gave products, and the products of the i7 8500f, 9500f, and 10500f primers increased by approximately 1000 bp, as expected from the placement of the primers. Sequencing of the i7 10500f forward and gene trap reverse primer PCR product indicated that the gene trap was inserted around nt 10797 of intron 7, with much of the targeting vector present before the gene trap cassette.

Based on the sequence information, I designed PCR screening primers. The forward primer was the i7 10500f primer described above, and the reverse primers

(pGTOlxRr1 and pGTOlxRr2) were designed to fall in the pGTOlxr targeting vector, about 500 base pairs upstream of the PITPβ intron 7 insertion site. The i7 10500f primer with both pGTOlxr reverse primers works on genomic ES cell DNA, providing two sets of primers that could be used to screen mice for the presence of the gene trap insertion.

AR0037 ES cells generate chimeric mice but do not transmit through the germline

AR0037 ES cells were grown up and injected into E3.5 embryos by the UNC Animal Models core. Two injections of separate batches of cells were performed, yielding 14 chimeric mice. The chimeras were mated with wild type mice, and 12 of the 14 chimeras produced offspring. A total of approximately 50 litters of mice were born from matings of the chimeras, and none of these mice were agouti, indicating that germline transmission of the gene trap did not occur. Possible reasons for the lack of germline transmission and future directions with the gene trap mouse project are covered in more detail in the discussion.

Part II: Transgenic PITPα/β mouse

Materials and Methods

Creation of a targeting vector to modify PITPα BAC

A PITPα BAC was modified to replace its C-terminal tail using the techniques and vectors described in ((Liu *et al.*, 2003)). Three fragments were cloned into the pL452 targeting vector: two flanking regions of PITPα and the coding sequence for the PITPβ C-terminal tail. pL452 has two multiple cloning sites (MCSs) on either side of a floxed kanaymycin gene; the kanamycin gene allows for selection of integrated pL452. Flanking regions were cloned by PCR and inserted into MCS 1 and 2. The PITPβ DNA

(encoding the C-terminal tail) intended for recombination into the BAC was synthesized by annealing of complementary primers that corresponded to 32 bp of PITPα intron 11 followed by PITPβ exon 12 (up to the stop codon) and the 30 nt of PITPα after its stop codon (all relevant primers shown in Table m2). This fragment was ligated into MCS2 of the PL452 vector (fig. m2).

The PITPα BAC was transformed into DY380 bacteria (DH10B [λc1857 (cro-bioA< >tet)])(Liu *et al.*, 2003). Heat inducible recombination enzymes in the DY380/PITPα strain were induced by a 15 minute incubation at 42ºC before transformation of a linearized pL452 targeting vector. The recombination enzymes promote homologous recombination between the pL452 and the BAC, and colonies where recombination had occurred were selected by growth on chloramphenicol (for the BAC) and kanamycin (for the recombined region of PL452). Recombined colonies were then transformed into EL350 (DH10B [λc1857 (cro-bioA< >araC-P_{BAD}cre)]). Activation of the arabinose-inducible Cre caused recombination of loxP sites and removal of the kanamycin cassette. Removal of the kanamycin resistance gene was confirmed by the inability of streaked colonies to grow on 25 μg/mL kanamycin/25 μg/mL chloramphenicol plates. Modified regions of the final PITPα/β BAC were sequenced to confirm that recombination had occurred correctly.

Modification of PL452 to target PITPα PAC

In order to allow recombination in a kanamycin resistant PAC, PL452 was modified to replace the kanamycin resistance gene with a chloramphenicol resistance gene. The chloramphenicol resistance gene (cat) was amplified from a pRIL plasmid (Stratagene, Cedar Creek, TX) with primers containing sites for BssHII and RsrII. The

cat gene was inserted into the BssHI and RsrII sites, disrupting the coding region of the kan gene. The colonies were screened for their ability to grow on chloramphenicol and not kanamycin.

The PITPα PAC (P1 clone 4232; a gift from Bruce Hamilton, University of California at San Diego) was targeted in the same manner as the BAC, except that where kanamycin was previously used, chloramphenicol was used instead, and vice versa.

Injection and screening of PITPα/β mice

The BAC and PAC were separately injected into C57BL/6JxC3H hybrid pronuclei at the University of North Carolina Animal Models Core. Potential transgenic animals were screened by PCR using a forward primer specific to the inserted region of the PITPβ tail (5′-cgtaagaagggttccgtccgaggcacgtcgg-3′), and a reverse primer in PITPα (5′-gcagataacttcctctcagcataacaagggac-3′).

Results

Generation of PITPα/β BAC

The C-terminal tail of PITPs is thought to play a critical role in their function. The C-terminal tail decreases the affinity of PITPα for membrane binding, and increases its rate of transfer. In addition, crystal structures and biochemical data indicate a change in the position of the C-terminal tail upon binding to the membrane(Tremblay *et al.*, 1996; Yoder *et al.*, 2001; Schouten *et al.*, 2002; Tilley *et al.*, 2004; Tremblay *et al.*, 2005). One of the regions of highest divergence between PITPα and PITPβ is at the C-terminal tail, and we recently showed that, in the context of a PITP molecule, the C-terminal tail of PITPα and PITPβ is sufficient to determine their localization(Phillips *et al.*, 2006). Further, a reported interaction between PITPα (but not PITPβ) and the DCC

receptor occurs via the C-terminal region of PITPα (Xie *et al.*, 2005). Thus, we hypothesize that the C-terminal tail of PITPα is critical for some or all of the physiological roles of PITPα.

In order to test the hypothesis that the C-terminal tail is critical for the function of PITPα, we created constructs that can be used to generate a PITPα/β transgenic mouse. In order to preserve as many of the regulatory regions of the gene as possible, the constructs were created in a PITPα BAC and PAC. Bacterial artificial chromosomes (BACs) or P1 artificial chromosomes (PACs) contain up to 300 kb, therefore the entire genomic sequence of the gene (introns and exons), along with surrounding genomic sequence are present in the BAC/PAC.

The PITPα BAC/PAC was modified to contain the PITPβ tail using recombineering techniques(Liu *et al.*, 2003). In this technique, a targeting vector, containing the PITPβ C-terminal tail flanked by PITPα sequence, is used to recombine the PITPβ tail into the PITPα BAC/PAC.

The PITPα/β chimeric BAC was made and injected first, since the resistance of the BAC (chloramphenicol) was compatible with the resistances of the pL452 targeting vector (ampicillin and kanamycin). The pL452 vector was linearized, and induced to recombine with the PITPα BAC. The final PITPα/β BAC was confirmed by digests and sequencing, and submitted to the UNC Animal Models Core for injection into pronuclei.

Screening of BAC PITPα/β transgenic mice yielded no positives

In order to determine whether mice have an integrated transgene, I developed a PCR screen using a forward primer in the PITPβ tail, and a reverse primer in the PITPα BAC. This PCR screen could detect as little as 20 pg of BAC, even in the presence of

mouse tail DNA (Figure m2). Three sets of injections with the BAC were done, with a total of 57 mice screened. Despite control PCRs indicating that the DNA preparations were of good quality, the BAC could not be detected by PCR in any of the mice.

Using a PAC to generate PITPα/β mice

Because of the large size of BACs, they sometimes do not integrate easily into the genome. The UNC Animal Modles Core was also unsuccessful in recent injections of BACs for other labs, suggesting that BACs were not the best way to make this mouse. Our lab has successfully made transgenic mice in the Animal Modles Core using PACs (Alb *et al.*, 2007), and so a PITPα PAC was modified to contain a PITPβ tail.

Unlike the BACs, which are chloramphenicol resistant, PACs are kanamycin resistant. Because the first step of the recombineering requires separate selection for both the targeting vector (which is kanamycin resistant) and the BAC/PAC, it impossible to use the same recombineering strategy for PACs. To circumvent this problem, the targeting vector was engineered to contain a chloramphenicol resistance gene that disrupts the normal kanamycin resistance. Recombineering was then performed as before, and the integrity of the PAC was confirmed.

PAC mice

The PITPα/β PAC was injected into fertilized oocytes as before. The same PCR screen was used to screen mice. 54 mice from 4 litters were screened, and none of the mice were positive for the transgene.

One possible reason for the lack of transgenic mice is that the PAC is partially integrated and/or there is selection against expression of the PITPα/β chimera. To determine if the PAC itself is present, primers in the PAC backbone were used to PCR

mouse tail gDNA. Of the 10 gDNA samples tested with these primers, none were positive for the PAC backbone (data not shown). This indicates a likely technical problem with injection of the PAC, rather than a specific problem with the targeted region of the PAC.

Part III: Floxed PITPβ mouse

Materials and Methods

Generation of a floxed PITPβ targeting construct

Recombineering was used to clone genomic DNA into a plasmid, for use as a targeting construct. Regions of DNA corresponding to nt 4607-5011 of intron 3 and nts 2725-3119 of intron 7 of PITPβ were cloned into pBluescript. The pBluescript/βintrons was linearized between the two genomic regions using the PstI site, and co-electroporated into the DY380 bacteria strain with a BAC containing PITPβ (number RP23 212N4). Recombination enzymes were activated as described earlier, and putative positive colonies were identified by screening for ampicillin resistance indicating that the pBluescript is intact. Positives were then further screened by PCR using primers in the genomic region, and digestion for those that contained the entire genomic region from intron 3 to intron 7.

Two loxP sites and a neo cassette were incorporated into the genomic DNA region of the plasmid in the following way. The neomycin reisistance gene was inserted in an orientation opposite to that of the PITPβ gene, since normal expression of neomycin did not occur when the gene was inserted in the forward direction (data not shown). The first loxP site was included in a primer that amplified the 3' end of a crippled neo

resistance gene (Tybulewicz *et al.*, 1991). Both the forward and reverse neo primers included KpnI sites, and the loxP/neo was ligated into a KpnI site in intron 3, and colonies were selected for those that had the loxP/neo ligated in the proper orientation. The second loxP site was created by synthesis of complementary primers corresponding to the loxP sequence: 5′- ATAACTTCGTATAGCATACATTATACGAAGTTAT -3′ with HpaI sites at both ends. It was ligated into an HpaI site in intron 6 of PITPβ.

An hsv-tk gene was also included in the targeting construct to allow for negative selection. The hsv-tk gene was amplified with primers containing NotI sites at both ends, and the hsv-tk was cloned into a NotI site in the pBluescript MCS 3' to the targeting construct.

The integrity of the plasmid was confirmed by digests with several different enzymes, which yielded bands of expected sizes. To prepare the DNA for electroporation, 20-30 μg of the targeting construct was linearized with AhdI, precipitated, washed in 70% EtOH and resuspended in sterile water.

Targeting ES cells

Approximately 2 x 10^7 ES cells were electroporated in the presence of linearized DNA using resistance of ∞, 250 μF capacity and 300 V. Selection with 200 mg/mL G418 and 2 mM gangcyclovir was begun 24 hours after electroporation. Colonies were clearly visible by 10 days after selection, and were picked and grown in individual wells.

Screening ES cells for homologous recombination of floxed PITPβ

ES colonies were screened by Southern blot. Genomic DNA was collected from p12 wells of ES cells using the Promega nuclei lysis and protein precipitation reagents. Approximately 10 μg of DNA was cut with SspI, separated on a 1.0% agarose gel, and

transferred to nitrocellulose membrane. Probes corresponding to nt 768 to 1079 or 2728 to 3004 of the floxed PITPβ targeting construct were PCR amplified and labeled by random primer extension with a ^{32}P labeled dATP. Standard Southern conditions for hybridization and washes were used (see ((Alb *et al.*, 2002))), and blots were exposed on a phosphoimager screen for 2-7 days.

Results

An inducible knockout model of PITPβ

Previous evidence from our lab suggests that PITPβ is an essential protein in cells. Homozygous null PITPβ mice do not survive to birth, and lethality likely occurs early in embryogenesis. Unsuccessful attempts to make homozygous knockout ES cells suggest that loss of PITPβ may be lethal to cells. Because it is difficult to assess cell lethality in a mouse model and difficult to get sufficient and reproducible knockdown by siRNA in cell culture systems, I created a genetic, inducible PITPβ knockout model. In this system, exons 4-7 of PITPβ are flanked by loxP sites. Upon treatment with the cre recombinase, the loxP sites recombine and intermediate regions are removed. Exons 4-7 encode regions of PITPβ that are likely critical for normal folding and function. In addition, the removal of these exons causes a frame shift and an early termination of the PITPβ message. Thus, after cre treatment, this model should serve as a functional knockout of PITPβ.

While this model is made by genetic modification of mouse ES cells, its primary purpose is for study at the cellular level. If PITPβ is essential, we can see the immediate effects of loss of PITPβ in cells leading up to cell death. If PITPβ is not essential, we can still assess effects on the cell (such as changes in cell cycle, trafficking ability, etc.) after

acute loss of PITPβ. Finally, should PITPβ prove to be not essential for cell growth, the cells can be used to generate a floxed-PITPβ mouse, and the role of PITPβ in various developmental stages and tissues can be assessed with cre containing mice.

An inducible knockout was created by homologous recombination of a targeting construct. The targeting construct contained regions of PITPβ flanking a selection cassette and loxP sequences inserted before and after essential exons of PITPβ (Figure 3). The region for targeting was obtained by recombineering. Small fragments corresponding to the 5′ and 3′ ends of the targeting regions were cloned into pBluescript (Stratagene, Cedar Creek, TX) and used to "capture" the entire targeting region from a PITPβ BAC. loxP sites were inserted in intron 3 and intron 7, and a neo resistance gene was inserted in the reverse direction directly after the intron 3 loxP site. An hsv-tk gene was ligated at the end of the targeting region. hsv-tk will not recombine into the genome if homologous recombination has occurred, and its presence causes sensitivity to gancyclovir, thus the insertion of hsv-tk provides a mechanism for negative selection.

The construct was linearized and electroporated into ES cells. Positive selection was performed with G418 and gancyclovir was used for negative selection. From five electroporations, a total of 289 colonies were isolated and screened. Initially, primers and conditions to perform a PCR screen were tested. Because of the large size of the fragment to be amplified (>4 kb), the PCR screen proved unreliable, and colonies were instead screened by Southern blot.

A southern blot strategy was developed where we could look for a 1.882 kb shift in a genomic fragment due to the integration of neo. We cut genomic DNA with SspI which, in the targeted region of the genome, would yield a wild type fragment of 10.83

kbp. If the targeting construct (with neo) recombined properly, the fragment would be 12.712 kbp for one of the two copies of the genes. The probe used to detect the genomic DNA fragments was PCR amplified from intron 3 of PITPβ. This region is not in the targeting construct, but is within the same 10.83 kb SspI fragment.

Genomic DNA from the 289 ES cell colonies was digested, separated, transferred and probed. We got clear Southern blot results for about 200 colonies, and only 2 colonies had two bands of similar intensity and correct sizes. Further screening with additional probes, however, indicated that these colonies were not correctly targeted.

The low targeting efficiency of this construct (0.5%) is likely a result of the genomic localization of the PITPβ locus. Screening of more colonies would likely yield a properly targeted, floxed PITPβ allele, however, because of results with siRNA in human cell lines, which addressed many of the same questions proposed for this project, the floxed PITPβ line was not pursued further.

Tables

primer name	primer sequence	purpose
β-geo1	from Jim Alb	rev screen in gene trap cassette
β-geo2	from Jim Alb	rev screen in gene trap cassette
β 100f	aactggtggtggagaaggaa	cDNA forward primer
β 200f	gagaagggacagtacacac	cDNA forward primer
β 400f	aaaccgttgaaattgtccac	cDNA forward primer
β 500f	gaccctgcattattccattcagtc	cDNA forward primer
β 600f	aagtggtgggggctgcagag	cDNA forward primer
i7 n1f	gtgagtactccttgatgtgtccc	intron 7 forward primer
i7 1500f	gaaggagtgttcctctttctcc	intron 7 forward primer
i7 3000f	ggctactggtttgctgtagattgc	intron 7 forward primer
i7 4500f	gtggtgtgttgaagtctcccac	intron 7 forward primer
i7 5500f	gagttgaaaatcttcattctc	intron 7 forward primer
i7 6500f	gccctcccggatgtctggagcc	intron 7 forward primer
i7 7500f	ggtggcatcagccaagcctgggc	intron 7 forward primer
i7 8500f	ctgggtgccgtttcactgcgtgtgc	intron 7 forward primer
i7 9500f	gtcaggaccaccactgtgcatgccc	intron 7 forward primer
i7 10500f	ccttctgaaggcagcagaaccatcc	intron 7 forward primer
i7 11500f	cggttaggggcattgtgtcgatgcc	intron 7 forward primer
pGT0lxr rev 1	GCTGAGGATGAGGGAGCAG GGC	reverse in gene trap vector, for mouse screening
pGT0lxr rev 2	CCCGGCGCTCTTACCAAAGG GC	reverse in gene trap vector, for mouse screening

Table A.1- Primers used for characterization of Gene trap Mouse

primer	sequence	purpose
gen1 5′ SacII	AAACCGCGGGAGGTGGGTGGATTTCTGGGTTTG	cloning PITP alpha region of homology
gen1 3′ NotI	AAAGCGGCCGCGCTTTTGTTGCTGATGGAACTTTACC	cloning PITP alpha region of homology
gen2 for EcoRI	AAAGAATTCCTTTCAATTTCCTTCTGCTTTTTCTGTTGCAGATGCGTAAGAAGGGTTCCGTCCGAGGCACGTCGGCTGCTGATGCCTAGCGC	PITPbeta tail with PITPalpha intronic DNA
gen2 rev BglII	AAAAGATCTGGTACTTACAGTGCAGAAAGGGCGGTGGCGCTAGGCATCAGCAGCCGACGTGCCTCGGACGGAACCCTTC	PITPbeta tail with PITPalpha intronic DNA
gen3 5′ BglII	AAAAGATCTGAGCTGTTGTCAGTGGGCTTGGGTCCTC	cloning PITP alpha region of homology
gen3 3’ SalI	AAAGTCGACGCCTAGCTAGCACGCACACAGGCCTGGGTG	cloning PITP alpha region of homology

Table A.2 – Primers used for construction of BAC/PAC transgenic mouse

Figures

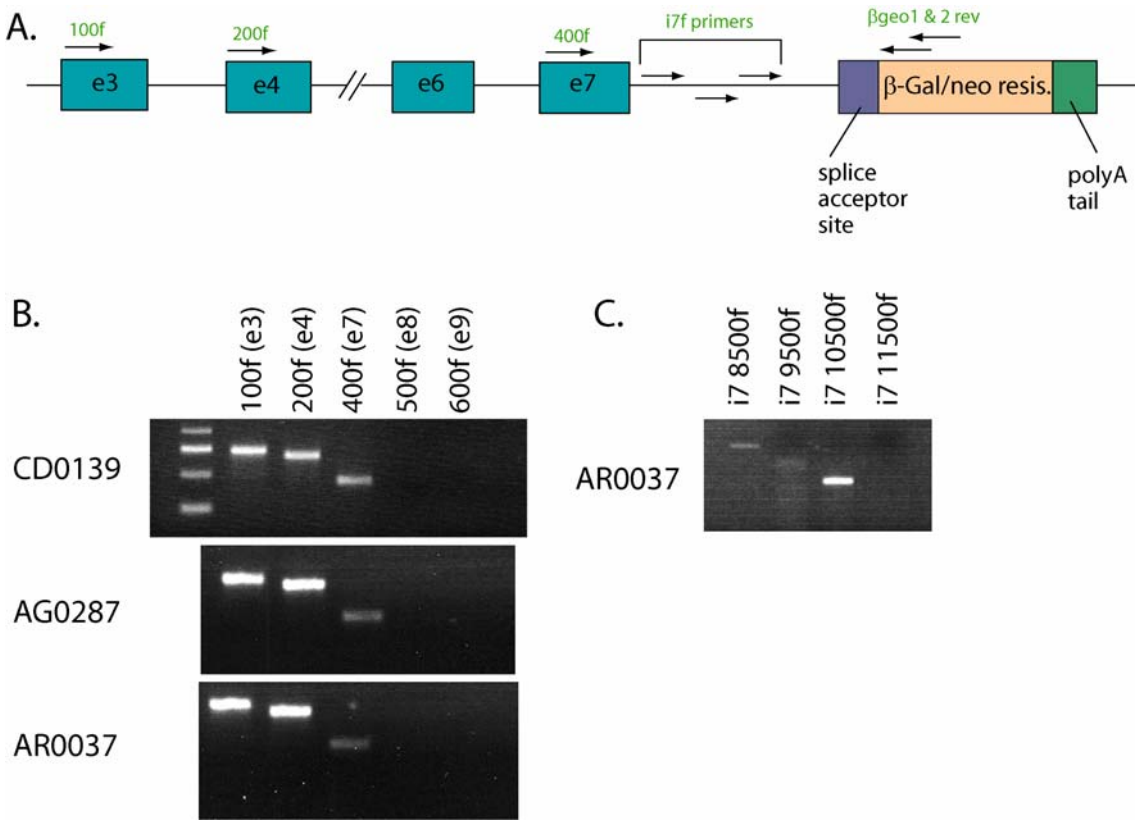

Figure A.1 – Three out of four PITPβ gene trap lines trap after exon 7. (A) A schematic of the gene trap indicates the critical features of the gene trap and several of the key primers (green text). Introns, exons, and primer locations are not drawn to scale. (B) Using forward primers in the PITPβ cDNA and a reverse primer in the gene trap (βgeo1), PCRs indicated that the gene trap fell within intron 7 (i.e. trapped after exon 7). (C) PCR reactions with forward primers in intron 7 and a reverse primer in the gene trap (βgeo2) showed that the gene trap in line AR0037 fell in the region of nt 10500-11500. Sequence analysis of the i710500 and βgeo2 PCR product indicated that the insertion site was around nt 10797.

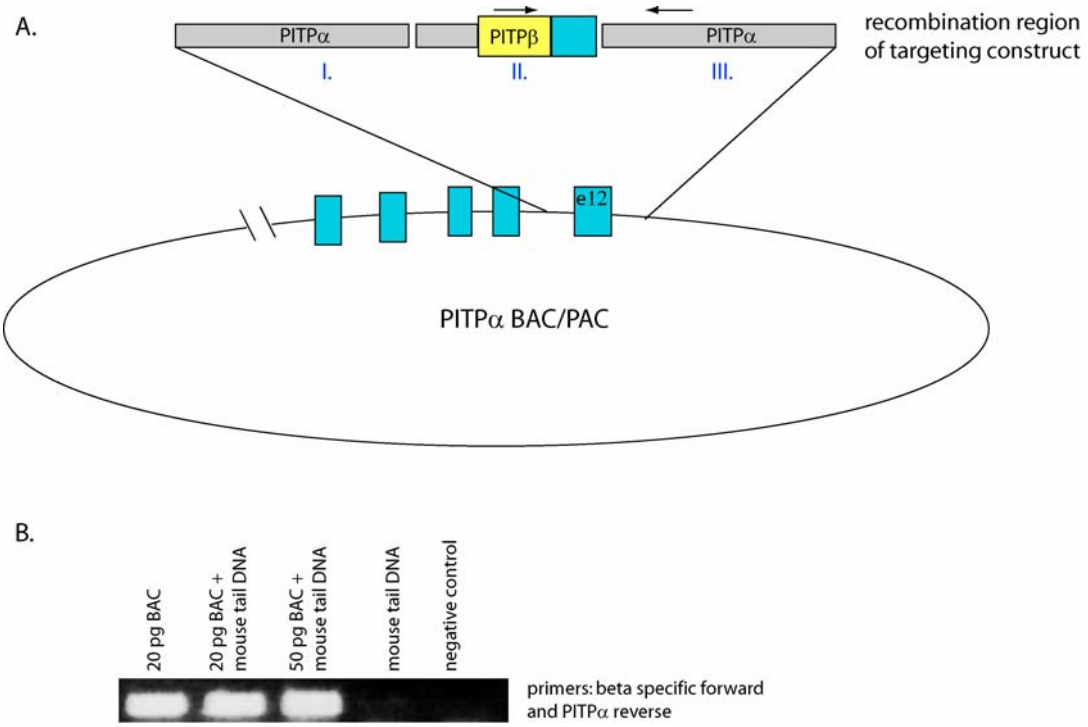

Figure A.2- A BAC/PAC was modified by recombination techniques to create a transgenic PITPα/PITPβ mouse. (A) A diagram of the PITPα and targeting plasmid are shown with introns indicated as a line (BAC/PAC) or in gray (targeting diagram), and exons in darker blue (PITPα) or yellow (PITPβ). The three fragments that were cloned to create the targeting construct are indicated by blue Roman numerals, and arrows indicate primers used to PCR screen animals carrying the transgene. (B) A PCR screen was developed to screen for animals carrying the transgene using primers indicated by arrows in part A. This PCR was sensitive and specific, picking up a band of the expected size from 20 pg BAC/PAC in the presence of mouse tail DNA.

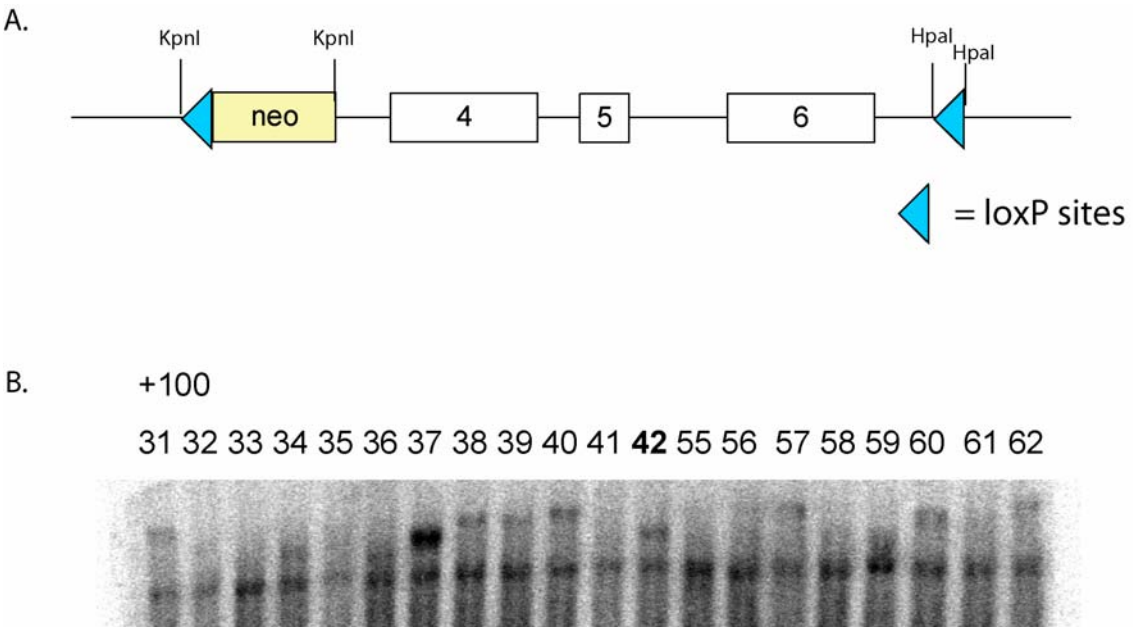

Figure A.3 – A targeting vector to create a conditional PITPβ knockout mouse is constructed. (A) The targeting region of the PITPβ targeting construct is composed of a genomic region starting in intron 3 and ending in intron 6. loxP sites, indicated in blue, were inserted in intron 3 and intron 6. A neo cassette (yellow) was inserted after the loxP site in intron 3. (B) A typical Southern blot for screening ES cell colonies. Genomic DNA is prepared from colonies grown in 12 well plates, and digested with SspI. The blotted DNA is probed with a fragment of PITPα that is outside of the targeting construct. In this Southern, there are several samples with multiple bands, but only one of them (142) has bands of equal intensity and of approximately the correct sizes. Further testing of this line indicated that it was not targeted.

References

Alb, J.G., Jr., Phillips, S.E., Rostand, K., Cui, X., Pinxteren, J., Cotlin, L., Manning, T., Guo, S., York, J.D., Sontheimer, H., Collawn, J.F., and Bankaitis, V.A. (2002). Genetic ablation of phosphatidylinositol transfer protein function in murine embryonic stem cells. Mol Biol Cell *13*, 739-754.

Alb, J.G., Jr., Phillips, S.E., Wilfley, L.R., Philpot, B.D., and Bankaitis, V.A. (2007). The pathologies associated with functional titration of phosphatidylinositol transfer protein alpha activity in mice. J Lipid Res *48*, 1857-1872.

Liu, P., Jenkins, N.A., and Copeland, N.G. (2003). A highly efficient recombineering-based method for generating conditional knockout mutations. Genome Res *13*, 476-484.

Phillips, S.E., Ile, K.E., Boukhelifa, M., Huijbregts, R.P., and Bankaitis, V.A. (2006). Specific and nonspecific membrane-binding determinants cooperate in targeting phosphatidylinositol transfer protein beta-isoform to the mammalian trans-Golgi network. Mol Biol Cell *17*, 2498-2512.

Schouten, A., Agianian, B., Westerman, J., Kroon, J., Wirtz, K.W., and Gros, P. (2002). Structure of apo-phosphatidylinositol transfer protein alpha provides insight into membrane association. Embo J *21*, 2117-2121.

Tilley, S.J., Skippen, A., Murray-Rust, J., Swigart, P.M., Stewart, A., Morgan, C.P., Cockcroft, S., and McDonald, N.Q. (2004). Structure-function analysis of human [corrected] phosphatidylinositol transfer protein alpha bound to phosphatidylinositol. Structure *12*, 317-326.

Tremblay, J.M., Helmkamp, G.M., and Yarbrough, L.R. (1996). Limited proteolysis of rat phosphatidylinositol transfer protein by trypsin cleaves the C terminus, enhances binding to lipid vesicles, and reduces phospholipid transfer activity. J Biol Chem *271*, 21075-21080.

Tremblay, J.M., Unruh, J.R., Johnson, C.K., and Yarbrough, L.R. (2005). Mechanism of interaction of PITPalpha with membranes: conformational changes in the C-terminus associated with membrane binding. Arch Biochem Biophys *444*, 112-120.

Tybulewicz, V.L.J., Crawford, C.E., Jackson, P.K., Bronson, R.T., and Mulligan, R.C. (1991). Neonatal lethality and lymphopenia in mice with a homozygous disruption of the c-abl proto-oncogene. Cell *65*, 1153-1163.

Vordtriede, P.B., Doan, C.N., Tremblay, J.M., Helmkamp, G.M., Jr., and Yoder, M.D. (2005). Structure of PITPbeta in complex with phosphatidylcholine: comparison of structure and lipid transfer to other PITP isoforms. Biochemistry *44*, 14760-14771.

Wiles, M.V., Vauti, F., Otte, J., Fuchtbauer, E.M., Ruiz, P., Fuchtbauer, A., Arnold, H.H., Lehrach, H., Metz, T., von Melchner, H., and Wurst, W. (2000). Establishment of a gene-trap sequence tag library to generate mutant mice from embryonic stem cells. Nat Genet *24*, 13-14.

Xie, Y., Ding, Y.Q., Hong, Y., Feng, Z., Navarre, S., Xi, C.X., Zhu, X.J., Wang, C.L., Ackerman, S.L., Kozlowski, D., Mei, L., and Xiong, W.C. (2005). Phosphatidylinositol transfer protein-alpha in netrin-1-induced PLC signalling and neurite outgrowth. Nat Cell Biol *7*, 1124-1132.

Yoder, M.D., Thomas, L.M., Tremblay, J.M., Oliver, R.L., Yarbrough, L.R., and Helmkamp, G.M., Jr. (2001). Structure of a multifunctional protein. Mammalian phosphatidylinositol transfer protein complexed with phosphatidylcholine. J Biol Chem *276*, 9246-9252.

Zambrowicz, B.P., Friedrich, G.A., Buxton, E.C., Lilleberg, S.L., Person, C., and Sands, A.T. (1998). Disruption and sequence identification of 2,000 genes in mouse embryonic stem cells. Nature *392*, 608-611.

Appendix B: Record of Plasmids generated

Part I: pRE plasmids

pRE number	previous name	short name	resistance	description
empty vectors				
pRE 1300	KI111	EGFP N1	Kan	clonetech, EGFP at C-terminus of protein
pRE 1301	KI102	EGFP C2	Kan	EGFP at N-terminus of protein
pRE 1302	KI103	pBluescript SK +/- (pSK)	Amp	
pRE 1303	KI117	BL21	Cam	Codon-Plus RIL - for protein expression (isolated from BL21)
pRE 1304	KI234	RSVrev (LL)	Amp	plasmid required for lentilox virus expression
pRE 1305	KI235	RRE (LL)	Amp	"
pRE 1306	KI236	vsv-g (LL)	Amp	"
pRE 1307		pLL5.0	Amp	
pRE 1308		pCMV-HA	Amp	
pRE 1309		pCDNA3.1	Amp	
pRE 1310		pDsRed-N1	Kan	
pRE 1311		pML2 mCherry N1		
pRE 1312		pL452	Amp	
mammalian PITPbeta mutants (in pEGFP-N1 unless otherwise specified; mutants made in betai1 (beta trad) unless otherwise specified)				
pRE 1313	KI200	PITPbeta i1-GFP	Kan	rat PITPbeta in pEGFP-N1 (C-terminal GFP)
pRE 1314	KI201	PITPbetai2-GFP	Kan	alternative spliceoform of pitp beta from mouse, C-term GFP
pRE 1315	KI206	ratPITPbeta i1-mCherry	Kan	rat beta with mCherry at C-terminus of protein
pRE 1316	KI207	mousePITPbetai2-mCherry	Kan	rat beta alt with mCherry at C-terminus of protein
pRE 1317		GFP betai1 CT	Kan	
pRE 1318	KI202	GFP-beta 2CT	Kan	last 2 helices of PITP beta (trad), N-term GFP

pRE 1319		PITPbetai1 W202A	Kan	
pRE 1320		PITPbetai1 W203A	Kan	
pRE 1321		PITPbetai1 WW202/203AA	Kan	
pRE 1322		PITPbeta L224F	Kan	
pRE 1323		PITPbeta I220L L224F	Kan	
pRE 1324	KI302, pRE779	ratPITPbeta T58D	Kan	pRE779; T58D introduced in 772
pRE 1325		PITPbeta F107A	Kan	
pRE 1326		PITPbeta FF107/108AA	Kan	
pRE 1327		human PITPbeta	Kan	
pRE 1328		PITPbeta box 1,2,&3 to alpha	Kan	
pRE 1329		pRE 955	Kan	aaab hybrid in EGFP-N1 (mislabeled in old stock list) alpha aas 1-182, beta aas 183-272
pRE 1330		pRE 956	Kan	bbba hybrid in EGFP-N1 (mislabeled in old stock list) beta aas 1-181, alpha aas 182-272
pRE 1331	KI232	PITPbetai1/IRES/GFP in pEGFPN1 background	Kan	bicistronic expression of beta and GFP in high expression pEGFP/N1 backbone.
pRE 1332	KI233	PITPbetai2/IRES/GFP in pEGFPN1 background	Kan	same as above. Cloned from pLL5.5 with __ and NotI into pEGFP
pRE 1333		PITPbetai1/IRES/mCherry in pEGFP backbone	Kan	bicistronic expression of beta and mCherry in high expression pEGFP/N1 backbone.
pRE 1334		PITPbetai2/IRES/mCherry in pEGFP backbone	Kan	bicistronic expression of beta and mCherry in high expression pEGFP/N1 backbone.
pRE 1335	KI301	si-resistant rat beta	Kan	4 silent mutations to make 772 resistant to siRNA
pRE 1336	KI303	ratPITPbeta T58D (pRE 779), si-resistant	Kan	4 silent mutations
pRE 1337	KI304	SM-mut si-resistant (I220L,L224F)	Kan	4 silent mutations

pRE 1338	KI305	955 si-resistant	Kan	4 silent mutations
pRE 1339	KI306	mbeta-alt si-resistant	Kan	4 silent mutations
pRE 1340		PITPbeta/alpha (box 1,2,3 to alpha) si-resistant	Kan	4 silent mutations
pRE 1341		956 si-resistnat	Kan	4 silent mutations
pRE 1342	KI307	PITPbeta/WW202,203AA, T58D	Kan	in pEGFP
pRE 1343	KI308	PITPbeta/WW202,203AA, 221,224 (SM) muts	Kan	in pEGFP
pRE 1344	KI309	beta/alpha/T58D	Kan	in pEGFP
pRE 1345		beta/alpha WW202,203AA	Kan	
pRE 1346		beta W203A T58D	Kan	
pRE 1347		beta W202A T58D	Kan	
pRE 1348		beta/alpha SM	Kan	
pRE 1349		beta/alpha L224F	Kan	
pRE 1350		PITPbeta QDPK T58D	Kan	
pRE 1351		PITPbeta KQE T58D	Kan	
pRE 1352		PITPbeta MTD T58D	Kan	
pRE 1353		PITPalpha KGSR to KGPR	Kan	
pRE 1354		PITPalpha KGSR to KGAR	Kan	
pRE 1355		PITPalpha KGSR to KGER	Kan	
myc plasmids from Scott				
pRE 1356		myc-PITPalpha	Amp	
pRE 1357		myc-PITPalpha KGSR	Amp	
pRE 1358		myc-PITPbeta	Amp	
pRE 1359		myc-PITPbeta S262A	Amp	
pRE 1360		myc-PITPbeta S165A S262A	Amp	
pRE 1361		myc-PITPbeta QDPK	Amp	
pRE 1362		myc-PITPbeta S165A	Amp	
pLL plasmids				
pRE 1363		pLL4.0/sh4/ratPITPbeta i1	Amp	
pRE 1364		pLL/sh4/mousePITPbeta i2	Amp	not sure whether these are in pLL4.0 or 5.0
pRE 1365		pLL/sh4/PITPalpha/beta	Amp	"

pRE 1366		pLL/sh4/PITPbeta/alpha	Amp	"
pRE 1367		pLL/sh4/PITPbeta T58D	Amp	"
pRE 1368		pLL/sh4/PITPbeta I220L L224F	Amp	"
pRE 1369		pLL/sh3/ratPITPbeta i1	Amp	"
zebrafish plasmids				
pRE 1370		pEGFP/zfPITPalpha	Kan	
pRE 1371		pEGFP/zfPITPbetai1	Kan	
pRE 1372		pEGFP/zfPITPbetai2	Kan	
pRE 1373		pEGFP/zfgamma	Kan	
pRE 1374	KI210	myoD	Amp	from Suk-Won for in situ control; cut with XbaI to linearize
pRE 1375	KI211	zfPITPbeta in pGEM	Amp	isoform 2, no restriction sites added; in ISH antisense direction (gene in same direction as T7 promoter)
pRE 1376	KI212	zfPITPbeta in pGEM	Amp	isoform 2, no restriction sites added; in ISH sense direction (gene in opposite direction to T7 promoter)
pRE 1377	KI213	zfPITPgamma in pGEM	Amp	cloned into pGEM using SalI/SacII (XhoI/SacII for vector, so SalI and XhoI sites lost); in ISH sense direction (gene in opposite direction to T7 promoter)
pRE 1378	KI214	zfPITPgamma in pGEM	Amp	no restriction sites added; in ISH antisense direction (gene in same direction as T7 promoter)
pRE 1379	KI230	pET28/zf actin	Kan	candidate for zpr1 antigen - not actual antigen
pRE 1380	KI231	pET28/zf arrestin-like 3	Kan	zpr1 antigen. cloned using pET28 his sites, so 6 His tags

pGEM				
pRE 1381		pGEM (empty)	Amp	
pRE 1382		pGEM/COS7beta	Amp	
pRE 1383		pGEM/KanMX	Amp	
pRE 1384		pGEM/loxP	Amp	
pRE 1385	KI203	pGEM/HpaI_loxP (6)	Amp	loxP flanked by HpaI sites
pRE 1386		pGEM/human PITPbeta	Amp	
protein expression plasmids				
pRE 1387	KI229	pET28	Kan	for protein expression
pRE 1388		pET28/ratPITPalpha	Kan	
pRE 1389		pET28/ratPITPbetai1	Kan	
pRE 1390		pET28/ratPITPbetai2	Kan	
pRE 1391		pET28/ratPITPalpha C95A	Kan	
pRE 1392		pET28/ratPITPbetai1 C94A	Kan	
Drosophila plasmids				pMT:Drosophila expression, metallothionein promoter; see Invitrogen catalog number: V4120-20 (modifed by Steve Rogers)
pRE 1393		pMT	Amp	Modification from Steve: EcoRI-GFP-NotI, EcoRI ACC delta TG
pRE 1394		pMT/ratPITPbeta i1	Amp	
pRE 1395		pMT/mouse PITPbeta i2	Amp	
pRE 1396		pMT/vibrator	Amp	
pRE 1397		pMT/vibrator WF to AA	Amp	
pRE 1398		pMT/vibrator G262D, R265K	Amp	
pRE 1399		pGEM/vibrator (with stop codon)	Amp	
pRE 1400		pGEM/vibrator G262D, R265K	Amp	
floxed PITPbeta				

mouse				
pRE 1401	KI219	pSK/floxed beta v4.28	Amp	neo in reverse, loxP at 3' of gene, works for targeting
pRE 1402	KI108	pPNT		targeting vector; has crippled neo and hsv-tk; http://www.med.umich.edu/tamc/mta.html#pPNT
pRE 1403	KI109	neo KpnI (pRE 561)	Amp	crippled neo for homologous recombination
PITPalpha/beta BAC and PAC				
pRE 1404	KI204	pSK/beta_gen2	Amp	genomic fragment for recombineering
pRE 1405	KI205	pSK/beta_gen3	Amp	second genomic fragment for recombineering
pRE 1406	KI209	BAC B4 in DY380	Cam	a PITPalpha BAC recombineered so that the C-terminal tail is beta (last alpha exon replaced with last beta exon)
pRE 1407	KI215	pL452/cat 8	Amp, Cam	cat (chloramphenicol resistance gene) cloned into Kan. Vector is now resistant to cam, but not Kan (for recombineering into PACs
pRE 1408	KI216	pL452/cat 11	Amp, Cam	same as above
pRE 1409	KI217	pL452/gen1,2,3 cat 4	Amp, Kan	targeting construct for alpha BAC
pRE 1410	KI218	pL452/gen1,2,3 cat 13	Amp, Cam	same as 1408/1409, except with sequence to make alpha/beta hybrid PAC
pRE 1411	KI220	PI4232 in DY380	Kan	PITP alpha PAC
pRE 1412	KI221	PI4232 in DY380	Kan	
pRE 1413		PAC B_ (in DH5alpha)		

lipid markers				
pRE 1414	KI227	pML2-FAPP-PH	Amp	from Lydia, mCherry
pRE 1415		TAPP1-GFP	Kan	from Amelia Lindgren
pRE 1416		GRP-GFP	Kan	from Amelia Lindgren
pRE 1417		PLCdelta-GFP	Kan	from Amelia Lindgren
pRE 1418		FAPP1-GFP	Kan	from Amelia Lindgren
pRE 1419		GFP-PKD-CRD	Kan	mine - see chapter 3
pRE 1420		PLC-PH-GFP	Kan?	from Scott
pRE 1421		PLD-PH-GFP	Kan?	from Scott
other vectors				
pRE 1422	KI224	PKD1-KD	Amp	PKDs with dominant negative kinase dead mutations, human? from Vivek Malhotra, tubulates Golgi?
pRE 1423	KI225	PKD2-KD	Amp	
pRE 1424	KI226	PKD3-KD	Amp	
pRE 1425	KI228	vsvg-mCherry	Kan?	from Lydia, cloned from vector from Sima Lev, ts mutation
more mammalian PITPbeta muts				
pRE 1426		betai2 CT	Kan	
pRE 1427		betai2 2CT	Kan	
pRE 1428		betai2 2CT S262P	Kan	
pRE 1429		772-1 IL220,224LF	Kan	C-term box 1, 2 or 3 to alpha and SM muts
pRE 1430		772-2 IL220,224LF	Kan	"
pRE 1431		772-3 IL220,224LF	Kan	"
pRE 1432		772-1 E247K	Kan	C-term box 1, 2 or 3 to alpha and PI muts
pRE 1433		772-2 E247K	Kan	"
pRE 1434		772-3 E247K	Kan	"
pRE 1435		pEGFP/PITPbetai1 K105A	Kan	
pRE 1436		pEGFP/PITPbetai1 K201A	Kan	
pRE 1437		pEGFP/PITPbetai1 KK201,208AA	Kan	
pRE 1438		pEGFP/PITPbetai1 F71A	Kan	
pRE 1439		pEGFP/PITPbetai1 VR72,73AA	Kan	

pRE 1440		pEGFP/PITPbetai1 MI74,75AA	Kan	
pRE 1441		pEGFP/PITPbetai1 W202A	Kan	
pRE 1442		pEGFP/PITPbetai1 W203A	Kan	
pRE 1443		pEGFP/PITPbetai1 MI74,75AA WW202,203AA	Kan	
pRE 1444		pEGFP/PITPbetai1 WW202,203II	Kan	
pRE 1445		pEGFP/PITPbetai1 WW202,203FF	Kan	
pRE 1446		pEGFP/PITPbetai1 KQE (box 1) WW202,203AA	Kan	
pRE 1447		pEGFP/PITPbetai1 KQE (box 1) WW202,203FF	Kan	
pRE 1448		pEGFP/PITPbetai1 QDPK (box 2) WW202,203AA	Kan	
pRE 1449		pEGFP/PITPbetai1 QDPK (box 2) WW202,203FF	Kan	
pRE 1450		pEGFP/PITPbetai2 C270D	Kan	
pRE 1451		pEGFP/PITPbetai2 S267A	Kan	
pRE 1452		pEGFP/PITPbetai2 CDD270-272DA	Kan	

Part II: pCTY plasmids (yeast expression)

pCTY number	**previous name**	**short name**	**resistance**	**description**
pCTY2025	pCTY1079	yEP/pSec14/PITPbeta	Amp	high copy plasmid with Sec14 promoter
pCTY2026		1079/WW201,202AA	Amp	
pCTY2027		1079/WW201,202II	Amp	
pCTY2028		1079/WW201,202FF	Amp	
pCTY2029		1079/MI74,75AA	Amp	
pCTY2030	pCTY1095	yEP/pPGK/PITPbeta	Amp	high copy plasmid with PGK (strong) promoter
pCTY2031		1095/WW201,202AA	Amp	
pCTY2032		1095/WW201,202II	Amp	
pCTY2033		1095/WW201,202FF	Amp	
pCTY2034		1095/MI74,75AA	Amp	
pCTY2035		1095/L224F	Amp	
pCTY2036		1095/I220L	Amp	
pCTY2037		pPGK/PITPbetai2	Amp	
pCTY2038		pPGK/human PITPbeta	Amp	
pCTY2039	pCTY1096	yEP/pPGK/PITPalpha	Amp	high copy plasmid with PGK (strong) promoter
pCTY2040		1096/L221I	Amp	
pCTY2041		1096/C95A	Amp	
pCTY2042		1096/F225L	Amp	
pCTY2043	pCTY1080	yEP/pSEC14/PITPalpha	Amp	high copy plasmid with Sec14 promoter
pCTY2044		pCTY1080/WW202,203 AA	Amp	
pCTY2045		PITPalpha WW202,203AA	Amp	in unknown yeast expression vector

				(probably yEP/pPGK)
pCTY2046		pCTY1109/WW AA	Amp	
pCTY2047		pCTY1092/WW AA	Amp	
pCTY2048		yCP lac 33-1	Amp	empty vector
pCTY2049		yEPlac 195	Amp	
pCTY2050		pDR195	Amp	
pCTY2051		pDR195/PITPbeta i1	Amp	
pCTY2052		pDR195/PITPbeta i2	Amp	
pCTY2053		pDR195/PITPbetai1 C95A	Amp	
pCTY2054		pDR195/human PITPbeta	Amp	
pCTY2055		pDR195/alpha	Amp	
pCTY2056		pDR195/alpha GFP	Amp	from Emily
pCTY2057		pDR195/alpha LL GFP	Amp	from Emily
pCTY2058		pDR195/alpha C95A 225C	Amp	
pCTY2059		yEPlac195/beta-GFP	Amp	
pCTY2060		pDR195/zebrafish PITPalpha	Amp	
pCTY2061		pDR195/zebrafish PITPbeta i1	Amp	
pCTY2062		pDR195/zebrafish PITPbeta i2	Amp	
pCTY2063		pDR195/zebrafish PITPgamma	Amp	
pCTY2064		pDR195/zebrafish PITPalpha T58D	Amp	
pCTY2065		pDR195/zebrafish PITPbeta i1 T58D	Amp	
pCTY2066		pDR195/zebrafish PITPbeta i2 T58D	Amp	
pCTY2067		pDR195/zebrafish PITPgamma T58D	Amp	
pCTY2068		pDR195/Sec14	Amp	

pCTY2069		pCTY705	Amp	
pCTY2070		pCTY706	Amp	
pCTY2071		pCTY705 R65A T236D	Amp	GFP Sec14 with PI-binding mutations
pCTY2072		pCTY705 S173I T175I	Amp	GFP Sec14 with PC-binding mutations
pCTY2073		pCTY705 M177W V194W	Amp	GFP Sec14 with pinched closed mutations
pCTY2074		pLac33/Hyde CDIPT	Amp	zebrafish PI synthase; cloned for tetrad analysis for Taylor in David Hyde's lab
pCTY2075		pLac33/wt CDIPT	Amp	
pCTY2076		pLac33/LOP CDIPT	Amp	loss of function mutation for CDIPT
pCTY2077		pDR195/Hyde CDIPT	Amp	cloned by Taylor (all CDIPT in pDR195)
pCTY2078		pDR195/wt CDIPT	Amp	
pCTY2079		pDR195/LOP CDIPT	Amp	

Appendix C: Protocols

From Litvak et al Nat Cell Biol. Volume 7 | Number 3 | March 2005

Washing buffer:

125 mM NaCl, 5 mM KCl, 5.6 mM glucose, 20 mM Hepes-NaOH, pH 7.2, 1.8 mM CaCl2 and 1.8 mM MgCl2

Washing buffer + 1mM xyloside

0.1N NaOH

Chondroitin sulphate (final: 0.6%)

Cetylpyridinium Chloride (final: 1%)

1% Cetylpyridinium chloride in 20 mM NaCl

2M NaCl

1. Plate cells in 6 well plates and treat with siRNA
2. Wash with washing buffer, and incubate with washing buffer + xyloside for 15 min. at 37ºC
3. Pulse-label with 80 μCi /ml of [35S]sulphate for 5 min at 37 °C.
4. Wash with serum-free DMEM, and incubate at 37 °C for ___(Litvak: 20, 40, and 60 min.; Godi: 10, 15, 20, 30 min.) in serum-free DMEM containing 0.1% bovine serum albumin.
5. Recover the supernatant from the cell media by centrifugation at 12,000 g for 10 min.
6. Extract the cell monolayers with 0.1 M NaOH for 1 h at 37 °C.

7. Precipitate cell supernatants and extracts by incubation for 12 h at 24 °C by the addition of chondroitin sulphate and cetylpyridinium chloride (0.6% and 1% final concentrations, respectively).

8. Centrifuge the samples at 2,600 g for 10 min, wash precipitates twice with 1% cetylpyridinium chloride in 20 mM NaCl.

9. Dissolve pellets in 2 M NaCl at 37 °C. Measure radioactivity in a scintillation counter. Data is expressed as the ratio of the 35S-glycosaminoglycans in the supernatant to the total 35S-glycosaminoglycans (cell pellet plus supernatant).

Immunoprecipitation

Solutions:

5X Pull down lysis buffer	50 mL
100 mM Tris, pH7.4	5 mL of 1 M stock
750 mM NaCl	18.75 mL of 2M stock
20 mM $MgCl_2$	2 mL of 0.5M stock
10 mM EDTA	1 mL of 0.5M stock
1% TritonX-100	500 µL

Protocol:

(Based on Upstate protocol)

1. Scrape cells into 1X Pull down buffer and put on orbital shaker for 15 minutes at 4ºC.
2. Wash agarose beads with PBS and make into a 50% slurry with IP buffer
3. Preclear lysate by adding 100 µL beads and shaking for 10 minutes at 4ºC.
4. Spin down lysate/beads, and collect cleared supernatant.
5. Incubate lysate, fresh beads, and antibody at 1:50 overnight at 4ºC.
6. Spin down beads and discard supernatant. Wash 3-4 x 15 minutes in lysis buffer.
7. Resuspend beads in sample buffer and boil. Spin down and run supernatant on a gel.

Protein G- mouse

Protein A - rabbit

siRNA protocol (Lipofectamine)

1. Plate cells at 60-80% confluency the day before siRNA treatment.

2. Into an eppendorf tube, add 50 µL OptiMEM and 1 µL Lipofectamine 2000 (or Lipofectamine) per 24 well. Mix gently and incubate at RT for 5 minutes.

3. Into another eppendorf, add 50 µL OptiMEM and 1.5 µL 20 µM siRNA per 24 well well. Mix gently.

4. Add contents of tube with siRNA to tube with Lipofectamine. Incubate for 20-30 minutes at RT (in hood).

5. Wash cells with OptiMEM. Add 100 µL of OptiMEM to each well (this provides enough volume to cover the cells). Add contents of tube to well.

6. After 4-8 hours, remove siRNA solution and add complete DMEM. Time of incubation with siRNA varies with cell type and siRNA.

7. Assay cells 24-72 hours after siRNA.

Generation of chemical competent cells (RbCl-method)

(GS 2008)

1. Inoculate fresh single colony in 4 mL LB and grow at 37°C over night.
2. Dilute 1 mL of overnight culture in 1L of LB (or YETM) media and grow at 28°C (or lower) temperature to OD 0.5
3. Chill cells on ice for 5 - 10 min and spin in pre-chilled centrifuge at 1700 g for 10 min. **From this moment on never let cells warm and never vortex them!**
4. Discard supernatant and resuspend pellet carefully (only swirling, no vortexing!) in 20 – 30 mL cold TFB1. Transfer cells to smaller tubes (e.g. 50 mL blue cap conical tubes) and spin at 1100 g for 10 min.
5. Discard supernatant carefully (pellet will be very loose) and add approx 20 mL of TFB2. Carefully resuspend and incubate cells on ice for 15 – 30 min.
6. Aliquot cells (we do 50 µL) in eppendorf tubes (on ice) using a multipipette. Close tubes and transfer to dry ice/ethanol mixture (use Styrofoam box) to snap freeze cells. Store cells at -80°C.

Transformation (heat shock)

1. Thaw cells on ice (5 – 10 min). Never let cells warm before heatshock!
2. Add 1-5 µL plasmid (ligation…) and mix by flicking and incubate for 5-10 min.
3. Heat shock for 35 seconds at 42°C in waterbath (do not use heated metal blocks).
4. Immediately put on ice and incubate for 3-5 min.

5. Add 800 µL prewarmed LB media (no antibiotics) and incubate for 1h at 37°C while shaking. (For increased efficiency use 10 mL Falcon tubes).
6. Plate cells on selective plates

Solutions:

YETM (1L)

5 g Yeast Extract

20g Tryptone

10 g $MgSO_4*7H_2O$

TFB1 (for 200 mL)

0.59 g KAc (30 mM

2.42 g RbCl (100 mM)

0.29 g $CaCl_2$ * $2H_2O$ (10 mM)

1.98 g (MnCl2) * $4H_2O$ (50 mM)

30 mL glycerol (15% v/v)

Adjust to pH 5.8 with acetic acid (not KOH!). Filter sterilize and store refrigerated at 4°C

TFB2, (for 200 mL)

0.42 MOPS (10 mM)

2.21 g $CaCl_2$ * $2H_2O$ (75mM)

0.24 g RbCl (10 mM)

30 mL glycerol (15% v/v)

Adjust to pH 6.5 with KOH. Filter sterilize and store refrigerated at 4°C

PC/SM transfer assay

1. Calculate amounts of lipid, heart mitochondria, and SET buffer:

    lipid: 8μL cold PC/2μL hot PC (SM) per 20 assays

    heart mito: 15 μL/assay (currently – differs per prep)

    total volume: 200 μL/assay + negative control+total+3-4 extra for error

2. Add 0.25, 0.5, 1 mg cytosol plus lysis buffer for a total volume of 500 μL. Make blank with 500 μL lysis and no protein.

3. Add appropriate amount of lipids to Falcon tube, dry down under nitrogen gas.

4. Sonicate lipid on ice: 1 minute sonication, 1 minute rest on ice.

5. Dounce homogenize BHM ~5 times.

6. To lipids, add bovine heart mitochondria and lysis buffer. Add 200 μL of lipid/BHM/lysis buffer mixture per tube and mix. Save 200 μL of lipid/BHM/lysis buffer for total count.

7. Incubate for 30 minutes at 37ºC.

8. During incubation, cool 14.3% sucrose solution in syringes.

9. After incubation, place samples on ice. Using 18 gauge needle, add 500μL 14.3% sucrose under the sample. Do not mix sucrose and reaction.

10. Spin for 10' at 12-14K (I prefer 14K/max).

11. Aspirate supernatant. Remove as much supernatant as possible, but do not aspirate pellet.

12. Add 100 μL 10% SDS to each tube. Resuspend by pipetting as much as possible. If pellet does not fully dissolve (normally it won't), either leave O/N at room temperature or boil for 5'.

13. Transfer the contents of the tube to a scintillation vial with 5 mL scint fluid. If samples were boiled, wash reaction tube with 100 μL methanol and transfer to scint vial.

14. Count samples on a ^{14}C setting.

PI transfer assay

1. Calculate amounts of lipid, rat liver microsomes, and lysis buffer.

    lipid: 25 μL PI/PC per sample

    RLM: 35 μL/assay (currently – differs per prep)

    total volume: 500 μL/assay + negative control+total+3-4 extra for error

2. Add appropriate amount of lipids to Falcon tube, dry down under nitrogen gas.

3. Sonicate lipid on ice: 1 minute sonication, 1 minute rest on ice.

4. Add 0.5, 1, 2 mg cytosol plus lysis buffer for a total volume of 500 μL. Make blank with 500 μL lysis buffer and no protein.

5. Add 200 μL 0.2M NaAc pH 5 (or pH 5.2) to tube of RLM. Spin down 10 minutes at setting 10.

6. Resuspend pellet in 1 mL lysis buffer. Dounce homogenize 10 times.

7. In 50 mL conical tube, mix lipids, RLM and lysis buffer.

8. Add 500 μL of lipid/RLM/lysis buffer mixture per tube. Mix. Save 500 μL mixture for total count.

9. Incubate for 30 minutes at 37ºC.

10. After incubation, put samples on ice and stop reaction by adding 200 μL 0.2 M NaAc.

11. Spin 10' setting 10 (4ºC or RT OK).

12. Count 1 mL of supernatant in 10 mL of scintillation fluid.

Tail preps

(from Jim Alb)

1. Make master mix for dissolving tails. Use glass pipettes to dispense.

Per tail: 500 µL Nuclei Lysis solution

100 µL 1M Tris pH 7.5

10 µL Proteinase K (for O/N digestion; 20µL for several hour digestion)

2. Add 600 µL of master mix per tail.

3. Make sure tail is in solution, vortex, and incubate at 55ºC for several hours-O/N.

4. Add 200 µL of protein precipitation solution.

5. Mix and put on ice for at least 10 minutes.

→ to stop at this point, put tubes in freezer

6. Spin 5 min. at max speed. Prep tubes for next step.

7. Pour into tubes with an equal volume of isopropanol (~600µL).

8. Mix 10-12x and spin 5 min. at max speed.

9. Wash 1x with 70% EtOH (200-500µL). Spin 5 min. at max speed.

10. Dry upside down for 30-45 min. Flip tubes and continue drying for ~1 hour (or until mostly dry)

11. Add 200 µL of sterile water and incubate at RT with DNA overnight. (If necessary, can be put at 37ºC for several hours, though resuspension won't be as good.)

12. Use 1µL per PCR

Transforming DY380 recombineering bacteria strain

From: P Liu, NA Jenkins, and NG Copeland, Genome Research 13:476-484, 2003.

Activation of recombination enzymes (heat shock)

1. Grow O/N culture of DY380.

2. Dilute 0.5 mL of culture into 10 mL of low-salt LB. Grow for 2-3 hours. (Turn on 42º shaking H2O bath at this time.)

Note: I've used this amount of cells for 2 transformations, though the protocol seems to say that you should use the entire 10 mL for one transformation.

3. Transfer 10 mL cultures to 42ºC and shake for 15 minutes.

4. After heat-shock, place cultures on wet ice and shake to cool quickly. Leave on ice for 5 minutes.

5. Spin down cultures and go to step 3 of the next protocol.

Transformation

1. Grow cells in 5 mL of LB broth (low salt recommended) O/N at 30ºC (not greater than 32ºC!).

2. Before beginning, put sterile H_2O on ice.

3. Spin down bacteria and resuspend in 888 µL of ice cold water.

4. Transfer to a pre-chilled eppendorf, and centrifuge for 15-20 seconds at RT.

5. Place tubes on ice and aspirate the supernatant.

6. Wash cells two more times with cold water as before.

7. Pellet cells and resuspend in 50 μL cold water. Transfer to a pre-cooled electroporation cuvette with a 0.1 cm gap.

8. Add DNA. They recommend 1 μL of BAC DNA (100 ng) or 1 ng of plasmid DNA. I've added more plasmid DNA and had success.

9. Electroporate under the following conditions:

    -1.75 kV

    -25 μF

    -pulse controller set at: 200 Ω

    Time constants will usually be around 4.0

10. Add 1.0 mL of LB to cuvette, transfer to blue-cap tube (or other sterile tube), and incubate at 32ºC for 1 hour.

11. Plate entire transformation.

Yeast FM4-64 labeling

1. Grow up yeast strains in YPD/selective media. Shift to restrictive temperature for 2 hours.

2. Label: Resuspend 4 OD in 100 µL media and label with 10 µM FM4-64 for 5-15 min at 25º or 37º.

3. Wash: wash cells 1-2 times and resuspend in 200 µL YPD (10-20 OD600 U/mL).

4. Chase: 10', 20', 30' (pilot experiment).

5. Stop endocytosis: spin down cells, resuspend in ice cold media, add energy poison (1 mM NaAz, 1 mM NaF), and keep on ice.

Immunofluorescent Staining of Yeast: SDS Permeabilization Method

modified from:

P. Brennwald

June 1993

For More information and alternative methods see: "Immunoflourescence Methods for Yeast" by Pringle et.al on pg. 565 in Guide to Yeast Genetics and Molecular Biology edited by Guthrie and Fink (Vol. 194 of Methods in Enzymology).

Materials:

1) 1.0M KPO_4 pH 6.5 : Make by mixing 33 mls of 1M K_2HPO_4 with 67 mls of 1M KH_2PO_4

2) 0.1M KPO_4 pH 6.5

3) 0.1M KPO_4 pH 7.5: Make 500 mls by mixing 41.7 mls of 1M K_2HPO_4 and 8.3 mls of 1M KH_2PO_4 with 450 mls of ddH_2O

4) 37% Formaldehyde

5) KS Buffer: 0.1 M KPO_4 pH 7.5/1.2 M Sorbitol

6) Zymolyase 100T: 5 mg/ml solution in 0.1M KPO_4/0.5% □-mercaptoethanol

7) □-mercaptoethanol

8) HS Buffer: 0.1 M Hepes pH 7.4/1.0 M Sorbitol

9) HS/SDS Buffer: 0.1 M Hepes pH 7.4/1.0 M Sorbitol/0.5% SDS

10) 0.1 % Polylysine (MW >300,000; Sigma Cat. No. P-1524) Stored in 1ml or 10 ml aliquots at -20°C. After thawing microfuge aliquot for 5 min. at 4°C before adding to slides.

11) Multiwell teflon masked slides (Carlson Scientific Inc. Peotone IL. Cat.No.100806)

12) PBT Buffer: PBS with1 mg/ml BSA and 0.02% Tween 20

13) Primary Antibodies: Affinity purified polyclonal antibodies or monoclonal antibodies from cell culture supernatant (not from ascites fluid). Dilutions must be determined emperically for each primary but common ranges are for affinity purified sera 1:10 to 1:100 in PBT Buffer. For cell culture supernatants 1:1 to 1:5 dilutions are normally used (if cell supernatants were concentrated by ammonium sulfate precipitation then 1:10 to1:50 dilutions are often used). After diluting in PBT buffer spin secondary in microfuge (at 4°C) for 5 min to pellet any debris.

14) Secondary Antibodies: Jackson Immunoresearch Laboratories makes high quality secondary antibodies which are good for both single and double labeling experiments. We've been using: Texas Red conjugated AffiniPure Donkey Anti-Mouse IgG (Cat#715-075-141) and Fluorescein (DTAF) conjugated AffiniPure Donkey Anti-Rabbit IgG (Cat#711-015-132). They are sent as freeze-dried powder which should be reconstituted with ddH2O according to directions and then aliquoted into 50 □l/tube (marked with name of Ab and Date) and frozen on dry ice and stored in the "Secondary Antibodies" Box in the -80°C Freezer. After thawing an aliquot keep it at 4°C--it should be good for about a month. These secondary Abs work very well for both double and single labeling and should be used at 1:50 to 1:100 dilutions each (in PBT

buffer). After diluting in PBT the solution should be microfuged for 5 min at 4°C to remove any precipitates that may have formed.

Method:

1) Grow up 2 x 5 mL of yeast to OD 0.5-0.8

2) Fix yeast directly in the culture by adding to each 5 mls of culture: 0.5 mls of 1.0 M KPO_4 pH 6.5 and 0.6 mls of 37% Formaldehyde directly to the culture flask. Incubate at room temperature with gentle shaking for 30 min.

3) Transfer an amount of cells that is equal to about 2.5-5 OD_{599} units and spin for 5 min.

4) Aspirate off the supernatant and resuspend each pellet in 2.5 mls of 0.1 M KPO_4 pH 6.5 and transfer to a 15 ml centrifuge tube. Add 0.3 mls of formaldehyde to each tube and incubate at room temperature for 1.5 hrs with gentle rocking.

5) Harvest fixed cells by centrifuging at for 5 min.. Aspirate off supernatant and resuspend in 2.5 mls of 0.1 M KPO_4 pH 7.5 and repeat spin. Aspirate off sup. and resuspend cells in 2.5 mls of 0.1 M KPO_4/1.2 M sorbitol. Fixed cells can now be stored overnight (or for several days) at 4°C.

6) Prepare Zymolyase solution by dissolving 2-5 mg of Zymolyase in 0.1 M KPO_4 pH 7.5 to give 5 mg/ml solution. Add β-mercaptoethanol to 0.5 % (i.e. 5 µl/ml), mix by gently vortexing and let sit at room temp. for 20-30 min to dissolve.

7) Harvest fixed cells at 2.2K RPM for 5 min. Aspirate off supernatant and resuspend in 0.5 ml of 0.1 M KPO_4 pH 7.5/1.2 M Sorbitol.

8) Transfer cells to a 13x100 mm glass culture tube (i.e. blue capped tubes). Add 22.5 µl of 5 mg/ml Zymolyase solution and 2.5 µl of β-mercaptoethanol and incubate at 30°C for 30 min with occassional mixing by finger-flicking.

9) Harvest spheroplasts for 5 min. Resuspend cells in 1.5 mls of HS Buffer and spin. Aspirate off supernatant and repeat wash one time.

10) To permeabilize cells resuspend spheroplasts in 1.5 mls of HS/SDS and incubate at room temperature for 5 min.

11) Centrifuge for 5 min and resuspend cells in 1.5 mls of HS Buffer and spin.

12) Aspirate supernatant and repeat wash with HS Buffer. Resuspend cells in 0.5 ml of HS Buffer. Do not store the cells for more than a few hours at this stage.

13) Set up an aspirator with "pulled" pasteur pipette at the end near to where the slides are to be processed to speed up the washing procedures.

14) Prepare slides by adding 20 µl of 0.1% polylysine to each well and incubate for 5-10 min. Aspirate off and wash each well 3 times with one drop of ddH_2O.

15) Place 20 µl of spheroplasted/permeabilized cell suspension on each well. Incubate for 5-10 min. Aspirate each well and add one drop per well of PBT Buffer. Repeat twice and let sit while primary Ab dilutions are prepared.

16) Prepare dilutions of primary antibodies in PBT and microfuge before use. Add 20 µl of diluted primary antibody and transfer slides to a plastic box with a moistened paper towel at the bottom. Incubate 60-90 min.

17) Carefully remove slides from box to benchtop for washing. To wash slides rapidly, hold aspirating pipette in one hand and another pastuer pipette with a rubber bulb containing PBT Buffer in the other hand. For each well aspirate the liquid and then add

one drop of PBT, aspirate add PBT, repeat this twice (leaving the well with a drop of PBT) and then move on to the next well. It is important that the wells do not dry out once antibodies have been added. Once all the wells have been washed move on the next slide. Then repeat this entire procedure twice so that each well has been washed at least nine-times. This may seem excessive but it often dramatically increases the quality of the images obtained and once you get the hang of using both hands it can be done fairly quickly.

18) Wrap plastic box used for primary Ab incubations in foil so it is light tight. Place slides inside and place 20 µl of secondary antibody in each well. Incubate for 60-90 min at room temperature.

13) Wash the wells as before with a total of at least 9-10 washes of PBT Buffer. Aspirate the wells dry after the last wash and let air dry underneath a piece of foil (make a tent) for 10-15 min.

14) Place 4 evenly spaced small drops of mounting medium in between the two columns of wells in the middle of the slide. Carefully place the coverslip over the slide and let mounting medium spread. Seal the slides with nailpolish, let dry 10-15 min. Then rinse off slides with ddH20, dry with a kimwipe and view immediately or store in dark at -20°C.

Zebrafish in situ hybridization

from: Parichy lab and C. Moens protocols

Probe preparation *All steps after 1b to be performed RNase free*

1. cDNA template preparation

a. linearize cDNA by digesting with appropriate restriction enzyme for 2 hr, 37 °C

Typically digest enough DNA so it can be used for multiple riboprobe syntheses, e.g.:

• 20 ug plasmid DNA + nano H_20 174 µl

• 10x restriction enzyme buffer 20 µl

• BSA 2 µl

• restriction enzyme (10U/ul) 4 µl

Avoid using restriction enzymes (e.g., Sac I, Kpn I, Pst I) that leave a 3' overhand, as this can result in inappropriate transcription of sense RNA that may contribute to background.

b. add equal volume phenol-chloroform-isoamyl alcohol (pH 8.0); vortex 10 sec; centrifuge

at maximum speed 5 min

c. remove aqueous (upper) phase to new RNase-free 1.5 ml tube (do not disturb interface between phases)

d. add 0.1x volume 3 M sodium acetate pH 5.2 and 2.5x volume 100% ethanol; vortex and

leave on ice 15 min

e. centrifuge at maximum speed 15 min at room temperature

f. remove supernatant and add 1 ml 70% ethanol; centrifuge at maximum speed 5 minutes at room temperature; draw off supernatant, air dry briefly

g. resuspend in nano H_20 at 1–2x original volume that you took from your plasmid prep

h. check cutting efficiency and determine template concentration on a 1% agarose gel

Run 0.1 µl of sample on gel (dilute 1 µl DNA into 9 µl TE, then dilute 1 µl of this into 9 µl TE). Run alongside 250, 500 ng lambda–Hind III to estimate concentration. Make sure that templates are completely linearized, as circular DNA will result in probes including the vector sequence

i. store cut DNA at –20 °C

2. Riboprobe synthesis

a. Ambion … kit

b. stop the reaction and precipitate the probe by adding:

• 0.5 M EDTA, pH 8.0 2.0 µl

• 4 M LiCl 2.5 µl

• 100% EtOH 75.0 µl

c. place at –80 °C, 10 min to overnight ; spin at maximum speed 30 min

d. remove supernatant and wash with 70% EtOH; spin 5 min; remove supernatant and air dry briefly

e. resuspend by vortexing in 100 µl nano H_20; add 1 µl Superasin RNase inhibitor

Check riboprobe quality on an agarose/MOPS/formaldehyde gel (optional):

prepare gel:

• 33 ml nano H20

• 4 ml 10X MOPS buffer2

• 0.6 g agarose

melt in microwave and when cool enough to touch add 2.2 ml 37%

formaldehyde, swirl, and pour immediately; cover gel box while gel sets

prepare samples:

to PCR tubes, add:

• 3 µl RNA loading buffer3

• 2 µl nano H20

• 1 µl riboprobe

prepare an extra tube as above for RNA ladder (stored at –80 °C)

heat all tubes at 65 °C for 15 min; quick chill on ice

It is essential to denature the single stranded RNA molecules, which otherwise will migrate as a smear or as irregular bands that cannot be evaluated.

run gel:

use 1X MOPS as running buffer, load all of sample and run at medium voltage (~100V);

do not add ethidium bromide (it is already in the RNA loading buffer)

inspect probe:

Successful probe synthesis should yield a single fragment at the expected size for intact probes and a smear at ~300 nt for fragmented probes. If this is not observed, DO NOT PROCEED with in situ hybridization!

f. Store probes at –80 °C after adding a small amount (~1 µl) of Ambion SUPERaseIn RNase inhibitor

Embryo Fixation and Hybridization

-Fix embryos in 4% Paraformaldehyde/PBS (PFA), 5 h. at room temp. or overnight at 4$_{o}$C

(Paraformaldehyde should be made fresh weekly as an 8% stock in sterile water and diluted 1:1 with 2x PBS before use. 8% PFA should be stored at 4°C)

optional: for long term storage, wash 1 x in 100% MeOH, 10 min., then store at -20oC in 100% MeOH. If embryos are stored in MeOH, before proceeding to next step, rehydrate embryos through 75% methanol/25% PBST, 50%methanol/50% PBST, and 25%methanol/75% PBST washes.

-Wash 5 x 5 min. at room temp in PBST (PBS/0.1% Tween-20). All PBST washes should be in

approximately 0.5 mls.

-For embryos older than ~10 hpf:

-permeabilize by treating with 10 ug/ml Prot. K in PBST, 5-20 min at room temp accordingto age: eg: 1 min for 2-4 somite embryos, 3min for 9-13 somite mbryos, 5 min for 18-24 hour embryos, etc. Do not over-digest or embryos will fall apart during subsequent steps.

-refix in 4% PFA in PBS for 20 min. at room temp.

-rinse 5 x 5 min. in PBST (not necessary if embryos were not proK'd)

-Prehyb for at least 1 hour at 65oC in hyb. mix (recipe below)

-Dilute 100ng labeled RNA probe in hyb. mix *(probe dilution is arrived at empirically, however asa first approximation, dilute probe 1/200 in hyb mix.)*

-Remove prehyb and add pre-warmed hyb mix plus probe to embryos.

-Hybridize overnight at 65°C

Day 2: post-hybridization washes

Notes:

a) Prewarm washing solutions before adding to embryos.

b) hyb mix containing probe can be removed, stored at –20°C and re-used many times without anyloss of signal.

c) *For the following washes, you can use hyb mix that does not contain tRNA or heparin if youwish to conserve these reagents.*

-Wash 5 min in 66% hyb mix, 33% 2 x SSC at 65oC.

-Wash 5 min in 33% hyb mix, 66% 2 x SSC at 65oC

-Wash 5 min in 2 x SSC at 65oC

-*Wash 1 x 20 min in 0.2 x SSC +0.1% Tween-20 at 65oC

-*Wash 2 x 20 min in 0.1 x SSC+0.1% Tween-20 at 65oC (high stringency)

-Wash 5 min in 66% 0.2 x SSC, 33% PBST at room temp.

-Wash 5 min in 33% 0.2 x SSC, 66% PBST at room temp.

-Wash 5 min in PBST at room temp

* Timing is critical

Anti-digoxigenin-Alkaline Phosphatase Binding (first antibody)

-incubate in blocking solution (PBST plus 2% sheep serum, 2 mg/ml BSA) 1 hour at room temp.

-prepare first antibody (eg, alkaline-phosphatase conjugated anti-digoxigenin) by diluting it in blocking solution; 1:5000.

-incubate in antibody for 2 hours shaking at room temp, or overnight at 4oC.

-wash 5 x 15 min in PBST *(may leave in the last PBST wash at 4oC overnight, or proceed directly to the next step)*

Day 3: First Colouration Step

-wash 4 x 5 min in Coloration Buffer2

-mix 45 ul nitro-blue tetrazolium (NBT) stock with 10 ml Coloration Buffer, then add 35 ul 5-bromo-4-chloro-3-indolyl phosphate (BCIP) stock.

- add 500 ul of this mix to embryos and incubate in the dark at room temperature until a blue reaction product is visible. *(colour should become visible within 3-4 hours at most. Coloration reaction can be sped up by incubating at 30oC, or slow by incubating at 4oC).*

-stop reaction by washing embryos 2-4 x in sterile water.

-store in PBST unless doing a two color in situ. *For single-colour in situs proceed to mounting.*

2. Colouration Buffer

(make fresh each use)

100 mM Tris-Hcl, pH9.5 5 ml of 1M

50 mM $MgCl_2$ 2.5 ml of 1M

100 mM NaCl 1 ml of 5M

0.1% Tween-20 250 µl of 20%

sterile water to 50 ml

"Fake" hybridization solution:

Same as hybridization solution, but without expensive components.

formamide 250 ml

20X SSC 125 ml

10% Tween-20 10 ml

1 M citric acid 4.6 ml

nano H_2O to 500 ml total

Store at room temperature.

Hybridization solution (T-hyb):

formamide 250 ml

20X SSC_{12} 125 ml

50 mg/ml yeast tRNA 5 ml

10% Tween-20 10 ml

1 M citric acid 4.60 ml

50 mg/ml heparin 500 µl

nano H_2O to 500 ml total

Antibody blocking solution:

5% heat inactivated goat serum, 2 mg / ml BSA in PBST2. Sterile filter and store at 4 °C. Goat serum is heat inactivated by incubating 45 min at 50 °C, aliquot and freeze at –20 °C.